

**THE IMPLICATIONS OF COMPARTMENT FIRE NON-
UNIFORMITY FOR THE MEMBRANE ACTION OF
REINFORCED CONCRETE SLABS**

Susan Deeny



Doctor of Philosophy

The University of Edinburgh

July 2010

Declaration

This thesis has been completed by Susan Deeny under the supervision of Dr Tim Stratford and Dr Stephen Welch and has not been submitted for any other degree or professional qualification. I declare that the work presented in this thesis is entirely my own except where indicated by full references.

Susan Deeny

July 2010

Abstract

Maintaining structural stability is an integral component of building fire safety. Stability must be ensured to provide adequate time for safe egress of the buildings occupants, fire fighting operations and property protection. Structural fire engineering endeavours to design structures to withstand the effects of fire in order to achieve this objective.

The behaviour of reinforced concrete in fire is not as well understood as other construction materials, such as steel. This is in part due to the complexity of concrete material behaviour and also due to concrete's reputation of superior fire performance. Concrete technology is, however, continually evolving; structures are increasingly slender, more highly stressed and have higher compressive strengths. A more robust understanding of concrete's behaviour in fire will enable predictions of the implications of changing concrete technology and also help to properly quantify the fire safety risk associated with concrete structures.

A fundamental key to understanding structural fire performance is the relationship between the thermal environment induced by the fire and the structure. Significant thermal variation has been found experimentally to exist within fire compartments. Despite this the design of structures for fire almost universally assumes the compartment thermal environment to be homogeneous. In this thesis the implications of compartment fire non-uniformity for concrete structural behaviour is investigated to assess the validity of the uniform compartment temperature assumption

The investigation is conducted using numerical tools; a detailed review of the necessary background knowledge, material modelling of reinforced concrete, finite element modelling of reinforced concrete structures and compartment fire thermal variation is included. The behaviour of a two-way spanning reinforced concrete slab is used as a structural benchmark. The membrane behaviour exhibited by two-way spanning RC slabs at high temperatures has been previously studied under uniform thermal conditions. They therefore are an ideal benchmark for identifying the influence of non-uniform thermal environments for behaviour.

The relationship between gas phase temperature variation and concrete thermal expansion behaviour, which is fundamental to understanding concrete high temperature structural behaviour, is first investigated. These preliminary studies provide the necessary fundamental understanding to identify the influence of gas phase temperature variation upon the membrane behaviour of reinforced concrete slabs.

The individual influences of spatial and temporal variation upon slab membrane behaviour are investigated and the behaviour under non-uniform thermal variation contrasted with uniform thermal exposure behaviour. The influence of spatial variation of temperature is found to be strongly dependent upon the structural slenderness ratio. The tensile membrane action of slender slabs is particularly susceptible to the distorted slab deflection profiles induced by spatial variation of gas temperature. Conversely the compressive membrane behaviour of stocky slabs is found to be insensitive to the deformation effects induced by spatial variation of temperature. The influence upon slender slabs is demonstrated under a range of temporal variations indicating that the thermal response of concrete is sufficiently fast to be sensitive to realistically varying distributions of temperature.

Contrasting behaviour induced by uniform and non-uniform thermal exposures indicates that uniform temperature assumptions provide both conservative and unconservative predictions of behaviour. The accuracy of the uniform temperature assumptions was also found to be dependent upon the type of fire, for example, fast hot and short cool fires. Additionally, the sensitivity of structural performance to deformations caused by spatial variation of temperature demonstrated in this thesis challenges the purely strength based focus of traditional structural fire engineering.

Spalling is an important feature of concrete's high temperature behaviour which is not currently explicitly addressed in design. The incorporation of spalling into a structural analysis is not, however, straightforward. The influence of spalling upon behaviour has therefore been dealt with separately. A spalling design framework is developed to incorporate the effects of spalling into a structural analysis. Application of the framework to case studies demonstrates the potential for spalling to critically undermine the structural performance of concrete in fire. It also demonstrates how

the framework can be used to quantify the effects of spalling and therefore account for these in the structural fire design addressing spalling risk in a rational manner.

Publications

Journal papers

Welch, S., Jowsey, A., Deeny, S., Morgan, R. and Torero, J. L. (2007). "BRE large compartment fire tests - Characterising post flashover fires for model validation." Fire Safety Journal **42**(8): 548-567

Conference papers

Deeny, S. and Stratford, T. (2010). Stability of RC structures under non-uniform thermal exposure. Structures in Fire: Proceedings of the sixth international conference, East Lansing, MI, DEStech Publications.

Deeny, S., Stratford, T., Dhakal, R., Moss, P. and Buchanan, A. (2009). Spalling of concrete: Implications for structural performance in fire. Applications of structural fire engineering Prague, Czech Technical University in Prague.

Deeny, S., Abecassis-Empis, C., Stratford, T. and Torero, J. L. (2007). The Dalmarnock Fire Tests on a Cast In-situ Concrete Structure. fib International workshop: "Fire Design of Concrete Structures - From Materials Modelling to Structural Performance", Coimbra, Portugal, Universidade de Coimbra.

Technical Reports

Concrete Society (2008). Assessment, Design and Repair of Fire-damaged Concrete Structures. Technical Report 68 (Contributing Author)

Acknowledgements

This thesis would not be here if not for the guidance and support of many colleagues and friends.

I would very much like to thank my supervisors at Edinburgh University, Dr Tim Stratford and Dr Stephen Welch and my industrial supervisor Dr Florian Block. The completion of this work is undoubtedly due Tim's expert guidance, keen observations and unending optimism. His natural good humour has made this project a thoroughly enjoyable experience. I would like to thank Stephen for introducing me to fire research as an undergraduate. His insightful comments are always valued. I would like to thank Florian for his advice, friendship and the perspective he has given to the project.

Thank-you to all my friends and colleagues at the BRE Centre for Fire Safety Engineering at the University of Edinburgh; a real fire engineering family. Thank you to Prof Jose Torero for the being the inspirational person he is to create this unique research environment. Kate, Angus, Joanne, Rory and Adam thank-you for your companionship, enthusiasm, distraction and empathy.

For their hospitality and kindness, I would like to thank Prof Andrew Buchanan, Dr Peter Moss and Dr Rajesh Dhakal of University of Canterbury, New Zealand. I would also like to thank the Royal Society of Edinburgh's JM Lessells scholarship for giving me the financial clout to visit them.

My friends and family I would like to thank for their good will, patience and feigned interest in concrete. I would like to thank my Mum for her unshakeable belief and in particular I would like to thank Ian Mackenzie. His continual encouragement, expert cheerleading, tea making and proofing saw this thesis to its end.

This research has been funded jointly by Buro Happold Ltd and EPSRC. This assistance is gratefully acknowledged.

Contents

DECLARATION	I
ABSTRACT	II
PUBLICATIONS	V
ACKNOWLEDGEMENTS	VI
CONTENTS	VII
TABLE LIST	IX
FIGURE LIST	X
NOMENCLATURE	XVIII
1 INTRODUCTION	1-1
1.1 MOTIVATION FOR RESEARCH	1-1
1.2 RESEARCH OBJECTIVES	1-4
1.3 CHAPTER OUTLINE	1-5
2 REINFORCED CONCRETE – MATERIAL BEHAVIOUR	2-7
2.1 THERMAL BEHAVIOUR	2-7
2.2 MECHANICAL BEHAVIOUR	2-14
2.3 CONCLUSIONS	2-47
3 COMPARTMENT FIRES AND STRUCTURAL FIRE FUNDAMENTALS	3-51
3.1 THE COMPARTMENT FIRE THERMAL ENVIRONMENT	3-51
3.2 THERMAL EXPANSION INDUCED STRUCTURAL BEHAVIOUR.....	3-60
3.3 CONCLUSIONS	3-83
4 BENCHMARK STRUCTURAL MODEL	4-85
4.1 BEHAVIOUR OF TWO-WAY SPANNING SLABS IN FIRE	4-85
4.2 FINITE ELEMENT MODELLING OF REINFORCED CONCRETE SLABS IN FIRE	4-89
4.3 FINITE ELEMENT ANALYSIS OF A TWO-WAY SPANNING RC SLAB	4-94
4.4 GEOMETRIC SENSITIVITY STUDIES	4-118
4.5 MATERIAL SENSITIVITY STUDIES	4-124
4.6 CONCLUSIONS: BENCHMARK SLAB MODEL	4-139
5 STRUCTURAL IMPLICATIONS OF NON-UNIFORM FIRES	5-142
5.1 INTRODUCTION	5-142
5.2 STRUCTURAL IMPLICATIONS OF SPATIAL VARIATION OF T_G	5-144
5.3 STRUCTURAL IMPLICATIONS OF TEMPORAL AND SPATIAL T_G VARIATION	5-160
5.4 CONCLUSIONS	5-173
6 CONSEQUENCES OF SPALLING	6-175
6.1 SPALLING BEHAVIOUR OF CONCRETE.....	6-176

6.2	DESIGN OF CONCRETE STRUCTURES FOR SPALLING.....	6-182
6.3	SPALLING DESIGN FRAMEWORK.....	6-185
6.4	CASE STUDY 1: CONTINUOUS TWO SPAN RC BEAM	6-195
6.5	CASE STUDY 2: TWO-WAY SPANNING SLENDER SLAB	6-204
6.6	CONCLUSIONS.....	6-216
7	CONCLUSIONS AND FURTHER WORK.....	7-218
7.1	INTRODUCTION	7-218
7.2	SUMMARY AND CONCLUSIONS	7-219
7.3	FURTHER WORK	7-227
	REFERENCES.....	229

Table List

Table 3-1 Concrete beam boundary conditions	3-65
Table 4.1 Boundary conditions examined.....	4-99
Table 6.1 Factors contributing to the spalling behaviour of concrete.....	6-179
Table 6.2 Example of hazard based scoring system for spalling of concrete structures (Lennon et al. 2007)	6-190
Table 6.3 Hazard categorisation for spalling of concrete structures (Lennon et al. 2007)	6-191
Table 6.4 Risk Assessment – possible template for risk profiling (Lennon et al. 2007)	6-192
Table 6.5 Possible risk categories (Lennon et al. 2007)	6-192
Table 6.6 Spalling hazard classification and spalling severities (Lamont et al. 2007)	6-193
Table 6.7 Fire resistance periods of continuous two span beam under spalling categories A-D	6-201
Table 6.8 Effect of sagging reinforcement distribution upon fire resistance periods in the event of spalling (Cat B) and without spalling.....	6-204

Figure List

Figure 2-1 Specific Heat of steel as specified by EC3.....	2-8
Figure 2-2 Eurocode 3 (2005) defined conductivity of steel at elevated temperatures	2-9
Figure 2-3 Density reduction for normal weight concrete at elevated temperatures according to Eurocode 2 (2004).....	2-11
Figure 2-4 Experimental and Eurocode 2 temperature dependent specific heat values for concrete (Malhotra 1982).....	2-12
Figure 2-5 Upper and lower thermal conductivity limits for normal weight concrete: Eurocode 2 (2004).....	2-13
Figure 2-6 Typical elevated temperature steel stress-strain curves indicated yield strength and proof strength	2-15
Figure 2-7 Residual proportional limit stress and maximum stress for hot rolled steel according to Eurocode 2 (2004).....	2-15
Figure 2-8 Young's modulus reduction factors at elevated temperatures according to Eurocode2 (2004).....	2-16
Figure 2-9 Uniaxial stress strain model for steel at elevated temperatures.....	2-17
Figure 2-10 Total thermal elongation o reinforcing steel (2004).....	2-18
Figure 2-11 Tensile Strength estimates related to compressive strength in EC2 (2004) and CEB-FIB Model Code (1990).....	2-21
Figure 2-12 Schematic of the stress-displacement relation for a concrete tensile test- 22	
Figure 2-13 Typical concrete uniaxial compressive stress strain curve.....	2-24
Figure 2-14 Eurocode 2 Part 1-2 recommended reduction factors for concrete compressive and tensile strength.....	2-27
Figure 2-15 Experimentally measured elevated temperature biaxial strength for gravel concrete reproduced from (Haksever and Ehm 1987)	2-29
Figure 2-16 Non-linear compressive stress-strain behaviour of concrete as described by Equation 2-3	2-31
Figure 2-17 (a) Concrete Fracture energy (b) Tension softening bilinear approximations for $G_F = 0.075 \text{ Nmm/mm}^2$ (Rots et al. 1984; CEB-FIP 1990).....	2-32
Figure 2-18 Free thermal strain for siliceous and calcareous aggregate concretes according to Eurocode2 (2004).....	2-33
Figure 2-19 Incorporation of Anderberg's transient creep term into concrete's constitutive stress - strain curve (Equation 2-3).....	2-37
Figure 2-20 (a) Schematic of shrinking failure surface (Drucker Prager) (b) Experimental biaxial compression failure envelope reproduced from (Haksever and Ehm 1987).....	2-38

Figure 2-21 (a) Schematic representation of multi-surface failure criteria (combined Drucker-Prager/Rankine) in plane stress (b) Lubliner yield function in plane stress space reproduced from (Lubliner et al. 1989).....	2-41
Figure 2-22 Series of events in cracking of reinforced concrete sections.....	2-45
Figure 2-23 Schematic load-displacement response of a steel bar and a concrete embedded steel bar.....	2-46
Figure 3-1(a) Pre flashover fire development in a compartment (b) post flashover fire	3-52
Figure 3-2 Progressive burning in a deep compartment with opening at one end (Buchanan 2001)	3-53
Figure 3-3 Fuel distribution and ventilation locations: Dalmarnock Test 1 compartment plan.....	3-54
Figure 3-4 Gas phase temperature measurements showing key events in fire development	3-55
Figure 3-5 Gas temperature plan contour plots at 50 mm below ceiling level (a) 400 (b) 700 (c) 860 (d) 1140 seconds	3-56
Figure 3-6 Temperature-time design fires available in Eurocode 1 (2002).....	3-57
Figure 3-7 Temperature-time compartment fire curves with different fire load densities for opening factor $A_w H^{1/2}/A_t(m^{1/2}) = 0.04m^{1/2}$ (Pettersson et al. 1976) ...	3-58
Figure 3-8 Parametric fire curves calculated according to Eurocode 1 (2002) for (a) opening factor, O (b) thermal absorptivity, b.....	3-59
Figure 3-9 Uniform heating of an (a) unrestrained and (b) axially restrained element	3-61
Figure 3-10 (a) Unrestrained and (b) axially restrained structural element subject to a uniform thermal gradient.....	3-62
Figure 3-11 Thermal expansion induced deflection response for various combinations of ϵ_{th} and $\epsilon\phi$ (Usmani et al. 2001)	3-63
Figure 3-12 Thermal effects for concrete: cross section (a) temperature (b) strain (c) stress.....	3-64
Figure 3-13 Deflection output locations for the thermal expansion analysis of a plain concrete element (a) maximum span deflection and lateral displacement (b) axial force.....	3-65
Figure 3-14 Plain concrete beam central deflection during 120 minutes exposure to the standard fire.....	3-66
Figure 3-15 (a) Simply supported beam lateral displacement (b) pinned beam axial force during 120 minute standard fire exposure	3-67
Figure 3-16 (a) Temperature profile and (b) thermal strain profile of a 100mm concrete element under standard fire exposure.....	3-68
Figure 3-17 Influence of cross-section depth for simply supported beam central deflections during 120 minute standard fire exposure	3-69

Figure 3-18 Effect of cross-section depth for the (a) simply supported beam lateral displacements (b) pinned beam axial force	3-69
Figure 3-19 (a) Linear variation of gas temperature along beam x-axis (b) evolution of gas temperature with time.....	3-71
Figure 3-20 Influence of a non-uniform thermal exposure for deformation of a horizontal concrete element: Simply supported beam deflection profile 60 minutes exposure	3-72
Figure 3-21 Influence of increasing horizontal variation in gas temperature upon the peak beam deflection.....	3-73
Figure 3-22 Influence of horizontal temperature variation for (a) simply support beam lateral displacement (b) pinned beam axial force.....	3-73
Figure 3-23 The influence of cross section depth for the deflection profile under horizontal gas temperature variation, $V = 80\%$	3-74
Figure 3-24 Influence of horizontal temperature variation upon (a) simply supported lateral beam displacements (b) pinned beam axial forces.....	3-75
Figure 3-25 Alpert correlation for maximum ceiling temperature and fire burning rate	3-76
Figure 3-26 Ceiling gas temperature distribution at 2 different time steps.....	3-78
Figure 3-27 Temperature distributions calculated according to Alpert (1972) for burning rates of 60, 38 and 20 MW and ceiling height 6m at $t = 0$ seconds.....	3-78
Figure 3-28 Spatial distribution of gas temperature in the beam x-coordinate for the fast burning rate at selected time steps.....	3-79
Figure 3-29 Sensitivity of concrete's thermal expansion deformations to a fast, medium and slow changing fire: Maximum vertical deflections and deflection profiles.....	3-81
Figure 3-30 Sensitivity of a deep concrete beam's ($d=250\text{mm}$) thermal expansion deformations to a (a) fast (b) medium and (c) slow changing fire: Deflection profiles.	3-82
Figure 4-1 Characteristic load-displacement curve for reinforced concrete slabs at ambient and elevated temperatures	4-86
Figure 4-2 Role of lateral restraint in the development of compressive membrane action	4-86
Figure 4-3 Tensile membrane action in an unrestrained floor slab.....	4-88
Figure 4-4 Reinforced concrete slab geometry and finite element analysis representation of RC concrete slab for heat transfer and stress-displacement analysis	4-95
Figure 4-5 Steel reinforcement stress-strain curves according to Eurocode 2 at elevated temperatures.....	4-97
Figure 4-6 Components of restraint surrounding structure imposes upon two-way spalling slab.....	4-98

Figure 4-7 Effect of boundary condition for the central deflection of a two-way spanning slab.....	4-100
Figure 4-8 Principal stress resultants (MPa) at 6 minutes exposure (a) unrestrained (b) laterally restrained (c) rotational restraint (d) lateral and rotational restraint. Supported Edge along X=0m and Y=3m.....	4-103
Figure 4-9 Principal stress resultants (MPa) at 60 minutes exposure (a) unrestrained (b) laterally restrained (c) rotational restraint (d) lateral and rotational restraint. Supported edges at X=0m and Y=3m.....	4-104
Figure 4-10 Reinforcement normalised stress profile across a centreline through the slab (y=0m) (a) Unrestrained slab (b) laterally restrained slab.....	4-105
Figure 4-11 Reinforcement normalised stress profile across a centreline through the slab (y=0m) (a) rotationally restrained slab (b) Laterally and rotationally restrained slab	4-106
Figure 4-12 Calculation of proportional equivalent plastic strains.....	4-108
Figure 4-13 Unrestrained slab proportional plastic equivalent strain at (a) Top (b) Mid and (c) Bottom surface and (d) y=2.925 m cross-section	4-110
Figure 4-14 Laterally restrained slab proportional plastic equivalent strain at (a) Top (b) Mid and (c) Bottom surface and (d) y=2.925 m cross-section.....	4-111
Figure 4-15 Rotationally restrained slab proportional plastic equivalent strain at (a) Top (b) Mid and (c) Bottom surface and (d) y=2.775 m cross-section	4-112
Figure 4-16 Rotationally and laterally restrained slab proportional plastic equivalent strain at (a) Top (b) Mid and (c) Bottom surface and (d) y=2.775 m cross-section ...	4-113
Figure 4-17 Reinforcement mechanical strain profile across a centreline through the slab (y=0m) (a) Unrestrained slab (b) Laterally restrained slab	4-114
Figure 4-18 Reinforcement mechanical strain profile across a centreline through the slab (y=0m) (a) Rotationally restrained slab (b) Rotationally and laterally restrained slab	4-115
Figure 4-19 Effect of slenderness ratio for the deflection of a slab exposed to the Standard Fire with (a) laterally restrained (c) laterally and rotationally restrained boundary conditions	4-119
Figure 4-20 (a) Development of slab central deflection during standard fire exposure (b) 6m span deflection profile after 60 min exposure to the standard temperature time curve.....	4-120
Figure 4-21 Square and rectangular slab maximum and minimum principal stress resultants for a rotationally and laterally restrained boundary condition.....	4-122
Figure 4-22 Reinforcement normalised stress profiles (a) Restrained slab, top and bottom reinforcement (b) Unrestrained slab, top and bottom reinforcement.....	4-123
Figure 4-23 Modification of the concrete tensile constitutive curve to include tension stiffening effect	4-125

Figure 4-24(a) Variation of post peak tension stiffening curve and (b) Tensile constitutive curves, TS= 5, for 20-500°C	4-126
Figure 4-25 von Mises stress contour plots at 3600 sec ISO fire exposure – bottom surface for TS values of (a) 0 (b) 5 and (c) 10	4-127
Figure 4-26 Variation in the slab mid span deflections with concrete tension definition for a 60 minute standard fire exposure	4-127
Figure 4-27 Effect of tension stiffening factor on the reinforcement normalised stress at the slab edge (a) Top location and (b) Bottom location and at the slab mid-span (c) Top location and (b) Bottom location.	4-128
Figure 4-28 Effect of tension stiffening factor on the reinforcement mechanical strain at the edge of the slab (a) Top location and (b) Bottom location and at the mid span of the slab (c) Top location and (d) Bottom location.	4-130
Figure 4-29 Incorporation of LITS term into the instantaneous stress-strain constitutive relations according to Anderberg and Thelandersson (1976) 300deg.....	4-131
Figure 4-30 Unrestrained slab (a) Mid span deflection profile at 60 minutes (b) slab central deflection and restrained slab (c) Mid span deflection profile at 60 minutes (d) slab central deflection.....	4-132
Figure 4-31 Material loading history for the restrained slab.....	4-133
Figure 4-32 Plan contour of unexposed surface plastic equivalent compressive strains at 10.5 min (a) Non-LITS model (b) LITS model	4-134
Figure 4-33 Effect of transient strain component for reinforcement mechanical strain at the slab edge slab (a) Top location and (b) Bottom location and at the mid span of the slab (c) Top location and (d) Bottom location.	4-135
Figure 4-34 Effect of reinforcement rupture strain definition for reinforcement normalised stress at the slab edge (a) Top location and (b) Bottom location and at the slab mid-span (c) Top location and (b) Bottom location	4-137
Figure 4-35 Effect of reinforcement rupture strain definition for reinforcement mechanical strain at the slab edge slab (a) Top location and (b) Bottom location and at the mid span of the slab (c) Top location and (d) Bottom location.....	4-138
Figure 4-36 Effect of reinforcement rupture strain definition on (a) central span deflection profile at 60 minutes standard temperature exposure and (b) central slab deflection for duration of 60 minute standard temperature time curve exposure.	4-139
Figure 5-1 (a) Linear variation of gas temperature across slab span (b) evolution of gas temperature with time	5-145
Figure 5-2 Mid span vertical deflection profile for a simply supported slab under linear gas temperature exposure.....	5-146
Figure 5-3 Horizontal deformation induced by a uniform ($V = 0\%$) and liner variation of T_g ($V = 80\%$) (deformation scale factor 10).....	5-146

Figure 5-4 The effect of a linear T_g spatial variation upon the compressive ring: minimum principle stress resultants in a pinned slab after 60 minutes exposure (a) $v=0\%$ (b) $v = 80 \%$	5-147
Figure 5-5 The effect of a linear T_g spatial variation upon the compressive ring: Proportional plastic equivalent concrete compressive in a pinned slab after 60 minutes exposure (a) $V=0\%$ (b) $V = 80 \%$	5-148
Figure 5-6 Effect of thermal variation and restraint condition for maximum crushing strains: maximum proportional plastic equivalent compressive strain after 60 minutes exposure	5-149
Figure 5-7 Effect of a linear gas temperature variation upon the distribution of reinforcement mechanical strains in a pinned slab: Contour plots mechanical strain of reinforcement spanning the same direction as the linear gas temperature gradient....	5-150
Figure 5-8 Slab cross-section showing zoning for comparison of reinforcement peak mechanical strains	5-150
Figure 5-9 Effect of linear thermal variation for maximum reinforcement strains at critical edge and mid span locations in a slender two-way spanning reinforced concrete slab.....	5-151
Figure 5-10 Alpert correlation plume location (a) slab edge and (b) slab mid span...5-	152
Figure 5-11 Effect of peak temperature location for slab deflection profile after 60 minutes exposure.....	5-153
Figure 5-12 Influence of peak temperature location for slab peak deflections (a) mid-span location (b) edge location	5-154
Figure 5-13 Effect of peak T_g location upon the compressive ring: Minimum principle stress resultant (a) Edge location (b)Mid-span location after 60 minutes exposure in a pinned slab	5-155
Figure 5-14 Effect of peak T_g location upon concrete crushing within the compressive ring: Proportional plastic equivalent plastic concrete compressive strains (a) Edge location (b) Mid-span location after 60 minutes exposure in a pinned slab	5-156
Figure 5-15 Effect of peak temperature location for concrete crushing: Max proportional plastic equivalent strain	5-156
Figure 5-16 Effect of reinforcement location for maximum reinforcement mechanical strains in a pinned slab	5-157
Figure 5-17 Effect of linear spatial T_g variation upon peak deflection of slab with (a) pinned (b) fixed boundary conditions	5-158
Figure 5-18 Temperature distributions and total exposure times for fast, medium and slow burning rates according to Alpert's (1972) correlation ($H = 6m$)	5-160
Figure 5-19 Spatial distribution of gas temperature in the slab x-coordinate for the fast burning rate at selected time steps.....	5-161

Figure 5-20 Effect of temporal and spatial variation of gas temperature upon the deformation behaviour of a slender two-way spanning reinforced concrete slab.	5-163
Figure 5-21 Effect of spatial and temporal variation of gas temperature upon the compressive ring: Minimum principle stress resultants under pinned boundary conditions	5-164
Figure 5-22 Corner crushing strains for different burning rates: Proportional plastic equivalent strains (a) Unrestrained slab (b) laterally restrained slab	5-165
Figure 5-23 Effect spatial and temporal variation of gas temperature upon the distribution of concrete crushing strains: Plan contour of top surface proportional plastic equivalent compressive strains (a) simply supported slab (b) pinned slab	5-166
Figure 5-24 Evolution of reinforcement strain distribution under pinned boundary conditions and fast fire exposure (a) 12 min (b) 15 min (c) 19 min	5-167
Figure 5-25 Effect of temporal changes in temperature spatial distribution for reinforcement behaviour: Pinned slab rebar mechanical strains (a) Fast fire 19 min (b) Medium fire 30 min and (c) Slow fire 58 min.....	5-168
Figure 5-26 Maximum and average uniform temperature exposures for the fast medium and slow fires	5-169
Figure 5-27 Evolution of maximum slab vertical deflection for non-uniform and uniform thermal exposure	5-170
Figure 5-28 Evolution of maximum crushing strain in the pinned slab under uniform and non-uniform thermal exposure	5-171
Figure 5-29 Evolution of maximum reinforcement strains under uniform and non-uniform thermal exposure at (a) slab mid-span ($x = 1.275 - 4.725$) and (b) edges ($x = 0 - 1.275, 4.725 - 6$).....	5-172
Figure 6-1 Flow chart of proposed design procedure for the consideration of spalling effects for concrete structural performance in fire	6-187
Figure 6-2 Two span continuous beam reinforcement distribution	6-195
Figure 6-3 Beam cross section temperature profiles ($^{\circ}\text{C}$)	6-197
Figure 6-4. Effect of spalling characterisation for (a) Bottom reinforcement temperature and (b) effective cross section area upon exposure to the standard temperature time curve.....	6-198
Figure 6-5 Cross section sagging and hogging moment capacity for (a) No spalling and (b) Category B spalling under standard fire exposure.....	6-199
Figure 6-6 Moment Redistribution in a two span continuous beam exposed to a fire (a) Ambient conditions (b) plastic hinge development at beam mid spans (c) plastic hinge develops at support – failure mechanism	6-201
Figure 6-7 Reinforcement redistribution to improve spalling performance of a two span continuous reinforced concrete beam	6-203
Figure 6-8 Effect of redistribution of sagging reinforcement for the sagging moment capacity without spalling (Cat A) and with spalling (Cat B).....	6-203

Figure 6-9 Reinforced concrete slab geometry	6-204
Figure 6-10 Composite shell section for approximation of spalling affected slab cross-section.....	6-206
Figure 6-11 Spalled material properties under (a) compression (b) tension. Above 50 °C material properties assumed unchanging showing how material properties are modified to effectively remove the concrete.....	6-207
Figure 6-12 (a) Temperature (b) thermal strain and (c) normalised concrete strength profile after sixty minutes exposure for spalling affected slab	6-208
Figure 6-13 (a) Thermal profile after sixty minute standard fire exposure (b) Evolution of reinforcement temperature during exposure to the standard fire.	6-208
Figure 6-14 (a) Reinforcement strength (b) average concrete compressive strength through shell cross-section.....	6-209
Figure 6-15 Central slab deflection of a laterally restrained two way spanning slender concrete slab for the case of spalling and no spalling	6-210
Figure 6-16 Peak reinforcement strain (a) Slab edge (0-1.2 m) (b) slab mid-span (1.2 – 3m)	6-211
Figure 6-17 Design option 1 and alternative design options 2 & 3 slab cross section showing the exposure cover (d) for each reinforcement layer.....	6-212
Figure 6-18 (a) No spalling and (b) Spalling affected temperature evolution for each reinforcement layer	6-212
Figure 6-19 (a) no spalling (b) spalling affected normalised equivalent reinforcement area.	6-213
Figure 6-20 Slab central deflection (a) No spalling (b) Spalling.....	6-214
Figure 6-21 Peak reinforcement strains for design options 1, 2 and 3 at the slab edge and mid-span	6-216

Nomenclature

Roman

A	Area (m^2)
c_p	Specific heat at constant pressure (J/kg.K)
d	Depth; diameter (m)
E	Young's modulus (N/m^2)
f	Material strength (N/m^2)
f_p	Steel proportional limit stress (N/m^2)
f_y	Steel maximum stress limit (N/m^2)
G_F	Concrete fracture energy (Nmm/mm^2)
H	Height (m)
k	Conductivity (W/m.K)
L	Length (m)
M	Moment (kNm)
M_p	Plastic Moment (kNm)
O	Compartment opening factor ($\text{m}^{1/2}$)
Q_c	Rate of heat release (W)
r	Radial distance (m)
r_{load}	Load ratio
R_{cold}	Ambient load capacity (kNm or kN)
S_0	Concrete crack transfer length (m)
T	Temperature ($^{\circ}\text{C/K}$)
t	Time (s)
u	Velocity (m/s^2)
V	Thermal variation (%) (Chapter 3 & 5)

w Concrete crack opening (m)

x,y,z Regular co-ordinates

Greek

α Co-efficient of thermal expansion; exponential growth rate
(Equation 5-1)

β Neilson coefficient (Chapter 2)

Δ Change in

ε Strain

δ Displacement (m)

ρ Density (kg/m^3)

σ Stress (N/m^2)

Subscript

0 Ambient conditions (20°C)

ave Average

b Biaxial; burnout (in Equation 3-8)

c Compression

cr Creep

d Drying

el Elastic

$fire$ Fire conditions

g Gas phase

$LITS$ Load induced thermal strain

max Maximum

<i>pl</i>	Plastic
<i>T</i>	Temperature (°C)
<i>t</i>	Tension; time
<i>th</i>	Thermal
<i>ttc</i>	Transient thermal creep
<i>tot</i>	Total
<i>u</i>	Ultimate
<i>v</i>	Ventilation
<i>x,y,z</i>	Regular coordinates
σ	Stress related

1 Introduction

1.1 Motivation for research

Maintaining structural stability is an integral component of building fire safety. Stability must be ensured to provide adequate time for safe egress of the buildings occupants, fire fighting operations and property protection. Structural fire engineering endeavours to design structures to withstand the effects of fire in order to achieve these objectives.

In this thesis the fire behaviour of reinforced concrete structures is specifically investigated. The behaviour of reinforced concrete in fire is not as well understood as other construction materials, such as steel. This is in part due to the complexity of concrete material behaviour and also due to concrete's reputation of superior fire performance. Consequently there are substantially fewer analytical tools for the design of concrete structures at high temperatures. High performance concretes are enabling more slender forms of concrete construction; to be able to develop analytical tools to design these structures for fire we need to more fully understand their behaviour in fire.

A fundamental key to understanding structural fire performance is the relationship between the thermal environment induced by the fire and the structure. This research, therefore, investigates the influence of spatial and temporal variation of gas temperature upon concrete structural behaviour. The motivation for this research is explained in more detail in sections 1.1.1 to 1.1.4. Section 1.2 outlines the research objectives and section 1.3 describes in more detail the content of each chapter of the thesis.

1.1.1 Structural fire behaviour

The means of designing structures to withstand fire loading has evolved from standardised fire tests of single elements to simple strength calculations, to detailed structural calculations considering strength loss, thermal expansion and boundary influences. The latter approach is "performance based design" and allows a better quantification of the fire safety risk for a given structural design. This approach requires a much greater understanding of high temperature structural behaviour.

The need for a greater understanding of high temperature structural behaviour has been exemplified over the last decade by a series of high profile fires. In 1990 a fire at the Broadgate construction site indicated that steel-concrete composite structures possessed hitherto unacknowledged reserves of strength in fire {The Steel Construction Institute, 1991 #237}. Full scale fire testing of a partially protected composite concrete-steel frame structure at Cardington subsequently confirmed this {Bravery, 1993 #179; Bailey, 2000 #214; Usmani, 2001 #138}. The collapse of the World Trade Centre One, Two and Seven towers in 2001 {NIST, 2005 #240; NIST, 2008 #239; Usmani, 2006 #241} and partial collapse of the Windsor Tower in 2005 {Fletcher, 2009 #238} served to further demonstrate knowledge gaps in the understanding of structural behaviour at high temperatures.

These experiences have prompted research into the behaviour of structures at high temperature. This research has predominantly focused on the behaviour of steel and steel-concrete composite structures; the behaviour of *concrete structures* in fire has received considerably less consideration.

1.1.2 Concrete structural fire behaviour

The behaviour of concrete structures in fire has not been afforded the same interest as that of steel structures due to a perception that concrete has inherent fire resistance. This inherent fire resistance can in reality be attributed to concrete's insulating nature arising from low thermal conductivity and high specific heat.

Concrete's slow thermal response causes the strength of only a small proportion of the cross section to be affected by high temperature. The reduction in bending capacity is therefore governed by the temperature rise in the reinforcement. By adopting minimum cross-section sizes and reinforcement cover levels high periods of fire resistance are achievable for a concrete element. There are a large number of documented cases of fires in concrete buildings where the building has withstood the effects of fire and been fully reinstated {Concrete Society, 2008 #62}.

Loss of bending strength is however only one mechanism of failure in a concrete structure. Real fire events have induced a number of different collapse mechanisms in concrete structures. Thermal expansion effects are reported by Beitel {, 2002 #66} to have caused collapse or partial collapse of a number of concrete structures. In

Gretzenbach in 2004 the flat slab roof of an underground car park collapsed due to shear failure {BBC news, 2004 #228}. Concrete structures are also susceptible to spalling which can seriously compromise both structural stability and integrity {Ulm, 1999 #229}. Spalling is further described in section 1.1.4.

There are still gaps in our understanding of concrete's behaviour in fire despite its reputation for good fire performance. Concrete technology is also continually evolving; structures are increasingly slender, more highly stressed and have higher compressive strengths. A more robust understanding of concrete's behaviour in fire will not only enable predictions of the implications of changing concrete technology but also help to properly quantify the fire safety risk associated with concrete structures.

1.1.3 Realistic thermal definitions

The thermal environment created by a compartment fire is influenced by the fuel load and distribution, the compartment boundaries, compartment size and the ventilation conditions. These influences cause both temporal and spatial variations of temperature within the compartment.

Only a very small number of full scale fire tests have been conducted where the gas phase has been instrumented at a sufficient resolution to capture the nature of this thermal variation. They include the Cardington NFSC3 {Bravery, 1993 #179} and Dalmarnock fire test series {Rein, 2007 #174}. The compartment sizes were relatively small, 144m² and 20m² respectively, compared with modern open office compartments. Despite this in both test series significant thermal variations were recorded for the duration of burning {Stern-Gottfried, 2010 #227}.

There are no experimental data available for large compartment fires; evidence from real fire events such as World Trade Centre 7 has suggested that variation will be greater as burning progresses through the compartment rather than becoming fully involved at any one time.

In current structural fire design the thermal exposure is typically characterised by a single temperature versus time curve. This characterisation is a significant assumption concerning the thermal exposure for the structure. The effect of thermal

variation upon concrete structural behaviour has, however, not been fully investigated to justify this assumption.

1.1.4 Consequences of spalling

Spalling involves the loss of concrete cross section during fire exposure; it therefore undermines concrete's insulating behaviour by exposing the reinforcement and increasing heat transfer through the section with potentially serious consequences for concrete structural stability.

Concern for the effect of spalling upon concrete structural performance has resulted in a significant research effort to understand and model the complex mechanisms responsible for spalling. There has been significantly less research focusing on the actual implications of spalling for concrete structural performance.

Understanding these implications will help to quantify the risk spalling can pose for a given structure and fire exposure. Identifying weaknesses and vulnerabilities of structural stability due to spalling can inform mitigating measures. The research in this thesis focuses on the implications of spalling rather than the mechanisms responsible for it.

1.2 Research objectives

The overarching aim of this research is to further our fundamental understanding of the behaviour and performance of reinforced concrete structures in fire. The research objectives are broadly summarised as follows:

- Investigate reinforced concrete structural behaviour at high temperatures using finite element software ABAQUS
- Establish the influence of non-uniform thermal environments or realistic fire conditions upon reinforced concrete structural behaviour
- Identify the implications of spalling for the mechanisms of reinforced concrete structural stability

The following more specific goals and the chapter outline in section 1.3 set out more specifically how this research proposes to achieve the above objectives:

- Comprehensive review of reinforced concrete material modelling and finite element modelling to establish the capabilities of a numerical investigation
- Formulate non-uniform thermal definitions for use in establishing the relationship between compartment fire thermal variation and concrete structural performance
- Assess the validity of the single temperature compartment fire assumption
- Develop a methodology which considers the effect of spalling in a structural analysis without modelling the mechanisms of spalling

1.3 Chapter outline

1.3.1 Chapter 2

Models of material behaviour underpin the validity of any structural analysis. Reinforced concrete as an inhomogeneous material exhibits complex material behaviour at high temperatures. The capabilities of reinforced concrete material modelling are established through discussion of the material behaviour and review of the available material models.

1.3.2 Chapter 3

The thermal environment created by a fire is discussed by reviewing fundamental compartment dynamics and full-scale fire test temperature data; the uniform temperature assumptions of structural design fires are then discussed. This discussion is used to formulate non-uniform thermal exposures for the investigation of structural implications.

The role of thermal expansion in explaining the high temperature behaviour of concrete structures is demonstrated using simple finite element analyses; the influence of non-uniform thermal distributions for concrete thermal expansion behaviour is established.

1.3.3 Chapter 4

A two-way spanning reinforced concrete slab is chosen as a benchmark structural model. Two-way spanning slabs have been studied previously under uniform thermal

conditions they therefore provide an ideal benchmark against which to investigate the implications of non-uniform thermal environments.

A finite element model is developed to analyse the slab behaviour under a range of boundary conditions. The behaviour of the slab is analysed under uniform thermal conditions to verify behaviour and develop performance indicators for investigating the influence of non-uniform thermal exposure.

The sensitivity of model predictions to material assumptions is presented and the influence of geometric parameters, aspect ratio and slenderness ratio are investigated.

1.3.4 Chapter 5

Using the benchmark finite element model the behaviour of the slab under non-uniform thermal exposure is analysed. The findings of the investigation of non-uniform thermal exposure effects upon thermal expansion behaviour in chapter 3 are used to interpret behaviour.

1.3.5 Chapter 6

The consequences of spalling for reinforced concrete structural performance are investigated. To achieve this, a methodology for the implementation of spalling effects in a structural analysis is developed. The methodology is demonstrated in the analytical analysis of a two-span continuous reinforced concrete beam and a finite element analysis of a restrained two-way spanning reinforced concrete slab.

1.3.6 Chapter 7

The research conducted is reviewed and the key conclusions identified. Any further investigation that has been highlighted by the research is recommended.

2 Reinforced Concrete – Material Behaviour

Numerical tools are heavily dependent upon the material definitions provided as an input; therefore in order to assess the adequacy of numerical methods to capture the behaviour of reinforced concrete structures at elevated temperatures a thorough investigation of the material models available to characterise concrete behaviour at elevated temperatures is also required. In this Chapter understanding of the material behaviour of concrete at ambient and elevated temperatures is summarised followed by an examination of the material models currently available to characterise such thermal and mechanical behaviour. The behaviour and material models for steel, concrete and concrete-steel interaction are discussed separately.

2.1 Thermal behaviour

The first step in an analysis of a structure exposed to a pre defined fire is to predict the thermal distribution in the structural section. The thermal properties required for conducting a heat transfer analysis for concrete and steel are described.

2.1.1 Steel thermal properties

The heating of reinforcement steel in a fire is dominated by conduction of heat from the exposed concrete provided the concrete cover is not removed through spalling or cracking. The prediction of heat transfer in reinforcing steel is therefore a relatively straight forward process requiring only the density, specific heat and conductivity to be defined. Steel's highly isotropic nature has meant that these properties have been well defined

Density

The densities of all steels (regardless of strength or application) remain unaffected by elevated temperatures. The density of steel is taken to be 7850 kg/m^3 as recommended by Eurocode 3 {, 2005 #117}.

Specific heat

For steel there is little variability in the specific heat between different steel strengths or applications. Its magnitude increases at elevated temperatures with a large spike around 730°C relating to a metallurgical change {Buchanan, 2001 #54}. The

expressions in Eurocode 3 {, 2005 #117} and Eurocode 4 {, 2005 #118} provide details of the specific heat of steel for the range 20-1200°C and this is plotted in Figure 2-1

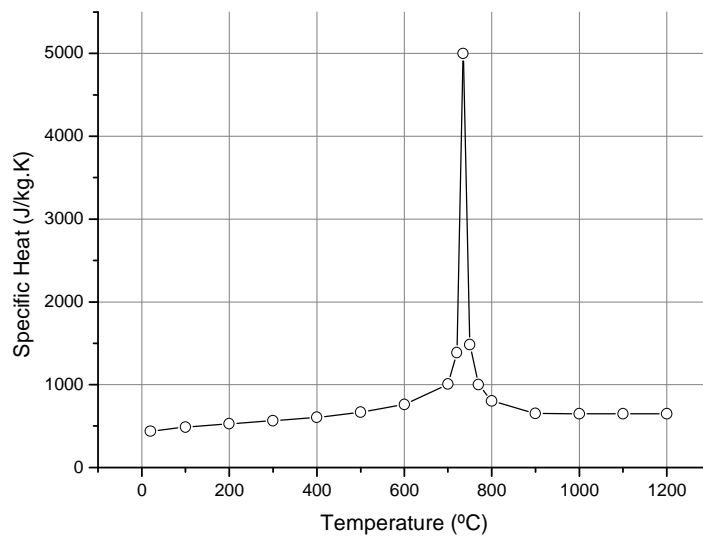


Figure 2-1 Specific Heat of steel as specified by EC3

Thermal conductivity

The thermal conductivity of steel decreases at elevated temperatures and some dependence on steel composition has been identified {Malhotra, 1982 #84}. Eurocode 3 {, 2005 #117} and Eurocode 4 {, 2005 #118} provide values for the thermal conductivity of steel in the range of 20°C -1200°C, these are plotted in Figure 2-2.

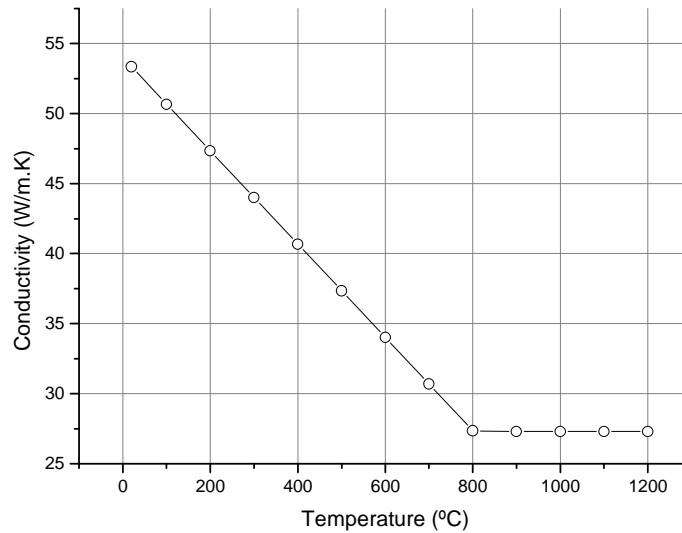


Figure 2-2 Eurocode 3 {, 2005 #117} defined thermal conductivity of steel at elevated temperatures

2.1.2 Concrete thermal properties

The process of heat transfer in concrete is more complicated than in steel. Concrete is a heterogeneous material with a porous structure containing free water. The process of heat transfer in concrete is therefore inextricably linked with the mass transport of this free water. Predicting the temperature evolution in concrete in detail therefore uses a system of coupled partial differential equations governing the heat and moisture transfer in porous media. Such models require the true rather than apparent thermal properties of concrete. These properties are very difficult to measure due to other effects occurring during heating such as changes to chemical composition, changes to physical structure and absorption of latent heats. The above changes are additionally influenced by the rate of heating thus the thermal properties of concrete are also a function of heating rate and history. Experimentally derived properties therefore represent apparent values {Bažant, 1996 #22}. Large amounts of experimental scatter have been witnessed as a result of this and true thermal properties typically need to be derived using a combination of experimental and theoretical considerations.

Apparent material properties are not without their use; such properties may be used to conduct decoupled heat transfer analyses where the heat flux is considered independent of the moisture flux. The effects of significant processes such as the evaporation of free water upon the heat transfer are mimicked through the use an

apparent or effective specific heat which includes a spike at temperatures of 100°C - 115°C.

Consideration of the complete heat and mass transport process is capable of yielding highly accurate results; however, it is completely dependent upon the quality of the material input, which is difficult to predict. For structural design purposes this level of detail concerning the concrete properties will not be known. Purkiss {, 2007 #86} compared the predictions of decoupled and coupled heat transfer analyses with experimental results and found both to provide reasonably accurate results. Similarly Lamont {, 2001 #136} achieved good agreement with experimental results using a decoupled thermal analysis. Thus it is possible to simplify our approach to heat transfer in concrete by assuming heat flux is independent of the moisture flux when apparent thermal properties are employed.

Density

The type of aggregate used will primarily dictate the density of the concrete. The density of the aggregate does not change significantly upon heating. The density of the concrete does change however because when heated to above 100°C free water within the concrete pores is driven off (often condensing and ponding on the unheated surface of slabs). This loss of free water leads to a reduction in the concrete's density. Eurocode 2 {, 2004 #27} provides an estimate of the reduction in density starting at 115 °C. The values supplied are valid in the range of 20 °C – 1200°C and are plotted in Figure 2-3.

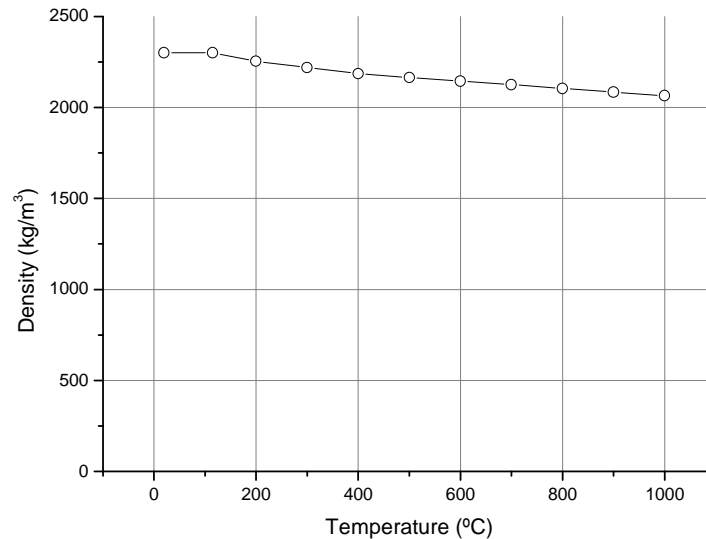


Figure 2-3 Density reduction for normal weight concrete at elevated temperatures according to Eurocode 2 {, 2004 #27}

Specific heat

The variation of concrete specific heat with temperature is very dependent on the type of aggregate used and the mix proportions. Malhotra {, 1982 #84} showed a large scatter in values for concretes of different aggregates reproduced here in Figure 2-4.

Despite the scatter in values Eurocode 2 provides values of specific heat applied to all normal weight concretes (all aggregate types). The spike in magnitude of the specific heat between 100°C and 115 °C is only introduced if one is unable to model explicitly the effects of moisture migration on heat transfer in the concrete cross section. Several peaks are provided depending on the moisture content. Eurocode 2 provides peaks for up to 3 % by weight moisture content and Eurocode 4 provides peaks between 3 and 10% moisture content by weight. This spike in specific heat is intended to simulate the latent heat of vaporisation of the free pore water.

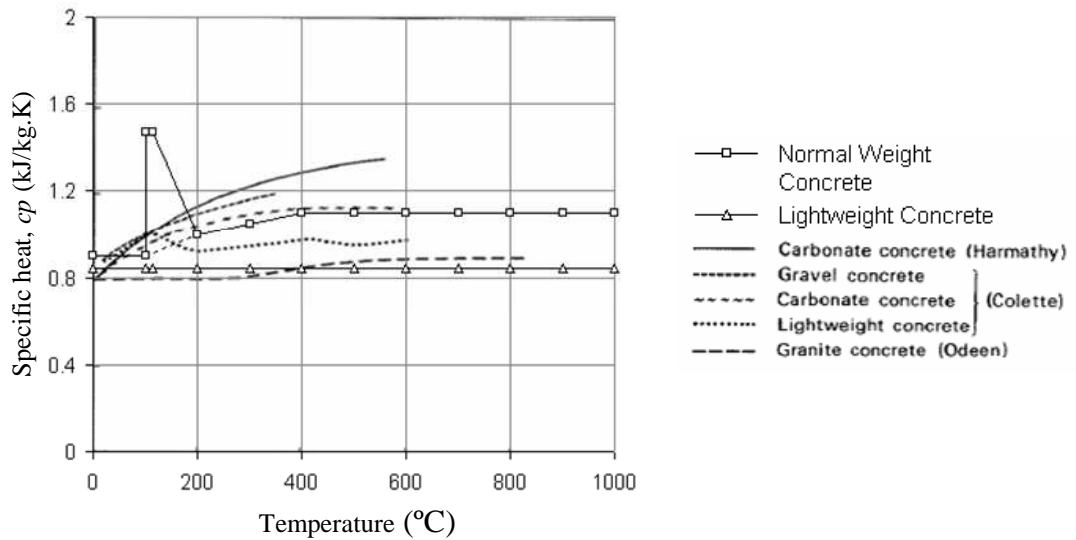


Figure 2-4 Experimental and Eurocode 2 temperature dependent specific heat values for concrete {Malhotra, 1982 #84}

Thermal conductivity

The type of aggregate used will influence the ambient magnitude of thermal conductivity. However, for all types of aggregate it has been found that thermal conductivity decreases at elevated temperatures. Eurocode 2 and 4 provide an upper and lower limit for thermal conductivity of normal weight concretes (again relating to all aggregate types). The upper bound is recommended for use in the analysis of concrete as part of a steel concrete composite system. The lower bound is recommended for use in the analysis of reinforced concrete structures; both expressions are plotted in Figure 2-5.

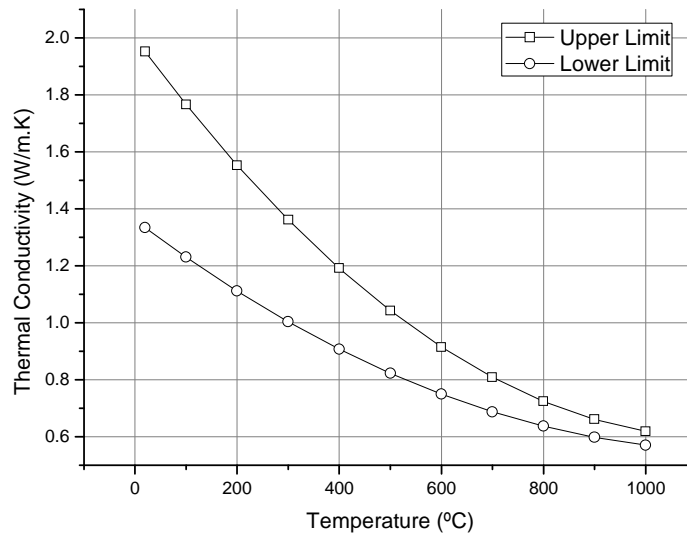


Figure 2-5 Upper and lower thermal conductivity limits for normal weight concrete: Eurocode 2 {, 2004 #27}

2.1.3 Summary

The thermal properties of steel are well defined, with little variation existing between types and applications of steel. When required the thermal properties provided in Eurocode 2 and 3 will be used for modelling heat transfer in steel.

The thermal behaviour of concrete contrasts significantly with that of steel having a significantly lower thermal diffusivity. The thermal behaviour of concrete is significantly dependent upon the type of aggregate used. Aggregates are typically locally sourced, therefore use of generic values is difficult to justify. One would assume that it would be conservative to choose those properties resulting in a more rapid transmission of heat, however, as will be shown, steeper thermal gradients may result in a more onerous condition for the structure in terms of spalling and deflections. It will therefore be necessary to conduct parametric studies to assess the structural sensitivity to the change in thermal distribution caused by possible variations in these properties.

Concrete's 'apparent' thermal properties (those measured experimentally) can be used to provide accurate descriptions of the thermal distributions arising in concrete exposed to fire when used as part of a decoupled heat transfer analysis.

2.2 Mechanical behaviour

The currently available material models proposed to characterise the mechanical behaviour of steel, concrete and steel-concrete interaction at elevated temperatures are reviewed in this section. Their ability to capture those aspects deemed important for predicting the behaviour of reinforced concrete structures in fire is assessed

2.2.1 Steel mechanical properties

The strength of steel is typically established through tensile testing and the compressive strength assumed to be the same. Reinforcing steel is predominantly under tensile loading, although compressive loading may occur in hogging regions of continuous structures and through restrained expansion when exposed to fire; typically though, the tensile behaviour dominates an analysis.

Tensile strength

The mechanical behaviour of steel at elevated temperatures can vary depending on the method of its production, i.e. hot rolled, cold worked, pre-stressing steel etc. The behaviour of structural steel is very similar to that of hot rolled reinforcing steels. Cold working of steel to produce reinforcement has the added benefit of increasing material strength. At elevated temperatures the proportional reduction in strength for hot rolled and cold worked steel is not dramatically different. However, the significantly higher initial strength of cold worked steels will lead to much larger absolute strength losses. Hot rolled steel is most commonly used in the UK with the exception of welded mesh fabric, which is often used in composite slabs. Due to its more common usage the reinforcement in this thesis will be assumed to be hot rolled.

Harmathy {, 1993 #15} collated published yield strengths of hot rolled steel at elevated temperatures and found a large amount of scatter in the data. Similarly Buchanan {, 2001 #54} compared the reduction functions provided in different codes of guidance and found them to be quite different. A commonly cited reason for the apparent scatter is variation in the definition of the steel yield strength. Figure 2-6 shows a schematic of a typical hot rolled steel stress-strain curve at 20°C and 400°C. It is apparent from this figure that at ambient temperature the yield point is clearly inferred, yet the yield point at elevated temperatures is less clear. Rather than providing the reduction function for yield strength Eurocode 2 {, 2004 #27}

therefore provides reduction functions for the proportional limit stress and maximum stress level which Hertz {, 2004 #131} has described as the 0.2% and 2.0% proof strengths respectively. Proof strength is illustrated in Figure 2-6.

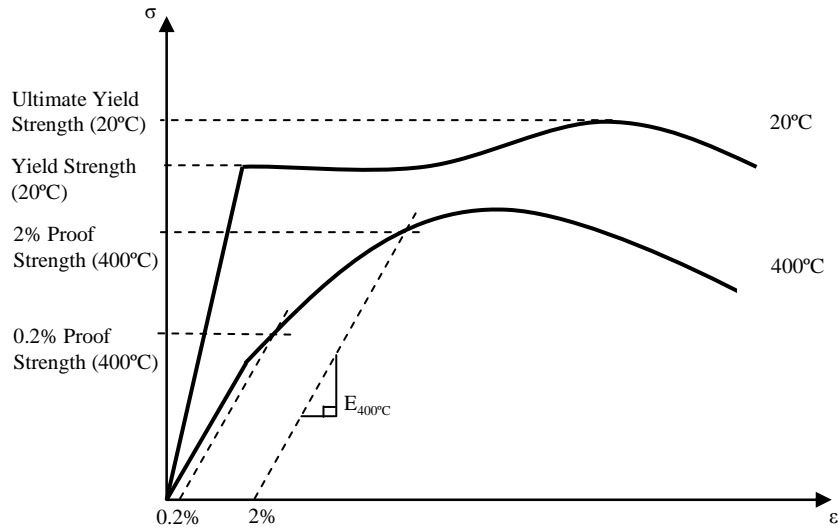


Figure 2-6 Typical elevated temperature steel stress-strain curves indicated yield strength and proof strength

The reduction functions are plotted in Figure 2-7 and may be used to define the shape of a constitutive curve for a numerical analysis.

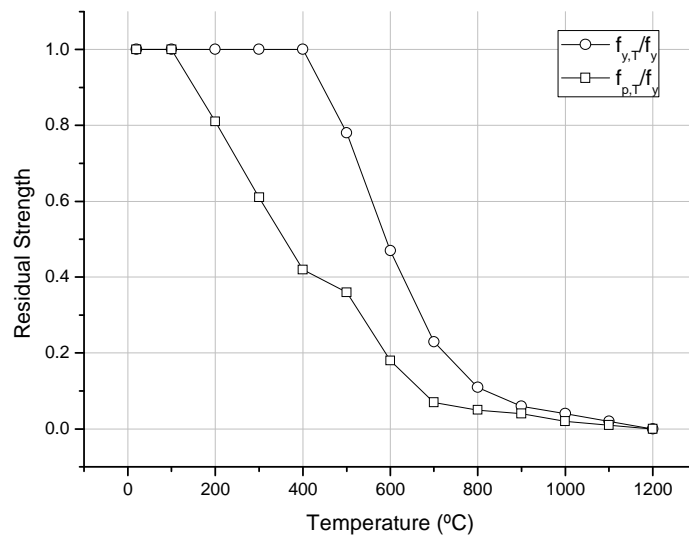


Figure 2-7 Residual proportional limit stress and maximum stress for hot rolled steel according to Eurocode 2 {, 2004 #27}

Modulus of elasticity

Steel stiffness reduces at increasing temperatures; this is evident from the schematic of the strength deformation behaviour in Figure 2-6. Eurocode 2 provides the reduction function plotted in figure 2-8.

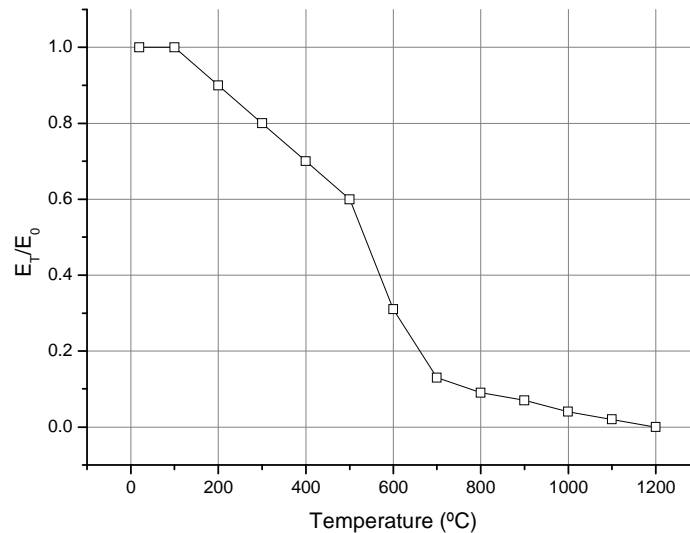


Figure 2-8 Young's modulus reduction factors at elevated temperatures according to Eurocode2 {, 2004 #27}

2.2.2 Modelling steel behaviour

The typical stress-strain behaviour found experimentally for typical hot rolled reinforcement at ambient and elevated temperatures is shown in Figure 2-6. Hot rolled steel experiences initially a degree of strain hardening at increased temperatures of up to 400°C. Beyond this the maximum stress decreases substantially. For design purposes hot rolled steel is treated as an ideal elastic plastic material. This section describes a uniaxial constitutive model for steel at elevated temperatures proposed by Anderberg {, 1986 #64} which has been widely adopted in both the literature and design.

Components of strain

The stress related strain described in section 2.2.1 is just one component of the strain behaviour of steel at elevated temperatures. The total strain exhibited by steel at elevated temperatures is generally taken to be composed of the three terms, as shown in Equation 2-1.

$$\varepsilon_{tot} = \varepsilon_{\sigma} + \varepsilon_{th} + \varepsilon_{cr}$$

Equation 2-1

Where ε_{σ} Instantaneous stress related strain

ε_{th} Free thermal strain

ε_{cr} Creep strain or time dependent strain

Instantaneous stress related strain (ε_{σ})

The strength deformation properties of steel are obtained by stress or strain rate controlled testing of thermally stabilised specimens. The rate of testing must be sufficiently high to isolate the stress related strains from creep strains which become significant for ordinary steels above 400°C {Anderberg, 1986 #64}. An analytical approximation of the experimental curves to describe uniaxial behaviour was proposed by Anderberg {, 1986 #64}. Eurocode 2 provides a similar constitutive curve defining the necessary parameters for hot rolled reinforcing steel.

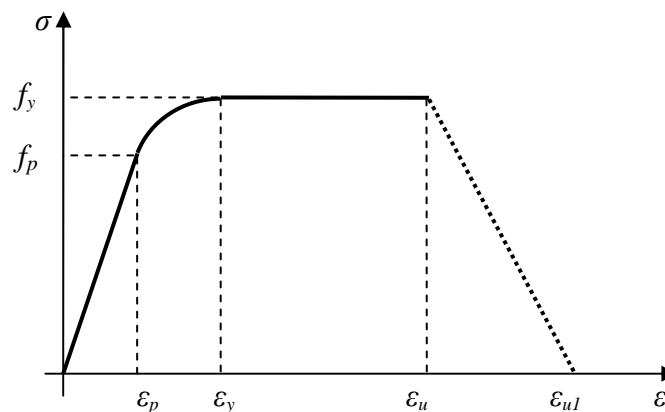


Figure 2-9 Uniaxial stress strain model for steel at elevated temperatures

The stress-strain behaviour is approximated by initially a linear elastic stage to the proportional limit, f_p , this is followed by an elliptical branch to the maximum stress level, f_y as shown in Figure 2-9. The material is assumed to be perfectly plastic beyond this point. A descending branch is included after strains of 15% are reached. The slope of the descending branch does not represent material behaviour; rather it provides a numerical method to reduce stress values. The rupture strain is assumed to remain constant at elevated temperatures. This contradicts research which indicates

that the rupture strain will increase as the ductility of steel increases {Cashell, 2010 #232}. There is, however, very limited information concerning the rupture strain of reinforcing steels at elevated temperatures.

Free thermal strain (ϵ_{th})

The free thermal strain of steel has been found to be relatively independent of the type or strength of steel. Anderberg {, 1986 #64} quotes the results of four studies of different steels which produced very similar results for free thermal strains. Eurocode 2 provides free thermal strain curve for reinforcing steels; this is presented in Figure 2-10.

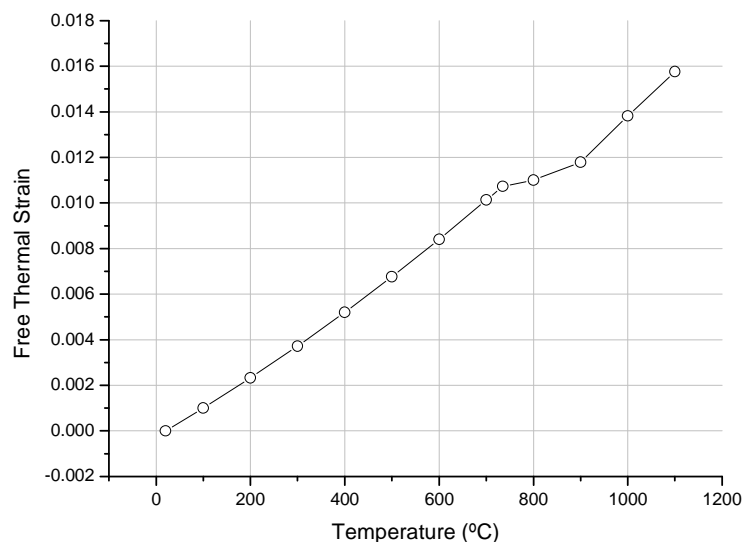


Figure 2-10 Total thermal elongation of reinforcing steel {, 2004 #27}

Creep strain (ϵ_{cr})

Creep strains are regarded as being relatively insignificant below 400°C for ordinary steels. It is often assumed that design instantaneous stress-strain curves implicitly allow for the creep strains which develop at elevated temperatures {Purkiss, 2007 #86}. During testing to establish the high temperature stress-strain curves creep strains will inevitably develop also. No correction is made for this and so it is assumed that creep is implicitly accounted for the measured stress-strain response. The rate of heating has a significant influence upon the development of creep strains; therefore, by assuming implicit consideration of creep strain in an analysis one is also assuming the rate of heating in the analysis and the original material test are the

same. However, these curves have primarily been formulated with steel structures in mind rather than steel reinforcement {Buchanan, 2001 #54}. Steel reinforcement is heavily insulated by the surrounding concrete resulting in a much slower rate of temperature rise than an exposed steel member, thereby making it possible to underestimate the creep strains which develop. The author is unaware of any research concerning the validity of assuming creep is implicitly accounted for or the possible effect of ordinary reinforcement creep for the performance of reinforced concrete in fire.

Multi-axial steel behaviour

The action of reinforcement in concrete is predominantly uniaxial. It is true that for ribbed reinforcement, the deformed profile introduces multi-axial interaction with the concrete. The scale at which this occurs would require modelling in far more detail than typically adopted or feasible in a structural analysis. Considering the action of steel reinforcement to be purely uniaxial is an acceptable approximation when the goal is determining overall structural behaviour.

2.2.3 Steel summary

Anderberg's {, 1986 #64} curvilinear constitutive model for steel provides a good approximation of the uniaxial deformation behaviour of steel for both ambient and elevated temperatures. Current inputs provided in Eurocode 2 do not specify an increase in rupture strain at elevated temperature; however, this is due to limited experimental data rather than a limitation of the model. The slope of the descending is not representative of reality but provides a means of introducing reinforcement rupture smoothly into a numerical analysis.

The treatment of creep strains remains simplistic. The assumption that they are implicitly measured in stress-strain experiments ignores the dependence of creep strain upon the heating rate which is substantially slower for insulated steel than the exposed steel which forms the basis of the high temperature steel data provided. The influence of creep strain for structural performance in fire is not considered

2.2.4 Concrete mechanical behaviour

In this section the mechanical behaviour of concrete at ambient and elevated temperatures is described. The material models devised to characterise this behaviour are described in section 2.2.5.

Concrete is a composite of cement paste and aggregate. The strengths of concrete under tension and compression are significantly different. Under tension, the strength is determined by the tensile strengths of the cement paste, the bond of the cement paste to the aggregate, and the aggregate. Under compression, dilation occurs transverse to the direction of loading (due to Poisson effects), and it is these transverse tensile stresses that govern the strength of the concrete. The compressive load confines the concrete so that the net compressive strength of a specimen is only reached once the tensile cracks have joined to form a compressive failure surface, across which aggregate interlock frictional mechanisms act. Concrete is thus much stronger in compression than in tension, but its compressive strength is a function of its tensile strength {Kotsovos, 1995 #82}. In this section the ambient temperature strength of concrete under compressive and tensile loading is explained in terms of the interactions of concrete's component parts (aggregate and cement paste). The effect of heating upon each of these components and the compatibility of their behaviour at high temperatures is summarised to explain changes to concrete strength at elevated temperatures.

Tensile behaviour of concrete

In ambient sectional design the tensile strength of concrete is often ignored; this is recommended by codified design (Eurocode 2) as a conservative assumption. When one is considering only the ultimate strength of a single cross section it is true that this simplification is conservative. In redundant structures, it is also reasonable to assume zero tensile strength at ambient temperatures, as stress redistribution can occur provided that there is sufficient ductility elsewhere within the reinforced concrete sections.

Under fire conditions, however, it is often the interaction between structural elements that dominates failure rather than the performance of individual structural elements alone, due to the interplay of restraint conditions and thermal expansion. Large

deformation mechanisms often occur under fire conditions, requiring a high degree of deformation capacity in the reinforcing steel and concrete. Consequently, it is not clear that neglecting the tensile strength of the concrete will always be conservative under fire conditions. In this investigation the tensile strength of concrete will be included so as to gain a more accurate insight into the behaviour of concrete structures in fire.

The tensile strength of concrete is strongly influenced by the size and surface texture of the aggregate and the environmental conditions for the curing and drying process. The tensile strength of concrete is more variable than its compressive strength, because it depends directly upon tensile failure between the components of the concrete {CEB-FIP, 1990 #158}. Due to the large number of influencing parameters the best method for establishing tensile strength is through direct tensile testing. This, however, is rarely feasible in the design process therefore the CEB-FIP Model Code {, 1990 #158} provides correlations between tensile strength and the compressive characteristic strength which is specified by the designer; these are plotted in Figure 2-11.

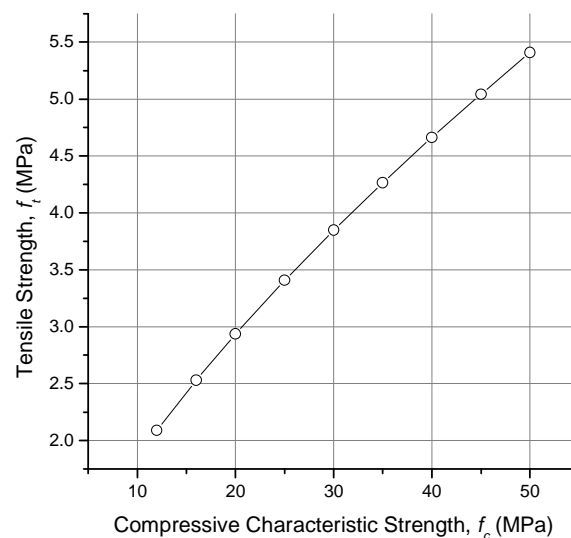


Figure 2-11 Tensile Strength estimates related to compressive strength in EC2 {, 2004 #169} and CEB-FIB Model Code {, 1990 #158}

The post-peak tensile behaviour is dominated by cracking. Figure 2-12 summarises the typical-stress displacement response of plain concrete under uniaxial tension and explains the mechanisms behind this brittle behaviour.

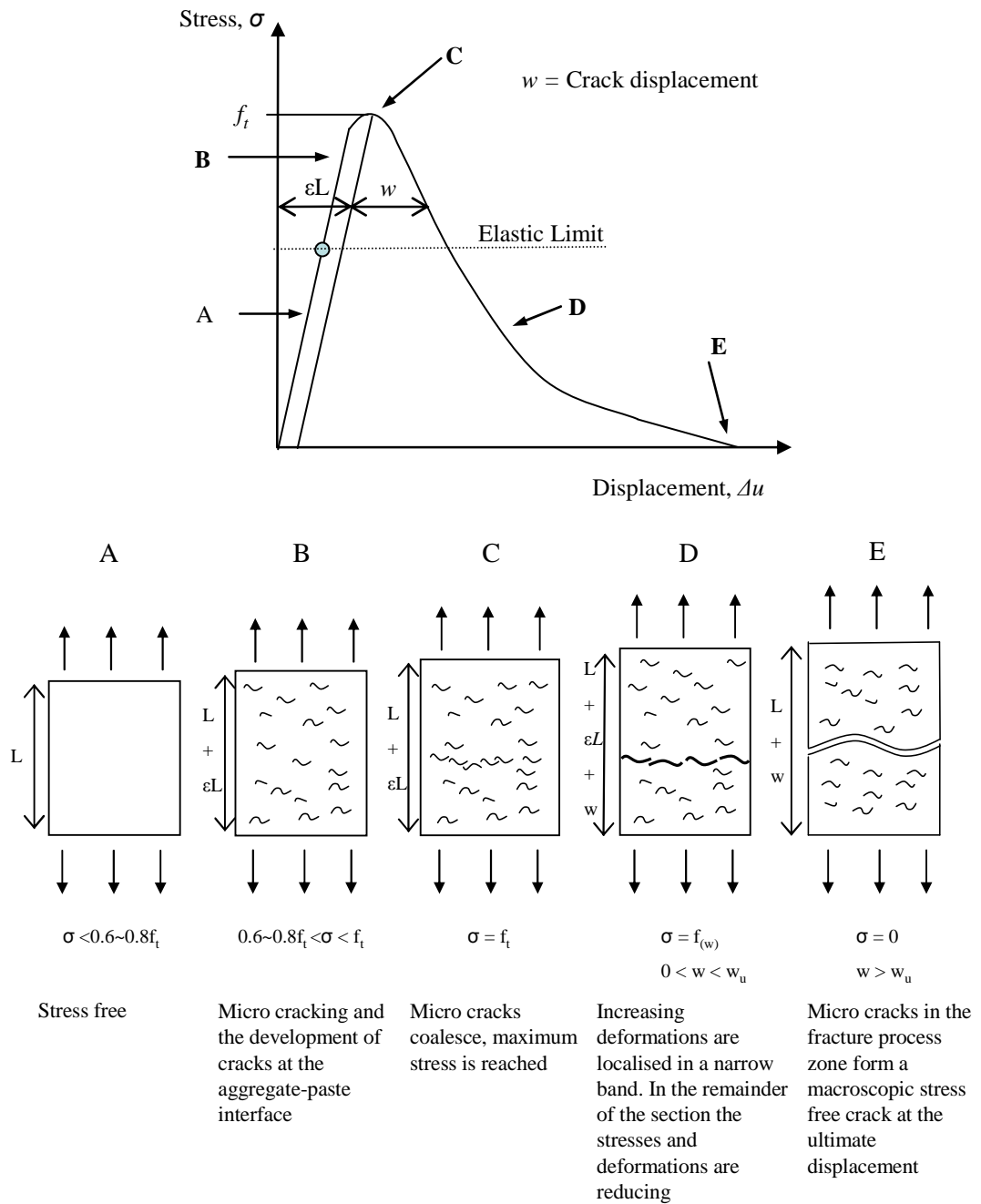


Figure 2-12 Schematic of the stress-displacement relation for a concrete tensile test

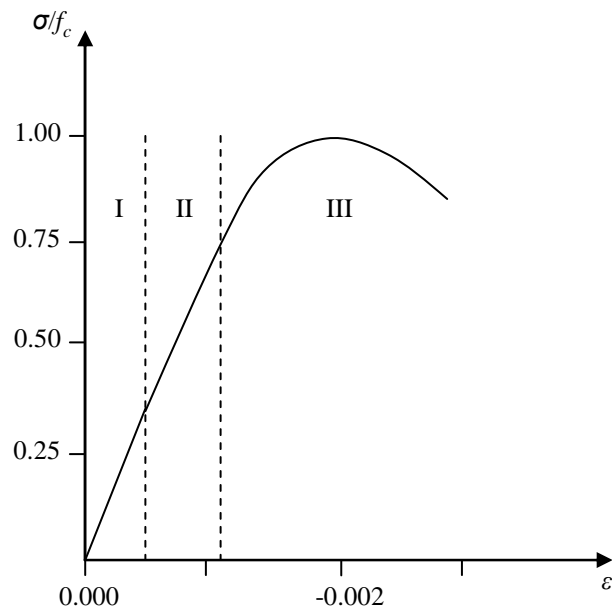
The limit of elastic behaviour for concrete under tension is reached at about 60-80% of the ultimate tensile strength {Chen, 1988 #159}. Beyond the elastic limit bond cracks at the aggregate interface begin to grow resulting in non-linear stress-deformation behaviour (Figure 2-12 $\sigma < f_t$). These bond cracks begin to coalesce towards the peak strength. This period of stable crack propagation is significantly

shorter under tension than it is under compression, in part due to the lack of confined frictional behaviour, resulting in concrete's brittle tensile nature.

Beyond the peak strength, deformations are localised in a narrow band known as the fracture process zone. Outside the fracture process zone, the stress and deformation decrease, so that they remain in equilibrium with the crack band. This gradual unloading of stress at increasing deformation (Figure 2-12 post-peak) is commonly referred to as 'tension softening' {Rots, 1984 #52}. Finally at a critical displacement the micro cracks in the fracture process zone form a stress free macroscopic crack separating the specimen into two parts.

Compressive behaviour of concrete

The non-linear strength-deformation behaviour of concrete under compression is caused by micro-cracking in the cement paste and the cement paste – aggregate interface. The compressive strength of concrete is defined as the peak stress in a stress-strain curve. Beyond peak stress the micro-cracks coalesce and the onset of macro-cracking occurs. The post-peak response is difficult to measure due to the localised nature of cracking. Van Mier {, 1986 #112} has shown the uniaxial post-peak response to be independent of specimen size when considered as a stress-displacement relationship similar to that described for tension. This approach has not yet been fully accepted (as demonstrated by available constitutive models described later) due to more complicated patterns of localisation under compression than occur in tension. Figure 2-13 summarises the behaviour under increasing compressive deformation. The compressive post-peak behaviour of concrete is less likely to affect the structural response than that of the tensile post-peak behaviour due to concrete's significantly weaker strength in tension. However in a structural analysis which aims to predict behaviour while the material is close to failure a more accurate definition of the compressive post-peak behaviour should be employed.



Phase	Stress Range	Concrete Behaviour
I	0 - 30%	Micro-cracks at aggregate-cement interface (bond cracks) remain unaffected – behaviour is linear elastic
II	30 - 75%	Bond cracks increase in length, width and number. Later some coalescing of nearby bond cracks. Material behaviour is non-linear, crack propagation remains stable
II	75% -	Beyond this stress level cracks through the cement coalesce with bond cracks forming crack zones. Cracking at this stage is unstable and leads to the progressive failure of the concrete

Figure 2-13 Typical concrete uniaxial compressive stress strain curve

High temperature behaviour of concrete

In a similar manner to the ambient behaviour of concrete, the high temperature behaviour of concrete is dictated by the heating characteristics of its components and by the compatibility of those components. The high temperature characteristics of the cement paste and aggregate are therefore looked at separately before discussion of the high temperature mechanical properties of concrete.

Cement paste

The cement paste refers to the hydrated cement at any part of the hydration process. About 70% of the paste is calcium silicate hydroxide (C-S-H gel) another 20% is calcium hydroxide. After exposure to temperatures of about 105°C for a sufficient length of time all evaporable water has been expelled from unsealed concrete, with only chemically bound water remaining {Bazant, 1996 #22}. Above 105°C the dehydration reactions begin and the C-S-H gel begins to decompose. As temperature increases the average pore size and specific internal pore surface area increases; Bažant and Kaplan {, 1996 #22} have attributed this increase to the progressive breakdown of the C-S-H gel structure during dehydration. At about 500°C around 70% of the C-S-H gel has decomposed; at 850°C it has been completely dehydrated causing shrinkage of the cement paste {Arioz, 2007 #21}. Between 400°C and 600°C the calcium hydroxide dehydrates, peaking at 500°C. This process produces water vapour and calcium oxide and contributes to the shrinkage of the cement paste. Upon cooling and exposure to moisture the calcium oxide re-hydrates, a process that is expansive and damaging to the residual strength of the concrete.

Aggregate

Aggregate makes up about 55-75% of the concrete mix {Khoury, 2000 #14}. Aggregates used in concrete fall largely into two groups;

- Calcareous: containing limestone, dolomite and anorthosites.
- Siliceous: containing quartzite, gravel, granite and flint.

The thermal expansion coefficients vary for each aggregate and indeed some aggregates experience anisotropic thermal expansion. Most aggregates used in concrete are virtually stable up to about 500°C {Harmathy, 1973 #28} and non-siliceous type aggregates are unlikely to undergo changes below 600°C. Siliceous aggregates, however, contain quartz which undergoes a number of transformations upon heating. The best known and applicable to the field of fire resistance of structural concrete is the transformation from α -quartz to β -quartz. This process is expansive and destructive to the concrete structure occurring at around 575°C. Calcareous aggregates decarbonate between 600°C and 900°C producing a

considerable amount of carbon dioxide gas {Arioz, 2007 #21}. This reaction is endothermic with significant heats of decomposition; however, the temperature intervals at which this occurs are too high to be of any real benefit to the concrete performance {Harmathy, 1993 #15}. Eurocode 2 provides different relations for thermal strain of concretes formed from siliceous and calcareous aggregates.

Concrete

In discussing the ambient behaviour of concrete, it was established that the development of micro-cracks at the cement paste – aggregate interface is responsible for influencing the material strength. At elevated temperatures this is exacerbated by the thermal incompatibility of the cement paste and the aggregate. From about 300°C the shrinkage of the cement paste and the expansion of the aggregate cause differential strains and internal stresses promoting increased cracking in the concrete micro structure {Hertz, 2005 #24}. At 550-600°C Khoury {, 2000 #14} discovered a marked increase in the basic creep of Portland cements and concrete. This corresponds to the dehydration of the cement paste and therefore represents a critical temperature above which concrete is considered no longer structurally useful. The wide variation in aggregate thermal expansion behaviour contributes to the significant variation seen in the strengths of different concrete's at elevated temperatures.

Given the difficulty in predicting the formation and propagation of the micro-cracks, which are so important to concrete behaviour, much experimental research has been undertaken to try to quantify the behaviour of heated concrete. Harmathy {, 1993 #15} summarised the broad conclusions drawn from a large body of testing:

- The fractional loss of strength is independent of the ambient temperature strength, therefore the cement-type and water-cement ratio does not play a significant role in strength loss at elevated temperatures.
- The aggregate-paste ratio has a significant effect on the loss of compressive strength. For rich mix concretes, relative strength losses are much higher than for lean mix.

- The highest fractional loss of compressive strength for normal weight concretes was with silicate aggregates.
- The residual strengths of unstressed specimens were lower than those which were tested stressed. It is possible that the load induced compression prevents the formation of micro-cracks.

In summary, the type of aggregate, aggregate-paste ratio and the presence of pre-stress are the most important parameters for determining the loss of strength at elevated temperatures. In Eurocode 2 only the first of these parameters is considered to have an effect upon the residual strength of concrete at elevated temperatures. Correlations are provided for siliceous aggregate and calcareous aggregate concretes which are plotted in Figure 2-14. Neither the aggregate-paste ratio nor the level of pre-stress is considered. Khoury {, 2000 #14} has suggested that the provision of ‘typical’ strength behaviour for all normal weight concretes in this manner is misleading unless specific information on mix design and environmental conditions are defined.

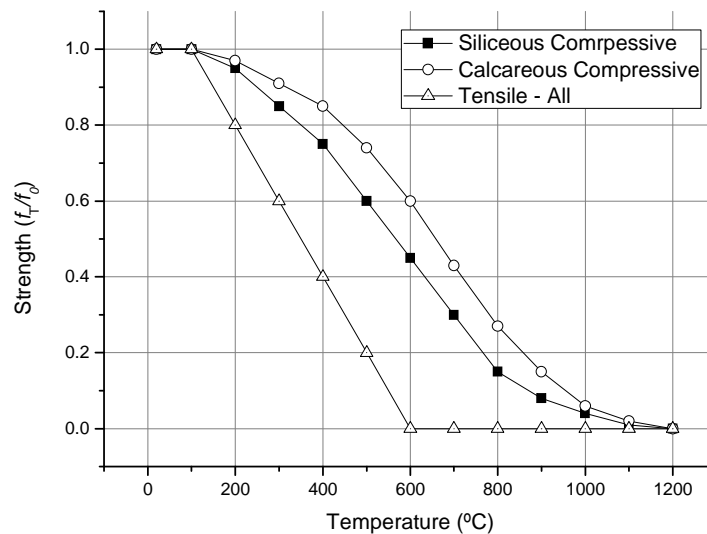


Figure 2-14 Eurocode 2 Part 1-2 recommended reduction factors for concrete compressive and tensile strength

From Figure 2-14 the tensile strength reduces more rapidly at increasing temperatures than the compressive strength, perhaps due to the tensile strength’s direct reliance on the aggregate – cement paste bond compared to the compressive strength, which also depends on the degree of frictional aggregate interlock.

Multi-axial concrete strength

The consideration of concrete structures for finite element analysis is generally required to be 2 or 3 dimensional. One dimensional idealisations and uniaxial material descriptions often applied to steel structures will fail to capture the significance that seemingly negligibly small stresses orthogonal to the principle stress direction have for concrete structural performance. Therefore 2D and 3D structural models will require material descriptions which refer to behaviour under these generalised stress states {Kotsovos, 1995 #82}.

The previous sections have described the uniaxial strength behaviour of concrete at elevated temperatures. Under generalised stress states however the behaviour of concrete varies quite significantly in both ultimate strength and post-peak behaviour (i.e. brittleness).

Much research has been undertaken in the field of multi-axial strength testing of concrete at ambient temperatures. Typically the biaxial strength of concrete is found to be higher than the uniaxial strength. Terro {, 1998 #149} quotes references of 16% higher. Considerably less research has focused on the multi-axial strength of concrete at elevated temperatures. Haksever and Ehm {, 1987 #70} conducted biaxial strength tests at temperatures up to 750°C. It was found that the relative increase of strength under a biaxial stress state was greater at higher temperatures. The maximum strength in the biaxial state also shifts to higher stress ratios. This is visible in the plane stress plot produced by Haksever and Ehm {, 1987 #70} in Figure 2-15. There is, however, very little further information on the effects of high temperature for multi-axial stress-states.

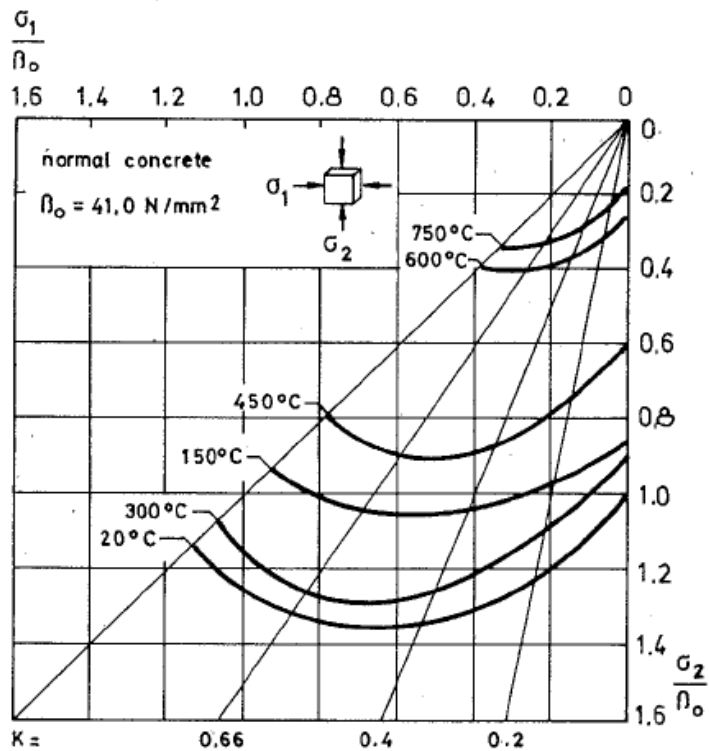


Figure 2-15 Experimentally measured elevated temperature biaxial strength for gravel concrete reproduced from {Haksever, 1987 #70}

2.2.5 Uniaxial material models of concrete behaviour

In this section the constitutive models proposed for capturing the behaviour of concrete at elevated temperatures described in section 2.2.4 are reviewed and discussed in the context of providing accurate input for high temperature structural analysis.

Components of strain

The strain behaviour of concrete under thermal exposure is more complicated than that of steel due to additional components arising from physiochemical changes in the concrete. The deformation behaviour of concrete at elevated temperatures is described by Equation 2-2 as resulting from three strain components. A number of models have been proposed to characterise these components. In the following sections the components of strain are described and the models available to characterise each are discussed and evaluated.

$$\boldsymbol{\varepsilon}_{tot} = \boldsymbol{\varepsilon}_{\sigma} + \boldsymbol{\varepsilon}_{th} + \boldsymbol{\varepsilon}_{LITS} \quad \text{Equation 2-2}$$

Where	$\boldsymbol{\varepsilon}_{tot}$	Total Strain
	$\boldsymbol{\varepsilon}_{\sigma}$	Quasi – instantaneous stress related strain i.e. strains read from stress-strain curves recorded at stabilised constant temperature
	$\boldsymbol{\varepsilon}_{th}$	Free thermal strain - due to thermal expansion or shrinkage
	$\boldsymbol{\varepsilon}_{LITS}$	Load Induced Thermal Strain - an umbrella term accounting for the physiochemical changes taking place on heating and at constant stress

Stress related strain ($\boldsymbol{\varepsilon}_{\sigma}$)

Cohesive-frictional materials such as concrete can be modelled in two different ways; as either a continuum (continuous models), or as discrete particles (discontinuous models). Discontinuous models require substantially greater computational effort, and research continues into the inter-particle relationships required to model concrete. Continuum approaches incorporating plasticity models, however, are computationally more efficient, more fully developed, and will be used in this investigation.

Continuum models are most commonly defined in terms of stress-strain curves, a definition that is appropriate for the pre-peak elastic behaviour of concrete. The post-peak deformation of a specimen, however, is the combination of two parts:

- a *stress-displacement* curve for the fracture process zone; and
- a *stress-strain* definition for the material outside the fracture process zone.

Under tensile loading the localisation patterns are more easily identifiable than under compression thus this approach has been more widely adopted for modelling tensile behaviour than for modelling compressive behaviour; thus compressive curves are still fully described by a stress-strain relation.

Constitutive compression models

The non-linear strength deformation behaviour of concrete is approximated using the parabolic function in Equation 2-3; n is taken as 3.0 for normal weight concretes.

$$\sigma_T = f_{c,T} \times \frac{\varepsilon_T}{\varepsilon_{c1,T}} \times \frac{n}{(n-1) + \left(\frac{\varepsilon_T}{\varepsilon_{c1,T}}\right)^n} \quad \text{Equation 2-3}$$

This function has been used by Anderberg and Thelandersson {, 1976 #31}, Schneider {, 1988 #77} and Eurocode 2 {, 2004 #27} for modelling the compressive behaviour of concrete at elevated temperatures. The high temperature peak compressive stress, $f_{c,T}$, is defined by Figure 2-14; these values have been used to plot the high temperature compressive behaviour of concrete for several temperatures in Figure 2-16.

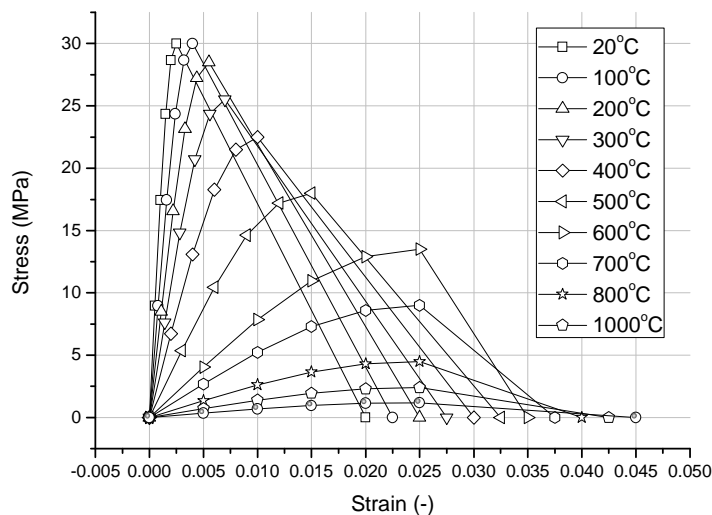


Figure 2-16 Non-linear compressive stress-strain behaviour of concrete as described by Equation 2-3

In Figure 2-16 the parabolic function has been used for both the pre-peak behaviour and the post-peak behaviour. It was described in section 2.2.4 that a stress-displacement relationship would more accurately describe the post-peak behaviour of concrete. In the absence of improved material data and models it is common to use the stress-strain relation of Figure 2-16 to define the post-peak behaviour of concrete under compression. Values of the strain at peak compressive stress, ε_{c1} , are taken from Eurocode 2.

Constitutive tension models

As described in section 2.2.4, the tensile behaviour of concrete is best represented by a stress-strain relation to describe pre-peak stress behaviour and a stress-displacement relation to describe the post-peak stress behaviour. The pre-peak behaviour is typically linear with some non-linearity developing close to the peak stress. However, for use in a numerical analysis the entire pre-peak range is assumed to be linear.

For the post-peak behaviour the shape of the tension softening curve is extremely difficult to measure experimentally. Consequently, there have been a variety of proposals for the form of the post-peak curve: linear {Hillerborg, 1976 #163}, bilinear {Rots, 1984 #52} and quadratic {Cornelissen, 1986 #165}. The area under these curves, however, remains a constant. This area is the energy required to open a unit area of crack and is termed the fracture energy, G_F (Nm/m^2). Hillerborg {, 1976 #163} has defined this as a material property rather than a structural property. Values of ambient temperature fracture energy for concretes of various strength and aggregate size are provided in the CEB-FIP Model Code {, 1990 #158}. Fracture energy is usually determined using a 3 point bending notched beam test {RILEM, 1985 #187}. These fracture energies and the recommended bilinear stress-displacement curves are presented in Figure 2-17.

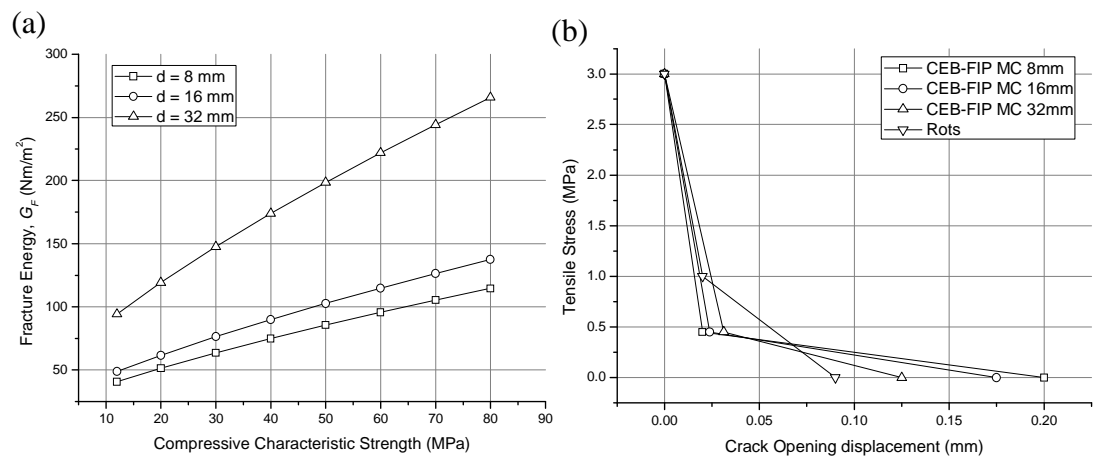


Figure 2-17 (a) Concrete Fracture energy (b) Tension softening bilinear approximations for $G_F = 0.075 \text{ Nmm/mm}^2$ {Rots, 1984 #52; CEB-FIP, 1990 #158}

Characterising the post-peak tension softening response of concrete can consequently be problematic, as it is not straightforward to transform the experimental stress-

displacement curve to a stress-strain curve. The stress-strain curve is not independent of the original specimen length, and is hence a structural property rather than a material property.

The appropriate modelling of tensile post-peak behaviour at ambient temperatures is still an ongoing topic of research in its own right. Information regarding the influence of temperature for the shape of the tension softening curve or the fracture energy property is lacking; in this investigation it is therefore assumed to remain constant.

Free thermal strain (ϵ_{th})

As described in section 2.3.2 at elevated temperatures aggregates typically expand and the cement paste shrinks, firstly due to dehydration processes and thereafter due to decarbonation {Khoury, 2000 #14}. It is extremely difficult to isolate these two phenomena experimentally; material models typically incorporate a thermal strain which is a combination of both. Experimentally derived properties of thermal strain will differ for sealed and unsealed concretes due to this embedded shrinkage component. It should, however, be noted that it is the expansive behaviour of the aggregate which dominates the free thermal strain term. For this reason free thermal strain terms are found in Eurocode 2 based on the type of aggregate used in the concrete; these are plotted in Figure 2-18.

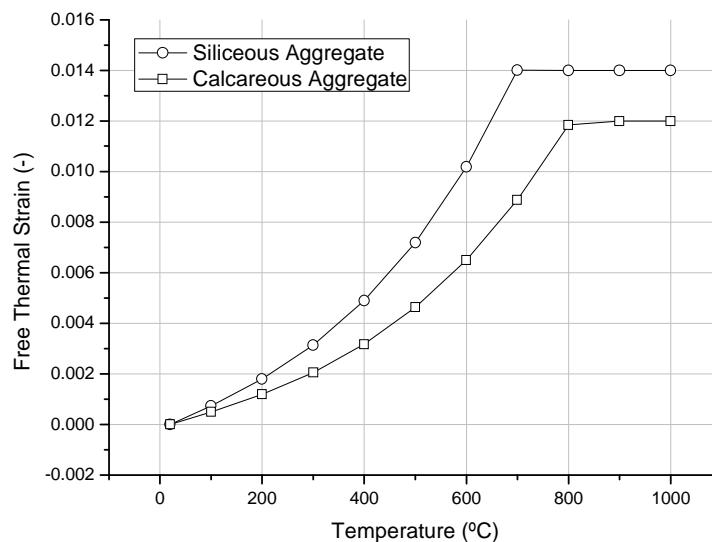


Figure 2-18 Free thermal strain for siliceous and calcareous aggregate concretes according to Eurocode2 {, 2004 #27}

The last 15-20 years in European research has seen a substantial amount of research recognising the importance of thermal expansion for understanding the behaviour of structures in fire. This subject is discussed further in chapter 3.

Load induced thermal strain (LITS) (ϵ_{LITS})

Load induced thermal strain (LITS) is an umbrella term for a number of strain components, related by the common attribute of all developing in specimens which are under constant stress during heating. The presence of LITS is widely accepted in the literature; however, it has not been widely recognised by structural engineers. The various components which make up LITS are described here followed by a discussion of the various empirical correlations available. Previous research considering LITS in structural analyses is reviewed to establish the consensus on the implications of LITS for structural behaviour.

The most obvious physical manifestation of LITS is seen when the deformations of an unloaded and loaded specimen are compared after heating. The unloaded specimen will elongate due to the free thermal strain. The deformation of the loaded specimen will be less than that dictated by the free thermal strain and under sufficiently large pre-stress will contract. This reduction in deformation is attributed to the presence of load induced thermal strain which is compressive and measured experimentally as the difference in deformation between a heated unstressed specimen and a heated stressed specimen.

The main components of LITS as defined by Khoury {, 2006 #72} are:

$$\epsilon_{LITS} = \epsilon_{tc} + \epsilon_{cr-d} + \epsilon_{ct-t-dep} + \epsilon_{\Delta el} \quad \text{Equation 2-4}$$

where	ϵ_{tc}	Transitional thermal creep – Irrecoverable strain occurring only upon first time heating in unsealed concrete under load
	ϵ_{cr-d}	Drying creep – Shrinkage caused by loss of chemically bound water
	$\epsilon_{cr-t-dep}$	Time dependent creep strain – Analogous to basic creep strain in thermally stabilised stressed specimens

$\varepsilon_{\Delta el}$ Changes in elastic strain – elastic components of LITS caused by the decrease in elastic modulus at elevated temperatures

Transitional thermal creep and drying creep are normally combined as one term referred to as transient creep/strain. This term represents the largest component of LITS and therefore is often mistaken for being the same thing. Both transitional thermal creep and drying creep are time dependent and irrecoverable. The time dependent creep strain is noticeable when stressed specimens are heated at different rates. None of the LITS correlations found in the literature are given, however, as a function of heating rate. LITS also contains an elastic or recoverable component caused by the reduction in elastic modulus at elevated temperatures leading to an increase in elastic strain.

Anderberg & Thelandersson {, 1976 #31} established an empirical correlation found in Equation 2-5 between a LITS component the transient creep strain and the free thermal strain at temperatures below 500°C. The coefficient k_{tr} is a constant between 1.8 and 2.35

$$\varepsilon_{tr} = -k_{tr} \frac{\sigma}{f_{c,0}} \varepsilon_{th} \quad \text{Equation 2-5}$$

Above 550°C they report a constant rate of straining for the siliceous concrete used in the experiment.

$$\frac{\delta \varepsilon_{tr}}{\delta T} = 0.0001 \frac{\sigma}{f_{c,0}} \quad \text{Equation 2-6}$$

There is however no physical justification for relating transient strain to thermal expansion and other researchers have found no relation between the two in their experimental data {Purkiss, 2007 #86; Khoury, 1985 #73}.

Correlations for LITS have also been produced by Terro {, 1998 #149}. These correlations are based on a wealth of experimental data produced at Imperial College where the major components of LITS were identified {Khoury, 1985 #73; Khoury, 1985 #74}. A linear expression is used to define the relationship between the load induced thermal strains and the stress/cold strength ratio in Equation 2-7. This is

called the master LITS curve which is independent of the aggregate used in the concrete.

$$\varepsilon_{LITS(\sigma/f_{c,0})} = \varepsilon_{LITS0.3} \cdot \left(0.032 + 3.226 \frac{\sigma}{f_{c,0}} \right) \quad \text{Equation 2-7}$$

The $LITS_{\theta,0.3}$ term describes the influence of temperature, for this Terro provides two expressions one for concrete of any aggregate other than Thames gravel and one for Thames gravel. These are found in Equation 2-8 and Equation 2-9 respectively.

$$\varepsilon_{LITS0.3} = -43.87 + 2.73T + 6.35 \times 10^{-2} T^2 - 2.19 \times 10^{-4} T^3 + 2.77 \times 10^{-7} T^4 \quad \text{Equation 2-8}$$

For $0 < T < 450^\circ\text{C}$

$$\varepsilon_{LITS0.3} = 1.48(-1098.5 + 39.21T - 0.43T^2 + 2.44 \times 10^{-3} T^3 - 6.27 \times 10^{-6} T^4 + 5.95 \times 10^{-9} T^5) \quad \text{Equation 2-9}$$

For $0 < T < 450^\circ\text{C}$

Despite the lack of physical justification for the Anderberg & Thelandersson correlation it has been more widely adopted than Terro {, 1998 #149} and Khoury {, 1985 #74} due to its more simple formulation. Neilson, Pearce *et al.* {, 2002 #35} have, however, adopted the Anderberg & Thelandersson LITS model with an important modification. Recognising the lack of physical justification for relating transient strain to thermal strain, Neilson proposed removing the thermal strain dependence and introduced a constant co-efficient of LITS derived by curve fitting to the empirically derived expression developed by Terro {, 1998 #149} (Equation 2-8 and Equation 2-9). The Neilson modified transient strain term is found in Equation 2-10. Thus Terro's fourth and fifth order polynomials are simplified to a linear expression. A constant co-efficient was used, but this was found to deviate from the experimental results above 400°C . A better fit could be achieved with a coefficient which is a function of temperature.

$$\varepsilon_{ir} = \beta T \frac{\sigma}{\sigma_{u0}} \quad \text{Equation 2-10}$$

Where: $\beta = 0.0000038$ for up to 400°C, Coefficient of LITS

The transient strain component can be calculated and combined with the stress-strain constitutive curve described previously for use in a numerical analysis. The effect of incorporation of this strain component upon the stress-strain curve can be seen in Figure 2-19. The blue curves represent concrete's constitutive curve with the added transient creep terms.

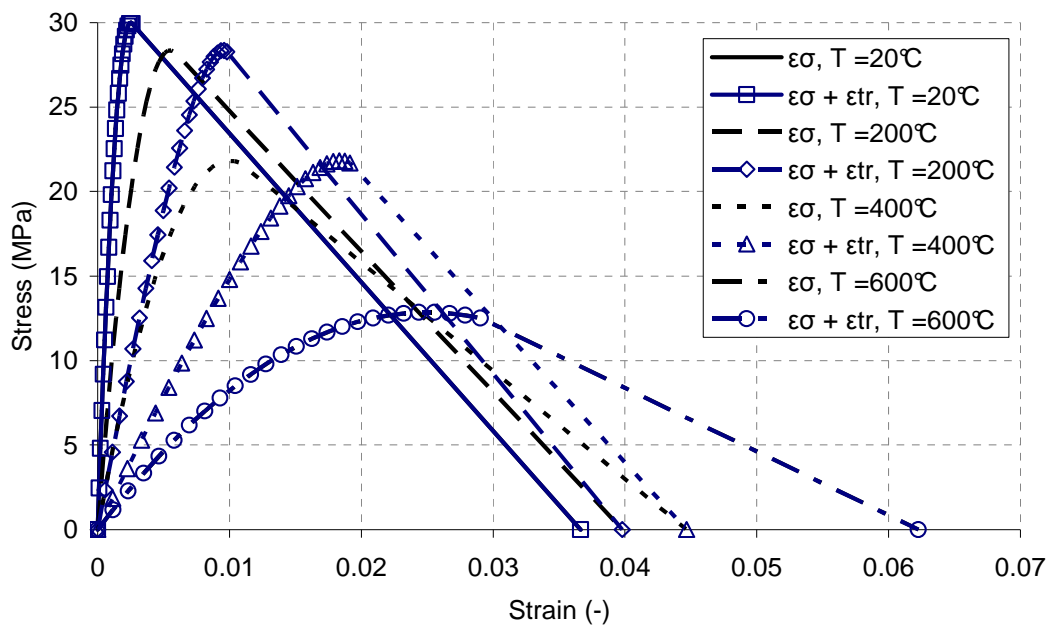


Figure 2-19 Incorporation of Anderberg's transient creep term into concrete's constitutive stress - strain curve (Equation 2-3).

Despite the details of LITS being well documented in the literature, it is not widely recognised by structural engineers. There is considerably less research documenting the implications of LITS for structural performance than there is concerning its representation in constitutive modelling. From a review of research focusing on the implications of LITS for structural performance {, 2007 #86; , 2008 #90; , 2007 #67; , 2002 #35; , 2008 #88} in fire there was a consensus that: the LITS term influences deformation behaviour, is important for predicting fire resistance periods of compression members, and that plastic strains are significantly underestimated when cooling is considered as part of the analysis.

Classical creep

The classical creep term has been deemed negligible for the analysis of concrete structures in fire by Anderberg and Thelandersson {, 1976 #31}, Schneider {, 1988 #77} and Li {, 2005 #32}. It is argued that the period of fire exposure is short compared with the age of the concrete. Similarly the constitutive curves provided in Eurocode 2 {, 2004 #27} are only applicable in the heating range of 2 to 50°C/min as classical creep effects are not considered.

2.2.6 Multi-axial concrete mechanical models

There has been little in the way of research focusing on 3D constitutive modelling of concrete at elevated temperatures. As described in section 2.2.4 there are few experimental data against which to validate any three and two dimensional formulations. The typical approach is to employ one of a number of the available ambient temperature 2 and 3D concrete constitutive models and ‘shrink’ the failure surface according to a reduction function for uniaxial compressive/tensile strength.

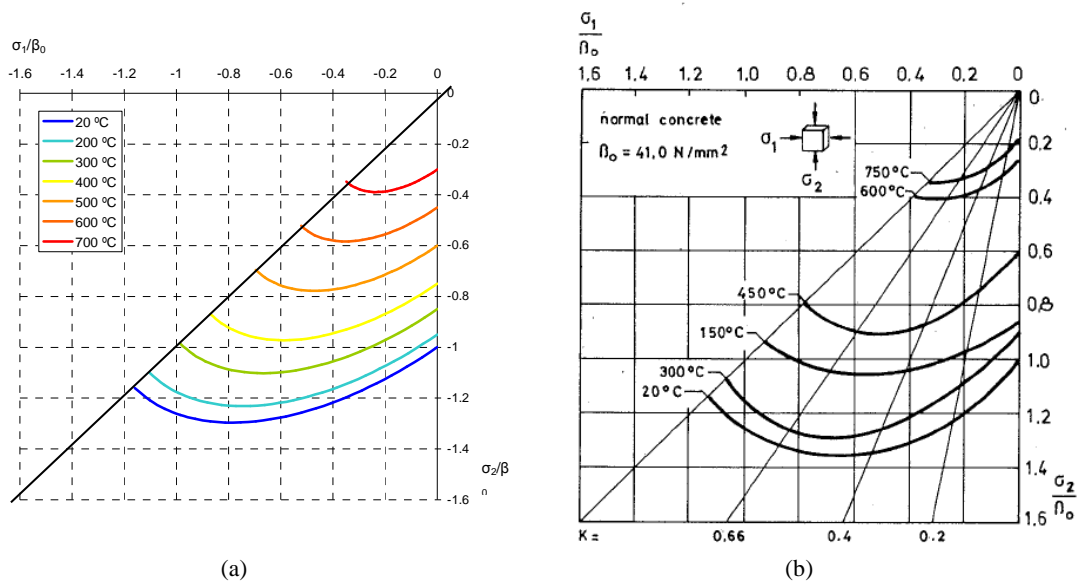


Figure 2-20 (a) Schematic of shrinking failure surface (Drucker Prager) (b) Experimental biaxial compression failure envelope reproduced from {Haksever, 1987 #70}

Figure 2-20 demonstrates using the Drucker-Prager criteria how the yield surface shrinks at increasing temperatures using this approach. The approach fails to account for, however, any changes in the shape of the yield surface at elevated temperatures. The experimental results which show the actual biaxial behaviour of concrete at

elevated temperatures, produced by Haksever and Ehm {, 1987 #70}, were discussed earlier and are presented here again for comparison. The experimental results indicate that at elevated temperatures the biaxial to uniaxial f_b/f_c compressive strength ratio changes with a subsequent change in the shape of the yield surface. Haksever's results suggest an increase in the f_b/f_c ratio at elevated temperature. The assumption typically made and shown in Figure 2-20 (a) is that the ratio remains the same thus making this a conservative assumption.

Several 3D constitutive models have been developed for typically ambient temperature usage, given the typical approach for high temperature analysis as outlined above, a discussion of these various models including their limits of applicability follows. Concrete behaviour is characterised by a non linear stress-strain relationship in multi-axial states of stress, a post-peak strain softening stage characterising cracking and crushing and different yield points in tension and compression {Yu, 2007 #113}. All of these characteristics must be captured by the constitutive model.

The essential elements of any model based on classical plasticity theory are the yield criterion, the flow rule and the hardening rule. The last is to be interpreted in a broad sense so that both hardening and softening may be accounted for {Lubliner, 1989 #96}.

Yield criteria

The yield criteria must fit the strength of the material in all quadrants that is biaxial compression, biaxial tension and tension-compression. The significantly different strength of concrete under compression and tension results in a difficult yield surface to formulate. As a consequence of this there a wide range of yield criteria that have been developed for concrete behaviour. These criteria range from the classic Drucker-Prager and Mohr-Coulomb yield surfaces to sophisticated descriptions requiring specification of numerous material parameters.

The simplest models require only a small number of parameters to define the yield surface. However modification of the yield surface parameters to fit behaviour in one quadrant (say biaxial compression) generally results in sacrificing accuracy in another. A consequence of this is a limited ability to capture accurately behaviour in

all quadrants. A common approach to amend this is to adopt two failure surfaces, one which characterises the biaxial compressive behaviour and another to characterise the biaxial tension and tension-compression behaviour. Jirasek and Bažant {, 2002 #80} have proposed that an approach such as that suggested by {Feenstra, 1996 #140}, combining a Drucker-Prager criterion in compression with a Rankine criterion in tension, could provide reasonable results for plane stress problems (shown schematically in Figure 2-21 (a)). Disadvantages of this approach are the need to define uncoupled behaviour along each principle strain or stress direction and the likely increase in computational cost associated with the simultaneous solution of two failure surfaces.

More sophisticated models such as shown in Figure 2-21 (b) typically involve a single yield surface with an increased number of modifiable parameters to allow the surface to fit in all quadrants. The most sophisticated criteria use up to 5 modifiable parameters and provide an excellent fit with experimental data {Yu, 2007 #113}. The large number of parameters required for their definition can make them difficult to apply where such information is limited counteracting the potential gain in material accuracy. Conversely the simplest models, despite their ease of implementation fail to capture behaviour reasonably in all quadrants. Yield criteria such as that of {Lubliner, 1989 #96} offer an appropriate compromise between material accuracy and ease of implementation.

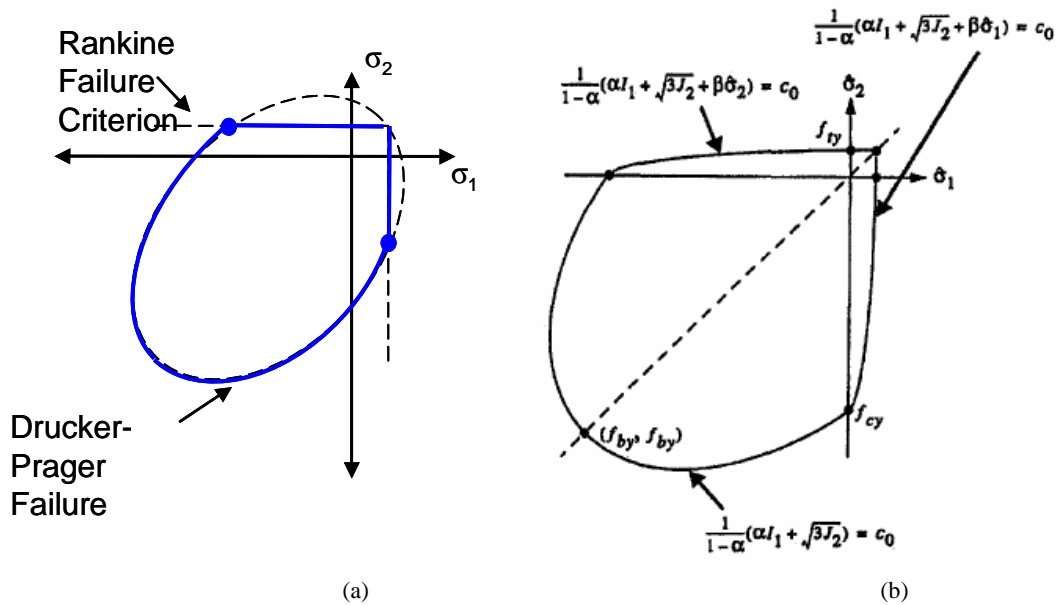


Figure 2-21 (a) Schematic representation of multi-surface failure criteria (combined Drucker-Prager/Rankine) in plane stress (b) Lubliner yield function in plane stress space reproduced from {Lubliner, 1989 #96}

Flow rule

The flow rule is used to evaluate the development of plastic strains when the material yields, this occurs when the equivalent stress reaches the yield surface. The flow rule commonly adopted for describing the behaviour of metals referred to as the associated flow rule assumes plastic straining is normal to the yield surface. Smith et al. {, 1989 #100}, however, have shown experimentally that the associated flow rule is inadequate for concrete as it overestimates volume dilation at peak stress. Jirasek and Bažant {, 2002 #80} have also recommended against using the associated flow rule for pressure sensitive materials. For concrete applications it is therefore common to employ a flow rule where the plastic potential and the yield criteria are not associated; termed the non-associated flow rule. A full description of the non-associated flow rule can be found in Jirasek and Bažant {, 2002 #80}. The disadvantage of a non-associated flow is the production of an unsymmetrical tangent stiffness matrix. In finite element analysis the tangent stiffness matrix is commonly assumed to be symmetrical to save computational effort. Therefore use of the non-associated flow rule is computationally more expensive.

Hardening rule

The ‘hardening rule’ is a broad term relating to both hardening and softening behaviour after initial yield. This behaviour means that yield surfaces are typically described in an incremental elasto-plastic constitutive law which prescribes the entire response curve of the material and characterises the strength envelope indirectly (such as the constitutive curve described in section 2.2.5). These should be established from experimental results (of both pre and post-peak behaviour). The yield criteria previously described are all open along the hydrostatic axis. Softening behaviour is not experienced in this direction however the material response is not linear; therefore the initial yield surface marking the onset of non-linearity must be enclosed. Several models have been developed to characterise this behaviour {Jirasek, 2002 #80} therefore the previously defined models (unless modified) should be applied only to conditions where confining pressures are low.

2.2.7 Concrete summary

In this section the complex and varied behaviour of concrete at ambient and elevated temperatures has been examined and the models available for characterising that behaviour reviewed. The following paragraphs summarise those findings.

The effect of high temperature upon concrete compressive strength has been studied in more detail than for tensile strength. Aggregate type, cement past – aggregate ratio and pre-stress have all been identified as being important for the residual strength of concrete at elevated temperatures. Currently only the aggregate type is considered by design guidance.

The highly non-linear compressive behaviour of concrete is well approximated in the pre-peak phase by a parabolic expression which has been widely adopted. For the post-peak phase behaviour would be best represented by a stress-displacement relation in the localisation zones and a stress-strain relation everywhere else. Identification of these localisation zones is difficult and reliable information is not available at ambient or elevated temperatures therefore the full stress-strain curve is used to describe compressive behaviour. Substantially more research has been conducted into the post-peak behaviour in tension; despite this, accurate descriptions of the descending branch shape and material properties are difficult to establish

accurately. It will therefore be necessary in any structural analysis to assess the sensitivity of the model to this definition.

Fitting a failure surface to the ambient multi-axial behaviour of concrete is difficult due to concrete's differing behaviour under compression and tension. Selection of a yield surface requires a compromise between accurate material characterisation and computational efficiency. Such a compromise is found by either combining two simple yield criteria or single criteria such as Lubliner {, 1989 #96} which requires relatively few parameters without sacrificing accuracy in all quadrants. The non associated flow rule has been found to describe the plastic flow of concrete better than the associated flow rule. It does however increase computational cost by creating non-symmetrical stiffness matrices.

Haksever's {, 1987 #70} work suggests that high temperatures influence the shape of concrete's failure surface. Attempts at developing a high temperature multi-axial constitutive model for concrete have however been thwarted by a lack of material data against which the models can be validated. The current approach is therefore to choose a suitable ambient temperature yield criteria (as described above) and shrink this at elevated temperatures based on the reduction in uniaxial strength, thereby assuming no change in multi-axial behaviour at elevated temperatures.

The presence of load induced thermal strains (LITS) has been well established and several empirical correlations have been formulated. Previous research has indicated that the LITS component influences deformation predictions, performance during the cooling phase of a fire and fire resistance periods of structures which have a high degree of axial compression. The correlations reviewed can be implicitly incorporated into the parabolic stress-strain to include LITS in a structural analysis. These correlations will be used in a comparative study to assess the importance of LITS in the structural analyses undertaken.

The free thermal stain term is of critical importance to understanding the behaviour of reinforced concrete structures in fire and should therefore always be included. The classical creep term however is ignored due to the relatively short period of heating a fire induces in a structure.

2.2.8 Steel-concrete interaction

The bond between the steel reinforcement and the concrete is critically important for the resistance of tensile loads in a reinforced concrete structure. When the concrete has cracked in tension, the tensile forces are carried by the steel reinforcement (there is little or no stress transfer across the cracked concrete). This mechanism is however dependent upon the transfer of stress from reinforcement to concrete in the uncracked concrete, between cracks. The transfer of stress is facilitated by the steel-concrete bond.

In this section the physical interaction between the steel reinforcement and the concrete is described, followed by a discussion of the effect this interaction has on the tensile and cracking behaviour of reinforced concrete.

The strength of the bond is determined by three components; chemical adherence (which is typically small), friction (which occurs once adherence has failed and there is relative movement between the concrete and the steel), and finally mechanical interlock (which occurs for deformed bars where there is interlock between reinforcement ribs and embedded concrete) {Girard, 2002 #166}. For plain bars the bond strength is determined by chemical adherence and friction; for deformed bars the bond strength is principally determined by the mechanical interlock. Due to the enhanced bond strength afforded by the mechanical interlock, deformed bars are now more commonly used than plain. Experimental estimates of bond strength are made by conducting pull-out tests for different reinforcement and concrete types. The results of such tests are bond stress-slip relationships.

The process of cracking in a reinforced concrete structural element is summarised in Figure 2-22 for the purpose of establishing the role steel reinforcement plays {after Beeby, 1978 #160}.

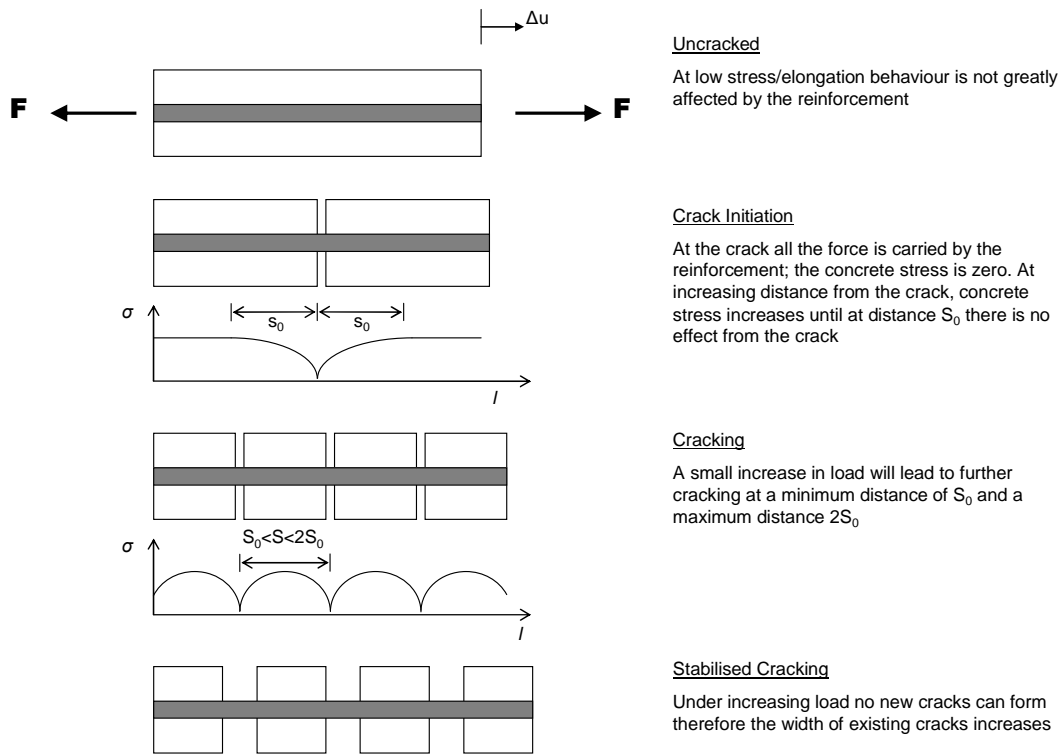


Figure 2-22 Series of events in cracking of reinforced concrete sections

The presence of reinforcement alters the cracking behaviour of the concrete. The stress transfer between the reinforcement and the concrete results in a pattern of multiple distributed cracks as opposed to the isolated cracks associated with plain concrete.

The transfer of stress between steel and the un-cracked concrete results in another effect referred to as 'tension stiffening'. Tension stiffening is distinct from the tension softening effect described in section 2.2.4, despite the somewhat interchangeable use of the terms. Tension softening refers to the gradual unloading witnessed at increasing deformations in the post-peak behaviour of plain concrete. Tension stiffening refers to the increased stiffness of a concrete-steel system compared to a plain steel bar. The transfer length described in Figure 2-22 results in a minimum crack spacing; between cracks the concrete is undamaged and contributes to the overall stiffness of the system via the bond between the reinforcement and the steel. The tension stiffening effect is evident in Figure 2-23 which compares the stiffness of two systems – a plain steel bar and a steel bar embedded in concrete. The

stiffness of the embedded-bar system is higher than that of the plain bar {Kotsovos, 1995 #82}.

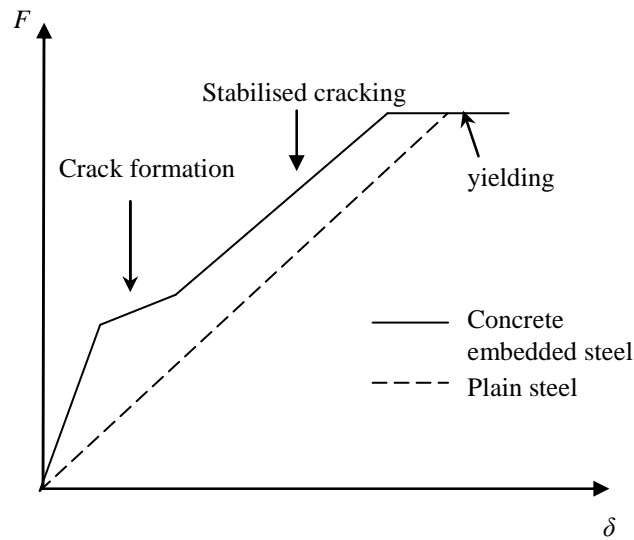


Figure 2-23 Schematic load-displacement response of a steel bar and a concrete embedded steel bar

The degree of tension stiffening is affected by reinforcement ratio, modular ratio, member dimensions and reinforcement dimensions. The effect of reinforcement ratio has been shown to be substantial with greater tension stiffening witnessed at lower reinforcement ratios. At higher reinforcement ratios, the stiffness of the reinforcing bar dominates the system stiffness rendering the contribution of the concrete negligible {Gupta, 1990 #171}.

2.2.9 Modelling steel – concrete interaction

The physical interaction between the reinforcement and the concrete is characterised by the use of either of the following models:

- Bond-Slip
- Tension Stiffening

Bond slip models are used to characterise the deterioration of the bond between concrete and steel at increasing deformation {Girard, 2002 #166}. Such models take the form of empirically derived bond stress-slip curves. They are typically used to define the behaviour of interface elements in finite element analyses between the reinforcement and the concrete. By defining the degree of bond strength these models can capture the tension stiffening behaviour of reinforced concrete and also

model the deterioration of bond strength under increasing slip. Bond-slip models provide a detailed representation of the physical interaction between concrete and steel, they therefore require that the cracking of the concrete is modelled in a semi-realistic manner also; they are typically combined with discrete or embedded crack models which are described in more detail in chapter 4.

Tension stiffening models do not define the bond strength, rather they assume perfect bond between the concrete and steel and instead modify either the steel or concrete material properties to account for the tension stiffening effect {Stramandinoli, 2008 #167}. These models are easily implemented in a finite element analysis. The better models include modifiable parameters such as reinforcement ratio to produce a range of possible tension stiffening definitions. Tension stiffening models made be used with more approximate cracking models such as smeared cracking (discussed in more detail in chapter 4); they are therefore capable of providing accurate global predictions of behaviour, but not local failure.

The objectives of the analysis will determine which method offers the best solution. Where it is desired to consider the influence of small scale interactions and phenomena for the global structural behaviour but such behaviour does not dominate the overall structural response, the tension-stiffening model approach provides an adequate solution. Where the small scale behaviour and phenomena will dominate the structural response and where reliable material data is available the more detailed bond slip model is the appropriate solution.

2.3 Conclusions

2.3.1 Reinforcing steel

The material parameters required for modelling heat transfer in steel are straightforward and have been defined in the literature. The process of heat transfer in concrete is more complicated involving a coupled relationship between temperature evolution and the mass transport of water vapour. It has been shown however that a reasonably accurate prediction of concrete temperature evolution in fire can be obtained using a decoupled heat transfer analysis (no mass transport considered) in combination with ‘apparent’ thermal properties; thermal properties

including the effects of moisture transport such as a spike in the specific heat term at 115°C to account for latent heat of vaporisation of water).

The behaviour of steel reinforcement may be adequately modelled using a uniaxial assumption of behaviour. Any biaxial effects occur on such a small scale as to be beyond the capabilities of a typical structural model to capture. Anderberg's uniaxial constitutive curves provide a good model for the behaviour of steel at elevated temperatures. The material data used to create this model was however primarily produced with exposed steel structures in mind; therefore the assumptions concerning the implicit consideration of creep do not apply for steel reinforcement. The implications of reinforcement creep for the behaviour of reinforced concrete structures at elevated temperatures is not understood.

There is limited information concerning the high temperature effects for reinforcing steel rupture strains. In the Eurocodes it is taken as a constant value. Rupture is modelled as an inclined descending branch to prevent numerical difficulties arising from the sudden loss of strength at rupture.

2.3.2 Concrete

The potential variation in concrete mix has a significant influence of the mechanical properties at elevated temperatures; despite this design guidance still provides mechanical properties predominantly for 'normal' weight concretes which cover a large range of possible concretes.

Modelling of concrete behaviour requires a complete description of the load deformation behaviour and an understanding of how elevated temperatures influence this behaviour. Constitutive models for the pre-peak phase of behaviour are able to capture the highly non-linear nature of concrete under compression and the chiefly linear response under tension provided reliable material data such as high temperature strengths are available.

The post-peak behaviour for both tension and compression is dominated by strain localisation; this behaviour is therefore best represented by a stress-displacement relation for localisation zones and a stress-strain relation elsewhere. We are currently unable to accurately model the post-peak behaviour of concrete under compression at ambient temperatures and consequently at elevated temperatures also. This problem

is perhaps not critical to some areas of ambient flexural analysis but under mechanisms where large compressive forces are induced it is less clear.

Ambient post-peak tensile behaviour is substantially better understood and described than the compressive post-peak behaviour. The fracture energy (area under the stress-displacement softening curve) is established as a material property. The effect of high temperatures for either the fracture energy or the tension softening curve is not understood.

There are several multi-axial models available which are capable of capturing the behaviour of concrete under biaxial and tri-axial states of stress. Attempts at developing a high temperature multi-axial model have been thwarted by a lack of material data to validate such models this is despite indications that at high temperatures the behaviour of concrete under multi-axial stress states alters.

There are several empirical correlations which describe the LITS component of concrete behaviour these can implicitly included in a numerical analysis.

2.3.3 Steel-concrete bond

The interaction between steel and concrete heavily influences the cracking behaviour of concrete under tensile loads. The transfer of stress between the concrete and the steel results in a distributed pattern of small cracks compared to the isolated larger cracks typically of plain concrete structures. The bond between the two will impose minimum and maximum crack spacings. The type of cracking is important for deciding what method of crack representation to use in a finite element analysis; this is discussed further in chapter 4.

The treatment of cracking is also important for the strain development in the reinforcement as it is through cracking that stress is transferred to the reinforcement.

The steel-concrete bond is also responsible for an effect for referred to as tension stiffening, where the concrete between cracks contributes to the overall system stiffness. This effect may be account for using detailed bond-slip models which explicitly model stress transfer between concrete and steel and the deterioration of the bond between the two, or it may be accounted for in a phenomenal manner by modifying the concrete or steel material properties. The latter assumes perfect bond

between the concrete and steel and is intended for use when the concrete steel interaction does not dominate the global structural response.

3 Compartment fires and structural fire fundamentals

Recent research into the spatial and temporal distributions of temperature within full scale fire tests has demonstrated that statistically significant thermal variation exists {Stern-Gottfried, 2010 #227}. An objective of this thesis is to establish if this variation could be significant for the concrete structural performance. It is first necessary to formulate thermal exposures which capture the spatial and temporal variations of temperature produced by a compartment fire.

The compartment fire thermal environment is examined by a discussion of compartment fire dynamics to establish the parameters which influence thermal variation. The temperature measurements of a full scale fire test are presented to demonstrate the potential thermal variation in a fire compartment. The conclusions of this discussion are contrasted with the assumptions implicit in current design fires for structural analysis.

The first step in establishing the significance of thermal variation in predicting concrete structural behaviour is to examine the implications for the thermal expansion behaviour. The thermal expansion behaviour of a structural element is a fundamental component to determining the high temperature structural behaviour {Usmani, 2001 #138}. Non-uniform thermal exposures are formulated to investigate the effect of both spatial and temporal variation of gas temperature upon the thermal expansion behaviour of a simple concrete element.

The conclusions of this investigation will be used to help interpret the behaviour of more complex structural forms under non-uniform temperature conditions in chapter 5.

3.1 The compartment fire thermal environment

In this section the nature of the temperature field within a compartment fire is considered. In section 3.1.1 compartment fire dynamics are briefly discussed to identify the parameters which influence the temperature field. In section 3.1.2 the temperature measurements from the Dalmarnock Fire Test One are presented to demonstrate the potential thermal variation within a compartment fire. Finally in

section 3.1.3 the assumptions of the current design fires for structural analysis concerning compartment thermal variation are discussed.

3.1.1 Compartment fire dynamics

A compartment fire refers to a fire that occurs within some boundary, such as the walls of an office, which confines combustion products and controls the ventilation supply. As we will see this strongly influences the burning behaviour of the fire.

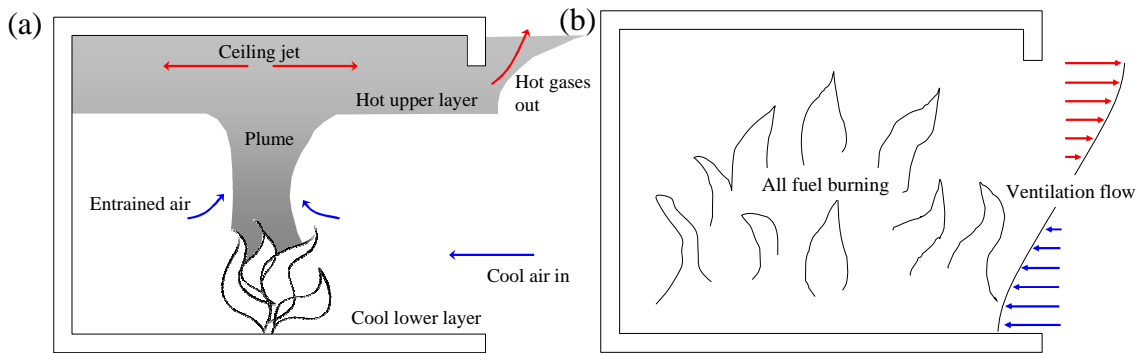


Figure 3-1(a) Pre flashover fire development in a compartment (b) post flashover fire

In the early stages of a fire the burning is largely unaffected by the compartment boundaries. Figure 3-1 (a) summarises the early stage development of a compartment fire. Hot combustion products rise vertically in a plume entraining cool air from the compartment as it does. The entrained air cools and dilutes the combustion products. When the plume reaches the compartment ceiling, flow is deflected horizontally until it reaches the compartment edge. Once it has reached the edge of the compartment a smoke layer is created that starts to increase in depth; hot gases will escape when it drops below the soffit of an opening in the compartment edge. The loss of hot gas is balanced by cool air drawn in through the openings.

Radiation from the hot smoke layer back to the fuel bed increases the burning rate and consequently the temperature of the smoke layer, further increasing radiation from the smoke layer to un-ignited fuel. At a critical value of radiative flux from the smoke layer it is possible for fuel remote from the fire source to ignite and begin burning. This leads to a rapid increase in both the burning rate and the temperature of the compartment. This process of fire spread to remote objects represents a transition in behaviour from a single burning item or collection of items within a compartment to full compartment involvement. This transition is referred to as flashover; a pre-

flashover fire therefore refers to behaviour prior to this point and a post-flashover fire after this.

During the post-flashover period temperatures are much higher than the pre-flashover period ($\gg 600^{\circ}\text{C}$) and the flow of gas within the compartment becomes turbulent (Figure 3-1 (b)). The burning rate is dictated by the relative abundance of fuel and ventilation; where ventilation is abundant but fuel is limited, the burning behaviour is referred to as fuel controlled and when there is limited ventilation but abundant fuel the burning rate is ventilation controlled. Thus the size, compartment openings and relative fuel layout in a compartment strongly dictate the thermal environment in a compartment fire. For example, in very large compartments typical of modern office construction the likelihood that the entire compartment will become fully involved at one point in time reduces; instead burning will progress through the compartment subject to fuel layout and ventilation conditions. This concept is presented by the schematic in Figure 3-2 of a deep compartment with an opening at one end.

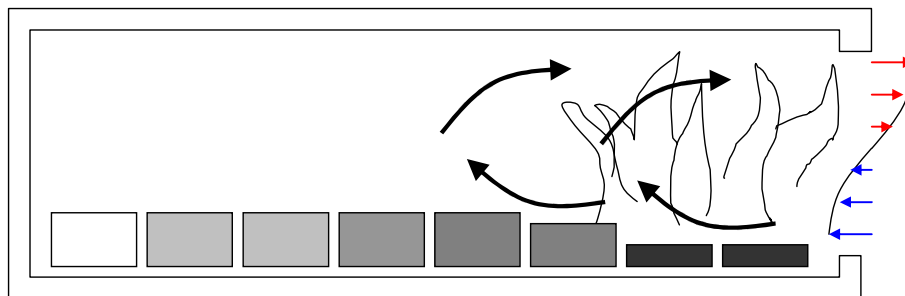


Figure 3-2 Progressive burning in a deep compartment with opening at one end {Buchanan, 2001 #54}

Post-flashover fires are considered to be most critical for structural performance due to the very high temperatures they can achieve. The design fires that have been developed for structural analysis try to characterise the environment created by a fire involving the entire compartment.

3.1.2 Full scale fire test temperature data

Typically a small number of temperature measurements are made of the gas phase temperature field during full scale fire tests; thus these tests offer little insight into the horizontal and vertical variations of temperature within a compartment.

Two recent full scale fire tests have included a large number of gas phase temperature measurements, the Cardington Natural Fire Safety Concept 3 (NFSC3) test series {Bravery, 1993 #179} and the Dalmarnock Fire Tests {Rein, 2007 #174}. In both of these tests it has been shown that there was statistically significant variation in compartment temperatures during burning {Stern-Gottfried, 2010 #227}. Temperature data from Dalmarnock Test 1 is presented to demonstrate the influence of both fuel distribution and ventilation conditions.

Dalmarnock Test 1 was conducted in July of 2006 in a 23 storey cast in situ reinforced concrete structure by the BRE Centre for Fire Safety Engineering. The test was conducted in a 4.75m x 3.5m x 2.95m (high) compartment. Figure 3-3 shows the natural fuel distribution within the compartment, sensor positions and ventilation locations. A total of 220 thermocouples were used to measure gas phase temperature field distributed over 20 thermocouple trees spread throughout the compartment.

The highest concentration of fuel is found in the north east corner of the compartment. The fuel load density in the compartment was estimated to be 32 kg/m², wood equivalent. Ventilation is provided through two open door ways in the south east corner and a closed double window in the west wall.

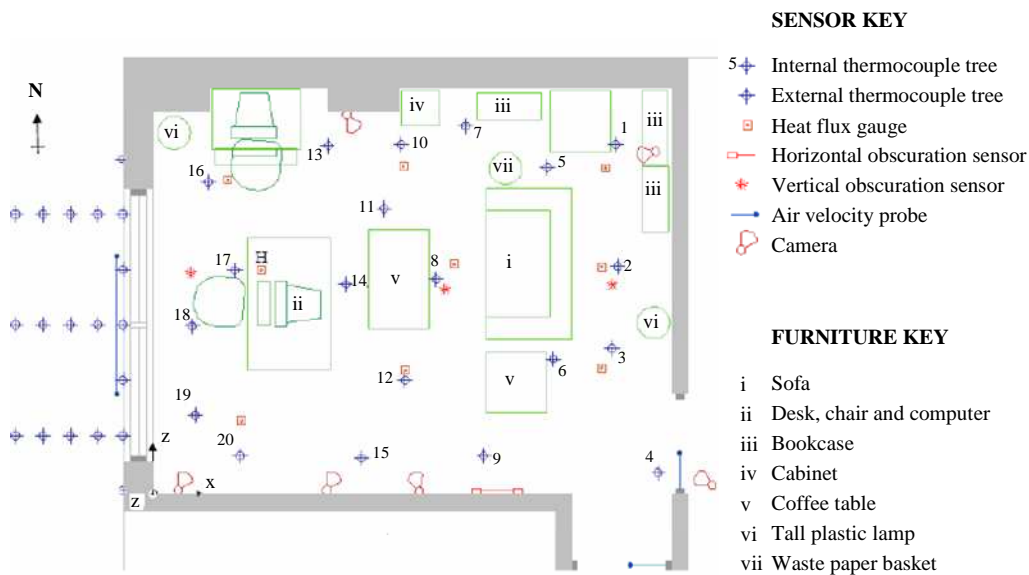


Figure 3-3 Fuel distribution and ventilation locations: Dalmarnock Test 1 compartment plan

The fire was ignited in the waste paper basket (vii - Figure 3-3) and subsequently spread to the sofa. Figure 3-4 presents the average gas phase temperature history for the fire; key events in the fire development have been marked.

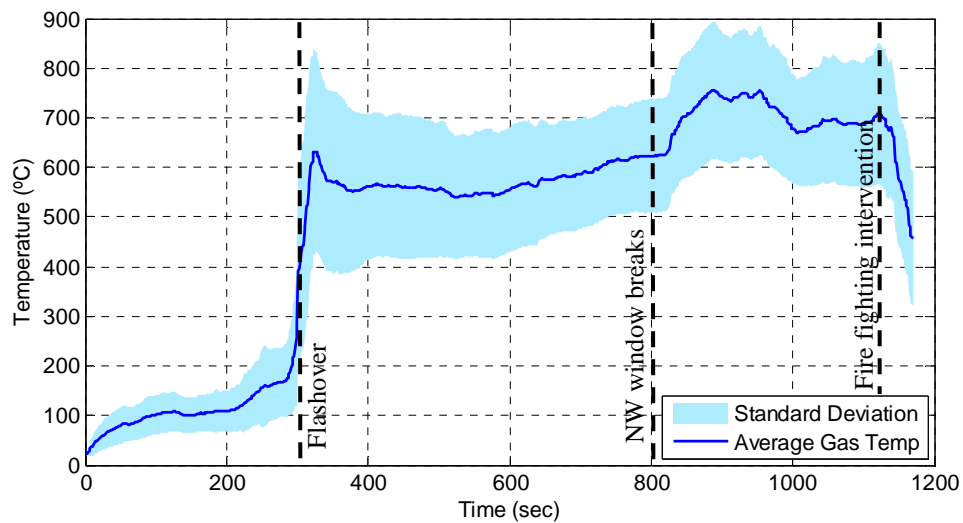


Figure 3-4 Gas phase temperature measurements showing key events in fire development

Flashover occurs 300 seconds after ignition; at this time there is a significant spike in compartment temperatures. The transition was confirmed by video footage showing remote ignition of fuel at this time. In the initial post flashover stages ventilation is provided through the south east corner doorways only. After 801 seconds the north-west window pane breaks; this not only increases the amount of available ventilation but introduces a new ventilation location. This event corresponds with a second spike in compartment temperatures. After 1140 seconds compartment temperature decrease due to fire fighting intervention.

Figure 3-5 presents plan contour plots of temperatures measured in the horizontal plane 50 mm below the compartment ceiling at selected time steps after flashover. These contour plots are presented to demonstrate the influence of the fuel load distribution and ventilation conditions on the measured temperature field close to the structure (concrete ceiling).

In Figure 3-5 initially peak temperatures are concentrated in the north east corner close to the ignition source and the highest fuel density; at this time ventilation is from the south east corner only. As fuel is consumed the temperatures in this location start to reduce (Figure 3-5 (b)). After the window breakage the greater availability of

ventilation increases the burning rate adjacent to the window. This can be seen by the peak temperatures developing in this region in Figure 3-5 (c) and (d).

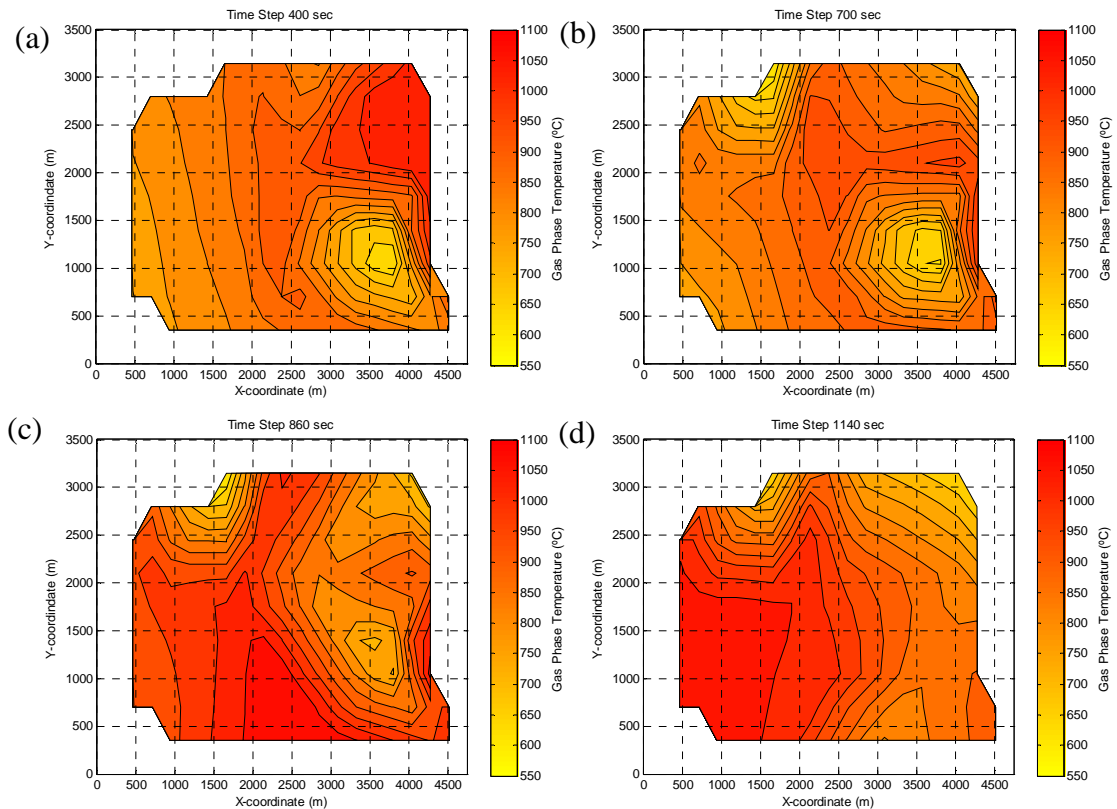


Figure 3-5 Gas temperature plan contour plots at 50 mm below ceiling level (a) 400 (b) 700 (c) 860 (d) 1140 seconds

3.1.3 Structural design fires

Early structural fire engineering was heavily dependent upon empirical data to determine the performance of structures in fire. To standardise the thermal loading used in the test procedure the ‘Standard Fire’ temperature-time relation was developed {Babrauskas, 1978 #157}. The standard fire takes the form of an ever increasing temperature-time relationship. This fire curve is still available in Eurocode 1 as the standard temperature time curve. This curve has been plotted in Figure 3-6.

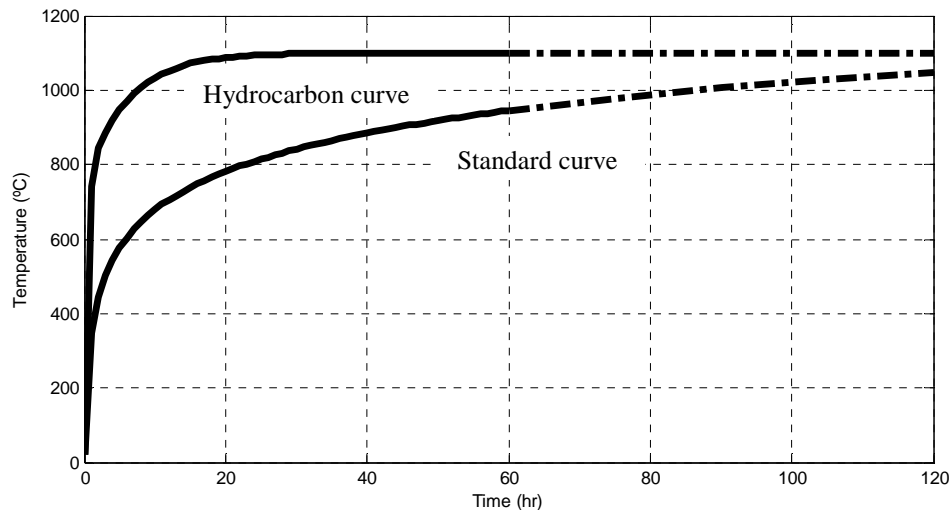


Figure 3-6 Temperature-time design fires available in Eurocode 1 {, 2002 #30}

Structural fire resistance is measured in time of performance under exposure to the standard fire; for example, 30 minutes fire resistance indicates the structure achieves its performance requirements (stability, integrity and insulation) for at least 30 minutes exposure to the standard temperature time curve. This convention stems from the empirical origins of structural fire engineering. It is therefore common for the standard temperature time curve to be used as a design fire in a structural fire engineering analysis. The standard temperature time curve has no physical basis {Drysdale, 1998 #17}. It is considered to adequately represent the severity of a compartment fire. No variation in the compartment temperature field is considered, temperature and heating rate are judged the most important factors for determining severity for structural behaviour. Where it is thought a more severe fire is likely to be encountered the hydrocarbon fire has been included in Eurocode 1 (also plotted in Figure 3-6).

Parametric fire curves

Parametric fire curves are a very simple form of fire model; the temperature-time data are calculated and published. The designer is only required to select the correct curve based on design variables {ASCE, 2009 #231}.

Pettersson's curves {Pettersson, 1976 #41} are the most commonly cited set of parametric fire curves. Pettersson et al. calculated their compartment temperature histories using the fundamental heat balance equation and Kawagoe's burning rate

equation {Kawagoe, 1963 #43}. The model is simplified by making the following assumptions:

- (i) combustion is complete and takes place within the compartment;
- (ii) temperature in the compartment is uniform at all times;
- (iii) a single heat transfer coefficient may be used for the compartment inner surface; and
- (iv) heat flow to and from the compartment is one-dimensional, that is, corners and edges are ignored and the boundaries are assumed to be 'infinite slabs'.

Despite these simplifications the calculation of temperature requires numerical integration. Therefore Pettersson et al. published a set of temperature-time data from which designers can choose the appropriate curve based on the compartment fuel load and ventilation factor. Ventilation factor relates the size of opening and the compartment size. A representative set of curves are presented in Figure 3-7.

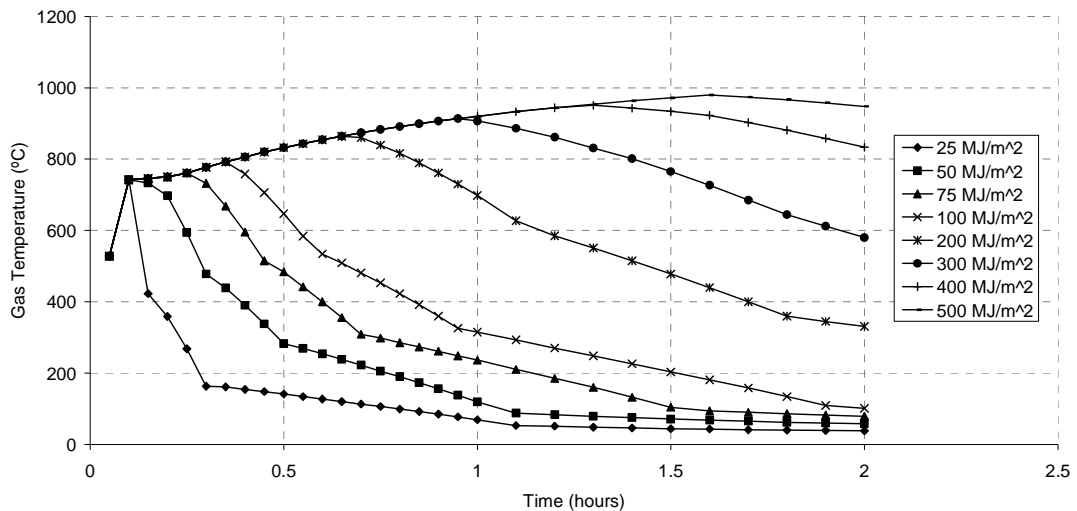


Figure 3-7 Temperature-time compartment fire curves with different fire load densities for opening factor $A_w H^{1/2} / A_f (m^{1/2}) = 0.04 m^{1/2}$ {Pettersson, 1976 #41}

The parametric fire curve available in Annex A of Eurocode 1 {, 2002 #30} is based on Pettersson et al. {, 1976 #41}. The temperature is defined according to the equation:

$$T_g = 20 + 1325 \left(1 - 0.324e^{-0.2t^*} - 0.204e^{-1.7t^*} - 0.472e^{-19t^*} \right) \quad \text{Equation 3-1}$$

Where $t^* = t\Gamma$ and $\Gamma = (O/b)^2 / (0.04/1160)^2$. O is the opening factor, $O = A_v(H)^{1/2}/A_t$, and b represents the compartment lining thermal absorptivity, $b = (k\rho c)^{1/2}$. Several parametric curves have been calculated using the above equation and are plotted in Figure 3-8 for different (a) opening factors and (b) boundary thermal properties.

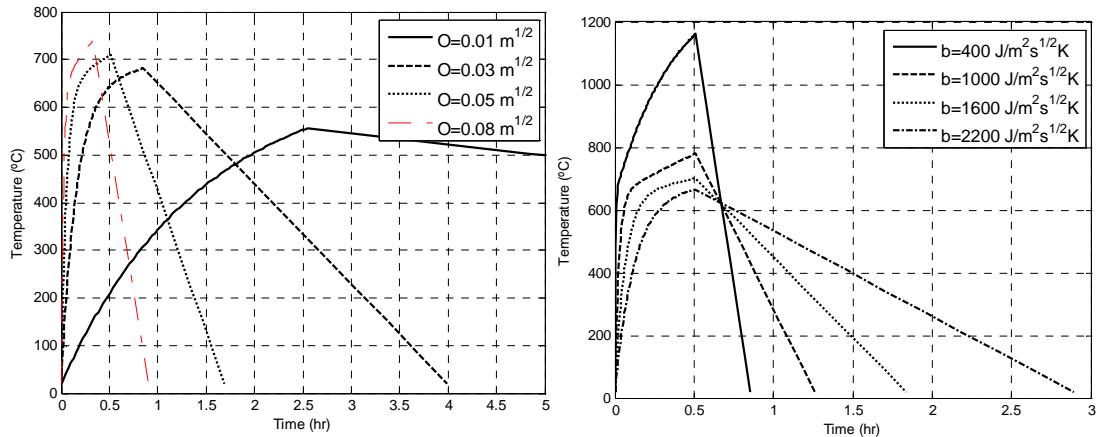


Figure 3-8 Parametric fire curves calculated according to Eurocode 1 {, 2002 #30} for (a) opening factor, O (b) thermal absorptivity, b .

The assumption of a uniform compartment temperature remains ingrained in parametric fire models. This assumption places an upper limit on the model applicability in terms of compartment size; in Eurocode 1 this limit is a compartment 500m² in plan and 4m in elevation. Experimental data from the Dalmarnock and Cardington fire tests demonstrated statistically significant thermal variation in compartments substantially smaller than this (16.6m² and 144m² respectively). These data contradict the assumption of compartment temperature homogeneity in small compartments. It is, however, not sufficient to just demonstrate that variation exists. The significance of that variation for structural performance must be demonstrated to establish whether spatial and temporal variation is an important design consideration. Furthermore in large compartments the variation in the compartment temperature field increases. The UK Eurocode 1 Annex permits use of parametric fires beyond the floor area limit of 500m², however. This is justified by assuming that all fuel is simultaneously burning producing a temperature homogeneous environment. It is thought that this will be the worst case scenario for the structure; this has not yet been demonstrated.

To demonstrate whether a non-uniform thermal environment is significant for the performance of a structure it is necessary to first to identify the effect upon structural behaviour. Section 3.2 investigates the influence of non-uniform temperature distributions for the thermal expansion behaviour of concrete; the thermal expansion behaviour is fundamental to understanding the structural behaviour at high temperatures.

3.2 Thermal expansion induced structural behaviour

Thermal expansion significantly influences structural performance in fire. The relationship between thermal expansion and fundamental structural behaviour has been established by Usmani et al. {, 2001 #138} for uniform thermal exposure. The implications of non-uniform thermal environments for structural behaviour can be explained by establishing their influence upon concrete's thermal expansion behaviour.

The concrete vertical thermal gradient dictates the thermal expansion behaviour of a structural element; this profile is a product of thermal exposure, material thermal properties and element geometry. Section 3.2.1 summarises the relationship between thermal profile and fundamental high temperature structural behaviour. The influence of specifically concrete's thermal response upon thermal expansion deformations is then analysed.

Having established the influence of concrete's thermal properties and geometry for thermal expansion behaviour section 3.2.3 investigates the influence of spatial and temporal temperature variations.

3.2.1 Thermal expansion effects for fundamental structural behaviour

Thermal strains arise from the expansion behaviour of materials under increasing temperature as discussed in chapter 2. The total strain, which dictates the structural deformation, is the sum of the thermal strains and any mechanical strains arising from restraint and/or applied load (Equation 3-2). It is the mechanical strains which determine the stress state of the structure.

$$\varepsilon_{total} = \varepsilon_{thermal} + \varepsilon_{mechanical} \quad \text{Equation 3-2}$$

If there is no applied load, when the element is unrestrained, thermal strains develop freely and the deformation is dictated purely by thermal expansion. The *mechanical strains* are zero therefore no stresses develop in the element (Equation 3-3).

$$\epsilon_{total} = \epsilon_{thermal}, \quad \epsilon_{mechanical} = 0 \quad \text{Equation 3-3}$$

If the element is then restrained against thermal expansion the *total deformation* is zero. The mechanical strain is therefore of an equal and opposite magnitude to the thermal strain (when the unloaded specimen remains straight) and gives rise to a restraining force in the element (Equation 3-4)

$$\epsilon_{total} = 0 = \epsilon_{thermal} + \epsilon_{mechanical} \Rightarrow \epsilon_{thermal} = -\epsilon_{mechanical} \quad \text{Equation 3-4}$$

The influence of thermal expansion for structural deformation has been described by Usmani et al. {, 2001 #138}. The influence has been described as two fold: pure thermal expansion and thermal bowing.

Pure thermal expansion

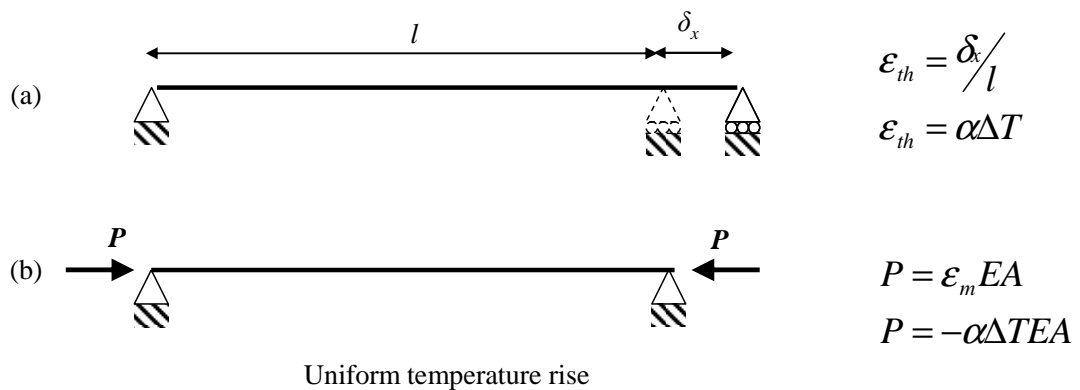
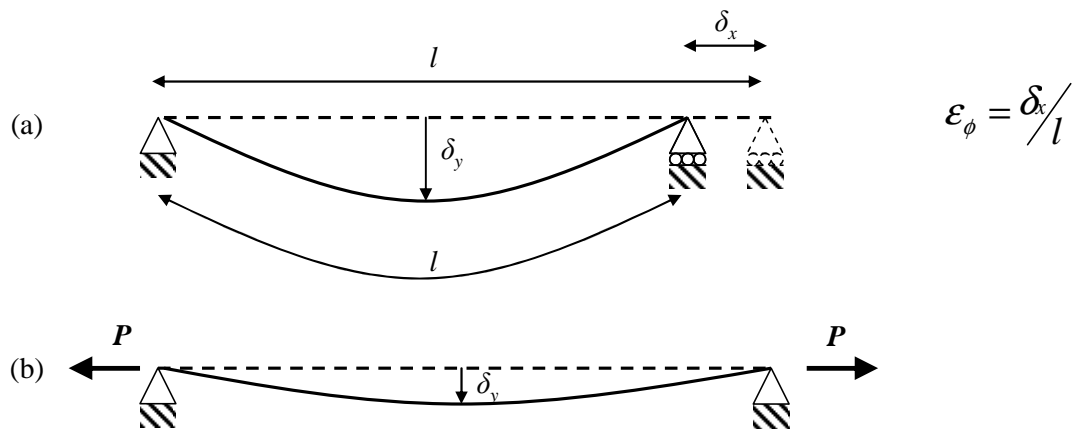


Figure 3-9 Uniform heating of an (a) unrestrained and (b) axially restrained element

An increase in the average temperature of an unrestrained element induces thermal expansion strains (ϵ_{th}) that increase the element length. Where this expansion is restrained, the axial restraining force will be compressive.

Thermal bowing



Uniform thermal gradient

Figure 3-10 (a) Unrestrained and (b) axially restrained structural element subject to a uniform thermal gradient

If there is a thermal gradient through the section, the differential rates of thermal expansion induce curvature. Where there is no increase in the centroidal temperature the length remains unchanged; however, the unrestrained ends of the element will contract to accommodate the thermal curvature. Restraint of this displacement will induce a tensile axial force in the element as shown in Figure 3-10.

The deformation response of a structure is a combination of thermal expansion and bowing. To compare the relative influence of each effect Usmani et al {, 2001 #138} have defined an effective strain where

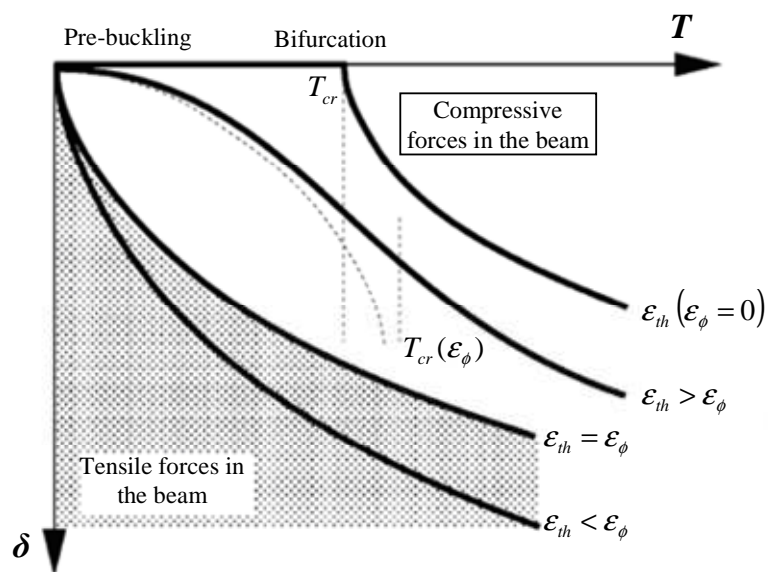
$$\epsilon_{eff} = \epsilon_{th} + \epsilon_{\phi} \quad \text{Equation 3-5}$$

The term ϵ_{ϕ} is an interpretation of the inwards displacement caused by thermal bowing as a contraction strain as shown in Figure 3-10.

Figure 3-11 summarises the spectrum of deformation responses that can arise from combinations of the thermal bowing effect and pure expansion effect. The deformation and stress behaviour is described for the case of pure expansion, dominant expansion, balanced expansion and bowing and dominant bowing. When expansion dominates the deflections are smaller and compressive restraint forces are

induced; when bowing dominates the deflections are larger and tensile restraint forces are induced.

The relative influence of each effect is determined by the through depth thermal gradient. This gradient is a product of the thermal exposure and the material thermal properties. The thermal properties of concrete are highly insulating resulting in steep thermal gradients thus increasing the influence of thermal bowing. Fast hot fires induce steeper thermal gradients compared to cool long fires which cause higher average temperatures.



Condition	Behaviour
$\epsilon_{th}(\epsilon_{\phi} = 0)$	Pure thermal expansion and no thermal bowing; when restrained induces large compressive stresses leading to either buckling, yielding or a combination of both depending upon slenderness and material strength
$\epsilon_{th} > \epsilon_{\phi}$	Expansion and thermal bowing; Expansion is dominant therefore restraining forces are compressive
$\epsilon_{th} = \epsilon_{\phi}$	Equal expansion and thermal bowing; Restraining force is zero
$\epsilon_{th} < \epsilon_{\phi}$	Expansion and thermal bowing; Thermal bowing is dominant, increased deflections and restraining forces are tensile

Figure 3-11 Thermal expansion induced deflection response for various combinations of ϵ_{th} and ϵ_{ϕ} {Usmani, 2001 #138}

3.2.2 Thermal expansion behaviour of a concrete element

The discussion of concrete's thermal properties in chapter 2 established that concrete is a highly insulating material; through depth thermal gradients in concrete are typically steep and non-linear. Figure 3-12 presents a cross-section of a typical concrete temperature profile and the associated strain and stress profiles.

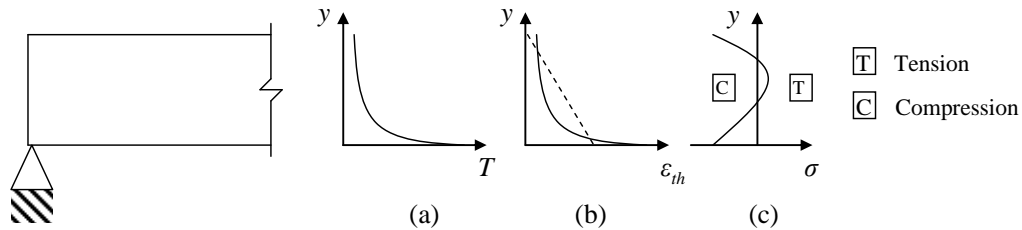


Figure 3-12 Thermal effects for concrete: cross section (a) temperature (b) strain (c) stress

The free thermal strain distribution is non-linear due to the non-linear temperature profile (Figure 3-12 (a)) and the non-linear variation of concrete thermal strain with temperature (Chapter 2). For the section to remain plane self equilibrating mechanical strains develop (Figure 3-12 (b)) resulting in stresses developing through the section despite an absence of load or restraint. The typical stress profile is presented in Figure 3-12 (c) stresses are compressive in the top and bottom extreme fibre and tensile in the mid depth region.

Thermal expansion induced deformations may be calculated using analytical methods {Usmani, 2001 #138}; however, these are complicated by concrete's non-linear thermal behaviour therefore a very simple finite element model of a plain unloaded concrete beam has been analysed using finite element software ABAQUS {, 2008 #120}.

The beam is 100 mm deep, 100 mm wide and 6000 mm in length. The heat transfer and subsequent mechanical analysis is conducted using shell elements. In an ABAQUS mechanical analysis shell elements provide greater thermal resolution through the element depth than beam elements. Up to 19 temperature definitions through the depth can be used in a shell element as opposed to 3 with a beam element; three temperature definitions is insufficient to capture the non-linear nature of concrete's thermal response.

The thermal and thermal expansion properties of concrete are taken from Eurocode 2 {, 2002 #30}. The mechanical behaviour is assumed to be linear elastic and independent of temperature to simplify the results. The deformation of the element is analysed for three restraint conditions, unrestrained, laterally restrained and laterally & rotationally restrained shown in Table 3-1.

Table 3-1 Concrete beam boundary conditions

Diagram	Name	Restrained component
	Fixed	Vertical Lateral Rotational
	Pinned	Vertical Lateral
	Simple	Vertical

The thermal expansion behaviour is interpreted using the peak span deflections, $\delta_{y,max}$, and where unrestrained the end lateral displacements, δ_x , or the axial force, P , when laterally restrained as indicated in Figure 3-13.

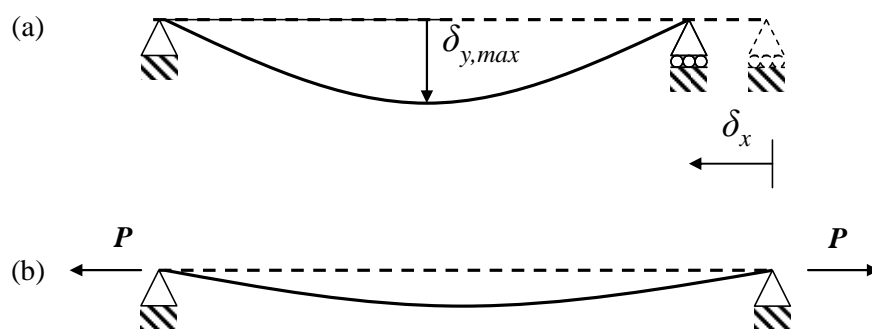


Figure 3-13 Deflection output locations for the thermal expansion analysis of a plain concrete element (a) maximum span deflection and lateral displacement (b) axial force

The thermal expansion behaviour of the plain concrete element is first investigated under uniform thermal exposure. The standard temperature time curve is used to define a uniform thermal exposure to the beam soffit. Figure 3-14 presents the central deflection of the element under each boundary condition.

A steep vertical thermal gradient induces the thermal bowing behaviour described in section 3.2.1. When thermal bowing dominates, deflection behaviour is characterised by a large increase in central deflection, this is evident in Figure 3-14. Rotational restraint opposes the curvature induced by the thermal gradient thus the central deflection for this case is zero.

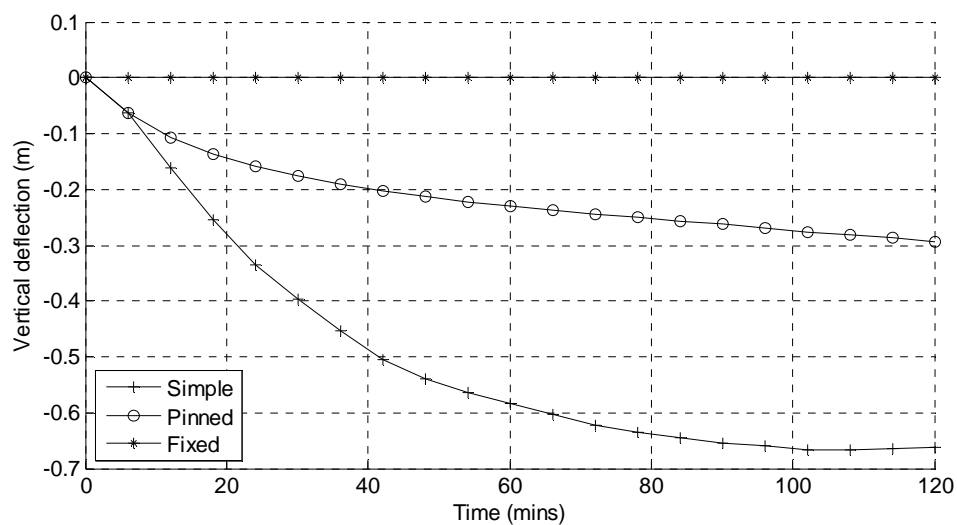


Figure 3-14 Plain concrete beam central deflection during 120 minutes exposure to the standard fire

Where the element is unrestrained the lateral displacement is negative (Figure 3-15 (a)) as the element ends ‘pull in’ to accommodate the increase in curvature. Lateral restraint opposes this pull in and therefore reduces the magnitude of central deflections which is evident when the simple and pinned cases in Figure 3-14 are compared. This restraint will also induce a tensile restraining force in the beam which can be seen in the plot of axial force in Figure 3-15 (b) (note positive values indicate tension).

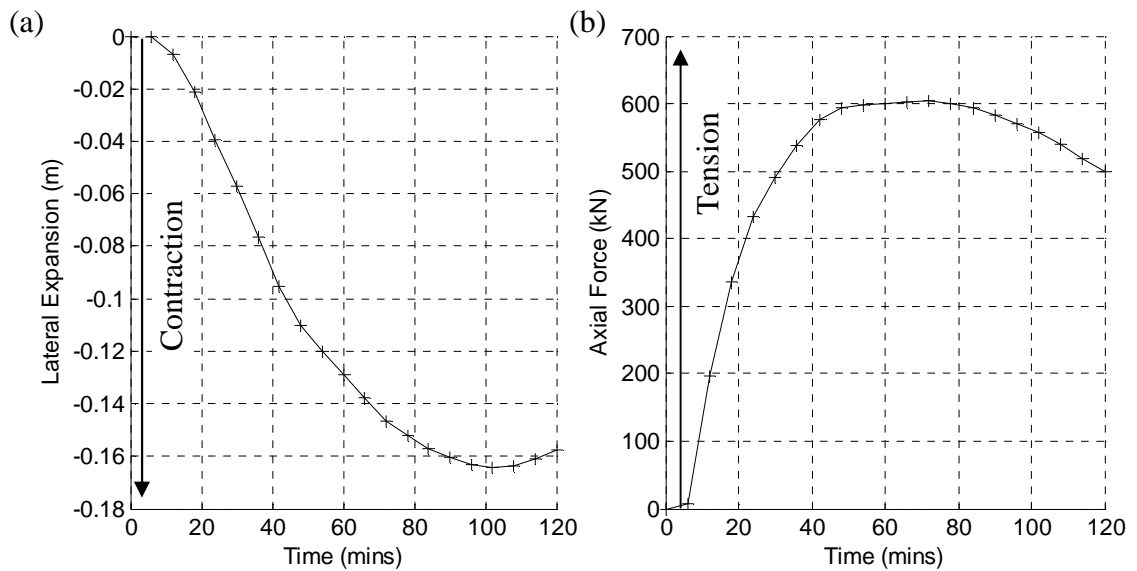


Figure 3-15 (a) Simply supported beam lateral displacement (b) pinned beam axial force during 120 minute standard fire exposure

After prolonged exposure (> 100 minutes of standard fire) the unrestrained element peak deflections and negative lateral displacement start to decrease. Figure 3-16 presents the temperature and thermal strain profiles at selected time steps. The magnitude of deflection is dictated by the curvature which is in turn dictated by the thermal strain differential through the element depth. Under prolonged exposure the differential decreases as the average temperature of the element increases and also due to the plateau in concrete thermal expansion strain at 700°C. The effect of the plateau upon the thermal strain vertical profile is visible in Figure 3-16 (b).

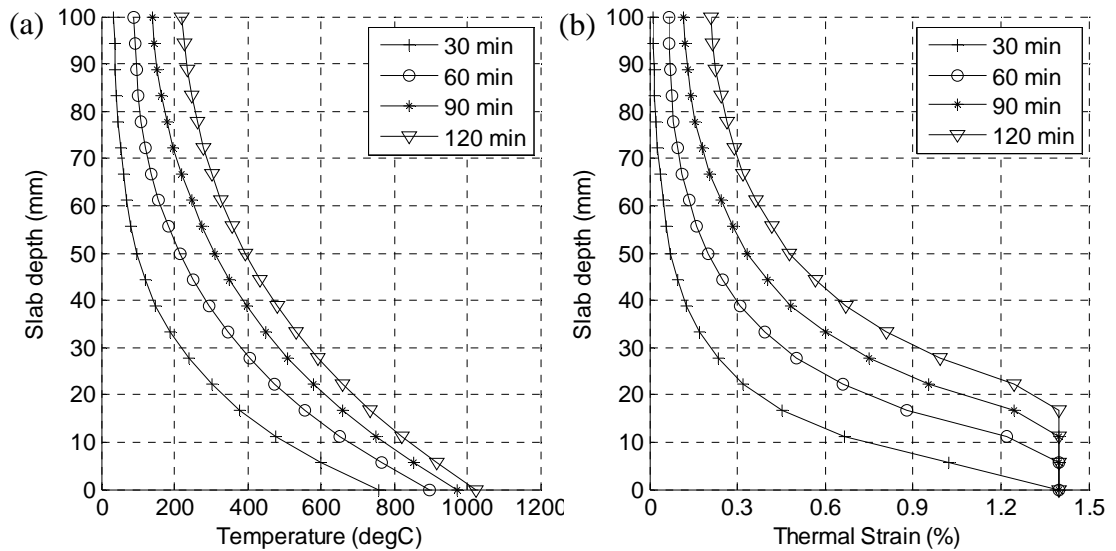


Figure 3-16 (a) Temperature profile and (b) thermal strain profile of a 100mm concrete element under standard fire exposure

Influence of element depth

The influence of increasing element depth upon the thermal expansion induced deformations is investigated. The concrete beam used in the previous investigation is reanalysed using depths of 100, 150, 200 and 250 mm. Increasing the depth of the cross section increases the proportion of cool concrete for the same exposure; this has the effect of reducing the thermal strain differential. As we saw in the previous analysis a decrease in the thermal strain differential decreases the thermal curvature and consequently the magnitude of deflection. The peak central deflections are presented in Figure 3-17. Figure 3-18 presents the (a) simply supported lateral displacements and (b) pinned beam axial forces.

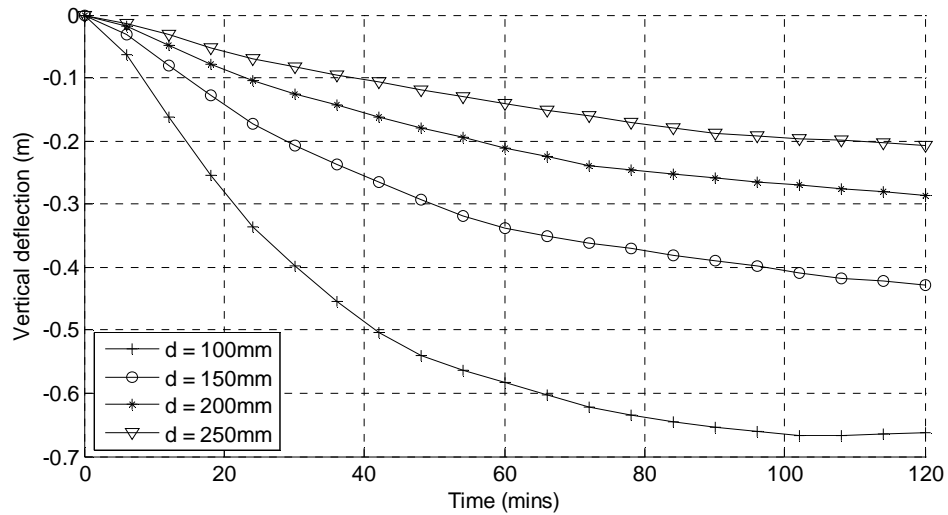


Figure 3-17 Influence of cross-section depth for simply supported beam central deflections during 120 minute standard fire exposure

An increase in element depth causes a substantial decrease in the magnitude of peak deflection and lateral displacement generated by thermal expansion. The lateral displacements we know result from the element pulling in to accommodate curvature; therefore as the curvature decreases so too does the negative displacement. In Figure 3-18 (a) it can be seen for the deepest cross-sections the lateral displacement is initially expansive. The surface temperature is not affected by the increased cross section depth. Thus the thermal strain differential in a deep cross section is reduced to such a degree that thermal expansion initially dominates over thermal bowing behaviour.

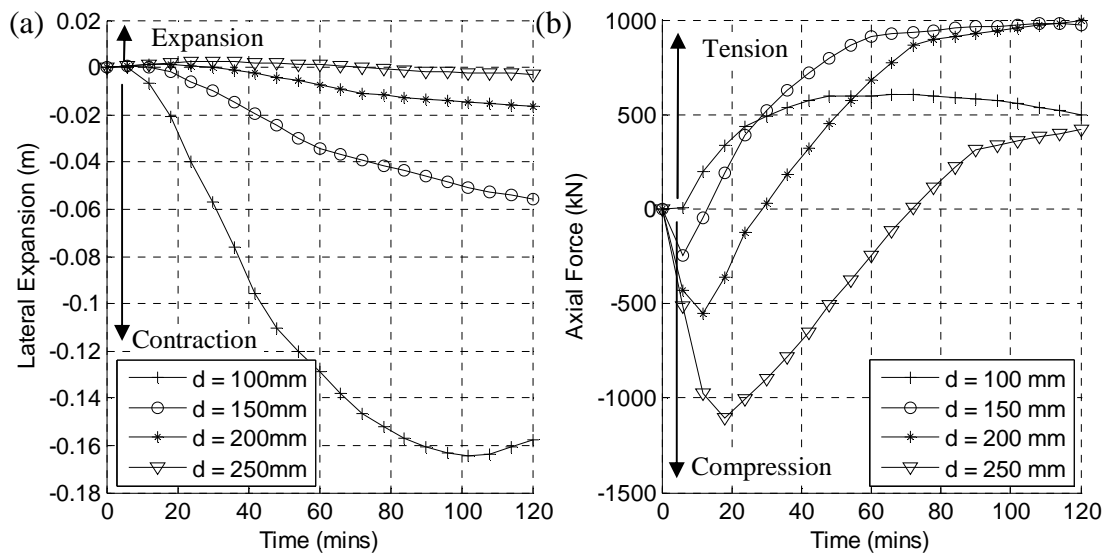


Figure 3-18 Effect of cross-section depth for the (a) simply supported beam lateral displacements (b) pinned beam axial force

Consequently in Figure 3-18 (b) we see that laterally restrained shallow elements develop significant tensile stresses whereas the behaviour of the deepest cross-section transitions from significant compression to tension.

3.2.3 Thermal expansion under non-uniform thermal exposure

The effect of a non-uniform thermal exposure is complicated by the simultaneous variation of gas temperatures both spatially and temporally. The objective of this section is to identify how non-uniform temperature distributions affect the thermal expansion behaviour of a concrete structural element. This complexity is simplified by:

- investigating first the effect of spatial temperature distributions,
- the significance of temporal variation of those distributions is then investigated.

The first step will involve analysis of thermal expansion behaviour under a static temperature distribution. This establishes theoretically what effect gas temperature variation can have upon thermal expansion behaviour.

The behaviour of the beam is then analysed for realistic spatial *and* temporal temperature exposures. This demonstrates the sensitivity of concrete's thermal response to different temporal conditions; that is, whether concrete's thermal response is sufficiently 'fast' to be affected by temporal changes encountered in a compartment fire.

Temperature spatial variations

Thermal exposure

To investigate the influence of spatial temperature variation for the thermal expansion behaviour of the concrete beam a simple linear variation of gas temperature along the beam length is used. A linear variation is an over simplification of the thermal variation found in a compartment fire. However, it allows for the thermal expansion behaviour of concrete under different magnitudes of variation with an equivalent average temperature to be contrasted. Figure 3-19 (a) presents the temperature spatial distribution schematically. Different magnitudes of variation, V %, about the average temperature, T_{ave} °C are considered. In this

investigation the thermal and mechanical response of the concrete element using $V = 0\%$, 20% , 40% , 60% and 80% is analysed. Figure 3-19 (b) presents the temperature history; the evolution of the average temperature with time is defined by the standard temperature-time curve.

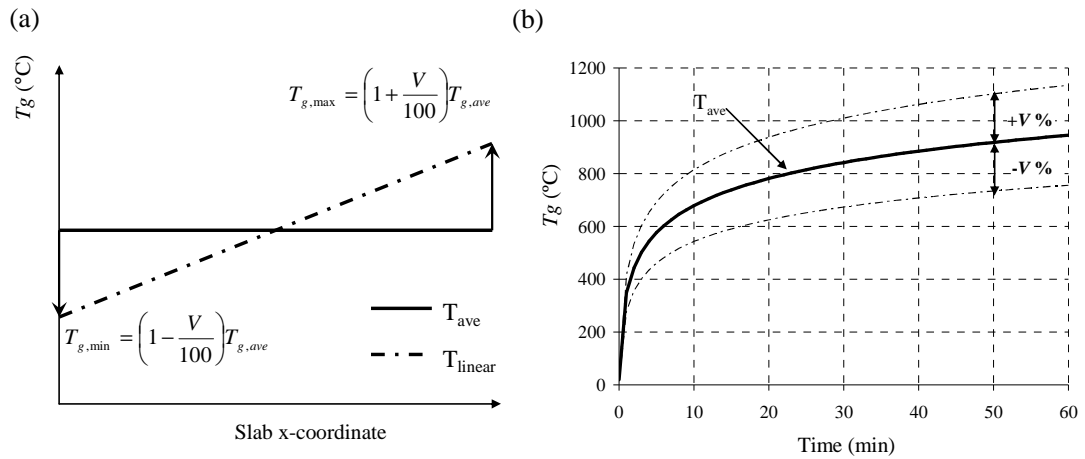


Figure 3-19 (a) Linear variation of gas temperature along beam x-axis (b) evolution of gas temperature with time

Structural response

Under exposure to a constant temperature in the x-direction the beam thermal curvature is constant hence thermal expansion produces a symmetrical deflection profile. If the gas temperature is variable in the x-direction the vertical thermal gradient responsible for thermal curvature will also vary in the x-direction. This longitudinal variation of thermal curvature distorts the element deflected shape. Figure 3-20 presents the deflection profiles for the simply supported element under increasing horizontal gas temperature variation, V .

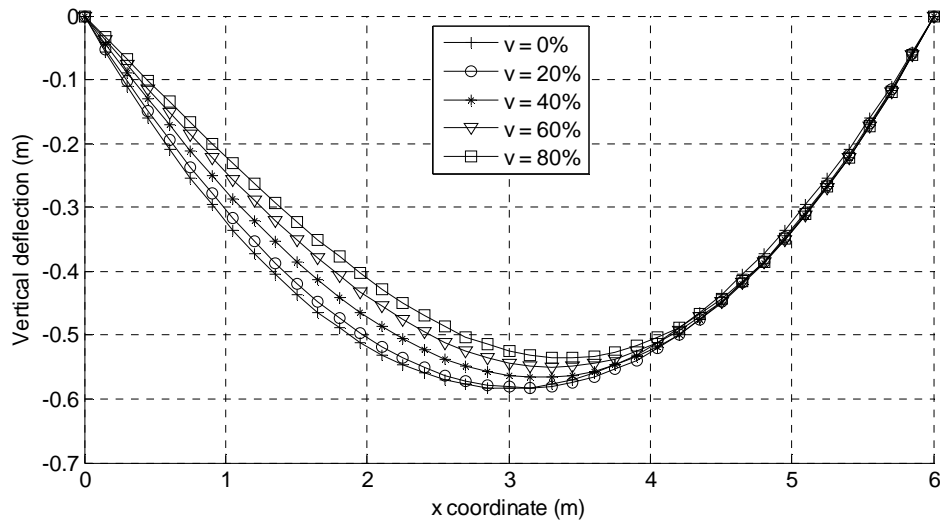


Figure 3-20 Influence of a non-uniform thermal exposure for deformation of a horizontal concrete element: Simply supported beam deflection profile 60 minutes exposure

Thermal curvature is greatest under the peak temperature ($x = 6 \text{ m}$); consequently the position of peak deflection shifts from the mid span towards the peak temperature location. The distortion of the deflection profile is most prominent for the most severe variation, $V = 80\%$ considered.

Figure 3-21 compares the evolution of peak deflection under increasing horizontal temperature variation (V). The magnitude of peak deflection is not substantially influenced by the thermal variation used in this investigation. Initially the highest thermal variation causes the largest peak deflections; however, under prolonged exposure the lowest variation (0%) produces the greatest deflections. As seen in section 3.2.2 this is due to the reduction in thermal strain differential caused by increasing average temperature and concrete's thermal strain plateau.

The effect for peak deflection magnitude is strongly dependant upon not just the distribution of temperatures but also the magnitude of temperature thus general conclusions concerning the effect of non-uniform temperatures for peak deflections cannot be drawn from this investigation.

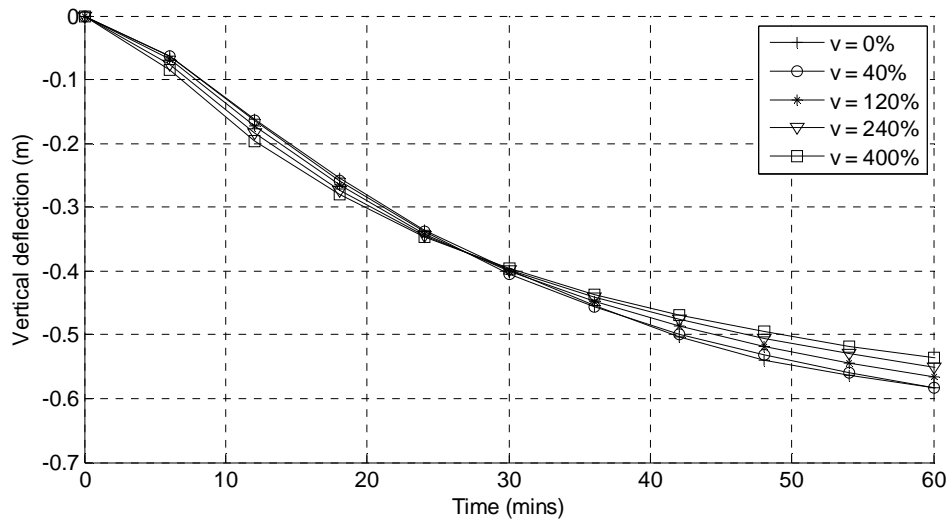


Figure 3-21 Influence of increasing horizontal variation in gas temperature upon the peak beam deflection

The same effect can be seen in the simply supported lateral displacements which are plotted in Figure 3-22 (a). The pinned beam axial force under increasing horizontal temperature variation (V) is plotted in Figure 3-22 (b); again the change in axial force magnitude is not substantial being linked to the lateral displacements.

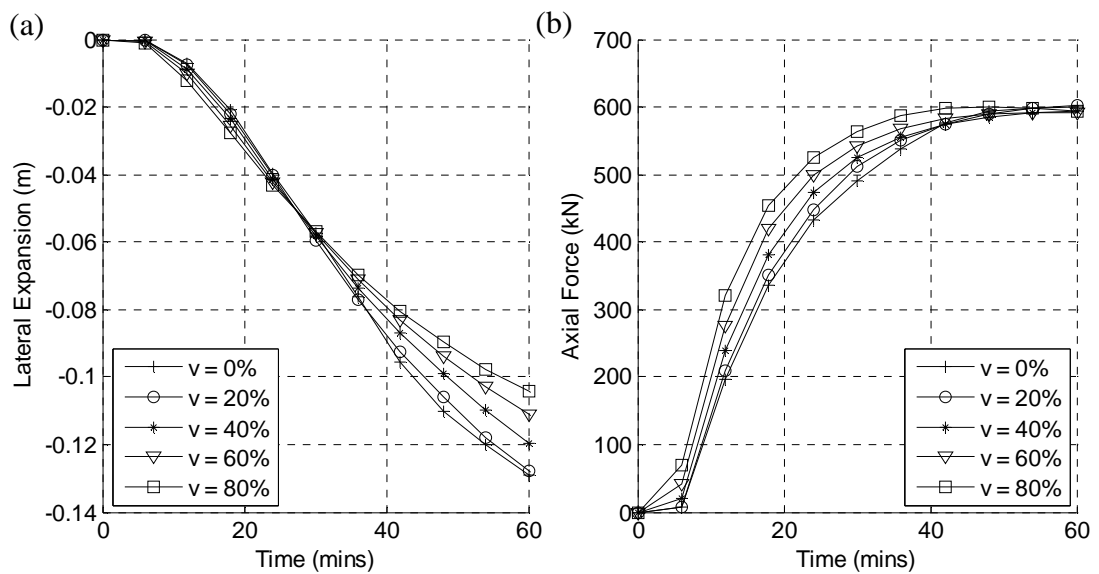


Figure 3-22 Influence of horizontal temperature variation for (a) simply support beam lateral displacement (b) pinned beam axial force

Influence of element depth

In section 3.2.1 it was shown that as the depth of section increases the dominance of thermal bowing decreases also and the influence of expansion increases. The

principle effect of a spatial variation in gas temperature for the shallow concrete element considered previously was to distort the deflection profile by inducing horizontal variation in thermal curvature. As the effect of thermal curvature diminishes in deeper cross sections it should follow that the distorting effect of a gas temperature variation decreases also. Figure 3-23 presents the deflection profiles for different depths (d) of beam for the most severe horizontal variation considered, $V=80\%$. As the depth of the cross section increases the distortion of the deflection profile is visually less evident.

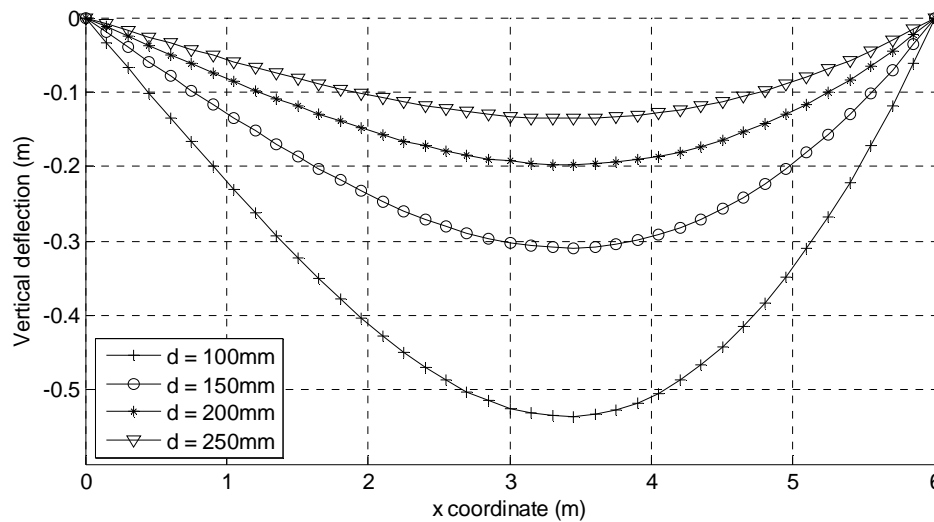


Figure 3-23 The influence of cross section depth for the deflection profile under horizontal gas temperature variation, $V = 80\%$.

Expansion dominated behaviour is characterised by elongation; therefore deflections are low and restraining forces are compressive. Figure 3-24 presents the influence of increasing thermal variation upon the (a) simply supported lateral displacement and (b) pinned axial force of the deepest cross section, $d = 250$ mm. The effect of increasing thermal variation for the thermal exposure considered is not substantial as each exposure has the same average temperature.

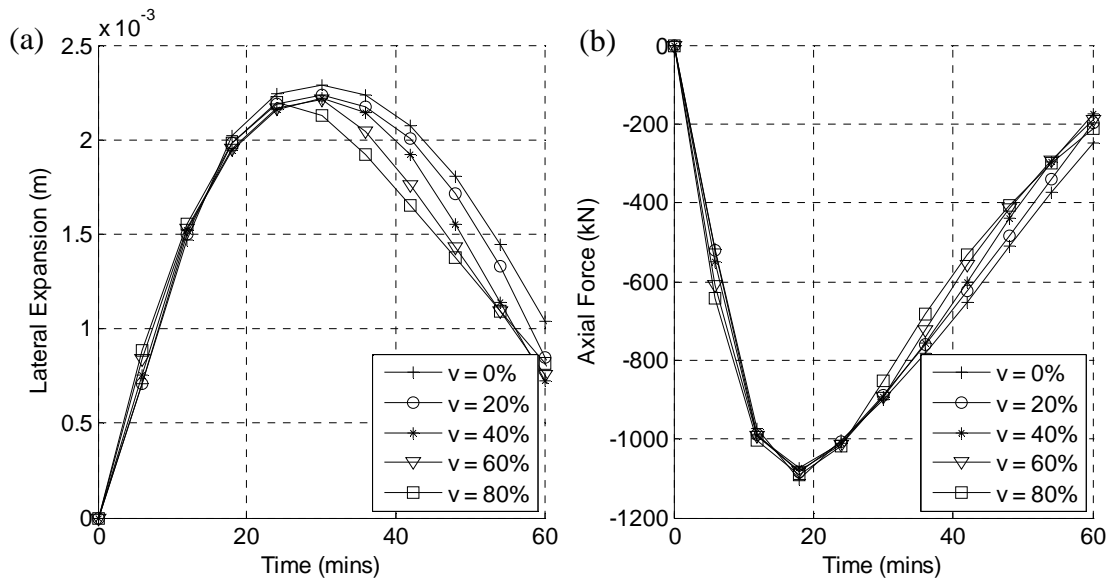


Figure 3-24 Influence of horizontal temperature variation upon (a) simply supported lateral beam displacements (b) pinned beam axial forces

Temporal changes in spatial distribution

The effect of a simple static temperature distribution for the thermal expansion behaviour of a concrete beam has been investigated. Having established the influence of a spatial gas temperature variation for the thermal expansion behaviour of a beam, the sensitivity of concrete's thermal expansion behaviour to spatially *and* temporally varying gas temperatures is now investigated. This will establish whether under realistic fire imposed thermal conditions concrete is affected by thermal variation. For this reason the spatial and temporal temperature variations employed in the investigation must be of a realistic nature.

Thermal exposure

A fire within a compartment produces a gas temperature distribution; as fuel is consumed that temperature distribution will change. The rate of fuel consumption is dependant upon the burning rate which also influences the gas temperature distribution. A high burning rate produces a fast changing thermal environment and high gas temperatures; a slow burning rate produces slow changing thermal environment and lower gas temperatures. Alpert {, 1972 #217} empirically correlated the burning rate Q_c and ceiling temperature $T_{ceiling}$ at radial distance r to the fire plume using Equation 3-6 and Equation 3-7:

For $r < 0.18H$

$$T_{ceiling} = 20 + \frac{16.9\dot{Q}_c^{2/3}}{H^{5/3}} \quad \text{Equation 3-6}$$

For $r \geq 0.18H$

$$T_{ceiling} = 20 + \frac{5.38(\dot{Q}_c / r)^{2/3}}{H} \quad \text{Equation 3-7}$$

Where H is the ceiling height (m); the correlation is based on a series of large scale tests which involved the burning of substantial fires (4.2 up to 98 MW) under flat ceilings at various heights (4.6 to 15.5m). The shape of the temperature distribution is presented in Figure 3-25.

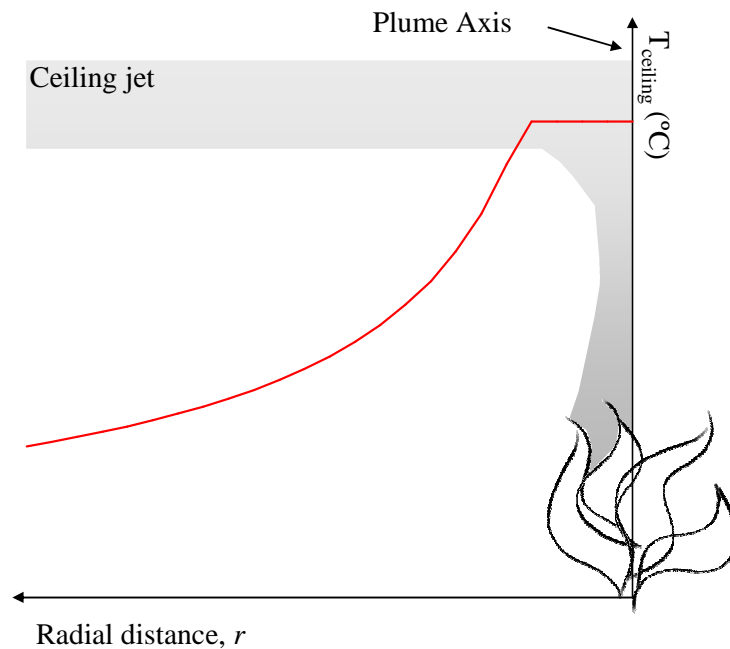


Figure 3-25 Alpert correlation for maximum ceiling temperature and fire burning rate

Alpert's correlation can be used to produce a range of static gas temperature distributions by varying the burning rate. Using the compartment fuel load and the burning rate we can calculate the total time for fuel consumption (burn out time). The temporal change in gas temperature distribution is achieved by moving the Alpert plume axis along the length of the compartment at a rate prescribed by the burn out time and the compartment geometry.

For this investigation burning rates of 60MW, 38MW and 20MW were chosen to represent a fast, medium and slow fire. The thermal exposure for each burning rate is formulated in two steps:

- 1) Calculate burn out time, t_b , and plume axis velocity, u_p
- 2) For each time increment calculate temperature distribution

Step 1: Burn out time and plume axis velocity

The burn out time is calculated using the fuel load density and the burning rate:

$$t_b = \frac{\text{Fuel Load Density}}{\dot{Q}_c} \quad \text{Equation 3-8}$$

Only one dimensional variation (x direction) is considered in this analysis therefore the fuel load density is expressed as a linear fuel load in the direction of variation. The plume velocity is calculated using the burn out time and the compartment length in the direction of variation:

$$u_p = \frac{t_b}{L} \quad \text{Equation 3-9}$$

Alpert's correlation is valid for smoke layers where horizontal travel is unimpeded and a static layer of gas does not develop. This is achieved if there is a clear horizontal distance of at least $3H$ between the plume axis and the nearest vertical impediment {Drysdale, 1998 #17}. This makes the correlation applicable for fires in large compartments where the fire is remote from vertical barriers. A compartment length of $L = 18$ m is used and a ceiling height, $H = 6$ m.

Step 2: Calculation of temperature distribution

The gas temperature distribution along the length of the compartment ceiling is calculated at each time, t_i . For each time step the location of the plume axis is first calculated:

$$x_i = u_p (t_{i-1} + \Delta t_i) \quad \text{Equation 3-10}$$

The magnitude of r at this location is set to zero and the Alpert temperature distribution calculated using Equation 3-6 and Equation 3-7. The gas temperature distributions at different time increments are shown schematically in Figure 3-26.

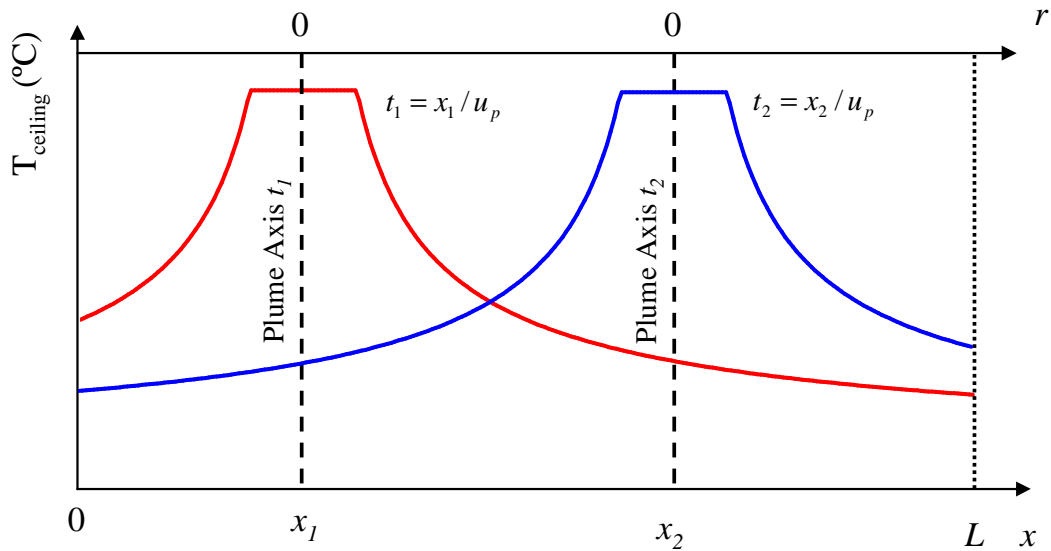


Figure 3-26 Ceiling gas temperature distribution at 2 different time steps

Temporal and spatial gas temperature distributions are calculated for each burning rate. In Figure 3-27 the temperature distributions for each burning rate considered are plotted at $t = 0$ for comparison. The maximum temperature increases as the burning rate increases, thus the fastest burning rate produces the hottest fire and the shortest burn out time.

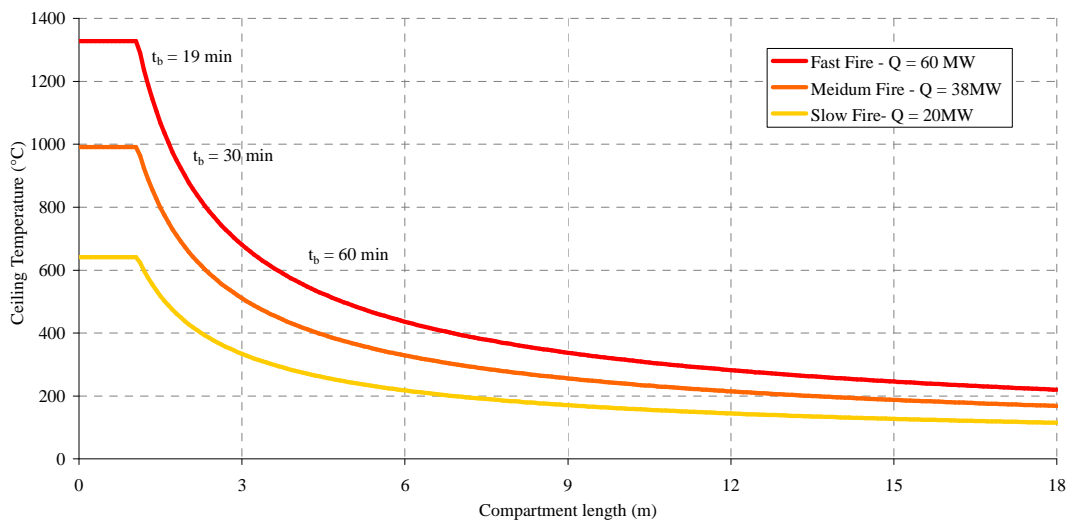


Figure 3-27 Temperature distributions calculated according to Alpert [1972 #217] for burning rates of 60, 38 and 20 MW and ceiling height 6m at $t = 0$ seconds

In this analysis the behaviour of a single element is considered and the surrounding structure is represented by a considering a range of boundary conditions. The

compartment length is in excess of the beam span considered therefore the 6 m plain concrete beam element is assumed to span from $x = 6 - 12$ m. Figure 3-28 presents the spatial distribution of gas temperature along the beam length at selected time steps for the fast fire.

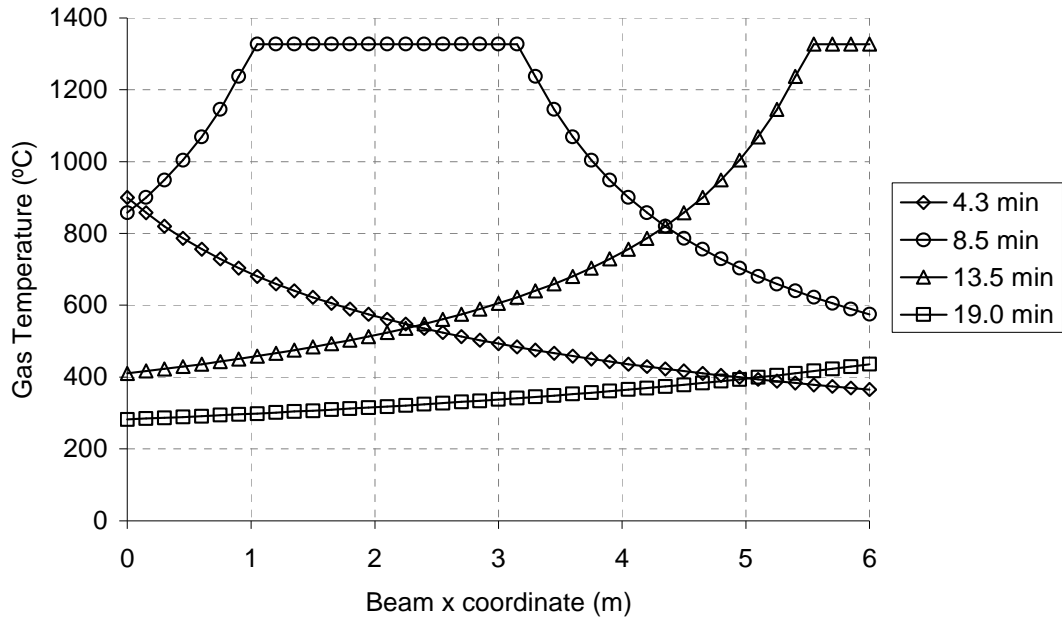


Figure 3-28 Spatial distribution of gas temperature in the beam x-coordinate for the fast burning rate at selected time steps.

Structural response

Figure 3-29 presents both the evolution of maximum vertical deflections and vertical deflection profiles in separate plots for each of the three fires: fast, medium and slow. The maximum vertical deflections are presented in the top row; for each fire the maximum vertical deflection for the pinned and simply supported boundary conditions are presented. The fixed boundary condition is not included as it was shown in Figure 3-14 that rotational restraint opposes thermal curvature producing zero deflection. The phase during the fire when the peak temperature traverses the element span is highlighted in yellow. The temperatures of the fast fire are higher than those of the slow fire; in concrete this increases the thermal bowing effect therefore the deflections in the fast fire are greater than those caused by the medium and slow fire. This behaviour has been previously documented {Lamont, 2003 #7}.

It is clear in each fire that the evolution of peak deflection exhibits three distinct phases: (a) gradual initial increase (b) a sharp increase as the plume & peak

temperature traverses the element (c) and finally a reduction after the peak temperature has passed.

Prior to the plume traversing the element temperatures increase gradually, hence the deflection response is gradual. As the plume and peak temperature traverse the element the surface temperature increases enhancing the thermal bowing effect and increasing the rate of deflection. The drop in temperature after the plume passes causes the surface temperature to drop. The influence of thermal bowing decreases and so the peak deflections decrease.

It has been shown in the previous investigations that spatial variation of gas temperature produces variation of thermal curvature along the beam element distorting the deflection profile. Figure 3-29 presents the deflection profiles under each fire separately for selected time steps. For each fire the distortion of the deflection profile is visually evident. As the peak temperature traverses the span the location of peak deflection shifts in response to the changing thermal curvature along the length of the element.

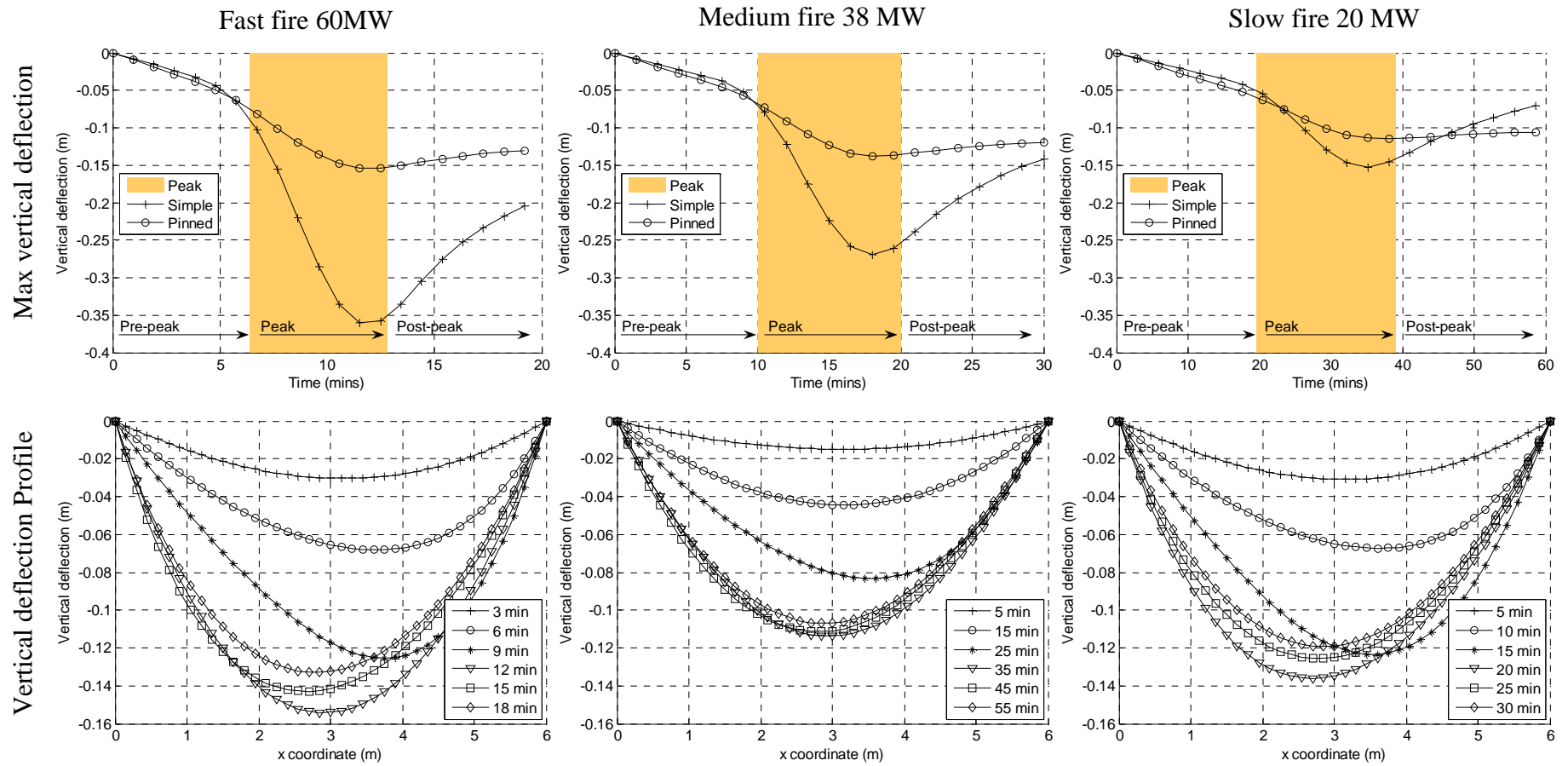


Figure 3-29 Sensitivity of concrete's thermal expansion deformations to a fast, medium and slow changing fire: Maximum vertical deflections and deflection profiles

Influence of cross-section depth

In section 3.2.1 it was shown that increasing cross-sectional depth reduced the effect of thermal bowing. The effect of spatial gas temperature variation for deep cross sections was substantially reduced. Figure 3-30 contrasts the deflection profiles of the simply supported 250 mm deep beam during the fast, medium and slow fires.

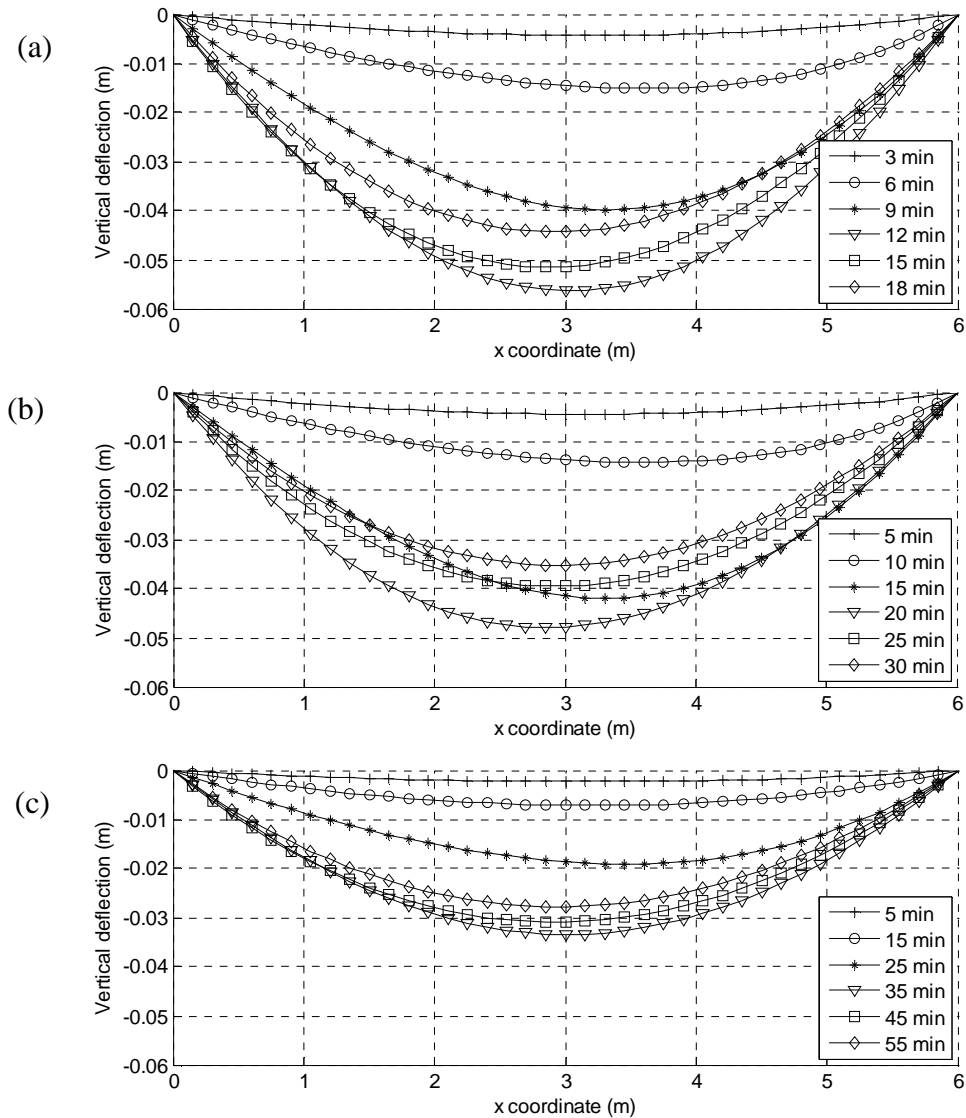


Figure 3-30 Sensitivity of a deep concrete beam's ($d=250\text{mm}$) thermal expansion deformations to (a) fast (b) medium and (c) slow changing fire: Deflection profiles.

Distortion of the deflection profile is still evident for all fire exposures. The distortion is however, much less significant than that exhibited by the shallow concrete beam.

3.3 Conclusions

Full scale experimental compartment fire data has shown that the temperature field within a fire compartment varies both spatially and temporally. From fire dynamics we know that this variation is likely to increase in larger compartments.

This variation is ignored in the analysis of structural performance at high temperature in both small ($< 500 \text{ m}^2$) and large ($>> 500\text{m}^2$) compartments. In small compartments it is assumed that the amount of thermal variation is not high despite recent contradictory experimental data. In large compartments is assumed that burning everywhere will produce a homogeneous compartment temperature which is the worst case for the structural performance. The implications of the likely spatial and temporal variations in temperature for structural behaviour have not been investigated to fully substantiate this justification.

The thermal expansion behaviour of structures is a fundamental component of understanding high temperature structural behaviour. The thermal expansion behaviour of concrete under uniform thermal exposure is investigated. It is found that the behaviour of shallow concrete cross-sections is dominated by thermal bowing which induces large deflections and tensile restraining forces. Increasing depth of section decreases the influence of thermal bowing and behaviour tends towards being dominated by expansion. Behaviour is then characterised by low deflections and compressive restraining forces.

The effect of a non-uniform thermal exposure for concrete thermal expansion behaviour was investigated in two stages to simplify the complexity of simultaneous spatial and temporal variation. The effect of a spatial variation was first investigated.

Spatial variation of the gas temperature causes variation in the vertical thermal curvature. In shallow concrete elements which are susceptible to thermal bowing effects this induces non-symmetrical deflection profiles. In deep concrete elements expansion dominates over thermal bowing behaviour therefore reducing the influence of the spatial gas temperature variation.

For both the shallow and deep concrete elements the gas temperature variation does not substantially influence the simply supported condition lateral displacements

under simply supported boundary conditions. This is due to the linear distribution of gas temperature and the common average temperature for each exposure.

Spatially and temporally varying gas temperature distributions have been formulated using Alpert's correlation of burning rate and ceiling temperature. A fast, medium and slow burning rate were chosen to compare the sensitivity of concrete's thermal expansion behaviour to temporally changing thermal environments.

It was found that for a shallow concrete beam the distortion of the deflected profile was evident for all three burning rates. The thermal expansion behaviour of the shallow concrete element is dominated by the temperatures near the surface which induce thermal bowing. The insulating nature of concrete's thermal response means the surface temperature responds quickly for all temporal variations considered and therefore the distortions they cause were also evident. The behaviour of the deep concrete beam however was increasingly less susceptible to this distortion as the burning rate decreased.

4 Benchmark structural model

In this chapter a benchmark structural finite element model is developed. A two-way spanning reinforced concrete slab is used as the benchmark structure. Reinforced concrete slabs have been studied extensively in the context of steel-concrete composite structures in fire due to performance enhancing stability mechanisms such as compressive membrane action and tensile membrane action they exhibit. Full scale fire tests were undertaken at Cardington {Bravery, 1993 #179} which in addition to smaller single span tests {Lim, 2004 #12} have been used to validate numerical models {Huang, 2003 #185; Elghazouli, 2000 #182; Foster, 2007 #183; Gillie, 2000 #186} and subsequent design methodologies {Bailey, 2000 #214; Usmani, 2004 #151} which have been employed here in the UK {Bailey, 2001 #65} and abroad {Clifton, 2006 #215}. The depth of understanding of the behaviour of these slabs in fire makes them an ideal case study for investigating the implications non-uniform thermal exposure has for well established mechanisms of stability.

Section 4.1 summarises the known behaviour of two-way spanning slabs at elevated temperature and section 4.2 discusses the finite element modelling of tensile membrane behaviour.

In section 4.3 the finite element model developed in this thesis is described and the behaviour of the slab analysed under uniform thermal exposure. There are two purposes to this analysis:

- Verify slab membrane behaviour
- Develop performance indicators for use in the investigation of non-uniform thermal exposure effects upon structural behaviour in chapter 5

Section 4.4 presents geometric parametric studies to identify any variations in slab behaviour. Section 4.5 presents material parametric studies to identify the model sensitivity to different material models discussed in chapter 2.

4.1 Behaviour of two-way spanning slabs in fire

Two-way spanning concrete floor slabs are a feature of traditional concrete construction where vertical support at all edges is provided by beams or walls. They

are also encountered in composite concrete-steel construction, where the steel frame supports concrete floor plates. Figure 4-1 presents the typical load-deflection behaviour of a reinforced concrete slab at ambient and elevated temperatures.

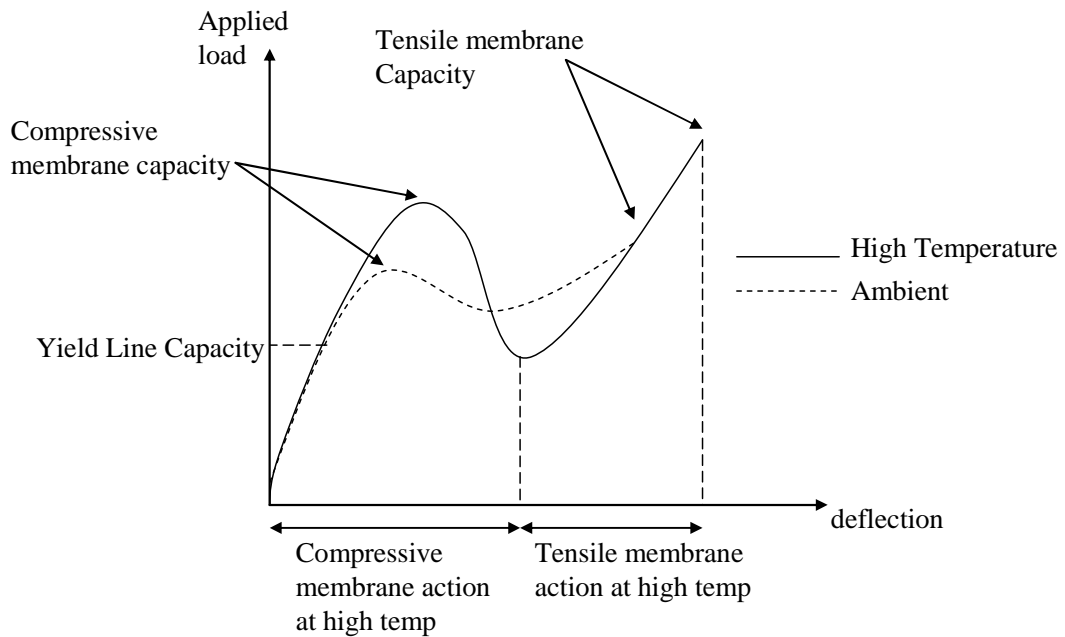


Figure 4-1 Characteristic load-displacement curve for reinforced concrete slabs at ambient and elevated temperatures

As slab deflections increase the flexural capacity either disappears or is significantly reduced. At the same time increasing deflection results in the slab pushing out at the edges, where restraint exists this induces in plane compressive stresses in the slab, hence this is known as compressive membrane action. The line of thrust generated by horizontal restraint through the slab is shown schematically in Figure 4-2.

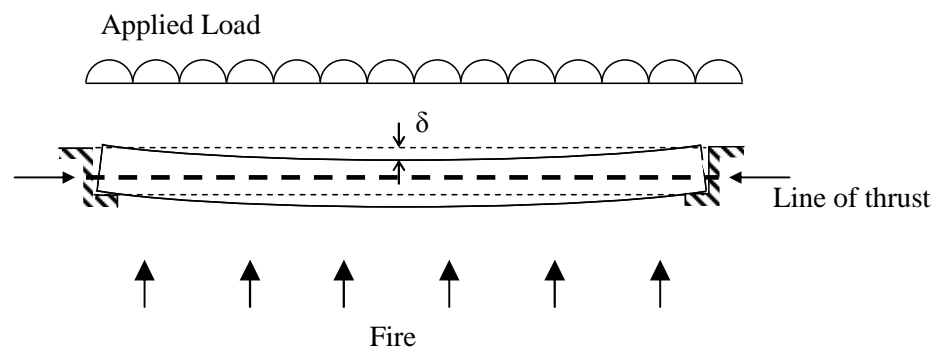


Figure 4-2 Role of lateral restraint in the development of compressive membrane action

When the central deflections increase beyond the level of this line of thrust tensile stresses and cracking develops at the mid span of the slab. The portion of the slab in tension hangs by catenary action anchored by either the surrounding ring of compression or lateral restraint where it exists; this is referred to as tensile membrane action.

The capacity afforded by tensile membrane action is similar to that of compressive membrane action; deflections can often therefore increase rapidly when transitioning from compressive membrane action to tensile membrane action. As the slab continues to deflect an increasing proportion of the slab is supported by catenary action. The slab ultimately fails due to either reinforcement rupture or crushing of the concrete at the slab corners {Bailey, 2007 #212}. In Figure 4-1 the tensile membrane capacity of the slab at elevated temperatures is shown to be greater than that achieved at ambient temperatures. The thermal bowing caused by exposure to fire (that is the curvature caused by differential rates of thermal expansion) enhances the tensile membrane capacity by increasing deflections without increasing mechanical strains {Lange, 2009 #180}.

4.1.1 Influence of restraint

Under fire exposure the development of compressive membrane action is dependent upon horizontal restraint resisting thermal expansion thereby inducing large in-plane compressive stresses in the slab. The position of this line of thrust was shown by Lim et al. {, 2004 #12} to be critically important for the development of compressive membrane action. From Figure 4-2 we can see that the higher the position of the line of thrust in the structural cross-section the more rapidly deflections will exceed this distance and the viability of compressive membrane action lost.

Lateral restraint is not necessary for the development of tensile membrane action in two way spanning reinforced concrete slabs. The slab deformation is one of double curvature; this geometric form leads to the development of a self supporting ring of compression at the slab periphery (Figure 4-3).

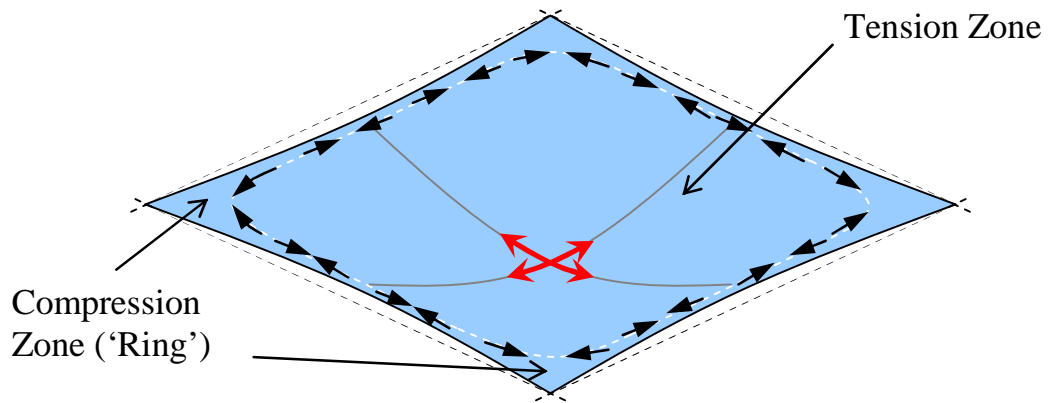


Figure 4-3 Tensile membrane action in an unrestrained floor slab

This ring of compression supports the internal portion of the slab which at large deflections is supported by catenary action. It is therefore very important that vertical lines of support are maintained at the slab edges to allow double curvature to develop. If the slab is laterally restrained, stability is less dependent on the compressive ring and a greater proportion of the slab can be supported by catenary action.

The initial slab lateral movements are expansive; however, at increasing deflections the slab mid-span edge starts to pull in to accommodate the large central deflections, thus any boundary conditions must be able to resist or accommodate this movement.

4.1.2 Failure mechanism

The definition of failure for a two way spanning slab in fire is difficult and dependent upon the circumstance. In structural fire engineering there are three criteria which can result in failure: integrity, insulation and stability. In this study we focus on failure by loss of stability.

Bailey and Toh {, 2007 #212} investigated failure mechanisms of small scale lightly reinforced concrete slabs at ambient and elevated temperatures. At ambient temperatures the failure mechanism has been found to be either rupture of the short span reinforcement at the mid span or by crushing of the concrete at the slab corners. Whether crushing or reinforcement rupture occurs will depend upon the reinforcement ductility and reinforcement ratio. High reinforcement ductility and/or ratios will result in failure of the slab by compressive concrete crushing. At elevated temperatures they consistently found reinforcement rupture to be the failure

mechanism. Bailey and Toh {, 2007 #212} stated that where the high temperature reinforcement ratio remained equivalent to the ratios leading to crushing failure at ambient temperature, concrete crushing is a possible failure mechanism. Their study focused on a lightly reinforced concrete slab typical of those used as part of concrete-steel composite construction; however, the reinforcement ratio in a concrete structure will be much higher.

Failure by crushing of concrete or by reinforcement rupture assumes that the surrounding structure is capable of resisting the pull-in forces generated at large deflections and that vertical lines of support are maintained at the slab edge. An accurate description of either failure mechanism requires detailed consideration of concrete cracking and crushing and reinforcement rupture. In the following section the characterisation of these features of behaviour in a finite element model are discussed.

4.2 Finite element modelling of reinforced concrete slabs in fire

4.2.1 Thermal modelling

It has been shown {Gillie, 2004 #210} that the thermal gradient through the structural cross section is primarily responsible for the deflections achieved and the reduction in material strength a secondary cause. It is therefore important to make a reasonable estimate of the through depth temperature gradients. This is particularly true when considering the effects of a non-uniform thermal environment which will result in a variation of the thermal profile in the concrete structure.

While the development of stress and strain is heavily dependent on the temperature distribution in the structure, the reverse is not true. Temperature evolution is generally deemed to be independent of the stress state. This allows the thermal and stress analysis to be decoupled which typically improves computational efficiency.

The thermal analysis may therefore be performed as a coupled heat and mass transfer analysis. Moisture migration, pore pressures and thermal distributions are analysed simultaneously, or moisture effects may be neglected and only thermal distributions calculated. Purkiss {, 2007 #86} has compared the predictions of a fully coupled heat transfer analysis and a simplified analysis considering only temperature evolution

with experimental results and found the simplified model (which neglects moisture effects) to provide adequate estimates of the temperature evolution.

4.2.2 Finite element requirements

It is computationally and mathematically advantageous to model a slab as a 2D surface rather than a 3D body. This involves sacrificing some of the detail of behaviour, however the mathematical advantages are sufficiently strong that this sacrifice is acceptable {Calladine, 1983 #213}; Shell theory has therefore been widely applied to the analysis of reinforced concrete slabs both at ambient and elevated temperatures {Gillie, 2000 #186; Huang, 2003 #193}. Finite elements that use both thick {Huang, 2003 #193} and thin {Lim, 2004 #12} plate theory have been validated against (separate) experimental results {Lim, 2004 #12}. Thin plate theory (Kirchoff) assumes that the transverse shear stiffness is negligible; thick plate theory (Mindlin/Reissner) considers shearing distortion to be important and therefore considers the transverse shear stiffness in the finite element formulation. As both thin and thick plate theory have provided satisfactory results it is unlikely that shear distortion is critical, particularly for slabs with a low slenderness ratio.

Previous research has shown that a high temperature finite element model of reinforced concrete slabs must be capable of capturing the following behaviour {Huang, 2003 #193; Gillie, 2001 #208}:

- non-linear thermal variation through depth;
- variation of material properties with temperature;
- thermal expansion;
- geometric non-linear behaviour; and
- material non-linear behaviour including the post peak behaviour under compression and tension (crushing and cracking).

The treatment of cracking and crushing has been an extremely active area of research in the field of numerical analysis of concrete it is therefore discussed in more detail in Section 4.2.3.

4.2.3 Modelling cracking and crushing in a finite element analysis

In Chapter 2 the behaviour of concrete under both compression and tension was discussed together with the material models formulated to describe that behaviour for a stress analysis. Under compressive loading the concrete strength-deformation response is highly non-linear and characterised by crushing after the peak stress has been reached. Under tensile loading cracking is the dominant behaviour. Both cracking and crushing are localised leading to a physical discontinuity in the concrete structure; special attention is therefore required to address both phenomena in a finite element analysis in which the concrete is assumed to be homogeneous.

The following section discusses how the material models from Chapter 2 are implemented in the finite element analysis in this study.

Tensile cracking

The cracks that occur within concrete are physical discontinuities which must be represented in the finite element mesh. A number of methods have been developed to represent tensile cracking in a finite element mesh, these include:

- discrete cracking;
- embedded finite element method (EFEM or XFEM); and
- smeared cracking.

Discrete cracking models are closest to reality, as an actual gap is introduced into the finite element mesh. Crack paths may be predefined (i.e. cracking is forced to occur along existing boundaries), or cracks may be allowed to propagate automatically requiring adaptive meshing techniques. For both methods, interface elements are inserted in the gap to model the tension softening behaviour across the crack. Predefined crack paths are possible only when the crack trajectory is known in advance. For more general cases automatic crack propagation is required. Either method provides a detailed description of crack evolution; however, there are several challenges associated with discrete automatic crack propagation models. Firstly, automatic crack propagation poses significant computational challenges including the use of complex remeshing algorithms and calculation of crack propagation criteria at the crack tip {Yang, 2004 #161; Yang, 2005 #162}. Secondly, increasingly

fine and complex meshes can arise from adaptive remeshing for tortuous crack paths. As the element size approaches the scale of the material constituents (for example aggregate), the assumption of material homogeneity becomes less valid.

Embedded FEM or XFEM (eXtended Finite Element Method) models have been developed more recently with the aim of providing a more detailed prediction of crack evolution associated with discrete crack models combined with the computational efficiency of the smeared crack model. Finite element displacement functions are enriched using additional displacement functions and degrees of freedom that represent a discontinuity (crack) within a finite element {d'Avila, 2008 #92}. The crack is therefore represented independently of the mesh and consequently this methodology has been referred to as mesh free or mesh-less crack modelling. The capability of the method to predict the opening of individual cracks has led to its use to predict integrity failure which may precede stability failure in the analysis of reinforced concrete slabs in fire {Yu, 2008 #168}.

With the *smeared crack* approach no gap is introduced into the finite element mesh. Instead, the crack is represented by a drastic change in material properties. Such an approach results in considerable improvements in computational efficiency; however, representing the crack in this manner 'smears' the crack across the area of a finite element represented by a material integration point. This area is substantially larger than that of a single crack. One consequence of smearing is the possibility of introducing mesh sensitivity (solutions are mesh dependent) into the numerical solutions when it is used to analyse concrete with large isolated cracks. In this case further mesh refinement does not lead to the development of additional crack bands changing the final solution. Where concrete is reinforced in tension the cracking behaviour is altered; crack sizes reduce and distribution increases. For this case mesh refinement will therefore lead to new crack bands forming which should be sufficient to allay mesh sensitivity concerns. Despite the smeared cracking methods simplification of the cracking process, it has been previously applied to the analysis of concrete structures in fire {Fox, 2007 #233; Cameron, 2003 #79} and has been found to provide accurate global descriptions of behaviour. It cannot, however, predict the growth of individual cracks which can be critical for establishing integrity

failure {Yu, 2008 #168}, reinforcement rupture {Giroldo, 2008 #129} or shear failures.

It is therefore possible to model the tensile cracking of concrete in a spectrum of detail. The more detailed approaches are appropriate when cracking will dominate behaviour and the simplified methods such as smeared cracking when the influence of cracking is only required to model global behaviour.

For the current investigation an accurate description of global behaviour is sufficient for establishing the implications of non-uniform heating for structural performance therefore a simplified approach is adopted with respect to concrete cracking. The concrete material mode employed is described more fully in section 4.3.1.

Compressive Crushing

The treatment of concrete crushing has received considerably less attention than that of concrete cracking. Tensile cracking occurs at significantly lower stresses than compressive crushing it is therefore more commonly encountered under serviceability conditions therefore demanding consideration. The pattern of localisation in crushing is also significantly more complex. The author is unaware of any attempts to formulate physical crushing behaviour in a finite element analysis. The softening behaviour that crushing is responsible for is therefore modelled phenomenologically. This softening behaviour is represented in a plasticity model as stress unloading at increasing strains.

4.2.4 Summary

It is possible to combine the computational efficiency of shell elements with the behaviour required for modelling reinforced concrete at high temperatures. The slab is modelled as 2D surface however integration points through the shell thickness allow one to consider: material non-linearity and variation at elevated temperatures, thermal expansion, geometric non-linearity and non-linear through depth temperature gradients. The concrete tensile post peak behaviour will be smeared, this approach is able to model the global behaviour of reinforced concrete structures accurately but unable to model crack propagation and the associated crack-reinforcement interaction.

4.3 Finite element analysis of a two-way spanning RC slab

A two-way spanning reinforced concrete slab is to be used as a benchmark structural model to investigate the effect of varying thermal conditions for structural fire performance. In this section the benchmark structural model is defined and a finite element model developed to analyse its behaviour under benchmark thermal conditions. The benchmark thermal condition used is the standard temperature time curve.

The behaviour under benchmark conditions is examined to firstly verify that the slab develops compressive and tensile membrane behaviour and secondly to establish aspects of behaviour which are critical for the performance of the slab. These aspects of behaviour will be used in subsequent analyses as relative performance indicators when contrasting the effect of the thermal definition for concrete structural behaviour.

In this investigation the general purpose finite element software ABAQUS {, 2008 #120} will be used to analyse both the thermal and mechanical response of the slab to heating. The structural model used is based on those demonstrated by Cameron {, 2003 #79} and Fox {, 2007 #233}. The thermal and structural analyses are performed sequentially, that is the thermal analysis is conducted first; the resulting thermal distributions are then read directly into the structural analysis.

4.3.1 Definition of the benchmark slab finite element model

The reinforced concrete slab spans 6m x 6m. The benchmark slab thickness is 100mm. The slab span to depth ratio is therefore 60 which is atypically slender when compared to typical concrete construction. Reinforcement is provided at the top and bottom of the slab by a 6 mm and 12 mm diameter mesh respectively. The mesh spacing is 200 mm for both. The axis distance (from the slab surface to the reinforcement mesh mid depth) is 30 mm for both top and bottom reinforcement. The applied load is 5 kN/m². In Figure 4-4 the slab geometry is summarised and the finite element representation depicted. The model takes advantage of symmetry so that a quarter of the slab is modelled, applying symmetry boundary conditions as indicated.

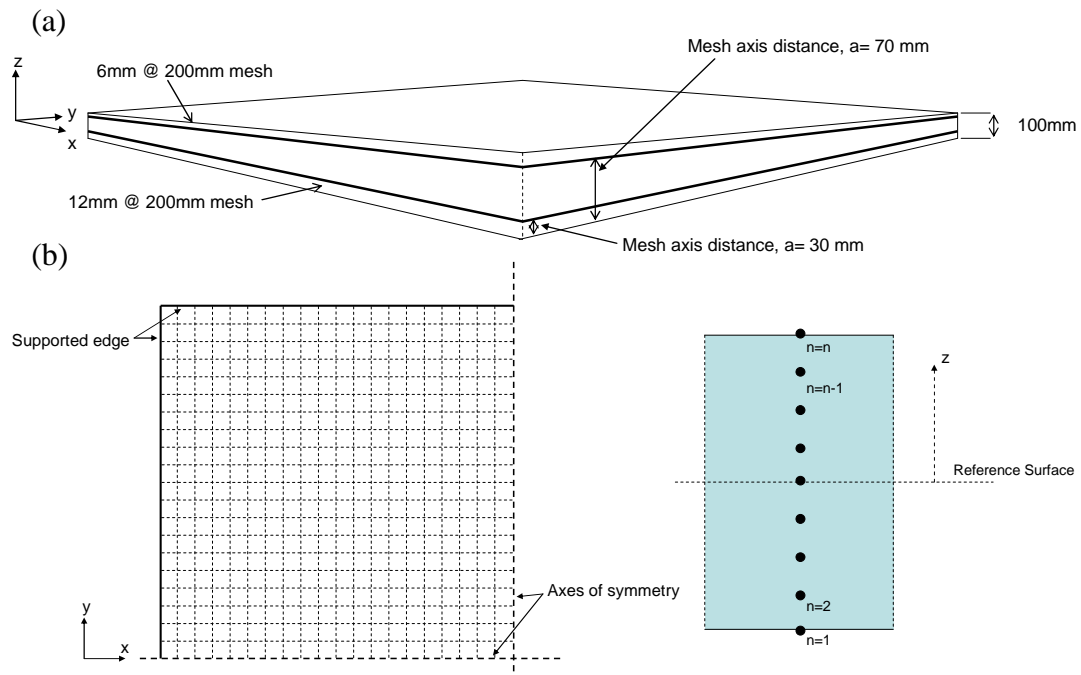


Figure 4-4 Reinforced concrete slab geometry and finite element analysis representation of RC concrete slab for heat transfer and stress-displacement analysis

Heat transfer numerical analysis

The thermal response of the slab is modelled using 4 node (DS4) heat transfer shell elements. Temperatures can be calculated at a number of evenly spaced integration points through the shell thickness. In this investigation temperatures are calculated at 19 points through the slab depth as this is the maximum number of points for which temperature can be defined in the structural analysis. For a 100mm slab temperatures are therefore defined every 5 mm. A steep thermal gradient develops in concrete due to its insulating properties, requiring a high degree of resolution through the depth.

For the initial verification of the finite element model, the Eurocode 1 {, 2002 #30} standard fire will be used to define the thermal exposure. The Eurocode 1 standard temperature time curve is the most widely adopted design fire in structural fire engineering; it has been used in most structural fire research and is used frequently in design. It is therefore appropriate to use this fire as the benchmark thermal condition. All references to time of exposure refer to exposure to the standard temperature time curve.

Structural numerical analysis

The slab is modelled using the ABAQUS {, 2008 #120} S4R shell element. S4R is a quadrilateral, stress/displacement general purpose shell element with reduced integration and a large strain formulation. In ABAQUS general purpose shell elements allow for transverse shear deformation. As the shell thickness increases they use thick shell theory and as the shell thickness decreases become discrete Kirchhoff thin shell elements; the transverse shear deformation becomes very small as the thickness of the shell decreases {ABAQUS, 2008 #120}. The S4R element uses a fully nonlinear formulation allowing large-displacement analyses to be conducted; the elements are allowed to distort from their original shape under increasing deformation.

The reinforcement is modelled as a smeared layer within the element that is a constant thickness equal to the area of one reinforcing bar divided by the reinforcement spacing. This method of modelling reinforcement for RC slabs has been widely adopted as an efficient means of defining the reinforcement within a shell. The implications of adopting such an approach mean that strains are evenly distributed over the width of an element. For profiled reinforcement, however, strains localise at the profiles where the reinforcement is mechanically anchored in the concrete as described in chapter 2. This method of modelling reinforcement will therefore likely under predict local strains.

The analysis is split into two steps: the mechanical load is first applied, followed by the temperatures. The definition of temperature evolution is read from the results of the separate thermal analysis. The analysis is solved using explicit dynamics (ABAQUS/Explicit) which is more efficient than implicit integration (ABAQUS/Standard) for extremely discontinuous events or processes. ABAQUS/Explicit accuracy checking is however less rigorous than ABAQUS/standard, it is therefore good practice to compare standard and explicit solutions to ensure the explicit solution is on track.

Material Models

The steel thermal and mechanical properties from Eurocode 2 {, 2004 #27} are used to define the behaviour of the reinforcement. The stress-strain curves are plotted in

Figure 4-5. A rupture strain of 15% as prescribed by Eurocode 2 is used in this preliminary analysis. The linear descending branch after strains of 15% is included to ease numerical solution. The real behaviour after rupture is an instantaneous loss of strength. Rupture strain is further considered in the material sensitivity studies in section 4.5.

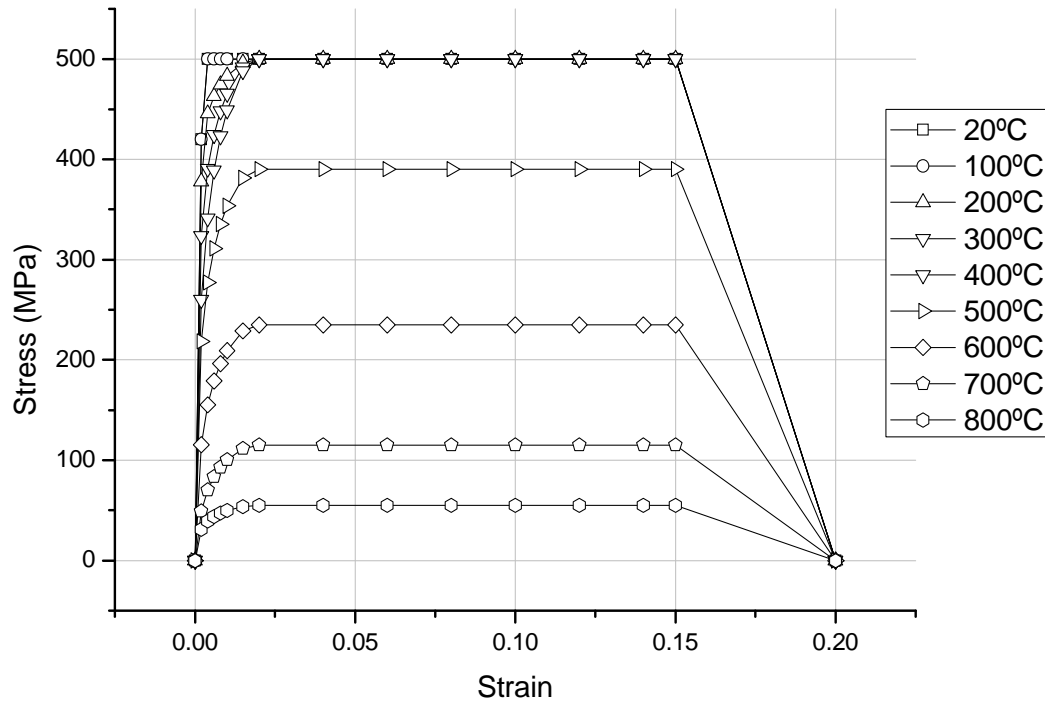


Figure 4-5 Steel reinforcement stress-strain curves according to Eurocode 2 at elevated temperatures

The concrete thermal and mechanical properties are taken from Eurocode 2. The concrete is assumed to be siliceous and the moisture content taken as 3 %. The peak ambient compressive strength is taken as 30 N/mm² and the peak tensile ambient strength is 3.39 N/mm². This was calculated according to the correlation in Equation 4-1 as reported by Shah et al. {, 1995 #60}.

$$f_t = 0.3(f_c + 8)^{2/3} \quad \text{Equation 4-1}$$

The concrete failure surface is described using the concrete damage plasticity model in ABAQUS. The concrete damage plasticity failure surface is based on that developed by Lubliner et al. {, 1989 #96} with modifications proposed by Lee and Fenves {, 1998 #126} to allow for the different evolution of stress under tension and compression. It provides a good description of the failure surface of concrete under

both compression and tension. The shape of the failure surface and the shrinkage of failure surfaces at elevated temperatures were presented in chapter 2.

Yielding under compression is described using a non-associated flow rule which has been shown to give more accurate results for concrete than the commonly adopted associated flow rule. Yielding under tension is described in terms of either a stress-strain, stress-displacement or fracture energy relation. In this case a stress-strain model is used; the tension stiffening effect described in Chapter 2 is included by increasing the slope of the concrete tensile stress-strain descending branch. A parametric sensitivity analysis is conducted to determine an appropriate degree of tension stiffening in section 4.5.1.

Boundary conditions

The boundary conditions that the surrounding structure exerts upon a single structural element can vary enormously. Continuity of the slab with both the edge beams and adjacent slabs imposes vertical, lateral and rotational restraint components upon the slab edge. This is shown schematically in Figure 4-6

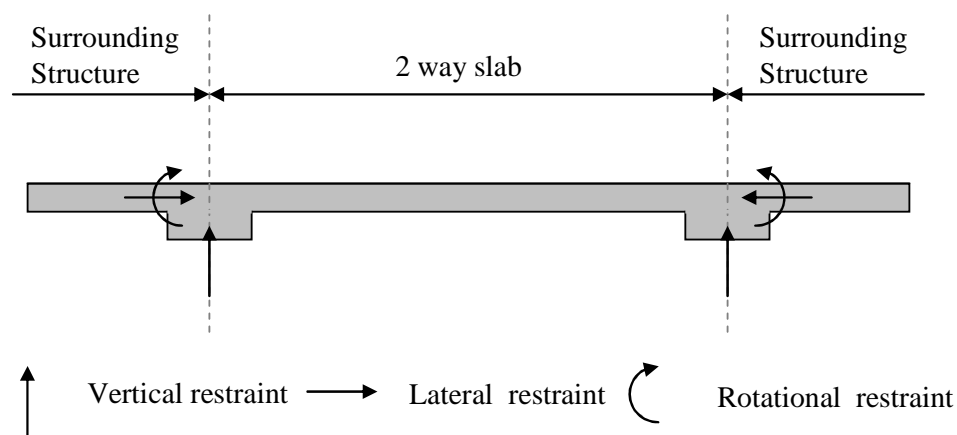


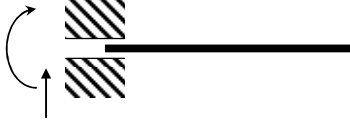
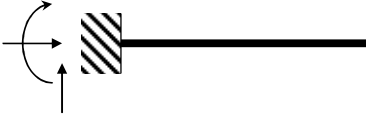


Figure 4-6 Components of restraint surrounding structure imposes upon two-way spalling slab

It is difficult to quantify the stiffness of this restraint, in particular at elevated temperatures when the cool surrounding structure restrains the thermal expansion of heated elements. Therefore a number of possible restraint configurations are applied to the slab to provide an envelope of possible conditions. The combinations applied are; unrestrained, lateral restraint, rotational restraint and lateral and rotational restraint. These have been summarised in Table 3.1. The range of combinations has

been chosen such that comparison of behaviour under each boundary condition will identify the contribution that each component of restraint makes to the global behaviour of the slab.

Table 4.1 Boundary conditions examined

Restraint Description	Restraint Condition
Unrestrained	
Laterally Restrained	
Rotationally Restrained	
Laterally & Rotationally Restrained	

4.3.2 Behaviour of the benchmark slab finite element model

This section looks in detail at the behaviour of the benchmark finite element model for two reasons: to verify the development of compressive and tensile membrane behaviour and to identify aspects of behaviour which can be used as an indicator of slab performance.

Verification of membrane behaviour

The deformation behaviour of the slab and the concrete and reinforcement stress state are used to verify the development of membrane behaviour in the benchmark finite element model.

Deformation behaviour

Figure 4-7 plots the central deflections of all restraint cases considered for 60 minutes of exposure to the standard temperature time curve.

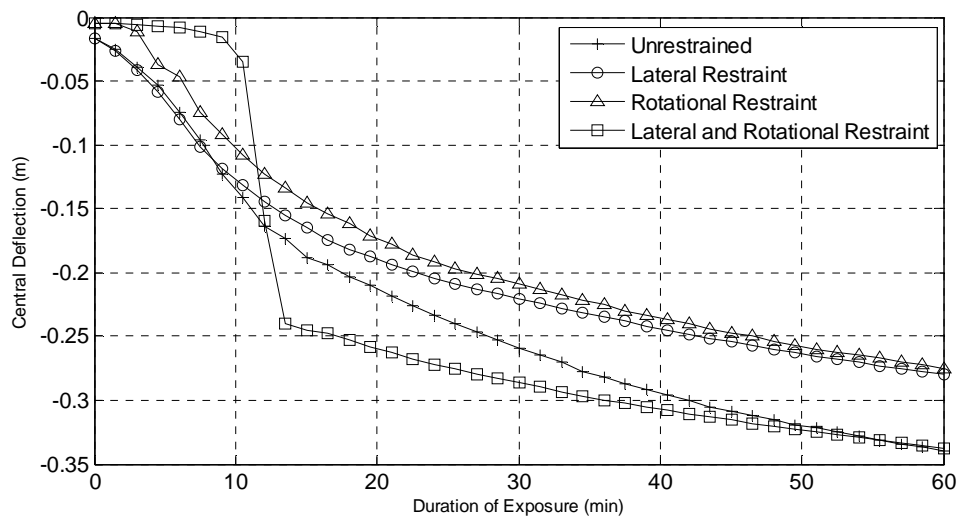


Figure 4-7 Effect of boundary condition for the central deflection of a two-way spanning slab

For all restraint cases large central deflections develop; these deflections are substantially bigger than would be feasible under pure flexure. There is a distinct difference in deflection behaviour between those slabs which are laterally restrained and those which are not. When lateral restraint is absent the slab experiences a gradual increase in deflection during exposure. Thermal bowing and high temperatures lead to a gradual reduction in flexural strength until the slabs transition to tensile membrane behaviour.

When lateral restraint is present the slab deflection initially increases very gradually due to the enhanced load carrying capacity arising from compressive membrane action. The additional capacity is lost when the slab central deflections exceed the line of thrust from the lateral support as explained in section 4.1. Tensile membrane action is mobilised at significantly larger deflections therefore the transition between the two mechanisms here is characterised by a dramatic increase in central deflection referred to as snap through.

Concrete stress state

The slab stress state is also indicative of the mechanism of stability. During compressive membrane action large in-plane stresses develop in the concrete cross-section. Under tensile membrane action the concrete stress state is characterised by a ring of compression surrounding a central tensile net. The stress state of the concrete and reinforcement is examined for evidence of the development of compressive and tensile membrane action.

The concrete stress state for each restraint case is presented in terms of the maximum and minimum principal stress resultants (Figure 4-8 and Figure 4-9). Stress resultants are calculated in the x, y and x-y direction by finding the integral of the through depth stress distribution at each integration point. Mohr's circle is then used to calculate the minimum and maximum principal stress for the section at that point.

Plan contour plots of principal section stress have been presented after 6 minutes of exposure (Figure 4-8) and 60 minutes of exposure (Figure 4-9). After 6 minutes the section stress of the laterally restrained cases Figure 4-8 (b) and (d) are predominantly compressive indicating the development of large in plane compressive stresses characteristic of compressive membrane action. For the restrained cases in Figure 4-8 (a) and (c) where lateral restraint is absent both cases show distinct regions of tension and compression, indicating flexure or tensile membrane action.

After 60 minutes exposure (Figure 4-9) all of the restraint cases are exhibiting the distinctive ring of compression and central region of tension associated with tensile membrane action. In the laterally unrestrained slabs, Figure 4-9 (a) and (c), stability is reliant on the support of the tensile net by the ring of compression. For the laterally restrained slabs' stability, Figure 4-9 (b) and (d), is not wholly reliant upon the

compression as the lateral restraint can support the reinforcement by catenary action. For this reason a greater proportion of the slab can develop tension. Comparing all four restraint cases the shape of the ring is noticeably different for the laterally restrained conditions and for the laterally unrestrained conditions. For the laterally restrained case the ring hugs the slab perimeter with a greater proportion of the slab in tension. The compressive stresses are also substantially higher. This is due to compression being induced in all directions by the restraint of the slab corner as it moves out to allow the slab to pull in.

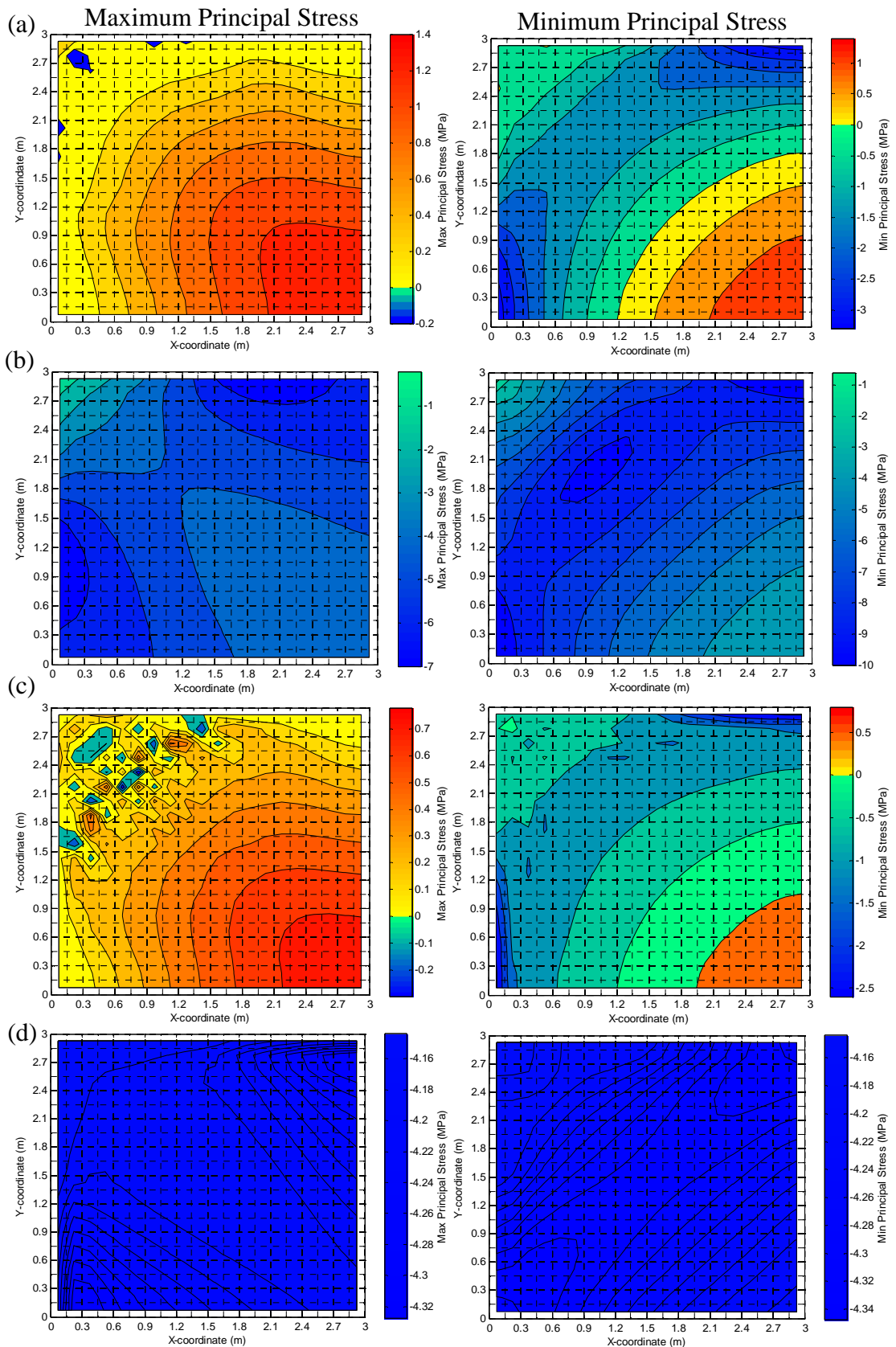


Figure 4-8 Principal stress resultants (MPa) at 6 minutes exposure (a) unrestrained (b) laterally restrained (c) rotational restraint (d) lateral and rotational restraint. Supported Edge along X=0m and Y=3m

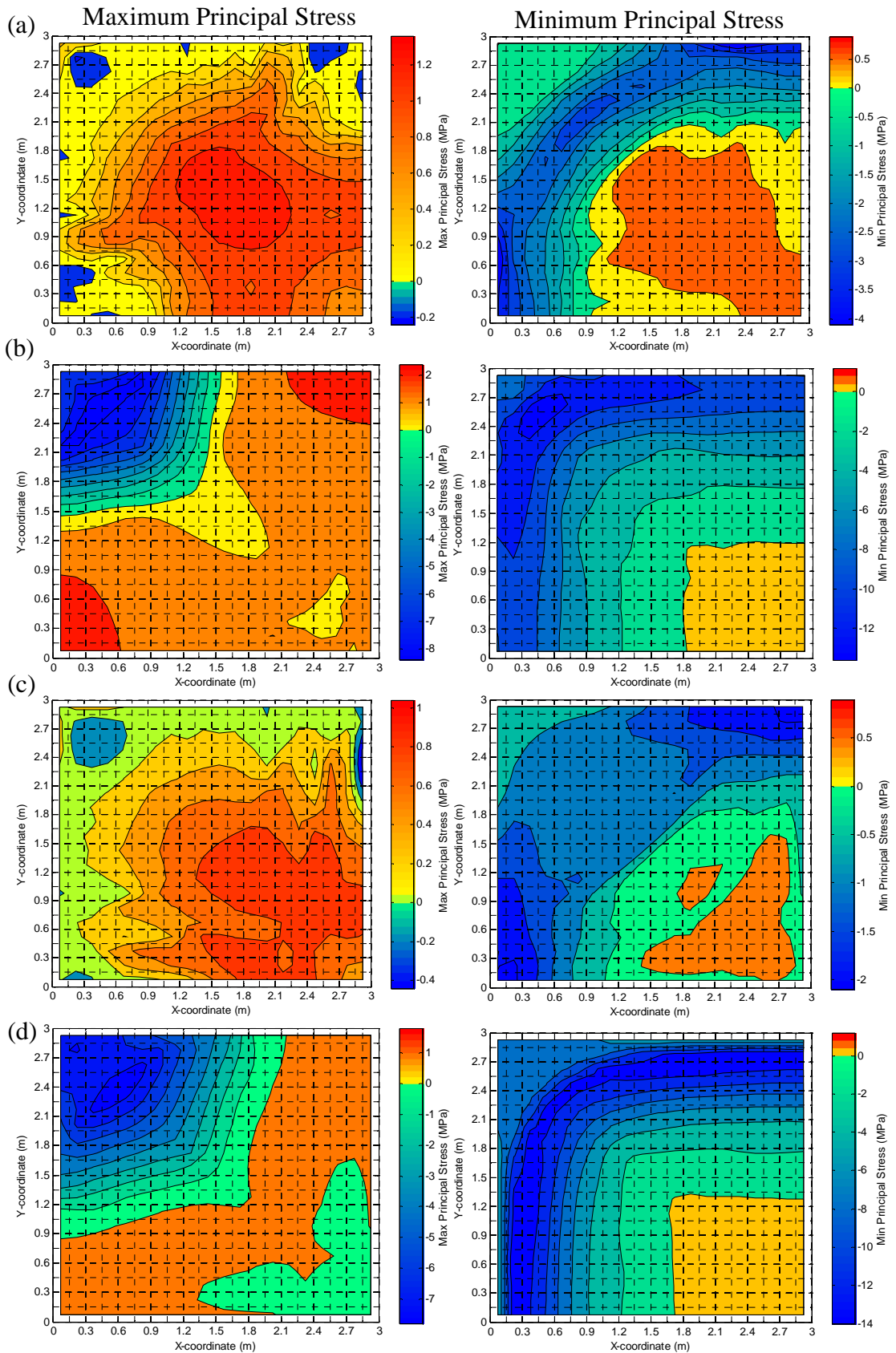


Figure 4-9 Principal stress resultants (MPa) at 60 minutes exposure (a) unrestrained (b) laterally restrained (c) rotational restraint (d) lateral and rotational restraint. Supported edges at $X=0m$ and $Y=3m$.

Reinforcement stress state

As introduced in Figure 4-4, the slab has two layers of reinforcement mesh, positioned 30 mm from the top and bottom surfaces. All of the restraint cases examined are exhibiting tensile membrane behaviour after 60 minutes of exposure (Figure 4-9). The reinforcement behaviour is examined to verify this behaviour. The net of concrete tension evident in Figure 4-9 is supported by the reinforcement; it is therefore expected that reinforcement stress will peak at the slab centre. Figure 4-10 and Figure 4-11 plot normalised reinforcement stress profiles across a centreline through the slab at $y = 0$ m. Profiles are plotted at selected time intervals to demonstrate the transition from flexure to compressive membrane behaviour to tensile membrane action. Reinforcement stresses are normalised by the temperature dependent maximum stress (Figure 4-5).

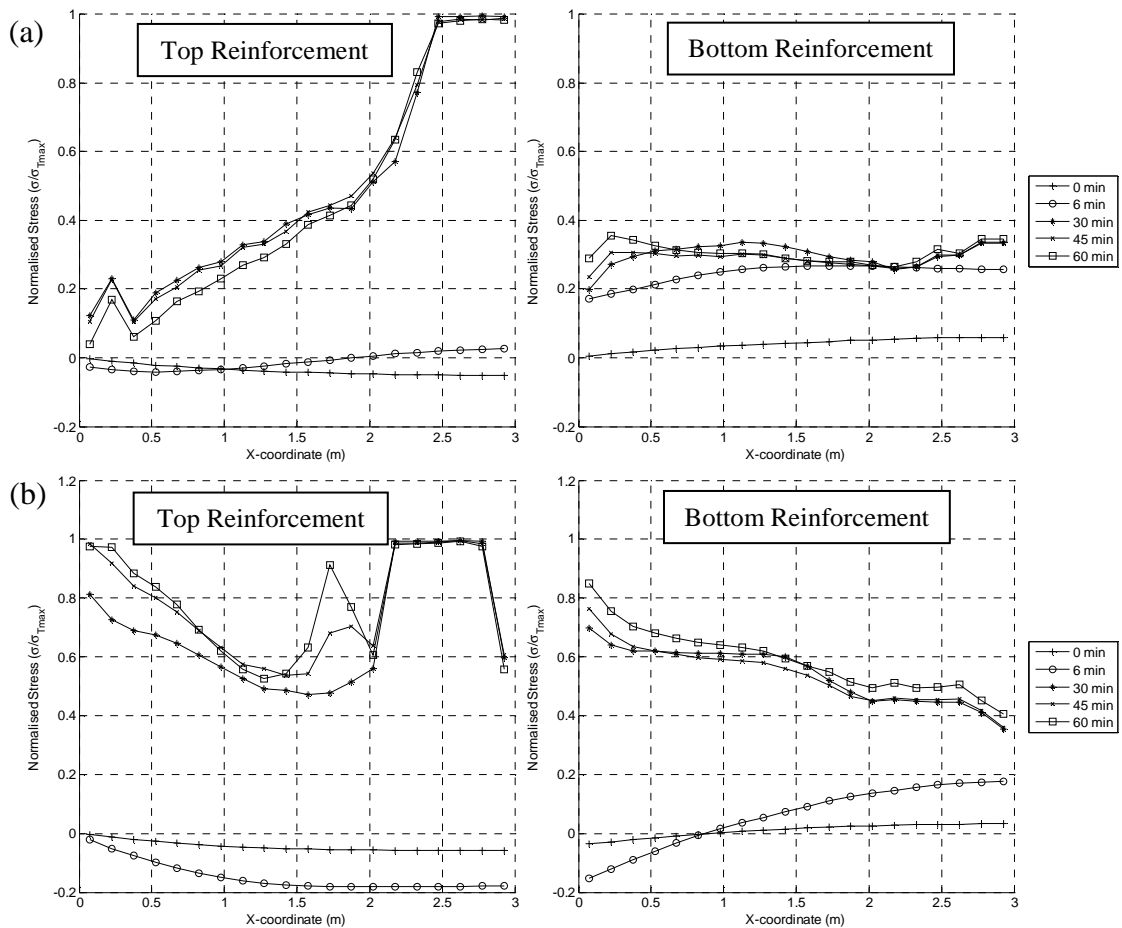


Figure 4-10 Reinforcement normalised stress profile across a centreline through the slab ($y=0m$) (a) Unrestrained slab (b) laterally restrained slab

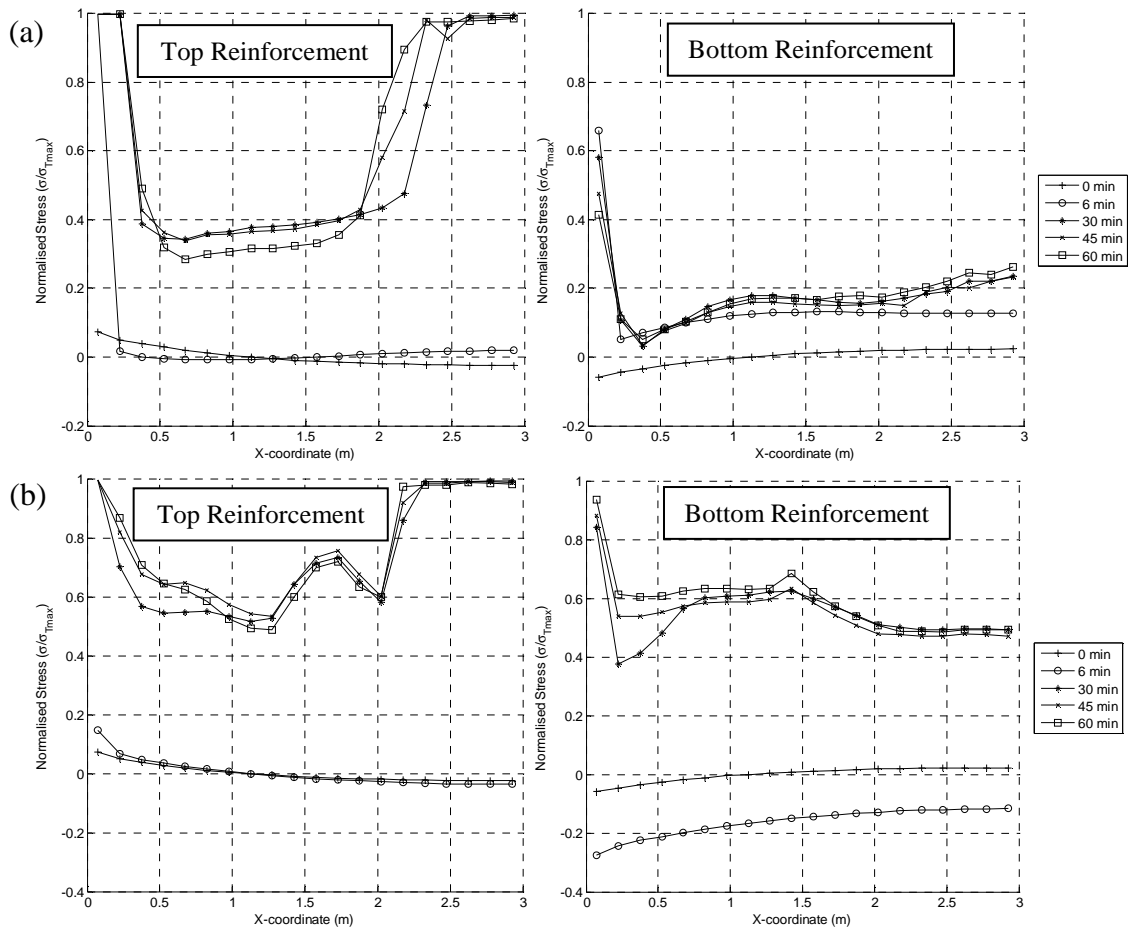


Figure 4-11 Reinforcement normalised stress profile across a centreline through the slab ($y=0m$) (a) rotationally restrained slab (b) Laterally and rotationally restrained slab

In the unrestrained case Figure 4-10 (a) the normalised reinforcement stress profiles show bending behaviour initially at zero minutes exposure with compression in the top layer and tension in the bottom layer. After 60 minutes of exposure both the top and bottom reinforcement are experiencing tension demonstrating catenary action. Stresses peak at the slab mid span where curvature is greatest. The top layer of reinforcement is significantly more stressed than the bottom reinforcement once catenary action is established; this is true for all restraint cases.

Lateral restraint initially induces compressive stresses in the reinforcement (Figure 4-10 (b) and Figure 4-11 (b)). Under tensile membrane action (profiles 30, 45 and 60 min) a second peak forms at the slab edge affecting both top and bottom reinforcement layers. This is due to restraint of the slab edges pulling in under increasing central span deflections.

Rotational restraint under pure flexure causes high reinforcement stresses at the slab edge. The top layer reinforcement experiences tensile stress and the bottom layer compressive stress. This is evident in Figure 4-10 (b) and Figure 4-11 (b) at zero minutes. Rotational restraint counteracts the large curvature which develops in the slab under tensile membrane action resulting in a significant increase in reinforcement stresses at the slab edge for both top and bottom layers.

Slab performance indicators

Failure of a slab under tensile membrane action is by either crushing of the concrete within the compressive ring or by reinforcement rupture. These two aspects of behaviour will be used to monitor slab performance.

Measuring concrete behaviour

Crushing is not explicitly modelled in this analysis; the concrete post peak constitutive curve is defined using a softening stress-strain definition. The development of plastic strains will be used to measure concrete failure; the strain at maximum stress in the constitutive curve is taken to represent the onset of crushing. The concrete strain state is represented by the equivalent plastic strain, which is calculated at each section point through the slab depth. The degree of concrete crushing is determined by the ratio of equivalent plastic strain to the strain at maximum stress. This is referred to as the proportional equivalent plastic strain; its calculation is summarised in Figure 4-12. A proportional equivalent plastic strain value greater than 1 indicates the onset of crushing at that location.

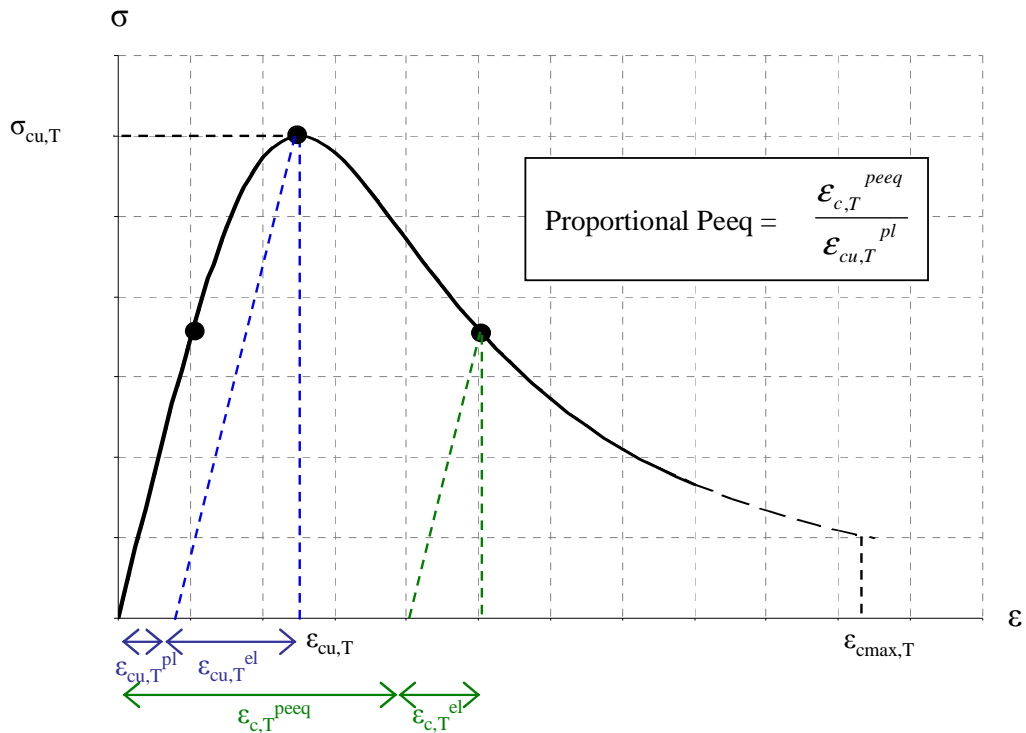


Figure 4-12 Calculation of proportional equivalent plastic strains

Figure 4-13 to Figure 4-16 present contour plots of the proportional equivalent plastic strain term for all restraint cases after 60 minutes of exposure to the standard fire. Plan contours are provided at the top, mid and bottom surfaces and a cross-section through the slab is presented.

After 60 minutes of exposure all of the restraint cases are exhibiting concrete crushing behaviour at the top surface in the corner of the slab. Where the slab is rotationally free (Figure 4-13 and Figure 4-14) the highest degree of crushing occurs. Crushing is evident across the entirety of the corner but the peak value is highly localised to the tip of the corner of the slab (coordinate (0,3)). Crushing is evident in the corners of the rotationally restrained slabs (Figure 4-15 and Figure 4-16) also. However, rotational restraint reduces curvature at the slab edge preventing crushing at the corner tip. The magnitude of crushing strains is therefore less.

Under tensile membrane action the slab edges start to pull-in to accommodate the increasing central deflections; in a two way spanning slab this results in the corner of the slab pushing outwards. Lateral restraint prevents this movement increasing the compressive loading along the slab edge. In the cross section plots Figure 4-14 (d)

and Figure 4-16 (d) it can be seen that this increased loading has caused compressive crushing along the slab edges.

For all restraint cases the peak crushing strain occurs in the slab corners on the top surface. In chapter 5 the top surface crushing strains will be used to contrast the influence of non-uniform thermal exposure for the performance of the compressive ring.

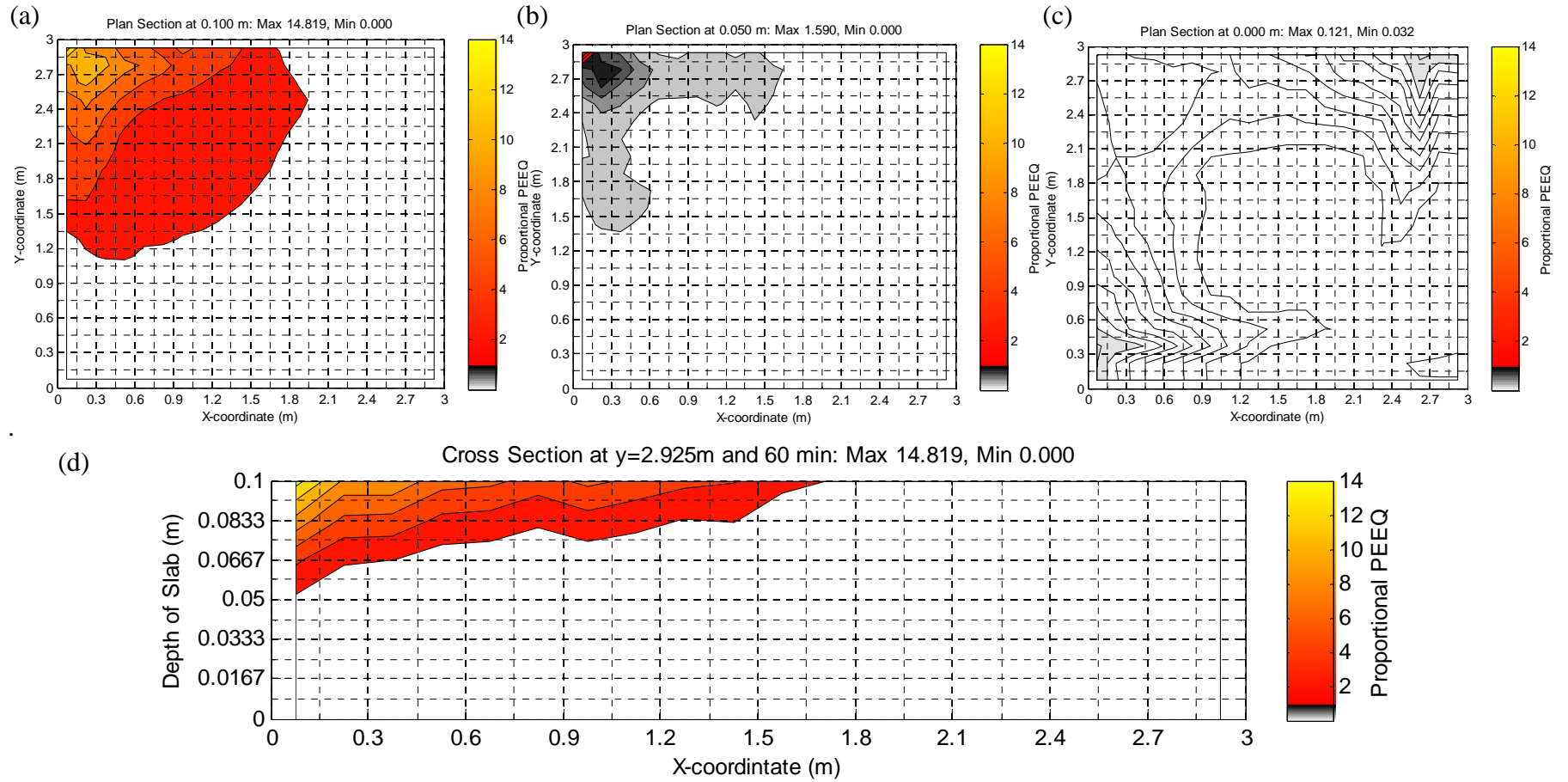


Figure 4-13 Unrestrained slab proportional plastic equivalent strain at (a) Top (b) Mid and (c) Bottom surface and (d) $y=2.925\text{ m}$ cross-section

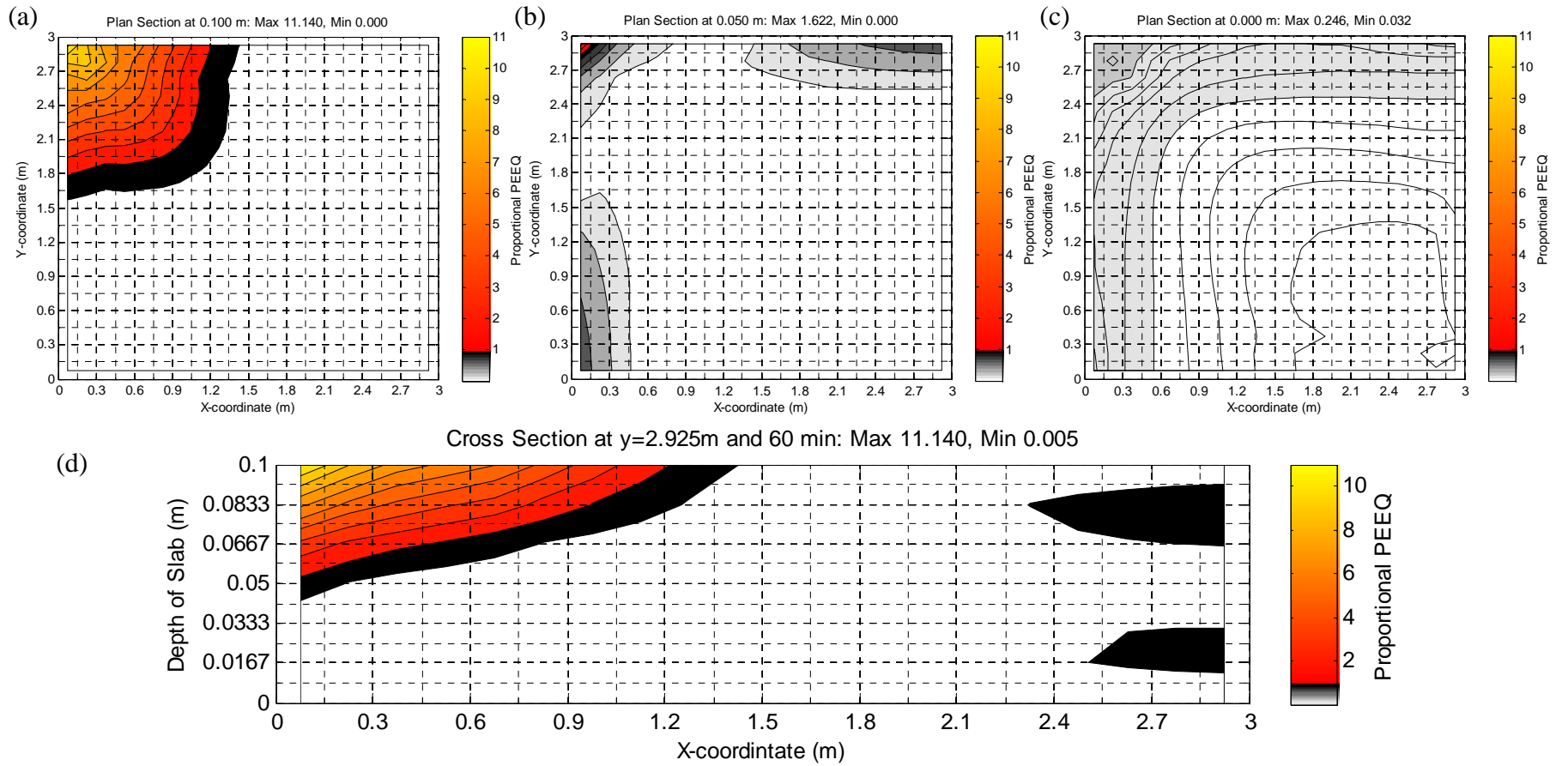


Figure 4-14 Laterally restrained slab proportional plastic equivalent strain at (a) Top (b) Mid and (c) Bottom surface and (d) $y=2.925$ m cross-section

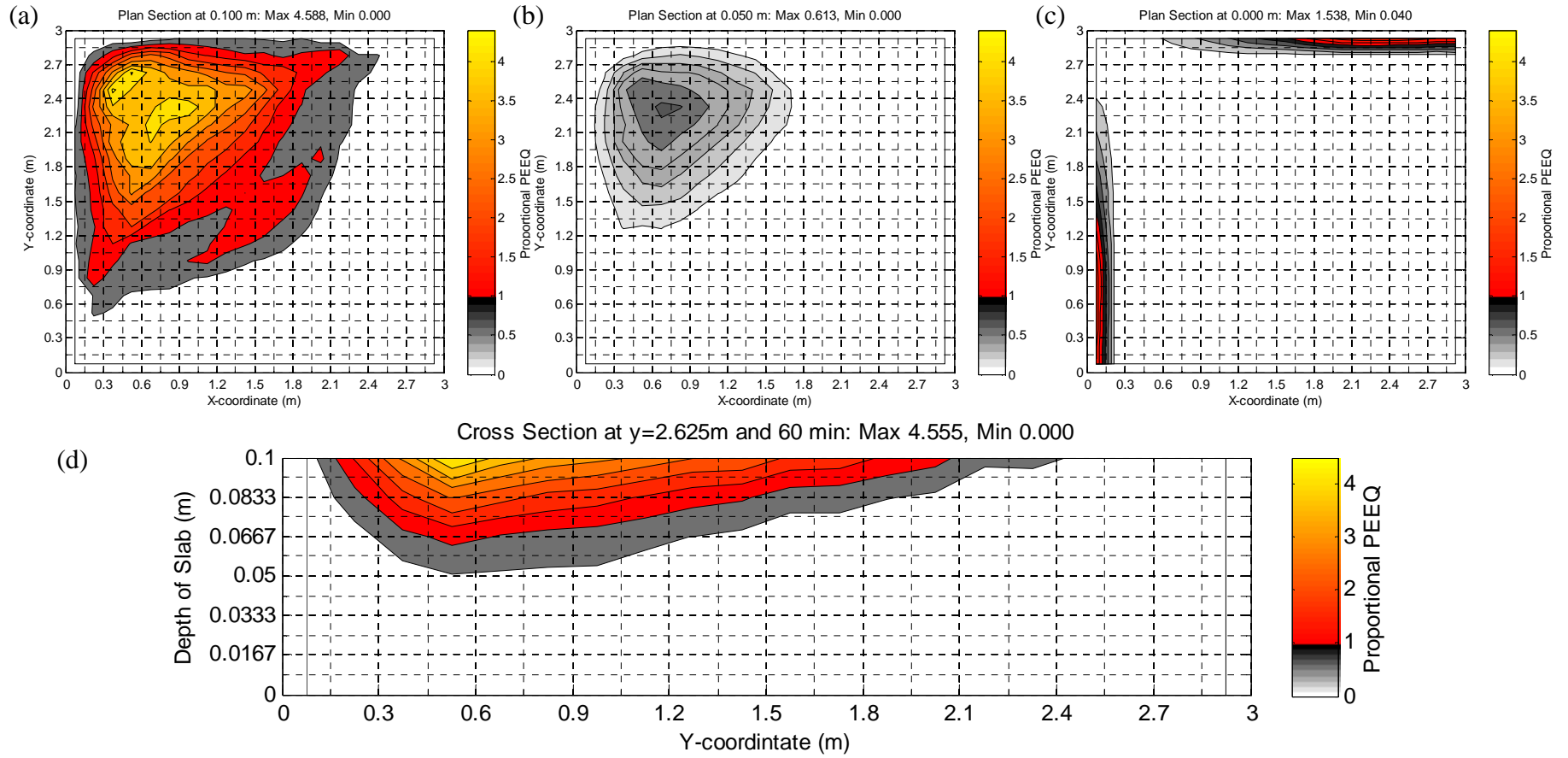


Figure 4-15 Rotationally restrained slab proportional plastic equivalent strain at (a) Top (b) Mid and (c) Bottom surface and (d) $y=2.775$ m cross-section

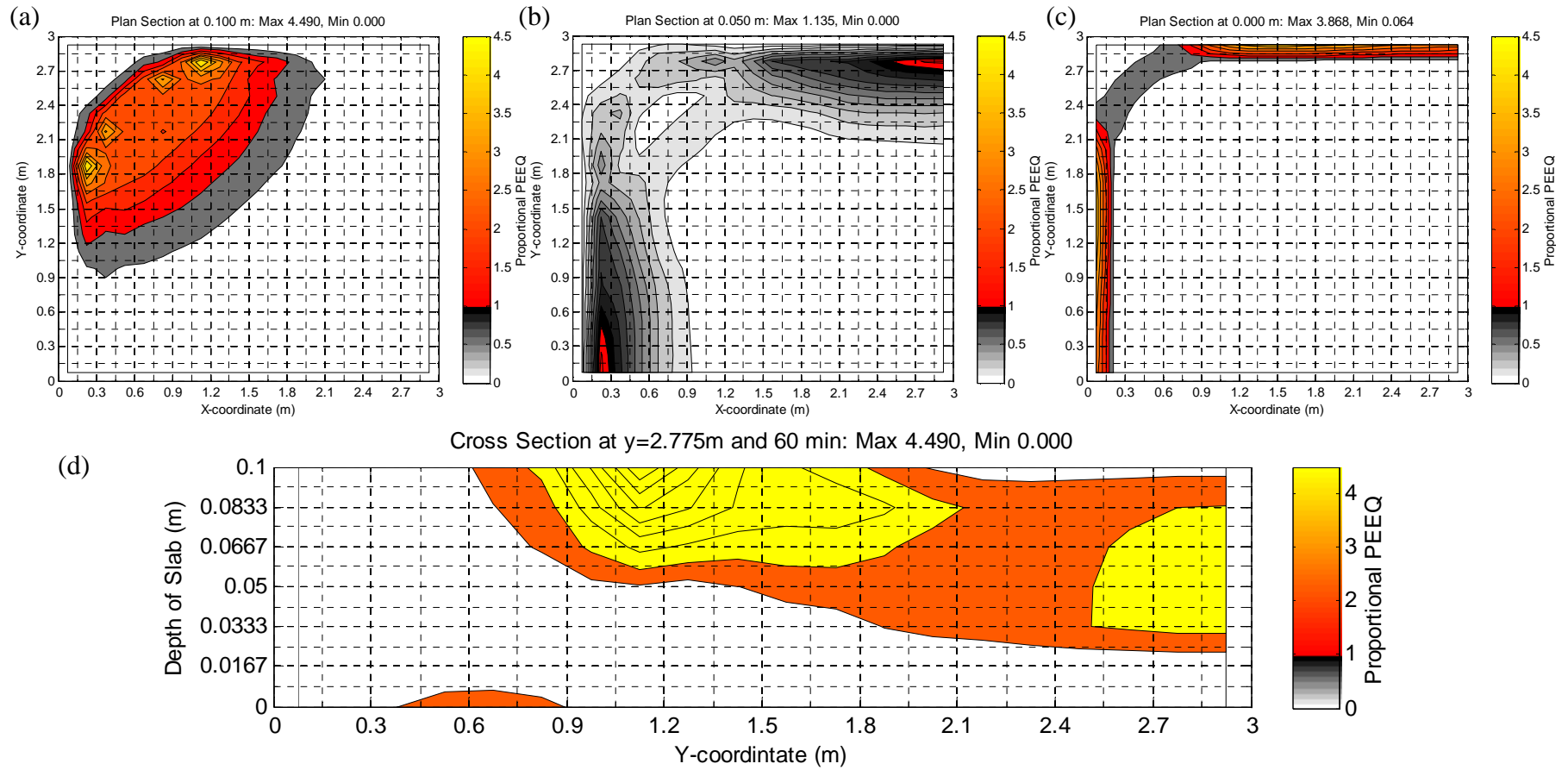


Figure 4-16 Rotationally and laterally restrained slab proportional plastic equivalent strain at (a) Top (b) Mid and (c) Bottom surface and (d) $y=2.775$ m cross-section

Measuring reinforcement behaviour

In Figure 4-10 and Figure 4-11 the reinforcement stress was presented. In this section the mechanical strains are examined to measure the relative behaviour of the reinforcement. Once the steel has yielded the strain history provides a better indicator of relative performance. It is not possible to model reinforcement rupture due to the smearing of the concrete's post-peak tensile behaviour and the reinforcement. In reality strains concentrate around the rib for profiled reinforcement where the reinforcement is mechanically anchored in the concrete. It is not possible to represent this given the current modelling approach so the development of large mechanical reinforcement strains will be interpreted as increasing the probability of rupture at that location. Estimates of when reinforcement rupture will occur are avoided.

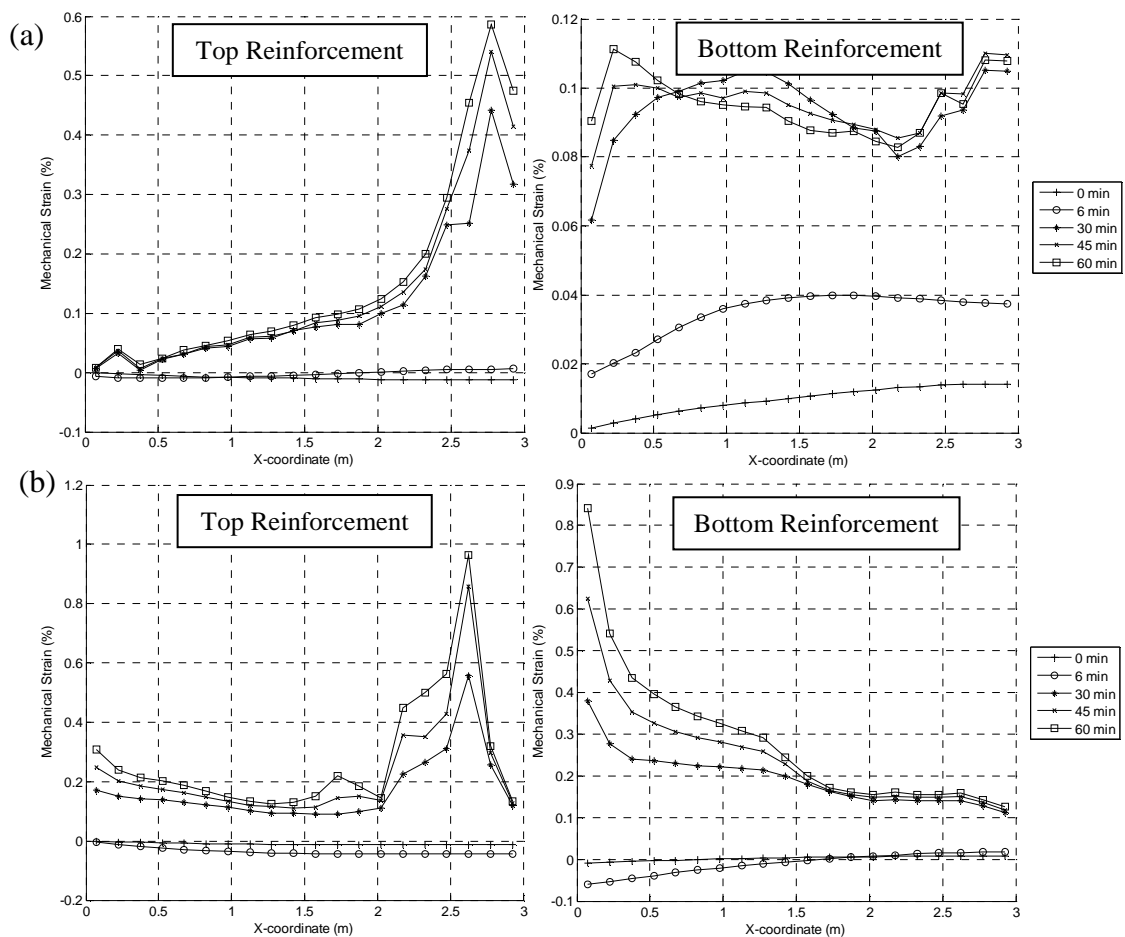


Figure 4-17 Reinforcement mechanical strain profile across a centreline through the slab ($y=0m$) (a) Unrestrained slab (b) Laterally restrained slab

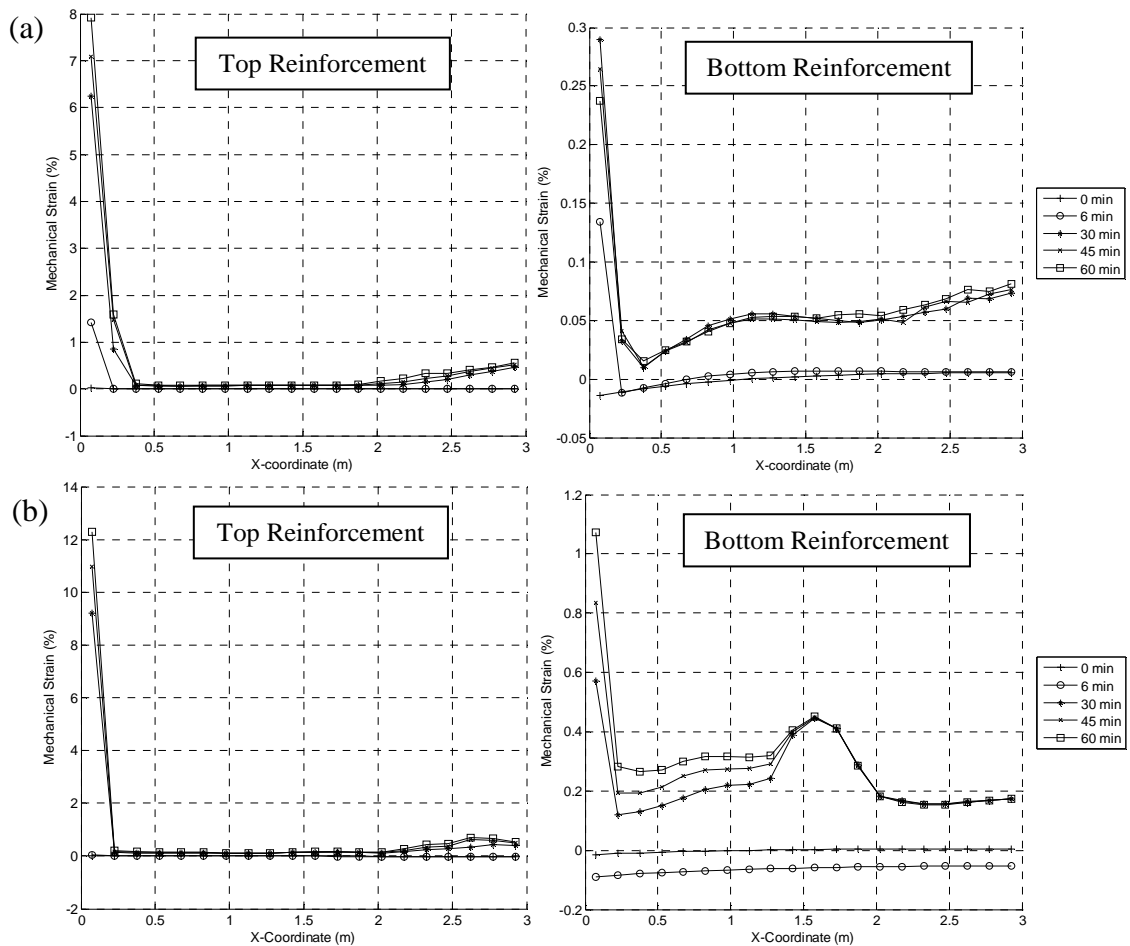


Figure 4-18 Reinforcement mechanical strain profile across a centreline through the slab ($y=0m$) (a) Rotationally restrained slab (b) Rotationally and laterally restrained slab

Figure 4-17 and Figure 4-18 present the mechanical strain profile across a centreline through the slab for the top and bottom layers of reinforcement. The distribution of strains closely reflects the stress distributions presented in Figure 4-10 and Figure 4-11. For all restraint cases the bottom layer reinforcement strains are typically lower than the top layer reinforcing strains. This is due to the relieving effect of thermal expansion. The bottom reinforcement is hotter and therefore is experiencing a greater degree of thermal expansion.

Figure 4-17 (a) presents the mechanical strains for the unrestrained slab, the peak strain occurs in the top reinforcement at the slab centre. Both lateral and rotational restraint exhibits a peak in strain at the slab centre and also at the slab edge (Figure 4-17 (b) and Figure 4-18 (a)). The edge strains induced by rotational restraint are substantially larger than those caused by lateral restraint; they are also much larger

than the mid span strains for all cases. The combination of lateral and rotational restraint (Figure 4-18 (b)) induces the largest edge strains.

The magnitude of reinforcing strains is substantially lower than the defined rupture strain of 15% in this investigation. For this slab the behaviour of the concrete is more critical for performance than the reinforcement. The relative importance of the concrete and the reinforcement for slab performance will depend on the reinforcement ratio. It is therefore possible that in other slab design the reinforcement behaviour will be critical. For this reason the behaviour of the reinforcement in subsequent analyses will be examined in addition to concrete behaviour.

Peak strains have been shown to develop both at the slab mid span and at the slab edge. Rupture of the reinforcement at the mid span has been shown experimentally {Bailey, 2007 #212} to cause failure of the slab. Rupture of the reinforcement at the slab edge will change the slab boundary conditions such that it behaves as an unrestrained slab. Continued stability will therefore depend upon the nature of the vertical support which is critical for maintaining stability. Cracking at the slab edge will also prove critical for the shear capacity of the slab. The model used here is not capable of capturing this effect or modelling shear failure.

The critical location for reinforcement in the unrestrained slab is in the top layer at the slab centre. For the laterally restrained slab the critical locations are in the top layer at the slab edge and the slab centre. For the rotational restraint and combined lateral and rotational restrained slabs the critical location is in the top layer reinforcement at the slab edge.

Summary

In this section the finite element predictions of the behaviour of a two way spanning reinforced concrete slab under standard fire exposure and a variety of boundary conditions have been discussed in detail. The predictions are in agreement with the prior knowledge of the behaviour of these slabs, demonstrating that the finite element model is able to model the membrane behaviour of slabs under a variety of support conditions.

Features of behaviour demonstrated include the development of compressive membrane action in laterally restrained slabs, the development of the concrete compressive ring and central net of concrete and reinforcement tension associated with tensile membrane action in unrestrained and restrained slabs and the clear transition between the two mechanisms for laterally restrained slabs.

The finite element model created is capable of modelling the global behaviour of reinforced concrete slabs. The prediction of localised concrete crushing and reinforcement mechanical strains are limited due to the simplifying assumptions in the smeared tension and shell model used. However they allow the comparative behaviour of the slab to be examined under different conditions.

The behaviour of the concrete and reinforcement has been further investigated to establish performance indicators for use in subsequent analyses. Performance is assessed in terms of concrete crushing and reinforcement rupture.

Concrete crushing is indicated by the proportional plastic equivalent strain, which is a ratio of the plastic equivalent strain to the strain at maximum concrete stress. The critical location for concrete crushing is the top surface of the slab.

The increased likelihood of reinforcement rupture is indicated by the development of large mechanical reinforcement strains. Reinforcement strains in the top reinforcement are substantially larger than the bottom reinforcement strains and are therefore taken to be more critical for performance. The restraint condition strongly affects the reinforcement strain distribution. For the unrestrained slab the mid span location is considered critical. For the laterally restrained condition, the mid span and slab edge strains are critical and for the rotationally restrained slabs the slab edge location is considered critical.

In the following sections the influence of other parameters upon structural performance is investigated. Section 4.4 investigates geometric parameters and Section 4.5 investigates material parameters.

4.4 Geometric Sensitivity Studies

In this section the influence of geometric parameters, slenderness ratio and aspect ratio upon the high temperature structural behaviour exhibited by a two way spanning reinforced concrete slab is investigated.

4.4.1 Slenderness ratio

The magnitude of deformation is very important for the behaviour of reinforced concrete two way spanning slabs. At low deflections flexure and compressive membrane action are the dominant load bearing mechanisms; at large deflections tensile membrane action dominates.

The influence of slenderness ratio for the two way spanning slab is investigated by varying the slab depth; depths of 100 mm, 150 mm, 200 mm and 250 mm are analysed. Cover to the sagging reinforcement is maintained at 20 mm as is the load ratio of 0.48 maintained in the benchmark analysis in section 4.3.1.

Increasing the depth of the slab has two important effects for the behaviour of the slab. Firstly, the depth at which compressive membrane action can be mobilised is increased. Secondly, in chapter 3 it was shown that an increase in cross-section depth decreases the magnitude of thermal induced deflections. These two effects enhance the compressive membrane behaviour of the slab.

Figure 4-19 contrasts central deflections of slabs of increasing depth when laterally restrained and laterally and rotationally restrained (compressive membrane action is not possible in unrestrained slabs). Compressive membrane action is identifiable from the deflection results of laterally restrained slabs by low deflections which increase slowly. This was confirmed in section 4.3.2 by examining the concrete maximum and minimum principle stresses. The principle stresses indicated the presence of large in plane compressive forces through the section typical of compressive membrane behaviour. Compressive membrane action is terminated when the peak deflections exceed the line of thrust generated by the lateral restraint. This is accompanied by a sharp increase in deflections until tensile membrane action is mobilised.

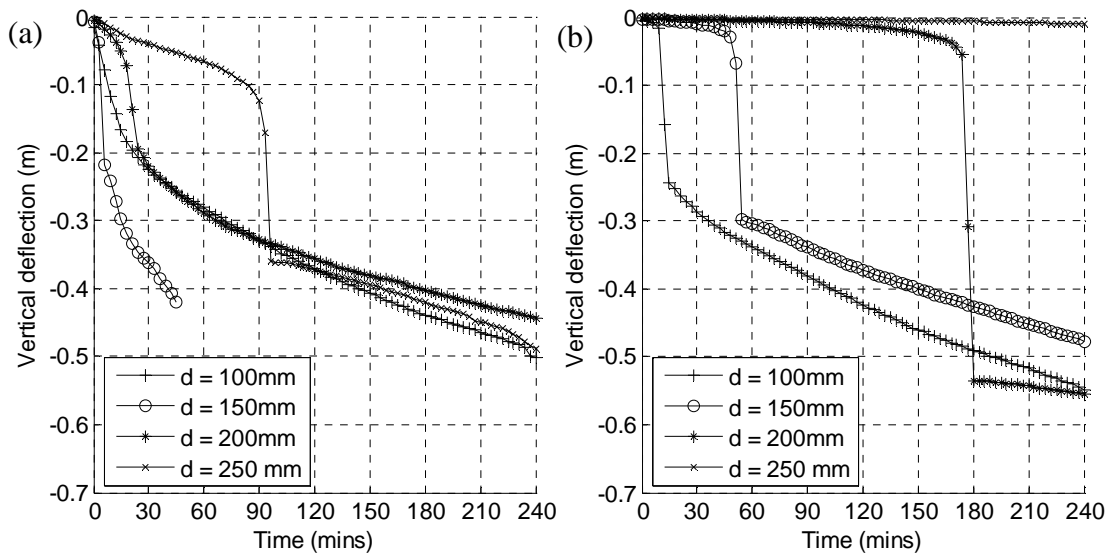


Figure 4-19 Effect of slenderness ratio for the deflection of a slab exposed to the Standard Fire with (a) laterally restrained (c) laterally and rotationally restrained boundary conditions

In Figure 4-19 increasing the slab depth or reducing the slab slenderness clearly increases the period of compressive membrane action. Under lateral restraint the period of compressive membrane action is increased to over 90 minutes of standard fire exposure. Where rotationally restrained this period is increased from less than 10 minutes to over 240 minutes. With such long periods of compressive membrane action it is entirely possible that under exposure to a real fire some concrete structures will never develop tensile membrane behaviour. It is also possible that by the time the slab does snap though to tensile membrane action the reinforcement will be substantially weakened reducing any contributions to strength. Thus for many forms of concrete construction compressive membrane action will be the dominant load bearing mechanism in fire. Such structures include the stocky solid slabs considered here and also flat slabs. Tensile membrane action requires vertical lines of support at the slab edge, in flat slabs where vertical support is provided by the columns the effect is diminished.

A stocky slab will be included in the investigation of non-uniform thermal exposure and explosive spalling in addition to the slender slab previously analysed. This will allow conclusions to be drawn concerning both tensile membrane behaviour and tensile membrane behaviour.

In investigating these effects relative performance will be judged by the effect on the period of compressive membrane action achieved. For example a reduction in the period of compressive membrane action will be considered a decrease in performance.

4.4.2 Aspect Ratio

The enhancement of strength two way spanning slabs achieve from catenary action at ambient and at high temperatures is dependent upon the double curvature nature of the deformed shape. This enhancement is at its greatest when the aspect ratio of the slab is closest to 1 {Lim, 2003 #218}. The previously examined model has assumed a square slab; in this section the influence for behaviour a rectangular geometry poses is investigated.

The behaviour of the 6m square slab (aspect ratio = 1) is compared here with that of a 6m x 4.5m slab (aspect ratio = 0.75). Advantage was taken of symmetry about both the x and y axes and a quarter of the slab was modelled. Figure 4-20 plots the evolution of the slab central deflection with increasing time of exposure and the deflection profile for each slab after 60 minutes exposure to standard temperature time curve; at this time both slabs are exhibiting catenary action. The central deflection of the rectangular slab is less than that of the square slab due to the stiffer response of the short span; consequently the transition from compressive membrane action to catenary action is delayed.

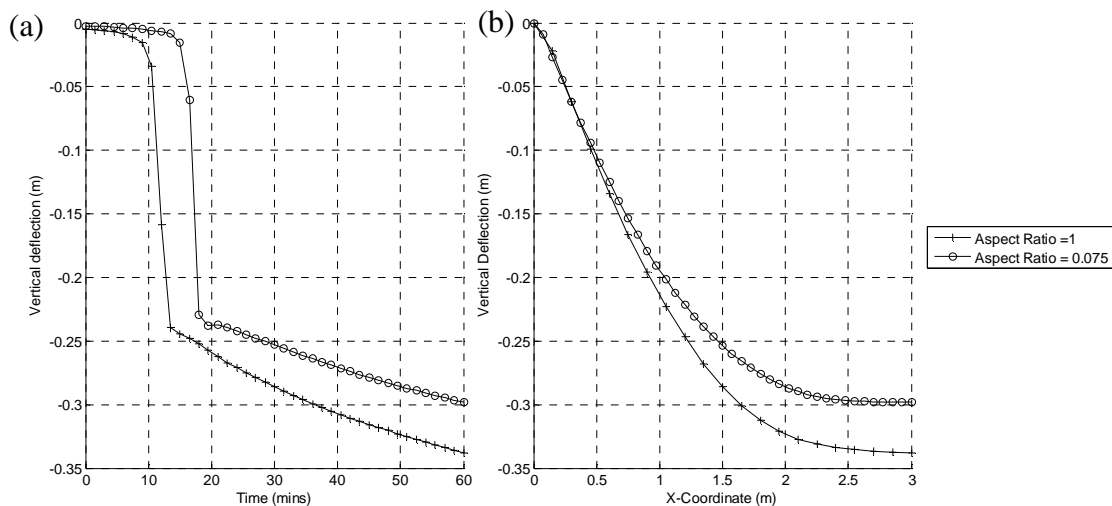


Figure 4-20 (a) Development of slab central deflection during standard fire exposure (b) 6m span deflection profile after 60 min exposure to the standard temperature time curve

The slab geometry influences the development of the compressive ring; Figure 4-21 compares the maximum and minimum principal concrete stress resultants of the rectangular and square slabs at 60 minutes exposure for the laterally restrained slab. In the rectangular slab compressive stresses across the short span edge increase relative to those which develop with a square geometry, those along the long span edge decrease.

It was seen in section 4.3.2 that under the increased deflections of catenary action the slab edges start to pull in. The geometry of a rectangular slab alters the proportion of pull in along the long and short span edges. The long span edges are able to pull in more than the short span edges, therefore in Figure 4-21 where the slab is restrained laterally we see an increase in tensile stresses at the edge of the long span and a decrease at the short span relative to the long span geometry.

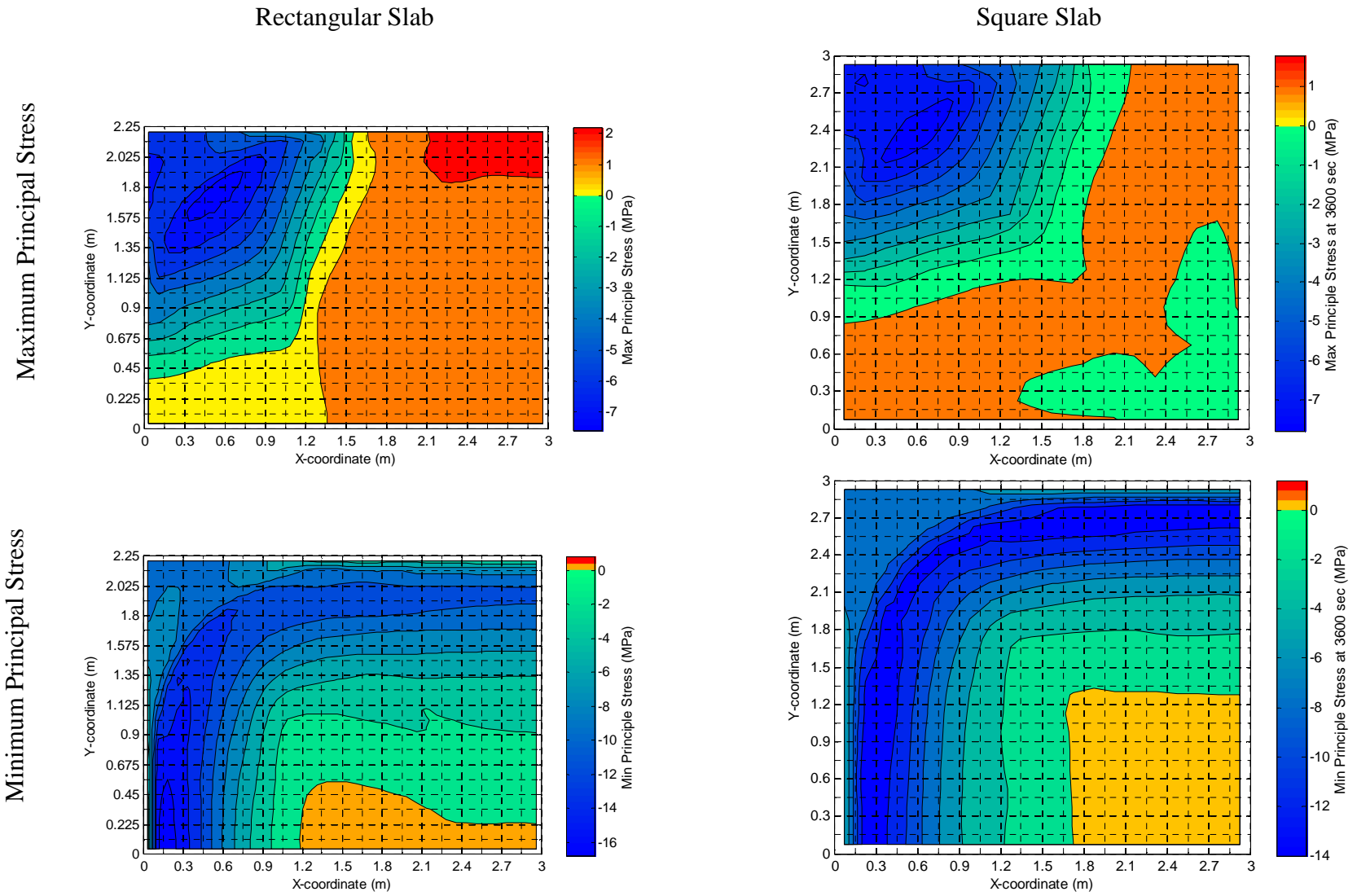


Figure 4-21 Square and rectangular slab maximum and minimum principal stress resultants for a rotationally and laterally restrained boundary condition

In a series of small scale tests on rectangular lightly reinforced and unrestrained concrete slabs, Bailey and Toh {, 2007 #212} found that ultimate failure at high temperatures was consistently by rupture of reinforcement in the long span direction. Increased pull in along the long span edge allows greater relaxation of the reinforcement spanning in the direction of the short span.

In Figure 4-22 reinforcement normalised stress profiles are presented for both the rotationally and laterally restrained case and unrestrained case. The profiles have been plotted for the long and short span of the rectangular slab, hence stress values have been plotted at normalised distances from the edge ($x = 0$) to the centre of the slab ($x = 1$).

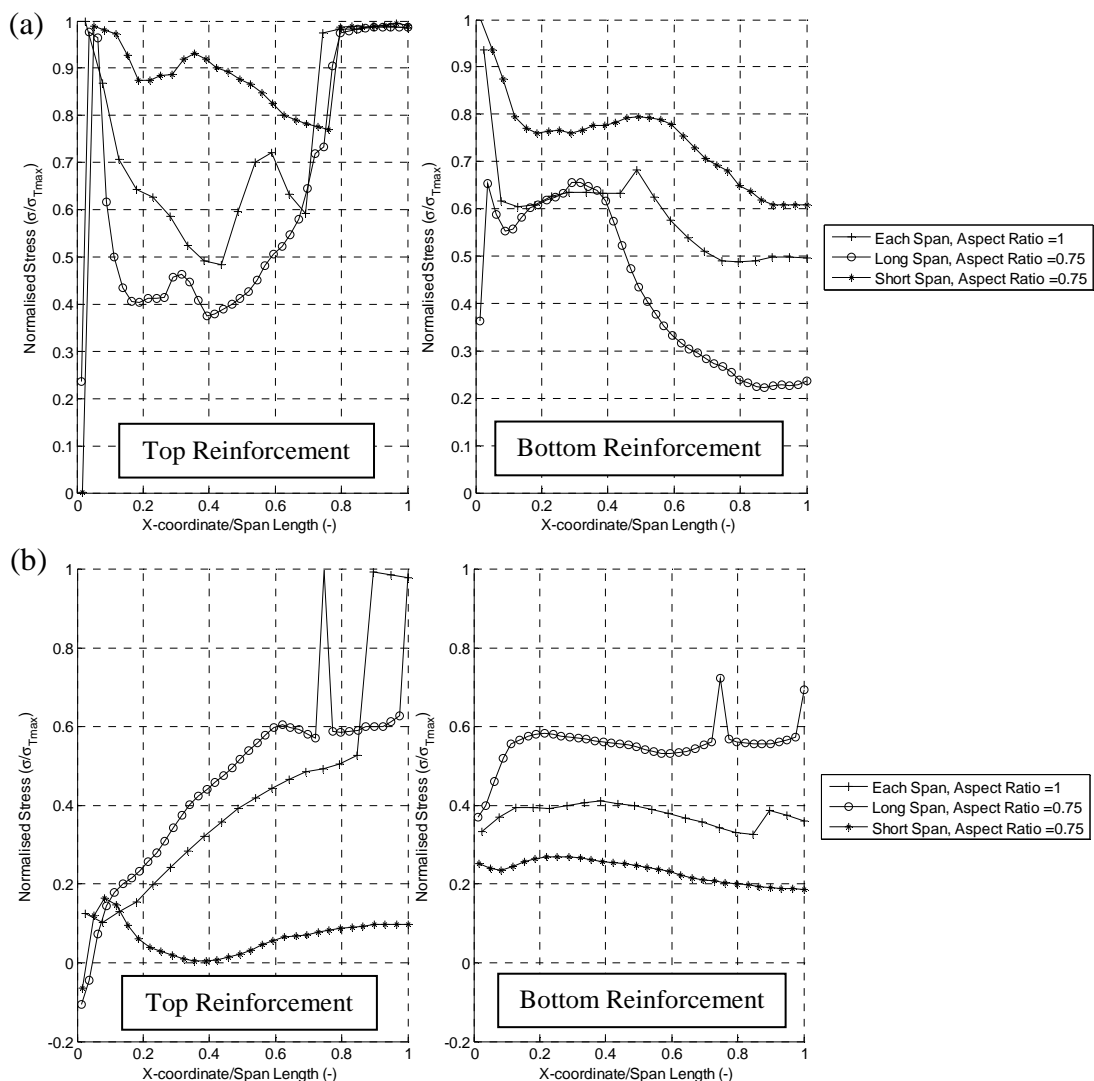


Figure 4-22 Reinforcement normalised stress profiles (a) Restrained slab, top and bottom reinforcement (b) Unrestrained slab, top and bottom reinforcement

For the unrestrained case it is evident in both the top and bottom reinforcement that reinforcement stresses in the short span reduce while those in the long span increase. This behaviour is reversed however when the slab is restrained laterally. Lateral restraint opposes the slab edges pulling in; consequently this increases the reinforcement strains in the short span reinforcement. In Figure 4-22 (a) it can be seen that the magnitude of reinforcement strain in the short span is greater than the long span strains and the square slab reinforcement strains.

4.4.3 Summary

The investigation of slenderness indicates that stockier slabs are less likely to develop tensile membrane action for an equivalent fire exposure than a more slender slab. For such slabs flexural strength and compressive membrane action will determine their fire performance, therefore it is important to consider the implications of non-uniform heating for these mechanisms in addition to tensile membrane action.

A rectangular geometry reduces the strength enhancement of a concrete slab by increasing maximum reinforcement mechanical strains. This is an important consideration for the design of reinforced concrete slabs; however, as the mechanism of behaviour has not changed the behaviour of rectangular slabs is not further investigated.

4.5 Material sensitivity studies

In chapter 2 a detailed review of the assumptions made in reinforced concrete material modelling was discussed. In this section the sensitivity of the finite element model predictions to some of those material definitions is investigated. The material definitions investigated include the tension stiffening definition in section 4.5.1, load induced thermal strain in section 4.5.2 and reinforcement rupture strain in section 4.5.3.

4.5.1 Tension stiffening

In the Chapter 2 the mechanisms responsible for the tension stiffening effect have been described and models devised to characterise this behaviour in a finite element

analysis discussed. In this section the significance of the degree of tension stiffening for the structural performance is investigated.

Chapter 2 has described how tension stiffening can be characterised for analysis by modifying the concrete tensile constitutive curve, typically reducing the slope of the post peak descending branch for increasing levels of tension stiffening. In this analysis the degree of tension stiffening will be termed the tension stiffening factor which is defined in Equation 4-2.

$$TS = \frac{\epsilon_{T,t}^u}{\epsilon_{T,t}^{ck0}} \quad \text{Equation 4-2}$$

Where, $\epsilon_{T,t}^{ck0}$, is the initial cracking strain (strain at peak strength) at temperature, T , and, $\epsilon_{T,t}^u$, is the ultimate tensile strain at temperature, T . The post peak descending branch is assumed to be linear, a typical tensile curve is shown in Figure 4-23

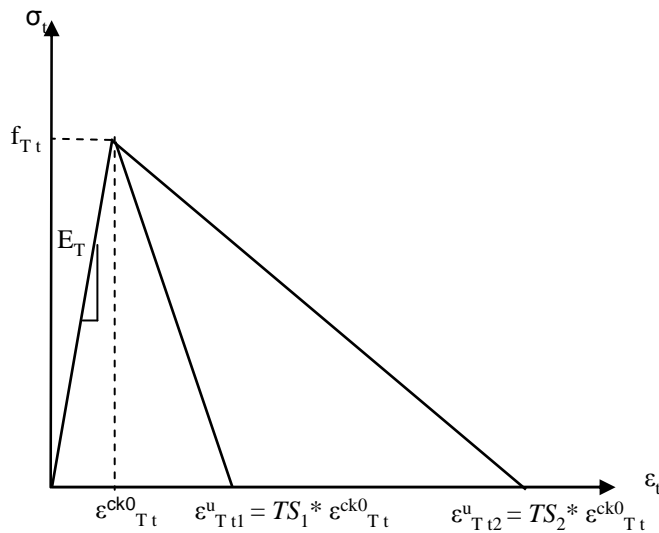


Figure 4-23 Modification of the concrete tensile constitutive curve to include tension stiffening effect

For the sensitivity study an increasing range of TS values of 0, 5, 10, 20, 40, 100, 200, and 400 are adopted. Figure 4-24 (a) presents the ambient post peak branches and Figure 4-24 (b) a set of temperature dependent concrete tensile curves for a selected TS value. It should be noted that the tension stiffening is assumed to be constant with temperature.

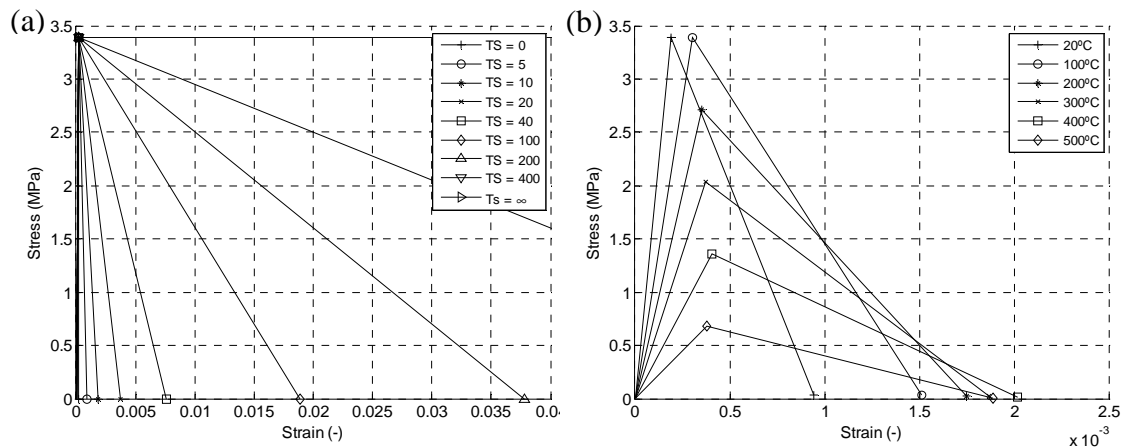


Figure 4-24(a) Variation of post peak tension stiffening curve and (b) Tensile constitutive curves, $TS=5$, for 20-500°C

The two-way spanning slab outlined in section 4.3.1 was analysed using each of these post peak definitions for a 60 minute standard fire exposure. Abrupt changes in material properties can cause numerical instabilities during the analysis therefore in addition to investigating the sensitivity of structural predictions to the concrete tensile model definition, numerical stability is also compared.

Numerical Stability of the Concrete Tension Model

Increasing the brittleness of the tensile post-peak descending branch reduces the numerical stability of the finite element solution. The abrupt change in an element's constitutive response when cracking occurs causes the solution to become temporarily unstable and equilibrium must be re-established. Unless an extremely small increment in solution time is applied, the solution will jump from the pre-peak response to past the end of the descending post-peak response. Equilibrium of the solution will be lost, particularly if multiple elements become cracked during the same solution increment. Conversely, increasing the length of the descending branch aids numerical stability but introduces an increasingly ductile concrete tensile response. Figure 4-25 presents contour plots of stress at the slab bottom surface for TS values of 0, 5 and 10. Local cracking due to numerical instability can be seen by the unsymmetrical behaviour of the slab with the most brittle definition (Figure 4-25 (a), $TS=0$). Such behaviour is not evident at higher TS values. Due to the numerically unstable results produced by the most brittle model, $TS = 0$, this definition will be excluded from subsequent comparisons in the sensitivity investigation.

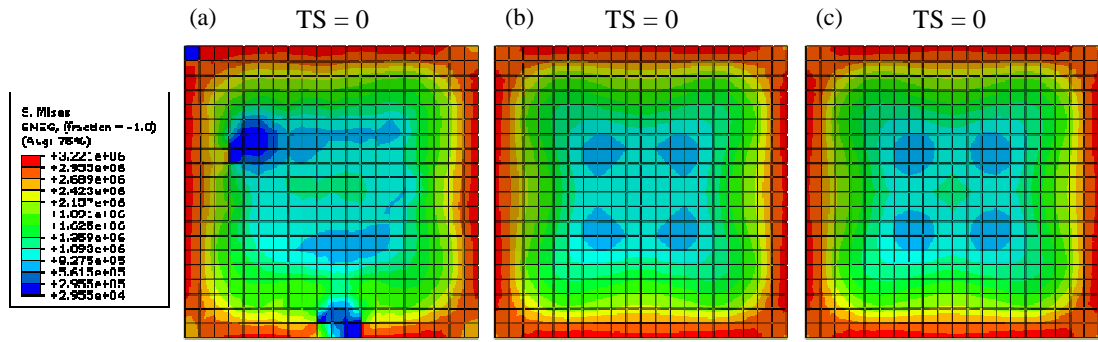


Figure 4-25 von Mises stress contour plots at 3600 sec ISO fire exposure – bottom surface for TS values of (a) 0 (b) 5 and (c) 10

Structural Sensitivity to the Reinforced Concrete Tensile Model

Figure 4-26, Figure 4-27 and Figure 4-28 present the sensitivity of the slab model to the tension stiffening factor. Figure 4-26 plots the slab central deflection against time of exposure for each of the TS values used. Figure 4-27 and Figure 4-28 present the effects for reinforcement stress and mechanical strain respectively.

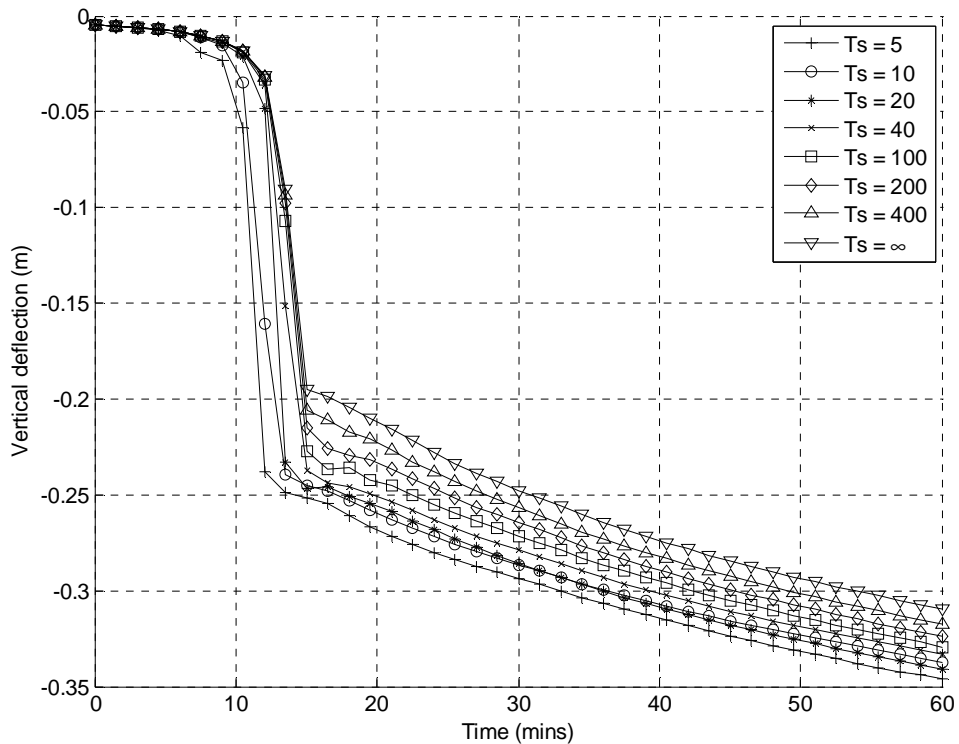


Figure 4-26 Variation in the slab mid span deflections with concrete tension definition for a 60 minute standard fire exposure

Figure 4-27 (a) and (b) present the top reinforcement stress at the edge and mid-span of the slab respectively. Figure 4-27 (c) and (b) present bottom reinforcement stresses again at the edge and mid-span locations as a proportion of the maximum steel stress defined by Eurocode 2 {, 2004 #27}.

Figure 4-28 presents the effect the tension stiffening factor upon the reinforcement mechanical strains. Again these have been plotted for the top and bottom reinforcement at the slab edge (Figure 4-28 (a) and (b) respectively) and for the top and bottom reinforcement at the mid-span (Figure 4-28 (c) and (d) respectively).

The increased stress transfer between reinforcement and concrete implied by a higher tension stiffening definition is significant for the behaviour of the two way spanning slab. From the plot of central deflections in Figure 4-26 it is evident that a high degree of tension stiffening leads to a significantly stiffer slab response.

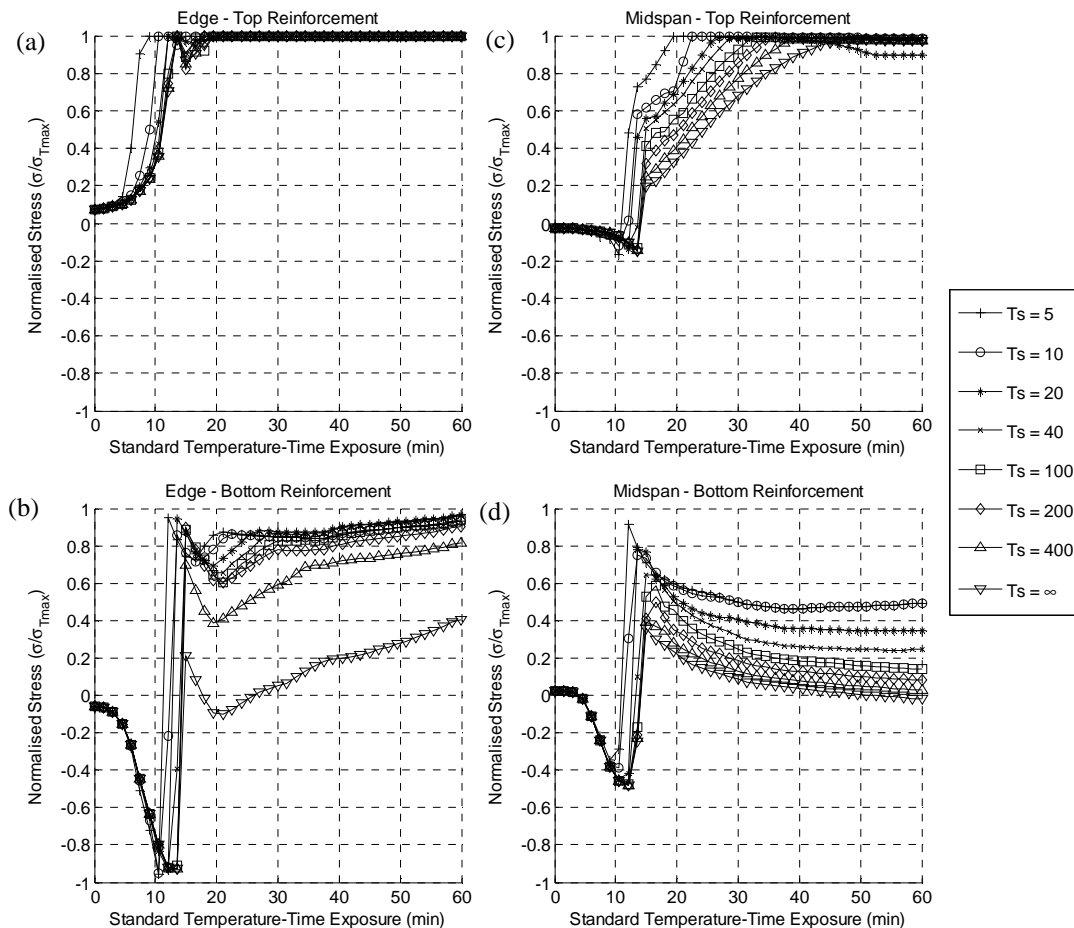


Figure 4-27 Effect of tension stiffening factor on the reinforcement normalised stress at the slab edge (a) Top location and (b) Bottom location and at the slab mid-span (c) Top location and (b) Bottom location.

The effect is most significant after the slab has snapped through from compressive membrane action to tensile membrane action where the central portion of the slab is predominantly in tension. Prior to snap-through stability is dependent upon flexural and compressive membrane action, therefore, the degree of tension stiffening has a negligible effect. The additional capacity of the concrete results in reduced reinforcement stresses and strains which have been plotted in Figure 4-27 and Figure 4-28.

This sensitivity study has shown that the cracking behaviour of concrete is a source of numerical instability in the analysis. The introduction of some tension stiffening which is a real effect can have the additional benefit of alleviating some of the numerical difficulties associated with softening behaviour. Increasing the quantity of tension stiffening has the effect of smoothing the influence of the concrete cracking and altering the structural behaviour. To avoid numerical problems it has therefore been decided to use a TS value of 10.

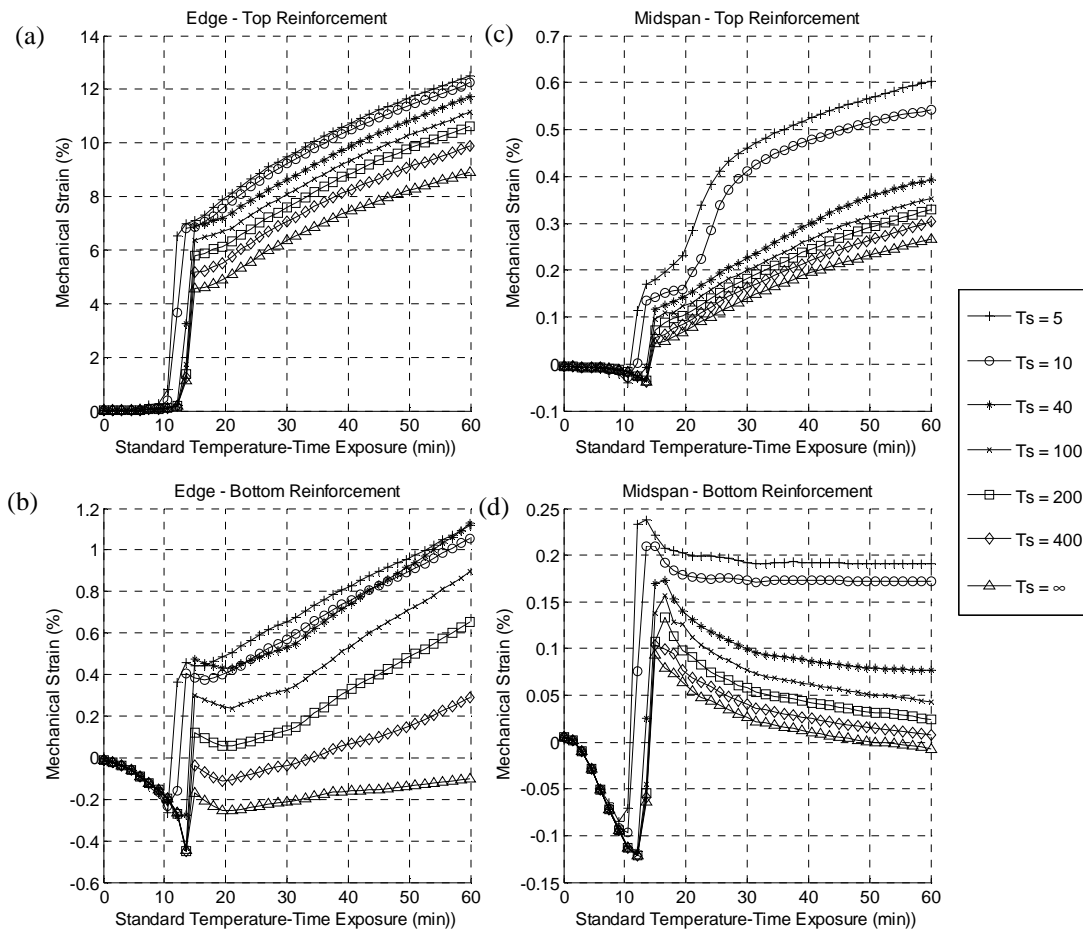


Figure 4-28 Effect of tension stiffening factor on the reinforcement mechanical strain at the edge of the slab (a) Top location and (b) Bottom location and at the mid span of the slab (c) Top location and (d) Bottom location.

Accurate representation of reinforcement behaviour is critically important for the prediction of tensile membrane behaviour in structures. The reinforcement behaviour is in turn inextricably linked to the concrete tensile definition.

In conjunction with the literature review of concrete behaviour in chapter 2 this study highlights the difficulties in accurately representing the tensile behaviour of concrete in a finite element analysis and the significant consequences of misrepresentation in predicting structural behaviour.

4.5.2 Load Induced Thermal Strain (LITS)

The influence of Load Induced Thermal Strain (LITS) upon the behaviour of a two way spanning slab is investigated in this study. Previous research concerning the importance of LITS for structural behaviour, summarised in chapter 2, has identified the strain term as important for compressive members such as columns and for

structures in cooling where it is important to predict the appropriate amount of non-recoverable strain. In this study the effect of the LITS term upon the behaviour of the two-way spanning slab is investigated.

Anderberg and Thelandersson's {, 1976 #31} correlation for transient strain (which is the largest non-recoverable component of LITS) was described in chapter 2. It is easily incorporated into the concrete constitutive curve used in the previous analysis. Figure 4-29 plots the amended curve at 300°C in which inclusion of the transient strain term changes the initial tangent modulus. Law and Gillie {, 2008 #88} demonstrated that using this new 'apparent' modulus rather than the actual material modulus in a structural analysis will lead to incorrectly calculating the proportion of elastic and plastic strain making up the total strains. If the slope of the apparent modulus is reduced it will therefore over predict the elastic strain quantity and under predict the plastic strain component. The actual modulus is therefore used in this investigation.

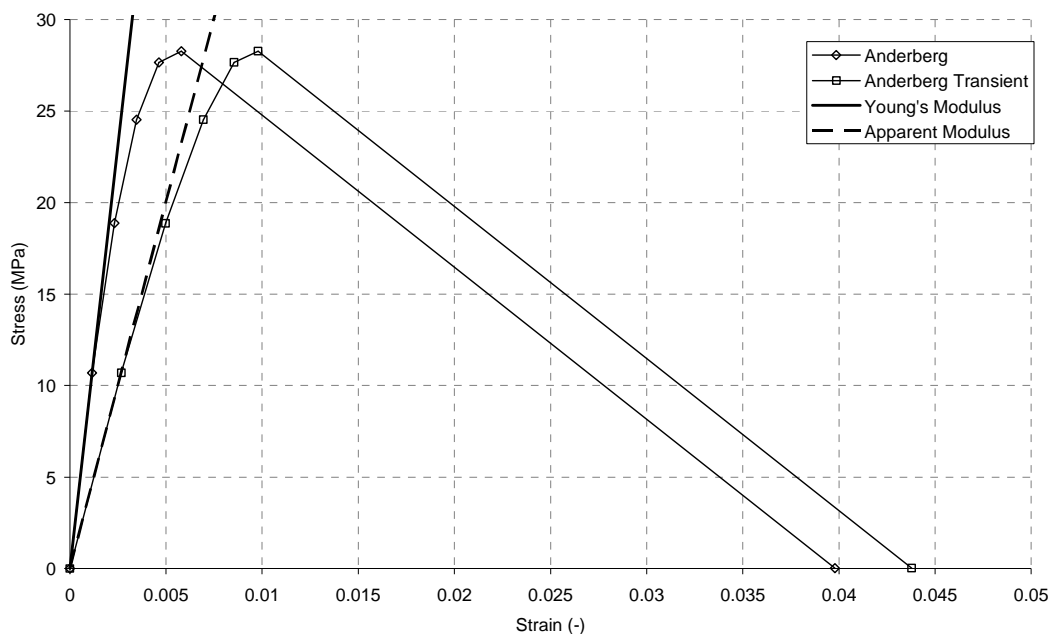


Figure 4-29 Incorporation of LITS term into the instantaneous stress-strain constitutive relations according to Anderberg and Thelandersson {, 1976 #31} 300deg

The slab is analysed for a 60 minute exposure to the standard-temperature time curve with both unrestrained boundary conditions and fully restrained boundary conditions. Figure 4-30 plots the deformation behaviour of both, Figure 4-30 (a) and (c) plot the

deflection profiles; Figure 4-30 (b) and (d) plot the evolution of the central slab deflection for the duration of exposure. The inclusion of the transient strain term has little noticeable effect upon the deformation behaviour of the unrestrained slab but does affect the deflections of the restrained slab once the slab has snapped through to tensile membrane action.

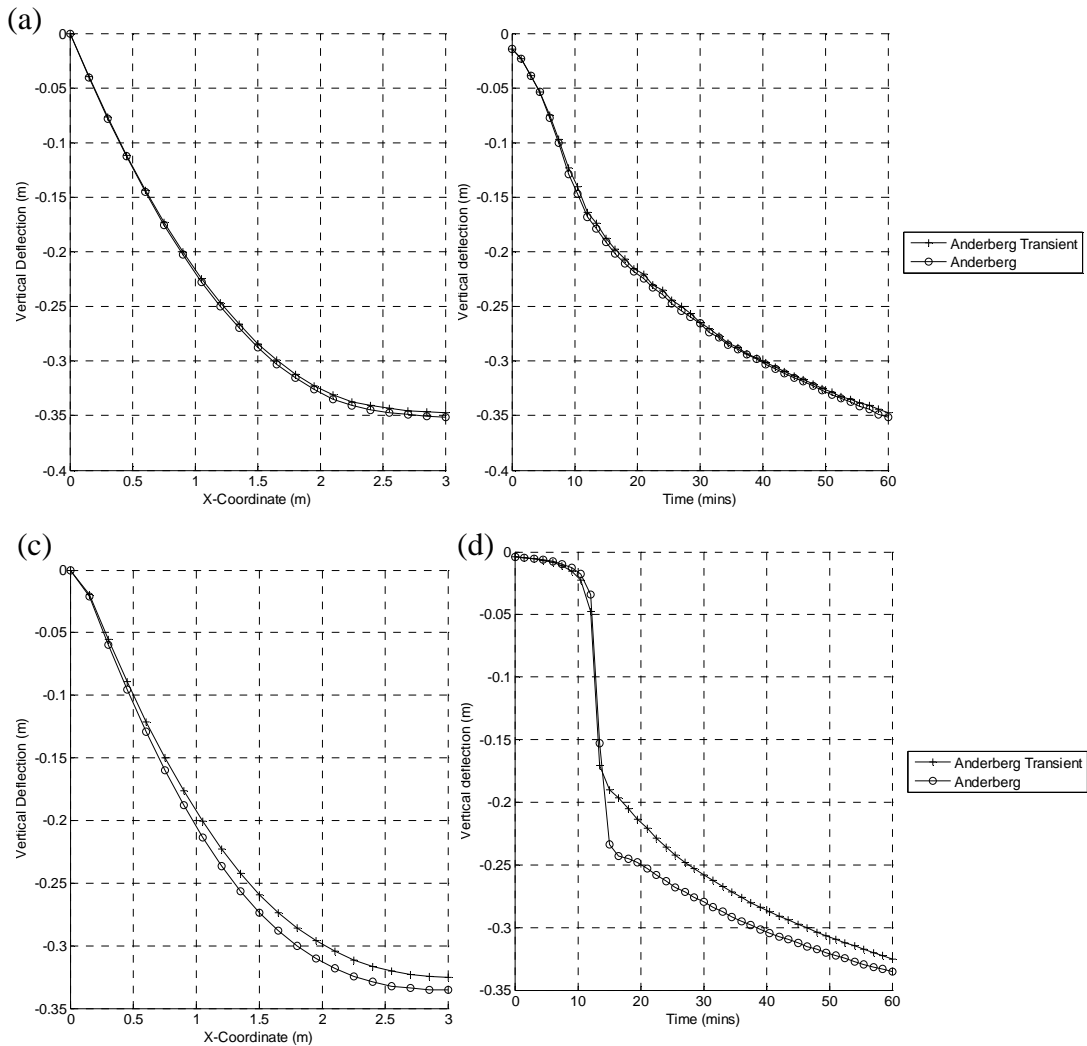


Figure 4-30 Unrestrained slab (a) Mid span deflection profile at 60 minutes (b) slab central deflection and restrained slab (c) Mid span deflection profile at 60 minutes (d) slab central deflection

The effect is a stiffer response from the material model including the transient term. This at first appears somewhat counter-intuitive as the inclusion of the transient strain term in the compressive stress strain curve ‘softens’ the compressive material response (Figure 4-29), but this can be explained by examining the slab response in more detail.

Figure 4-31 presents schematically the material loading history for the central portion of the restrained slab. In the early stages of exposure the slab experiences compressive membrane action (1). For the same strain under compression the LITS modified material model develops a larger plastic strain component ($\epsilon_{c,pl}$) for the same total strain than the model which does not include LITS. The equivalent plastic strains for each analysis are plotted in Figure 4-32 after 10.5 minutes of exposure which is just prior to the slab snapping through to tensile membrane action. The magnitude of equivalent plastic strains for the model including the transient strain term is significantly larger than that for the material model excluding the transient strain term.

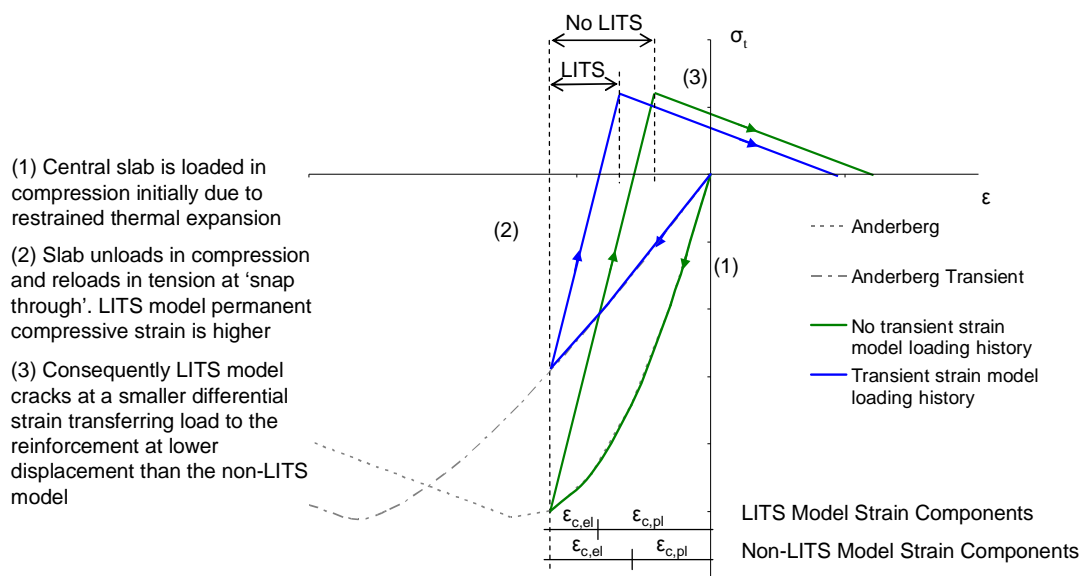


Figure 4-31 Material loading history for the restrained slab

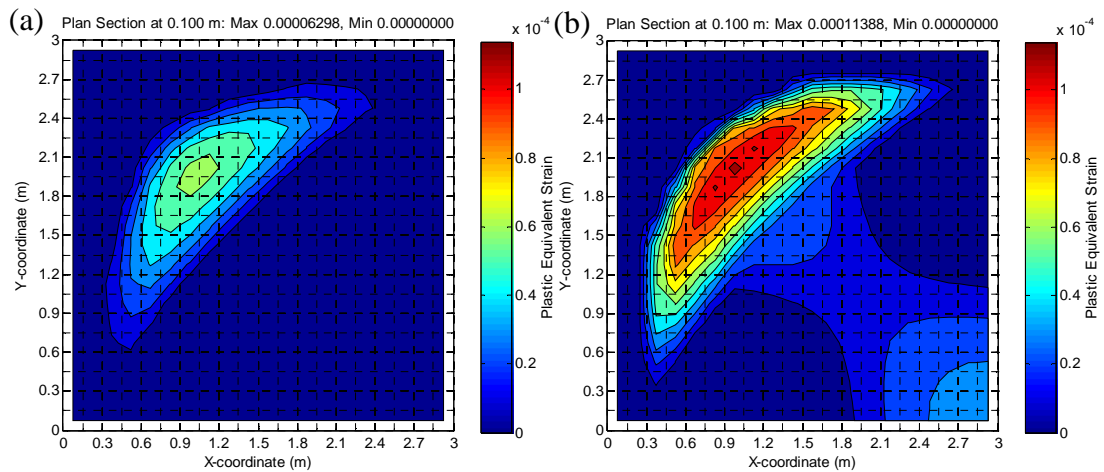


Figure 4-32 Plan contour of unexposed surface plastic equivalent compressive strains at 10.5 min (a) Non-LITS model (b) LITS model

The proportion of plastic and elastic strain making up the total strain is important when the slab unloads in compression and reloads in tension which occurs when the slab ‘snaps through’ from compressive membrane action to tensile membrane action after ten minutes of exposure (Figure 4-30 and (2) in Figure 4-31). Upon reloading in tension the additional non-recoverable transient strain component results in the concrete cracking at a lower total deformation than the non LITS model and transferring load to the reinforcement. Tensile membrane action is therefore mobilised at smaller slab deflections and the response is stiffer as seen in Figure 4-30. The effect is not noticeable for the unrestrained case as it lacks the lateral restraint to allow compressive membrane action to develop.

Figure 4-33 presents the reinforcement mechanical strains for each material model. For this scenario neglecting the transient strain term results in a conservative estimate of the reinforcement strain therefore the LITS terms has not been included in subsequent analyses.

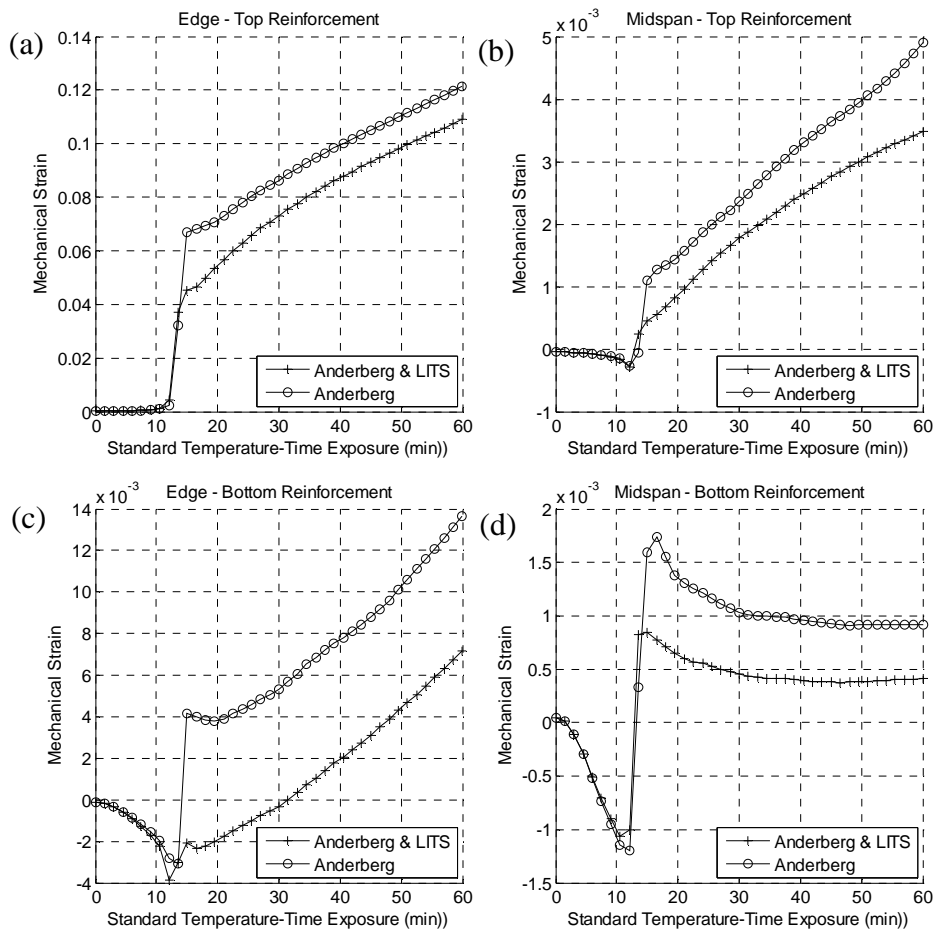


Figure 4-33 Effect of transient strain component for reinforcement mechanical strain at the slab edge slab (a) Top location and (b) Bottom location and at the mid span of the slab (c) Top location and (d) Bottom location.

This study has highlighted the importance of the transient strain term where unloading of the structure occurs during heating for predicting behaviour. Previous research has predominantly focused on the effects for compressive members such as columns and in some cases the cooling behaviour. The importance of LITS for predicting concrete structural behaviour has, however, not yet been widely adopted by the design community this is despite the application of performance based engineering principles to the design of reinforced concrete slabs in the context of concrete-steel composite structures.

4.5.3 Reinforcement Rupture Strain

In this section the sensitivity of the finite element model to the reinforcement rupture strain is assessed. Given the current model formulation it is not possible to model the physical process of concrete tensile cracking leading to reinforcement rupture. The

cracking behaviour of concrete in tension is characterised using smeared cracking concepts and reinforcement rupture is characterised through a sharp decrease in strength at high strains. Both the concrete cracking and reinforcement strains are averaged across the width of one element, therefore accuracy is particularly limited. The aim of the study is to assess the sensitivity of the model to reinforcement rupture rather than to make predictions of cracking and reinforcement rupture behaviour under membrane action. Rupture is assumed at strains of 4% and 8% and compared with the Eurocode recommended 15%. The slope of the descending branch adopted by the Eurocode is adopted for the 4% and 8% analyses. A sloped descending branch is unrealistic; however, it is needed for numerical stability

These definitions were used in the analysis of the fully restrained slab where rotational restraint at the slab edges results in large strains of the top reinforcement under catenary action. The results of these analyses are presented in Figure 4-34 to Figure 4-36. Figure 4-34 plots the top and bottom reinforcement normalised stress at the mid span slab edge and at the slab centre. Figure 4-35 plots the top and bottom reinforcement mechanical strain for the same locations. Figure 4-36 plots the mid span deflection profile and slab central deflection.

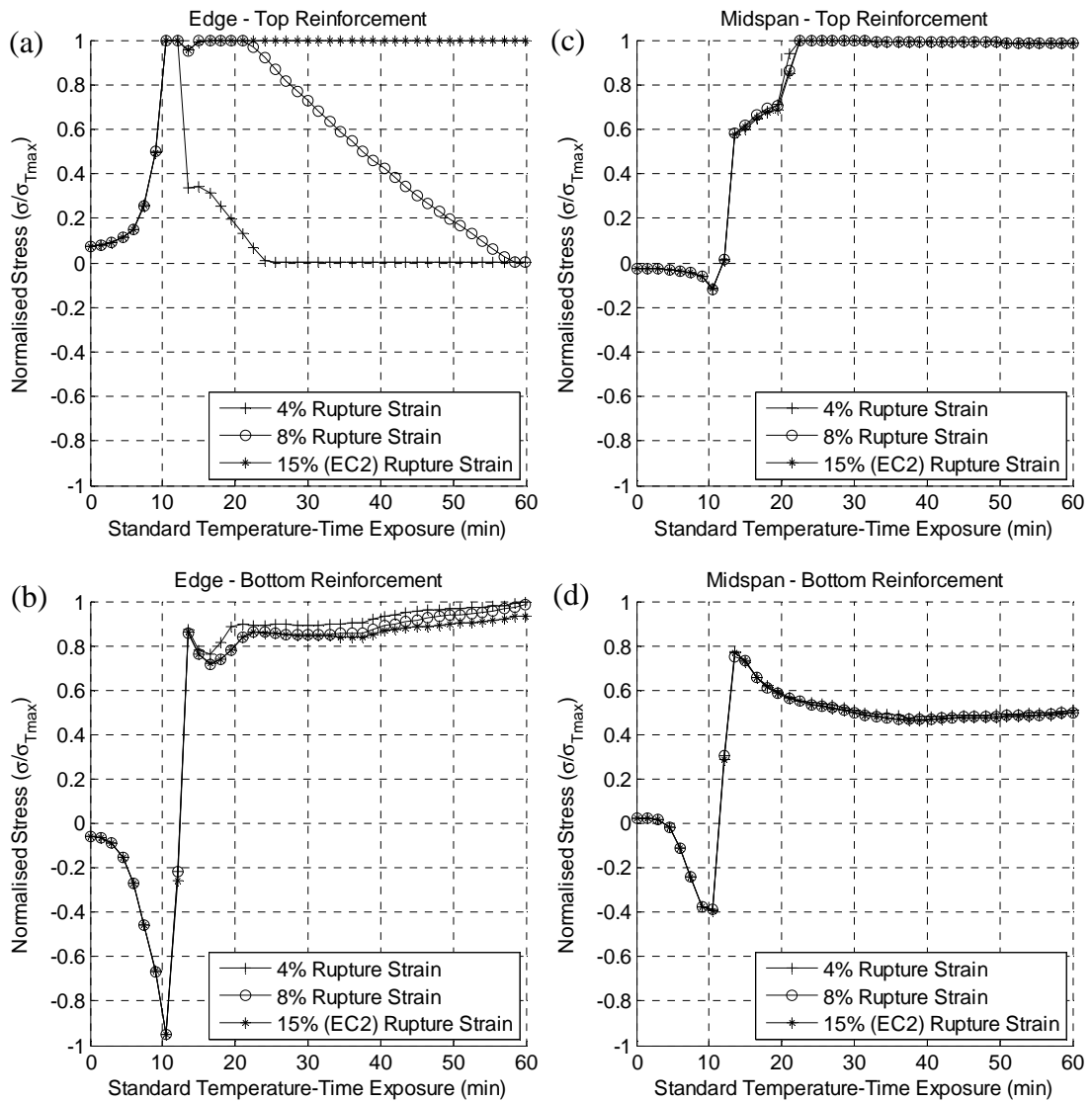


Figure 4-34 Effect of reinforcement rupture strain definition for reinforcement normalised stress at the slab edge (a) Top location and (b) Bottom location and at the slab mid-span (c) Top location and (b) Bottom location

The evolution of stress in Figure 4-34 (a) indicates that for the 4% and the 8% rupture strain definitions the top reinforcement at the slab edge has ruptured. The gradual ‘load shedding’ exhibited is of course unrealistic. The consequences of sudden load transfer that would occur are not captured in this analysis; it is not clear what effect this would have for the stability of the slab.

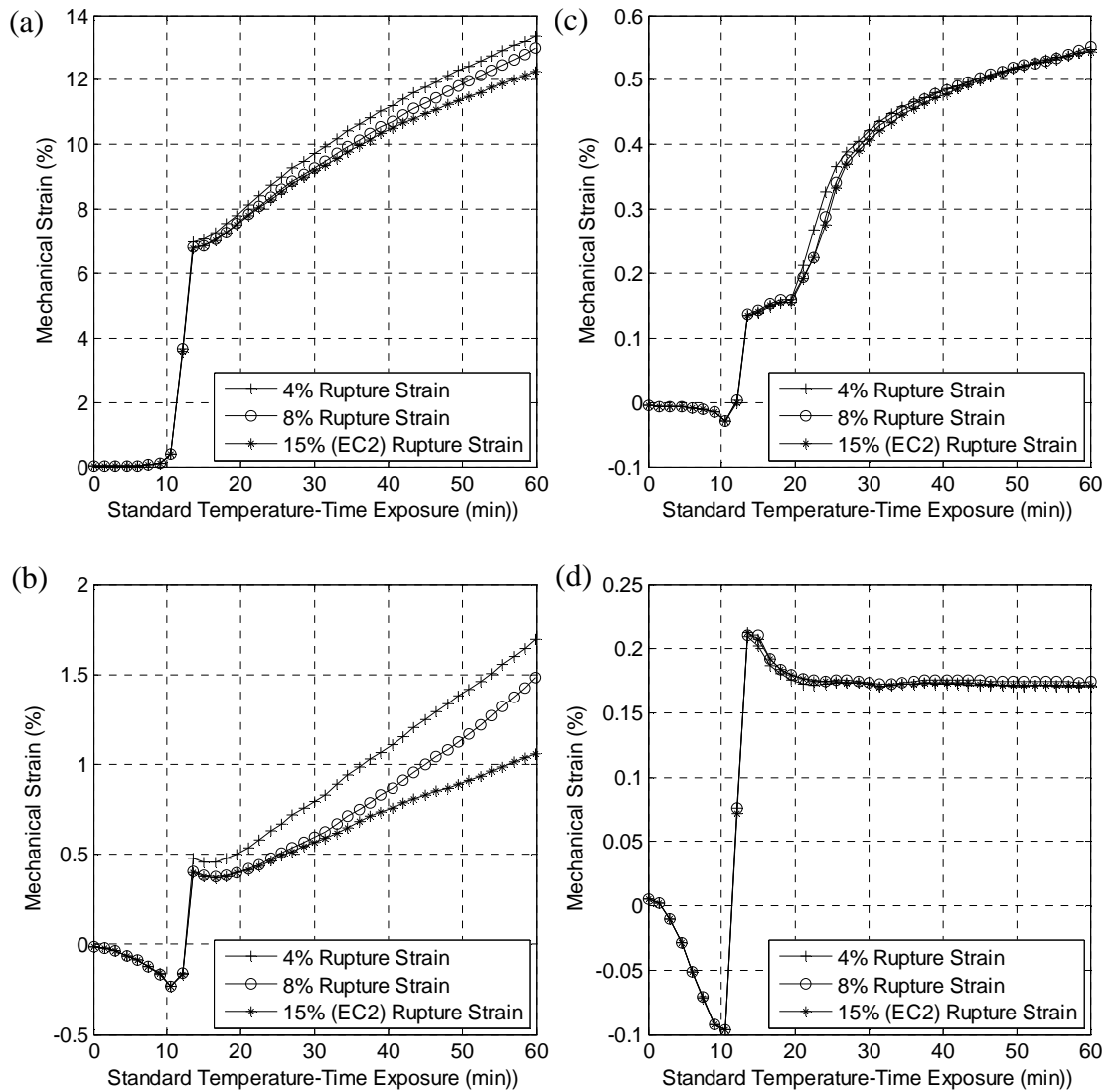


Figure 4-35 Effect of reinforcement rupture strain definition for reinforcement mechanical strain at the slab edge slab (a) Top location and (b) Bottom location and at the mid span of the slab (c) Top location and (d) Bottom location.

From inspection of the mechanical strain response in Figure 4-35 the loss of strength in the top reinforcement results in increased straining of the bottom reinforcement at the slab edge as the slab edges continue to pull inwards. There is no significant effect upon the development of strains in either the top or bottom reinforcement at the slab centre.

Figure 4-36 compares the increase in slab central deflections for each reinforcement material definition and also the deflected profile after 60 minutes exposure.

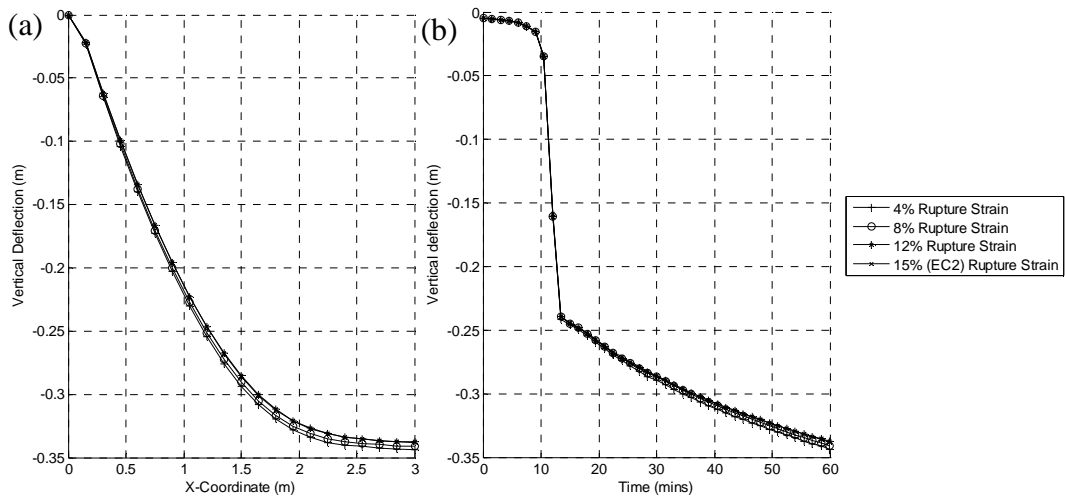


Figure 4-36 Effect of reinforcement rupture strain definition on (a) central span deflection profile at 60 minutes standard temperature exposure and (b) central slab deflection for duration of 60 minute standard temperature time curve exposure.

Despite the complete loss of strength in the top reinforcement the definition has an almost negligible effect on the deformations of the slab. This is due to the smearing of the effect of the crack and the reinforcement rupture across the width of one element and the infinite strength of the boundary conditions defined, thus preventing any real increase in rotation at the slab edge.

4.6 Conclusions: Benchmark slab model

4.6.1 Finite element model of a two way spanning RC slab

In this chapter a finite element model has been developed to investigate numerically the behaviour of two way spanning reinforced concrete slabs exposed to fire. A great deal of research has been conducted in this field; this research has been drawn on to establish a benchmark finite element model that includes the features required for subsequent analysis of the slab.

The general purpose finite element software ABAQUS was used to undertake both the heat transfer analysis and the stress/displacement analysis. Computationally efficient shell elements were used to model the slab. These elements are capable of modelling: non-linear thermal variation through the slab depth, thermal expansion and geometric and material non-linearity which have been found to be necessary for the modelling of reinforced concrete slabs at high temperature.

The predictions of the finite element model for the behaviour of the reinforced concrete slab under standard fire exposure was in agreement with the state of the art understanding of their behaviour in fire and models the compressive and tensile membrane behaviour of these slabs. The model's capability for predicting ultimate failure due to concrete crushing or reinforcement rupture is limited by the use of a smeared crack simplification, but allows comparative studies to be performed.

The investigation of behaviour has shown that concrete plastic equivalent strains and reinforcement mechanical strains can be used as performance indicators in chapter 5 to judge the influence of non-uniform thermal exposure upon slab performance.

4.6.2 Geometric Sensitivity Studies

The influence of slenderness ratio upon the membrane behaviour was considered for a two way spanning slab. The slenderness ratio strongly influences the development of slab deflections and therefore the compressive and tensile membrane behaviour. The reason is two fold:

- Increasing depth of cross section reduces the magnitude of vertical deflections from thermal expansion (demonstrated in Chapter 3)
- Compressive membrane action is feasible at greater deflections in deep cross-sections

The consequence of these effects is that increasingly slender reinforced concrete slabs will develop tensile membrane action whereas stocky slabs will be dependent upon flexure and if possible compressive membrane action. The investigation of non-uniform thermal exposure will study both slender and stocky cases.

The aspect ratio of the slab is known to affect the fire performance of reinforced concrete slabs. The effect of aspect ratio is upon the development of concrete stress and reinforcement mechanical strains have been reviewed. The analysis predicts increased reinforcement strains across the short span for restrained slab and a reduction for an unrestrained slab. Although the aspect ratio is important for performance it does not alter the behaviour exhibited by the slab. The investigation of non-uniform thermal exposure will therefore not consider aspect ratio.

4.6.3 Material Sensitivity Studies

In Chapter 2 a detailed review of the material behaviour of reinforced concrete at high temperatures was undertaken. This review highlighted some shortfalls in our current capability to characterise the behaviour of concrete at ambient and at elevated temperatures thus during the development of a benchmark model sensitivity analyses were conducted to assess the significance of these gaps in current knowledge.

The *post peak tensile behaviour of concrete* and the tension stiffening effect associated with reinforced concrete were investigated. Reducing the amount of tension stiffening increases numerical instability while increasing tension stiffening improves stability. However, it also smothers the cracking behaviour of concrete, leading to under predictions of reinforcement strain. It was found that a tension stiffening value of 10 provides a numerically stable analysis without significantly compromising accuracy and will be used in future studies

A significant amount of research has been conducted concerning the occurrence of *load induced thermal strain* but its effect on slab performance has not been considered in depth. The effect upon behaviour of the two-way spanning slab was found to be significant where the slab unloaded in compression and reloaded in tension such as the transition from compressive membrane action to tensile membrane action. For this type of load history accurate prediction of the development of plastic strains is important. For the scenario considered here neglecting the transient strain term caused the reinforcement strains to increase.

The *reinforcement rupture strain* provided in Eurocode 2 is relatively high; a sensitivity analysis was conducted to establish the effect of rupture strain upon deformation and reinforcement stresses and strains. The reduction of the reinforcement rupture strain definition resulted in reinforcement ‘rupture’ at the slab edge where rotational restraint is applied. It was found however to have a negligible effect upon behaviour. This is due to the modelling methodology rather than a real behaviour.

The finite element model developed in this chapter will be used in chapter 5 in the investigation of the implications of non-uniform thermal exposure for structural behaviour.

5 Structural implications of non-uniform fires

5.1 Introduction

In this chapter the structural behaviour of two-way spanning reinforced concrete slabs exposed to non-uniform thermal conditions is investigated. The investigation builds directly on the findings of the investigations in chapters 3 and 4. These chapters demonstrated the effect of non-uniform thermal exposure upon concrete thermal expansion behaviour and the uniform thermal exposure behaviour of two-way spanning slabs respectively

The high temperature behaviour of the two-way spanning slab was shown to be dominated by tensile membrane action under a range of restraint conditions. The analysis exhibited the key features of tensile membrane action under biaxial deformation: the self supporting peripheral concrete ring of compression and the central net of reinforcement tension. The analysis of the slab under uniform thermal conditions was performed not only to verify and establish behaviour but to identify performance indicators for the tensile membrane mechanism.

Failure of the compressive ring is by crushing in the region of the slab corners where the effect of biaxial bending is greatest. As the concrete material model is based on plasticity, crushing is not explicitly modelled. Concrete plastic straining is therefore used to indicate the onset of material crushing. The plastic equivalent strain is used to indicate the degree of plastic straining in an element. This strain is expressed as a proportion of the strain at peak stress; a value greater than unity indicates the onset of crushing.

The performance of the tensile net is dependent upon the reinforcement behaviour. Under large deflections and high temperatures the material yields quickly therefore strains are used to measure behaviour. The accurate prediction of reinforcement strains is compromised by smearing concrete's post peak tensile behaviour; however, they provide a useful indicator of relative performance.

These performance indicators will be used to measure the structural implications of non-uniform thermal definitions for the tensile membrane mechanism exhibited by the slender slab.

The tensile membrane mechanism at high temperatures is strongly influenced by thermal expansion behaviour. Chapter 3 investigated the effects of non-uniform thermal exposures upon the thermal expansion behaviour of simple concrete elements. The temperature field within a fire compartment varies both spatially and temporally. The influence these temporal and spatial variations upon behaviour is complicated by the different characteristic timescales associated with changes in the gas phase temperatures and changes in the concrete temperature.

To simplify this complexity the effect of spatial variation of gas temperature only upon thermal expansion deformations was first investigated. The spatial variation in gas temperature caused a similar variation in thermal gradient and hence thermal curvature along the length of the beam. This had the effect of distorting the deflection profile; the peak gas temperature locally increases the thermal curvature shifting the peak deflection towards its location.

Behaviour under spatial *and* temporal variation was then investigated. Different temporal variations were employed to identify the sensitivity of concrete's response relative to temporal changes encountered in the gas phase. Shallow concrete elements were found to be sensitive to spatial gas temperature variations in even fast changing thermal environments. In shallow concrete elements the surface temperatures strongly influences the thermal curvature. As concrete is an insulator the surface temperature reacts quickly to changes in the gas phase.

The investigations of chapter 3 have shown the deformation behaviour of shallow concrete cross sections to be sensitive to spatial variation in gas temperature. The tensile membrane mechanism exhibited by the slender slab is strongly influenced by deflections. In this section we will therefore investigate the implications of these deformation effects for tensile membrane performance by examining the more specific questions:

- 1) What are the effects of deflection profiles from spatial T_g variations upon tensile membrane behaviour
- 2) Are these effects still evident under temporal variation?

- 3) Are uniform T_g assumptions capable of capturing behaviour exhibited under non-uniform thermal exposure?

The investigations are performed using the 100 mm deep finite element slab model from chapter 4 under simply supported, pinned and fixed boundary conditions. Section 5.2 investigates the effect of a distorted deflection profile for tensile membrane action by analysing the behaviour of the slab under a static gas temperature variation. In section 5.3 the effect of a spatially and temporally varying temperature distribution is investigated and finally in section 5.3.2 behaviour under a uniform and non-uniform temperature distribution is contrasted.

Chapters 3 and 4 also examined the effect of slenderness ratio upon the behaviour demonstrated. In chapter 3 it was shown that as the depth of the concrete cross-section increases the influence of thermal bowing decreases and expansion increases producing larger lateral displacements and lower vertical deflections during thermal exposure.

Subsequently the analysis of the high temperature behaviour of slabs of reducing slenderness in chapter 4 demonstrated that this thermal expansion behaviour increases the compressive membrane capacity of the slab. The compressive membrane behaviour is further enhanced in deeper concrete cross sections as the depth at which compressive membrane action can be mobilised.

From these findings we can conclude that stocky slabs reduced susceptibility to vertical thermal expansion deformations will make them less susceptible to the effects of spatial and temporal variations of gas temperature. This will be investigated in section 5.2.3.

5.2 Structural implications of spatial variation of T_g

In this section the effect of a spatial variation in gas temperature upon the tensile membrane behaviour of the slender concrete is investigated. The effect is investigated in two stages:

- First the sensitivity of the tensile membrane action to the magnitude of spatial gas temperature variation is investigated using a simple linear gas temperature variation of increasing slope.

- Then the effect of the peak temperature location for tensile membrane action is investigated using static gas temperature distributions with different peak temperature locations.

5.2.1 Tensile membrane sensitivity to spatial T_g variation magnitude

The linear gas temperature distribution used in this investigation is summarised in Figure 5-1; it is the same distribution as used in section 3.2.3. Variation values of $V = 0\%$, 20% , 40% and 80% are used.

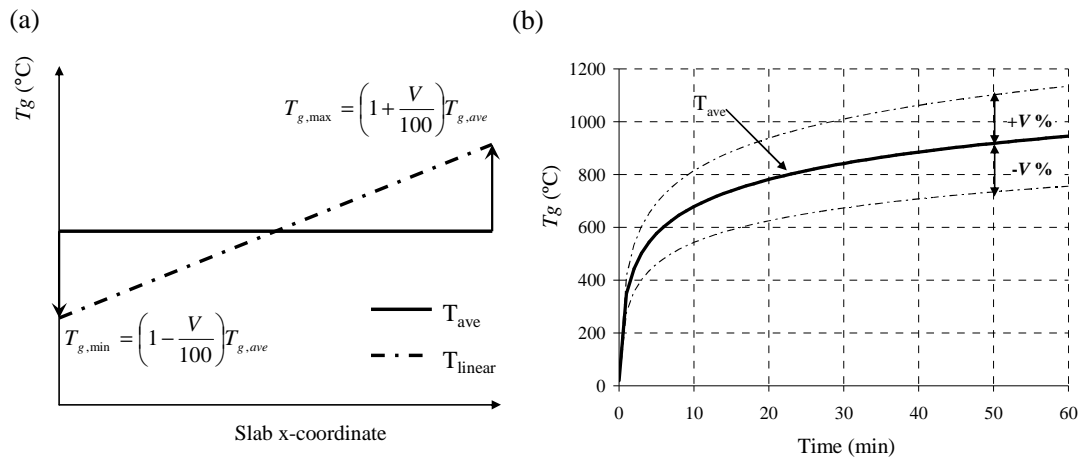


Figure 5-1 (a) Linear variation of gas temperature across slab span (b) evolution of gas temperature with time

Figure 5-2 presents the deflection profile after 60 minutes exposure for increasing values of V . Thermal expansion deformations are a substantial component of the deflection of a slab at high temperatures. Thus in Figure 5-2 the non-symmetrical deflection profile produced by spatial variation of gas temperature is evident. Under increasing variation the degree of curvature under the temperature peak increases, exaggerating the distortion of the slab profile. The peak deflection increases in the unrestrained slab results presented due to the combination of the localised increase in curvature and material degradation. The results for $V = 20\%$ are absent due to the analysis' inability to converge.

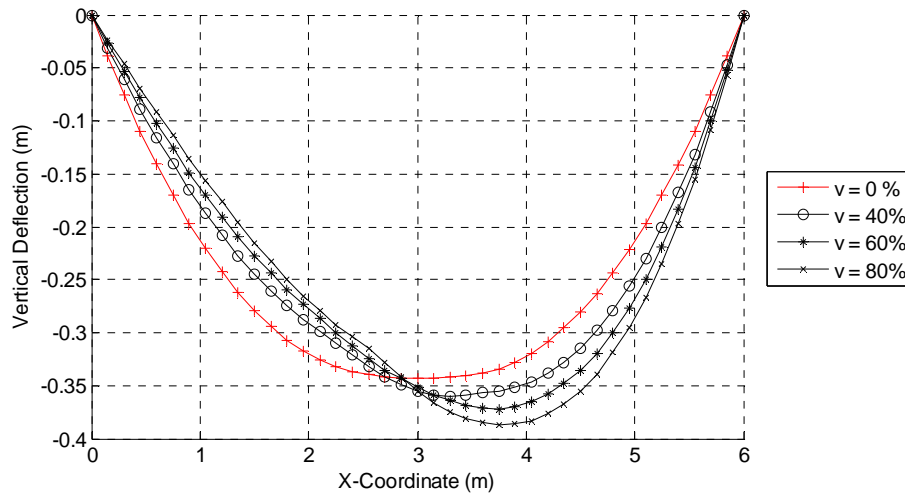


Figure 5-2 Mid span vertical deflection profile for a simply supported slab under linear gas temperature exposure

The unsymmetrical profile increases slab pull-in local to the hot slab edge. Figure 5-3 presents a plan view of the slab lateral displacements for 0% and 80% variation showing the localised increase in slab pull in for $V = 80\%$. The localised effect upon slab pull-in increases under increasing variation.

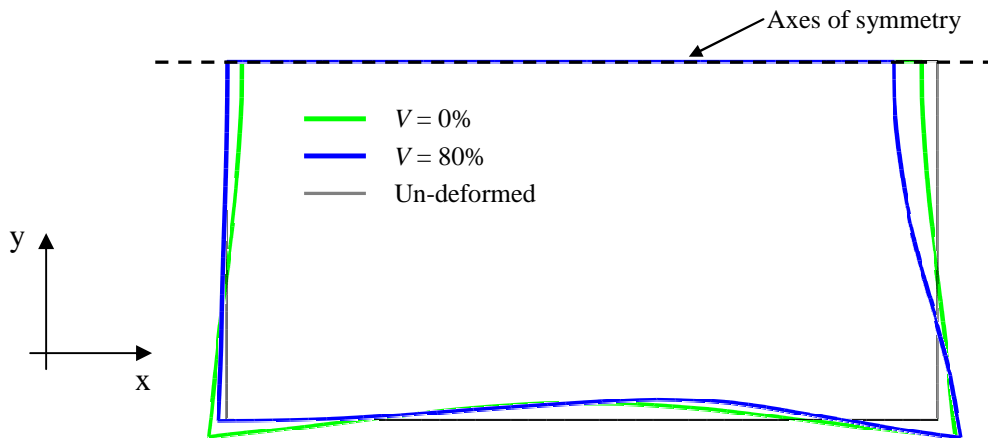


Figure 5-3 Horizontal deformation induced by a uniform ($V = 0\%$) and linear variation of T_g ($V = 80\%$) (deformation scale factor 10)

The effect of this distortion upon the tensile membrane action is examined in terms of the effect upon the compressive ring and the tensile net in the following sections.

Effect of linear T_g variation upon the compressive ring

The shape of the compressive ring is visible by plotting the net principle stresses through the depth of the slab, the principle stress resultants. Figure 5-4 presents the minimum principle stress resultants as a contour plot for the cases of 0% and 80%

variation. The ring of compressive stresses arises from the double curvature of bi-directional bending; therefore any distortion of the deflected shape affects the development of the compressive ring.

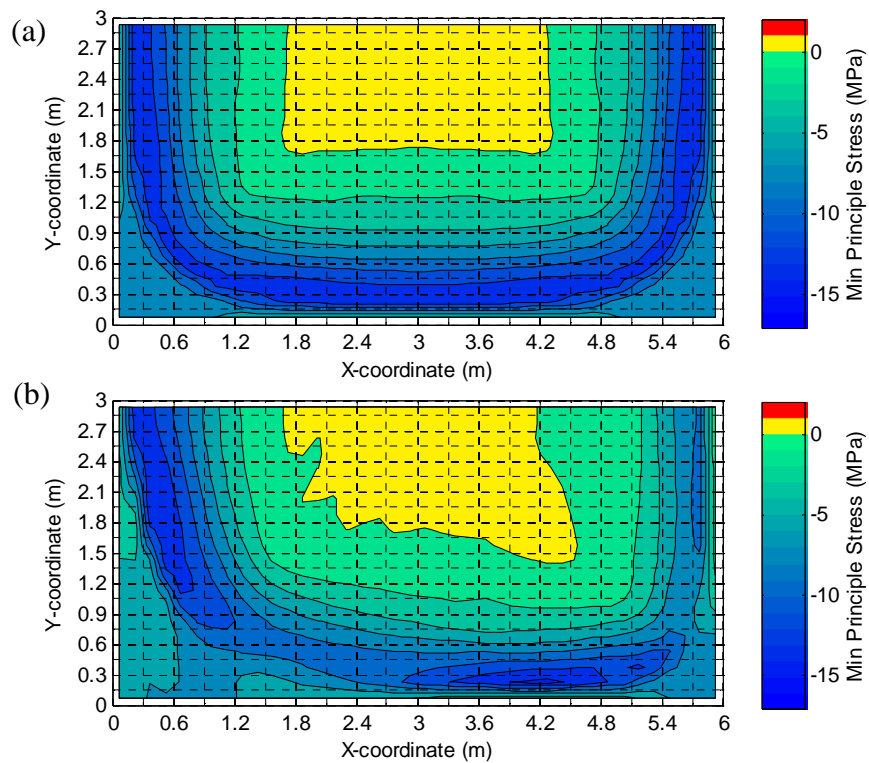


Figure 5-4 The effect of a linear T_g spatial variation upon the compressive ring: minimum principle stress resultants in a pinned slab after 60 minutes exposure (a) $v=0\%$ (b) $v = 80 \%$

The effect of spatial variation of temperature is visible in the shape of the compressive ring. Peak temperatures are located at the right hand side of the slab in Figure 5-4. The increased thermal curvature in this area further increases the stress concentration at the bottom right corner producing an unsymmetrical ring and increasing compressive strains.

Figure 5-5 (a) and (b) contrast the distribution of these compressive strains for the same analyses; they are presented as a proportion of the strain at peak stress to indicate the relative degree of crushing. From chapter 4 we know that crushing failure in the compressive ring initiates at the slab corners where the compression arising from bi-directional bending is greatest.

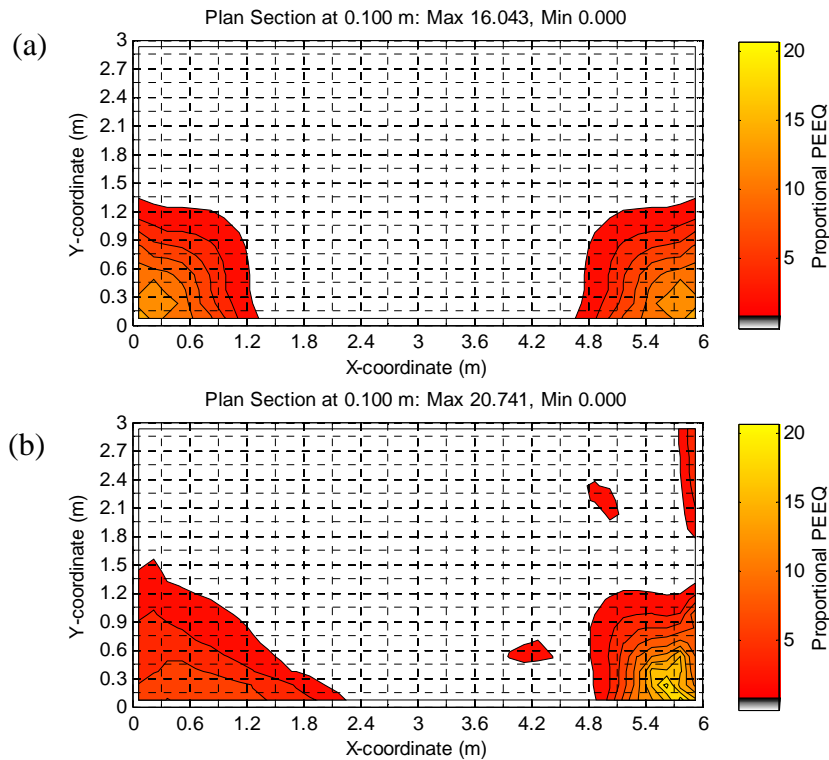


Figure 5-5 The effect of a linear T_g spatial variation upon the compressive ring: Proportional plastic equivalent concrete compressive in a pinned slab after 60 minutes exposure (a) $V=0\%$ (b) $V=80\%$

From these contour plots it is clear that a linear variation of gas temperature causes an increase and concentration of crushing strains in the corner closest to the peak temperature; strains are reduced and more distributed under the cooler temperature regions.

Figure 5-6 compares the maximum crushing strain predicted for the simple, pinned and fixed boundary condition under increasing thermal variation. The result for $V=20\%$ and simply supported boundary conditions is absent due to the analysis' inability to converge. The maximum crushing strain correlates positively with increasing thermal variation due to the higher thermal curvature associated with the increasing peak temperatures. For all boundary conditions increasing thermal variation increases the peak crushing strain, this can be considered a decrease in the performance of the slab. The increase is greatest for the simple case. For the pinned and fixed boundary conditions restraint reduces curvature at the slab edge; lateral restraint prevents the slab from pulling in and rotational restraint induces an opposing moment at the slab edge. Localised increases in curvature are missed by the average temperature uniform assumption.

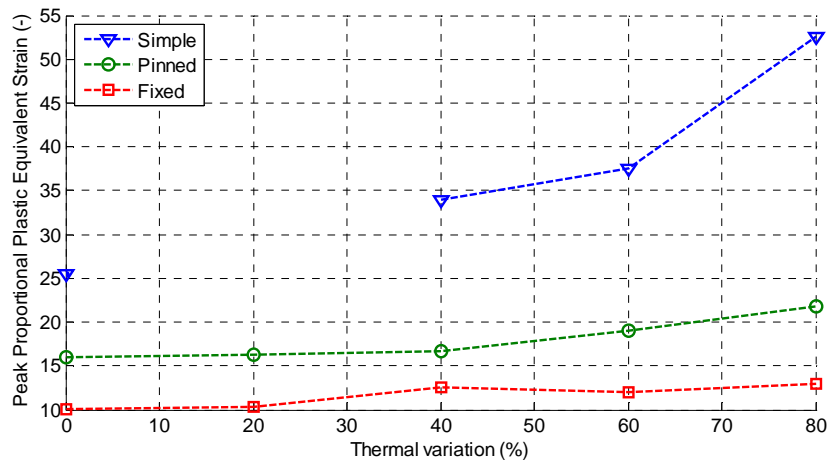


Figure 5-6 Effect of thermal variation and restraint condition for maximum crushing strains: maximum proportional plastic equivalent compressive strain after 60 minutes exposure

Effect of linear T_g variation upon the tensile net and reinforcement

Under tensile membrane action the reinforcement strains are greatest at the slab mid span where deflections are greatest and also at the slab edges when restrained. The large edge strains arise from the tensile force required to prevent the slab from pulling in and the hogging moment induced by restraint of rotation. Figure 5-7 (a-b) presents plan contour plots of the top and bottom layer reinforcement mechanical strain under uniform exposure ($V = 0\%$) and pinned boundary conditions. The peak strains are evident at the mid span location ($x = 3\text{ m}$) in the top layer and at the slab edges ($x = 0\text{ \& } 6\text{ m}$) in the bottom layer of reinforcement.

The linear variation in gas temperature causes an increase in the peak mid-span deflection and a local increase in the amount of slab pull in. The effect upon reinforcement distribution is dependent upon the support conditions. In the unrestrained slab the mid span strains increase with the peak deflection; in the restrained slabs the edge strains increase with the tensile restraining force. Figure 5-7 (c-d) present the top and bottom layer reinforcement mechanical strains for 80% thermal variation. The slab is laterally restrained and the localisation of strains at the slab edge is clearly visible.

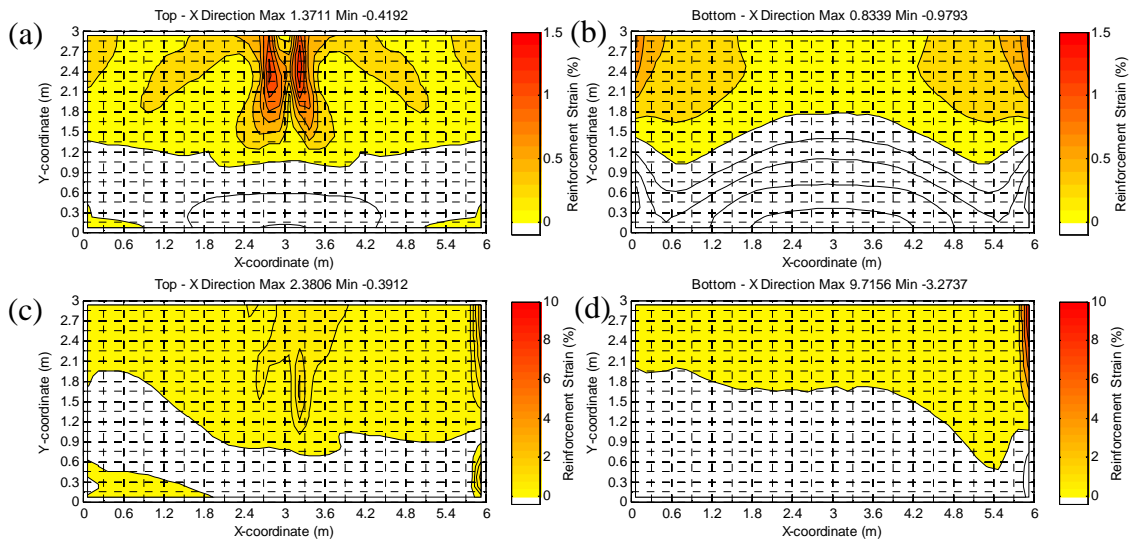


Figure 5-7 Effect of a linear gas temperature variation upon the distribution of reinforcement mechanical strains in a pinned slab: Contour plots mechanical strain of reinforcement spanning the same direction as the linear gas temperature gradient

We therefore expect under increasing thermal variation to see an increase in reinforcement mechanical strain at the ‘hot edge’ and a reduction at the ‘cool edge’. The effect of increasing thermal variation upon the reinforcement is examined by contrasting the maximum mechanical strain in three zones shown schematically in Figure 5-8.

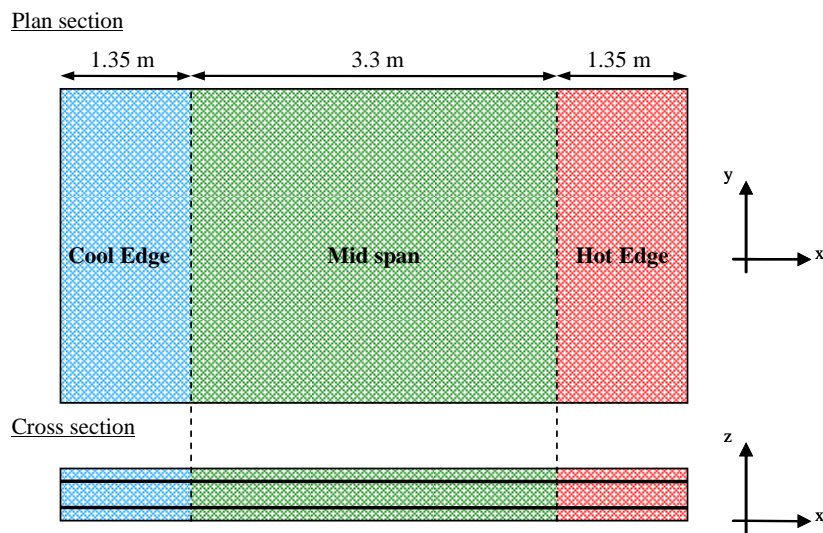


Figure 5-8 Slab cross-section showing zoning for comparison of reinforcement peak mechanical strains

These maximum strains are presented in Figure 5-9 for each boundary condition. The unrestrained slab peak deflections increase under increasing thermal variation thus

there is an initial increase in the maximum mid span mechanical strain. At increasing thermal variations these begin to decrease as the proportion of thermal strain increases at higher temperatures relieving some of the mechanical strains. The increase of reinforcement strains at the hot edge and decrease at the cool edge is evident in both the pinned and fixed slabs in Figure 5-9 (b) and (c).

In Figure 5-9 it can be seen that under increasing thermal variation the magnitude of reinforcement strain at the hot edge becomes extremely large. The finite element model used is not capable of realistically modelling large through depth cracks and reinforcement rupture. Relative comparison of the strain magnitudes indicates that the likelihood of reinforcement rupture increases substantially. This analysis demonstrates that the uniform average temperature assumption under predicts locally high reinforcement strains. This effect is increasingly prominent under more restrained boundary conditions (pinned and fixed) which are more akin to the boundary conditions encountered in reinforced concrete structures.

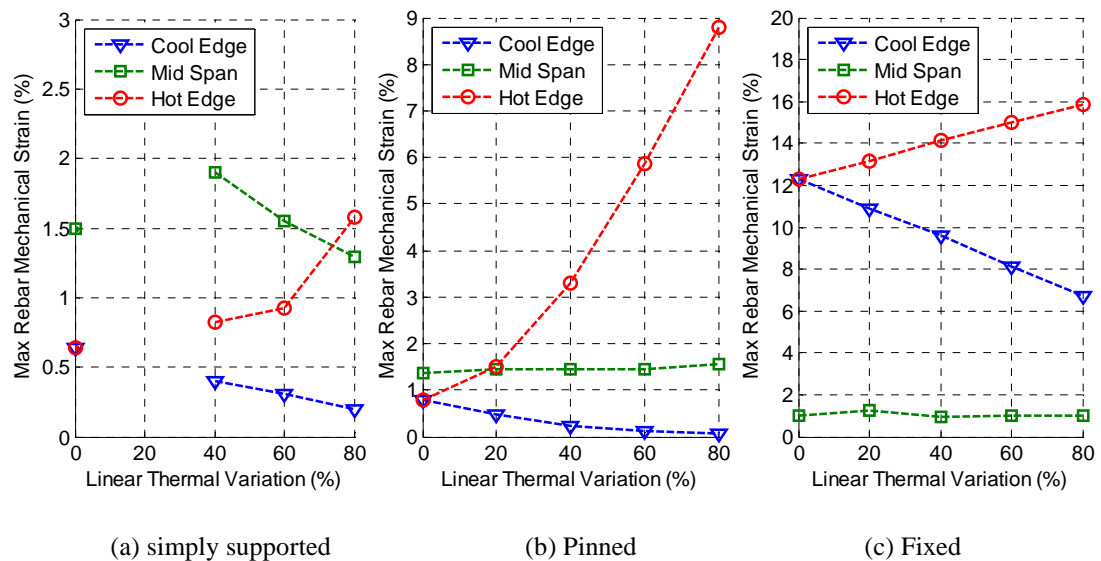


Figure 5-9 Effect of linear thermal variation for maximum reinforcement strains at critical edge and mid span locations in a slender two-way spanning reinforced concrete slab

Thus we can conclude from this study that the increased distortion arising from high levels of thermal variation has serious implications for the development of the compressive ring and tensile net that is critical to tensile membrane action. Locally high concrete crushing strains and reinforcement mechanical strains will not be captured by an assumption of gas temperature uniformity as is used in design.

5.2.2 Tensile membrane sensitivity to peak T_g location

The influence upon the tensile membrane mechanism of the location of the temperature peak is now investigated. Alpert's correlation {, 1972 #217} which was described in chapter 3 will be used to provide a realistic static spatial distribution of gas temperature. In Alpert's correlation the plume axis corresponds to the location of peak temperature. The behaviour of the slender slab will be analysed assuming the plume axis in two locations: at the slab edge, which is akin to the previous analysis but using a realistic temperature distribution and at the slab mid-span. The spatial distribution of temperature for each case is shown schematically in Figure 5-10.

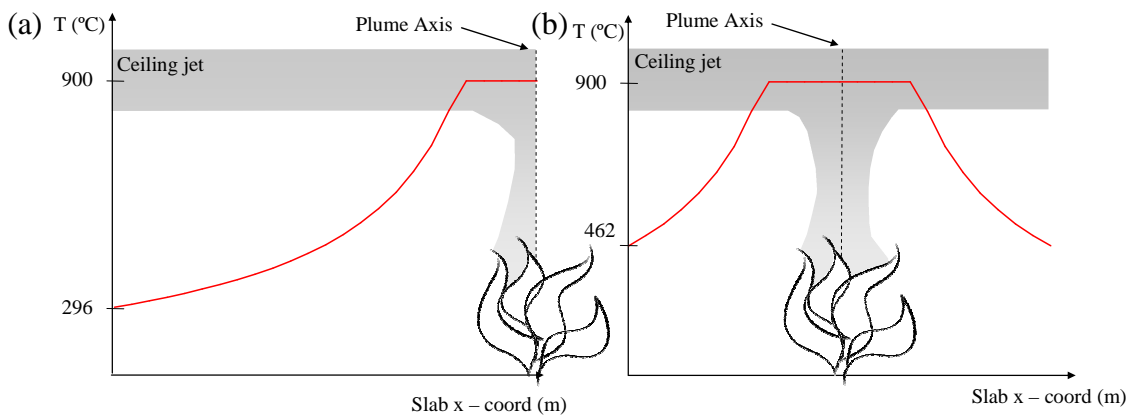


Figure 5-10 Alpert correlation plume location (a) slab edge and (b) slab mid span

The Alpert temperature distributions calculated are static, that is, independent of time; however, direct exposure to high temperatures creates numerical difficulties. To minimise this the temperatures are evolved using the exponential function in Equation 5-1 using $\alpha = 0.005$ which provides a moderate growth rate {Flint, 2005 #226}.

$$T_{(t)} = T_0 + (T_g + T_0)(1 - e^{-\alpha t}) \quad \text{Equation 5-1}$$

The influence of the location of the peak temperature upon the deflection profile is demonstrated in Figure 5-11. Increased thermal bowing at the slab edge as we have seen produces an un-symmetrical deflection profile. Positioning the temperature peak at the mid span produces a symmetrical temperature distribution; consequently the slab deflection profile remains symmetrical also. The increase in thermal curvature at the slab mid-span does, however, increase the peak deflection.

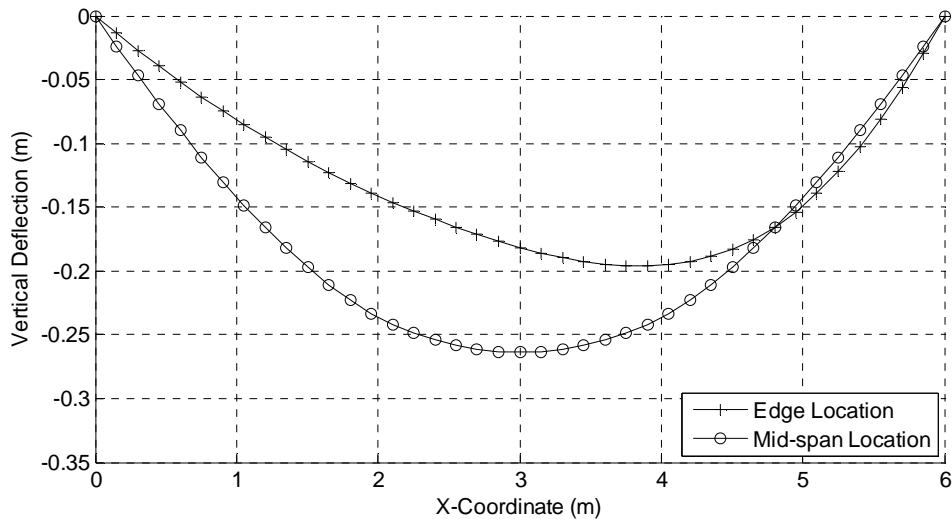


Figure 5-11 Effect of peak temperature location for slab deflection profile after 60 minutes exposure

Figure 5-12 contrasts the evolution of peak deflection for both exposure cases. The peak deflections under exposure to the mid-span peak temperature case increase noticeably faster. A consequence of increased deflection rate is the more rapid development of tensile membrane action. The transition to tensile membrane action under a fixed boundary condition is clearly evident by a sharp increase (snap through) in peak deflection. In Figure 5-12 snap through for the mid-span peak temperature location is after approximately $t = 10$ minutes; the slab exposed to the edge peak temperature location does not snap through until approximately $t = 15$ minutes.

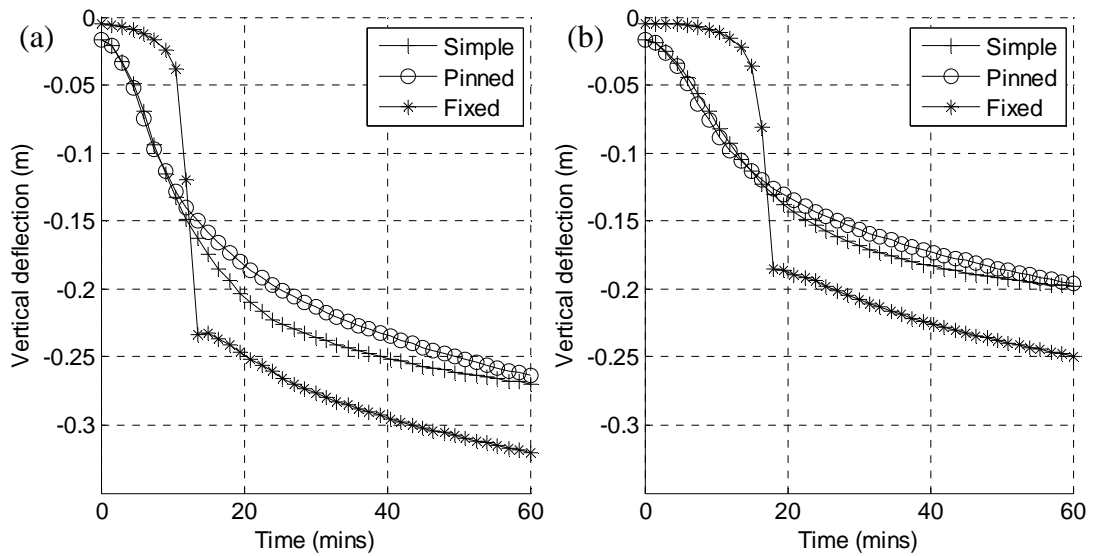


Figure 5-12 Influence of peak temperature location for slab peak deflections (a) mid-span location (b) edge location

In the previous investigation it was shown that the unsymmetrical deflection profile produced by a linear variation in gas temperature has adverse effects for tensile membrane action by increasing concrete crushing strains under low restraint conditions and increasing reinforcement strains under high restraint conditions.

The deflection profile produced by the mid-span peak temperature location exposure is symmetrical. The implications of this symmetrical profile upon the concrete compressive ring and reinforcement behaviour are contrasted in the following sections with the behaviour produced by the edge peak temperature location.

Effect of peak T_g position upon the compressive ring

Figure 5-13 contrasts the distribution of compressive stresses in the slab under pinned boundary conditions for the (a) edge peak temperature location and (b) the mid-span peak temperature location. Due to its symmetrical deflection profile the effect of the mid-span peak temperature location upon the distribution of stresses in the compressive ring is more subtle than the effect of the edge peak temperature location.

While the edge peak temperature location stresses are concentrated in the bottom right corner due to locally increased curvature at the hot edge. The peak curvature for the mid-span peak temperature location is at the mid-span and curvature decreases

towards the slab edges. This has the effect of reducing the magnitude of compressive stresses along the $x = 0$ and $x = 6$ m edges.

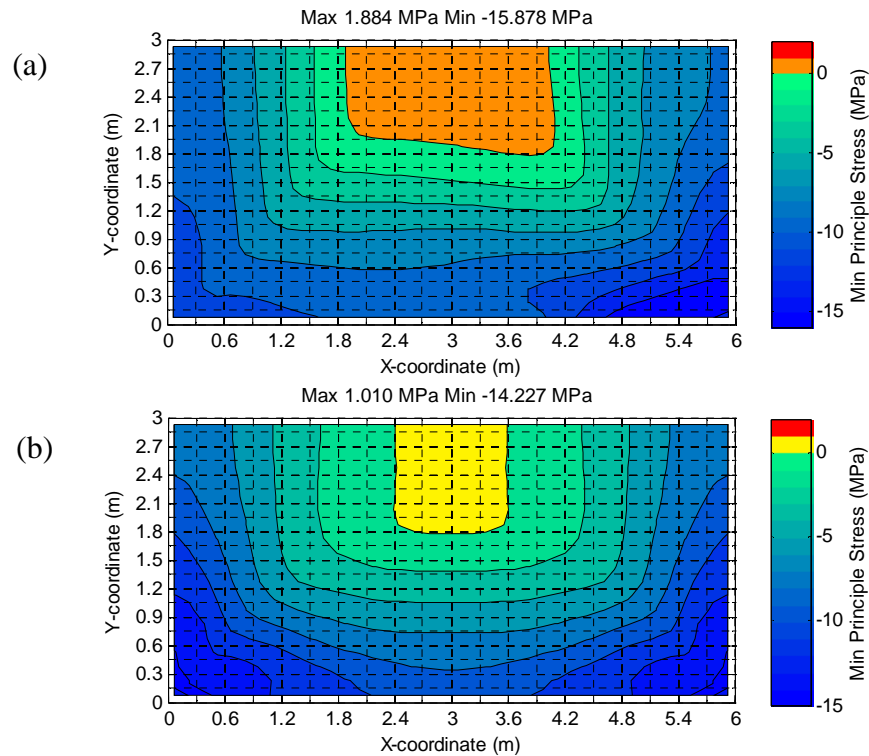


Figure 5-13 Effect of peak T_g location upon the compressive ring: Minimum principle stress resultant (a) Edge location (b) Mid-span location after 60 minutes exposure in a pinned slab

The reduction in edge compression stresses is not significant for the crushing behaviour of the pinned slab, however. Crushing on the top surface of the slab is concentrated in the corner regions where the effect of biaxial bending is strongest in producing compression stresses. Figure 5-14 contrasts the distribution of crushing strains on the top surface for the edge and mid-span peak temperature locations. It can be seen that the edge peak temperature location produces the highest crushing strains, almost twice the magnitude caused by the mid-span peak temperature location.

The effect upon the magnitude of crushing strains is investigated by contrasting the evolution of maximum crushing strain for each exposure case. Figure 5-15 presents the evolution of maximum crushing strain in the top surface of the slab under, simple, pinned and fixed boundary conditions for each the edge and mid-span peak temperature location.

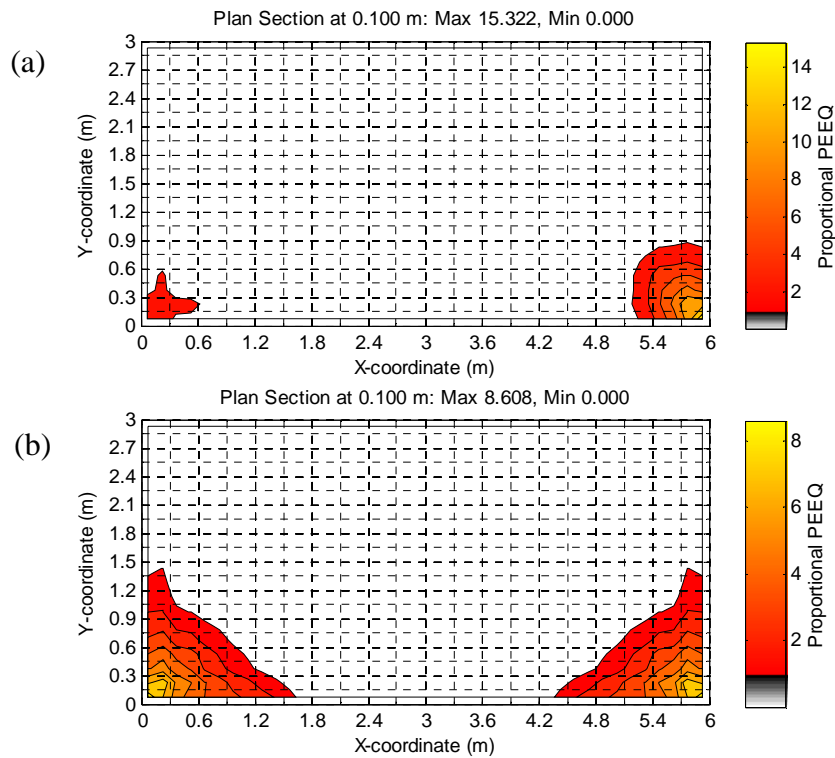


Figure 5-14 Effect of peak T_g location upon concrete crushing within the compressive ring: Proportional plastic equivalent plastic concrete compressive strains (a) Edge location (b) Mid-span location after 60 minutes exposure in a pinned slab

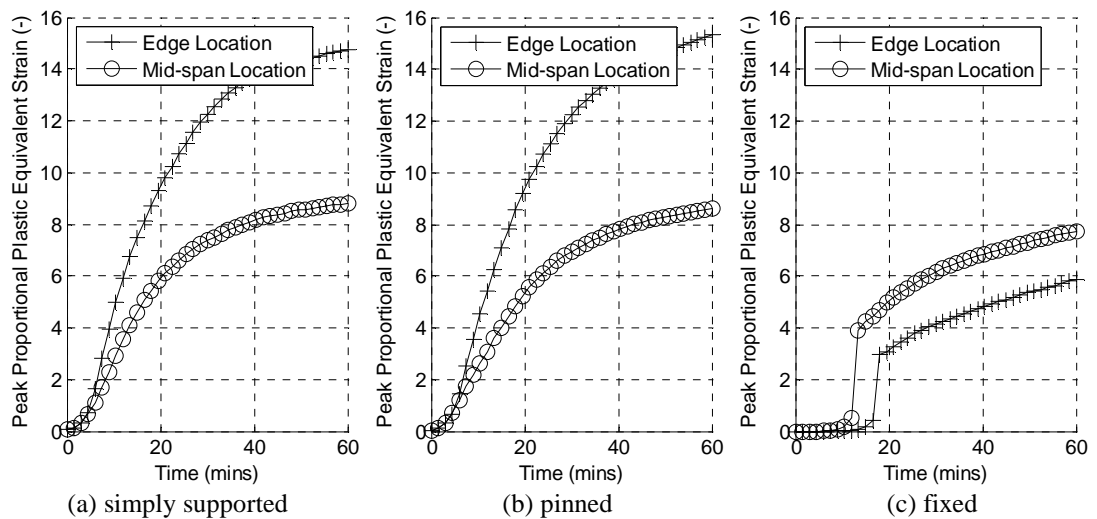


Figure 5-15 Effect of peak temperature location for concrete crushing: Max proportional plastic equivalent strain

Typically the magnitude of crushing strains increase as the slab peak deflections increase. This is true for a uniform thermal exposure where increasing deflection

corresponds to a uniform increase in curvature along the slab length. It is specifically the curvature at the slab edge however which dictates the magnitude of the concrete crushing strains. For this reason we see increased maximum crushing strains for the edge peak temperature location and lower crushing strains in the mid-span location despite the larger deflections associated with the latter.

The results for the fixed boundary condition appear to contradict this behaviour as the mid-span peak temperature location induces greater crushing strains. However, this occurs due to the rotational restraint component dampening the effect of any increased edge curvature in the edge peak temperature location.

Effect of peak T_g position upon the tensile net and reinforcement

The deflection profile (Figure 5-11) produced by the two exposure cases is quite different; consequently the effect upon reinforcement mechanical strain is also different. Figure 5-16 compares the development of maximum reinforcement strain at each edge of the slab and the mid-span as defined by Figure 5-8. The effect of the edge peak temperature is to increase edge strains on the heated edge and reduce them on the cool edge as seen in the previous investigation. The effect of mid-span peak temperature is to increase the mid-span strains due to the increased mid span deflections. Again this localised increase would not be captured when using a uniform average T_g assumption.

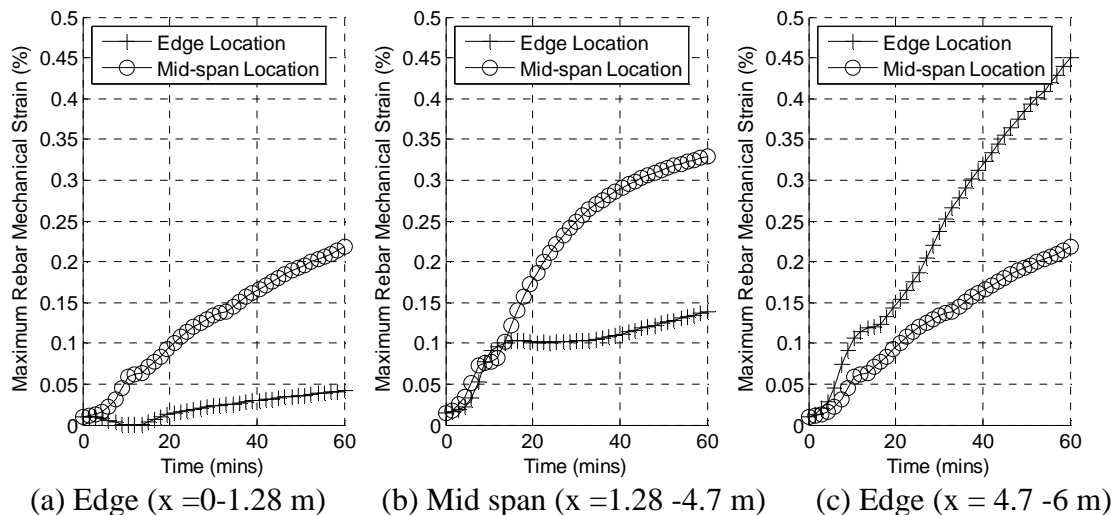


Figure 5-16 Effect of reinforcement location for maximum reinforcement mechanical strains in a pinned slab

5.2.3 Slab slenderness ratio

It was shown in chapter 4 that for slabs of reducing slenderness the compressive membrane behaviour at high temperature is enhanced due to reduced vertical thermal expansion deflections. In this section the response of the stockiest slab analysed in chapter 4, $d = 250$ mm is investigated under the linear spatial variation of gas temperature employed in section 5.2.2.

Figure 5-17 presets the vertical deflection response of the slab with lateral restraint under increasing values of thermal variation, V . Under pinned boundary conditions the sharp increase in deflection after 120 minutes exposure indicates the transition from compressive to tensile membrane action. The vertical deflections of the fixed boundary condition slab remain very low due to the additional rotational restraint; compressive membrane action and flexure provide structural stability.

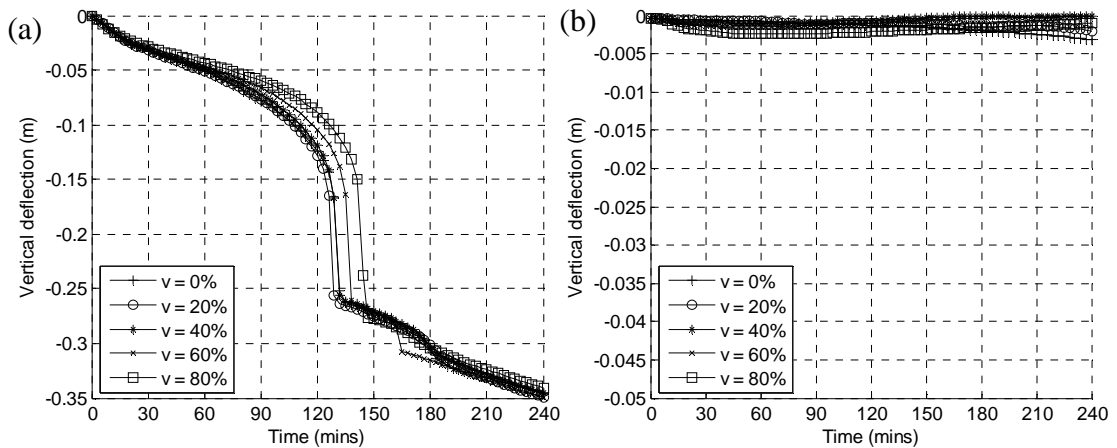


Figure 5-17 Effect of linear spatial T_g variation upon peak deflection of slab with (a) pinned (b) fixed boundary conditions

The increasing magnitude of thermal variation has little significant effect upon the deflection behaviour of the slab. Only the largest magnitude of variation, $V = 80\%$, which is in excess of the scale of variation likely to be encountered in a real fire has a noticeable effect upon the deflection response of the slab.

This investigation has demonstrated that the effect of spatial gas temperature variation upon the thermal expansion behaviour of a deep concrete cross section does not significantly influence the slab structural performance.

Unlike the slender concrete slab considered in section 5.2.1 and 5.2.2 the stocky slab is less susceptible distortions of the vertical deflections which are substantially smaller than the slender slab. The largest variations considered in this analysis are in excess of those likely to be encountered in a real fire therefore we can reasonably conclude that stocky restrained slabs are not susceptible to deformation effects from spatial variations of gas temperature. The performance of stocky slabs is therefore not further considered in this chapter.

This investigation has not considered explicitly the implications of non-uniform fires for material strength. This would require a more detailed analysis of the slab capacity and so is beyond the scope of this thesis. It is, however, an area of potential further study.

5.2.4 Summary of spatial variation effects

This section has investigated the implications of the distorted vertical deflection profile caused by gas temperature spatial variation for the structural behaviour of the two way spanning reinforced concrete slab.

It has been shown that distortion of the slender slab deflection profile can have adverse effects upon the compressive ring and tensile net which are critical for tensile membrane behaviour. This distortion, however, had no significant effect for the compressive membrane behaviour of a stocky restrained slab.

The design of concrete structures is predominantly concerned with establishing the maximum temperature reached by the concrete and/or reinforcing steel and the associated reduction in material strength. This investigation demonstrates that the deformation behaviour of a structural element can also influence high temperature structural behaviour when the behaviour is dominated by a mechanism that is strongly dependent upon deformations such as tensile membrane action.

Having established the implications of spatial variation of gas temperature for the slender slab structural behaviour, in sections 5.3 and 5.3.2 the influence of temporal variations is considered.

5.3 Structural implications of temporal and spatial T_g variation

5.3.1 Influence of temporal variation

In chapter 3 spatially and temporally varying temperature distributions were formulated to investigate the sensitivity of concrete's thermal expansion deflections to temporal and spatial variation of gas temperature. These temperature distributions will be used again here to investigate whether the structural implications of spatial gas temperature variation demonstrated in section 5.2 are evident under temporal variation also.

The temporally and spatially varying temperature definitions were formulated using Alpert's {, 1972 #217} static correlation of burning rate and radial ceiling temperature which was described in chapter 3. Temporal variation was introduced by assuming Alpert's plume axis to traverse a compartment at a speed determined by the compartment length and the burn out time; the burn out time being calculated from the burning rate and the compartment fuel load. The same fast – 60 MW, medium 40 MW and slow 20MW burning rates used in chapter 3 are used here. The resulting Alpert static gas temperature distributions are shown in Figure 5-18.

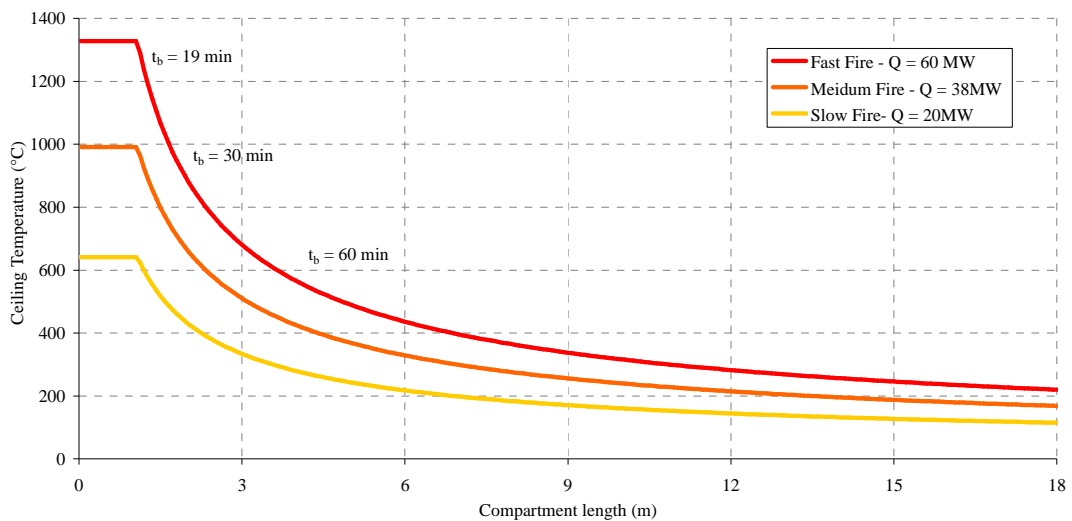


Figure 5-18 Temperature distributions and total exposure times for fast, medium and slow burning rates according to Alpert's {, 1972 #217} correlation ($H = 6m$)

As in chapter 3 the length of the slab is shorter than the compartment length. The slab is considered to span from $x = 6 - 12$ m. Figure 5-19 presents the spatial

distribution of gas temperature along the slab length at selected time steps for the fast fire.

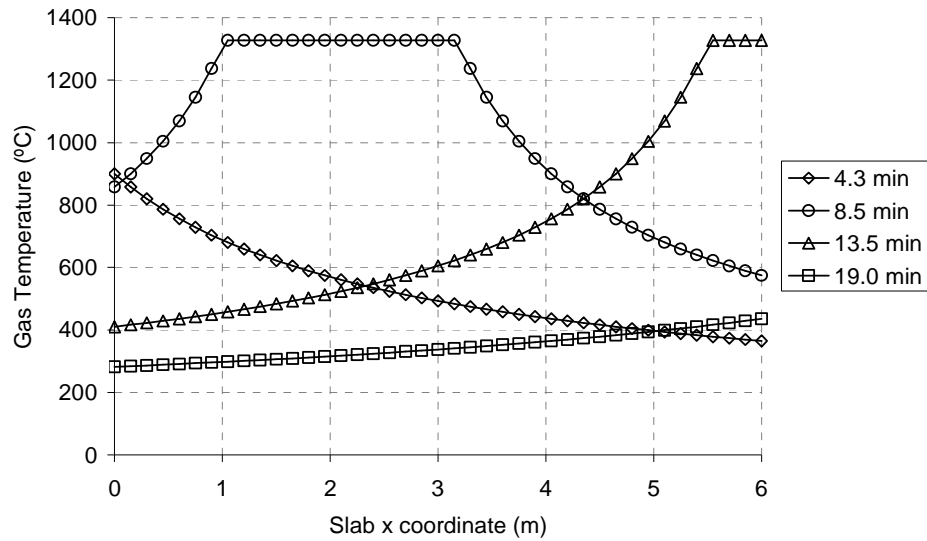


Figure 5-19 Spatial distribution of gas temperature in the slab x-coordinate for the fast burning rate at selected time steps

Figure 5-20 presents both the evolution of slab maximum vertical deflection and vertical deflection profiles in separate plots for each of the three fires: fast, medium and slow. The slab maximum vertical deflections under simply supported, pinned and fixed boundary conditions are presented in the top row for each fire. The period during exposure when the peak temperature traverses the slab span is highlighted in yellow

As we saw in chapter 3 the fast hot fire produces the largest deflections as under short exposures to high temperatures thermal bowing dominates the thermal expansion response. The effect of the traversing peak is also clear from the peak slab deflections. For each fire prior to the peak traverse the increase in deflections is gradual; as the peak traverses the slab span there is a noticeable increase in deflection rate for the pinned and simply supported slabs and the fixed slab snaps through from compressive membrane action to tensile membrane action. After the peak temperature traverse the rate of deflection increase drops almost to zero.

The deflection profiles at selected time steps for the pinned slab are presented in the bottom row of Figure 5-20; each fire is presented in a separate plot. The distortion of the deflection profile is clearly evident for each fire. The peak temperature traverses

from the right hand side of the slab ($x=6$ m) to the left hand side ($x = 0$ m), as it does so the shape of the deflection profile changes as the peak deflection shifts towards the position of peak temperature. Thus for each fire the final deflection profile is less distorted than under a static gas temperature spatial distribution.

In section 5.2 it was shown that the location of the peak gas temperature is important in determining the implications of the gas temperature variation for the tensile membrane mechanism. In the following sections the effect of spatial and temporal gas temperature variation upon the compressive ring and the reinforcement tensile net is investigated.

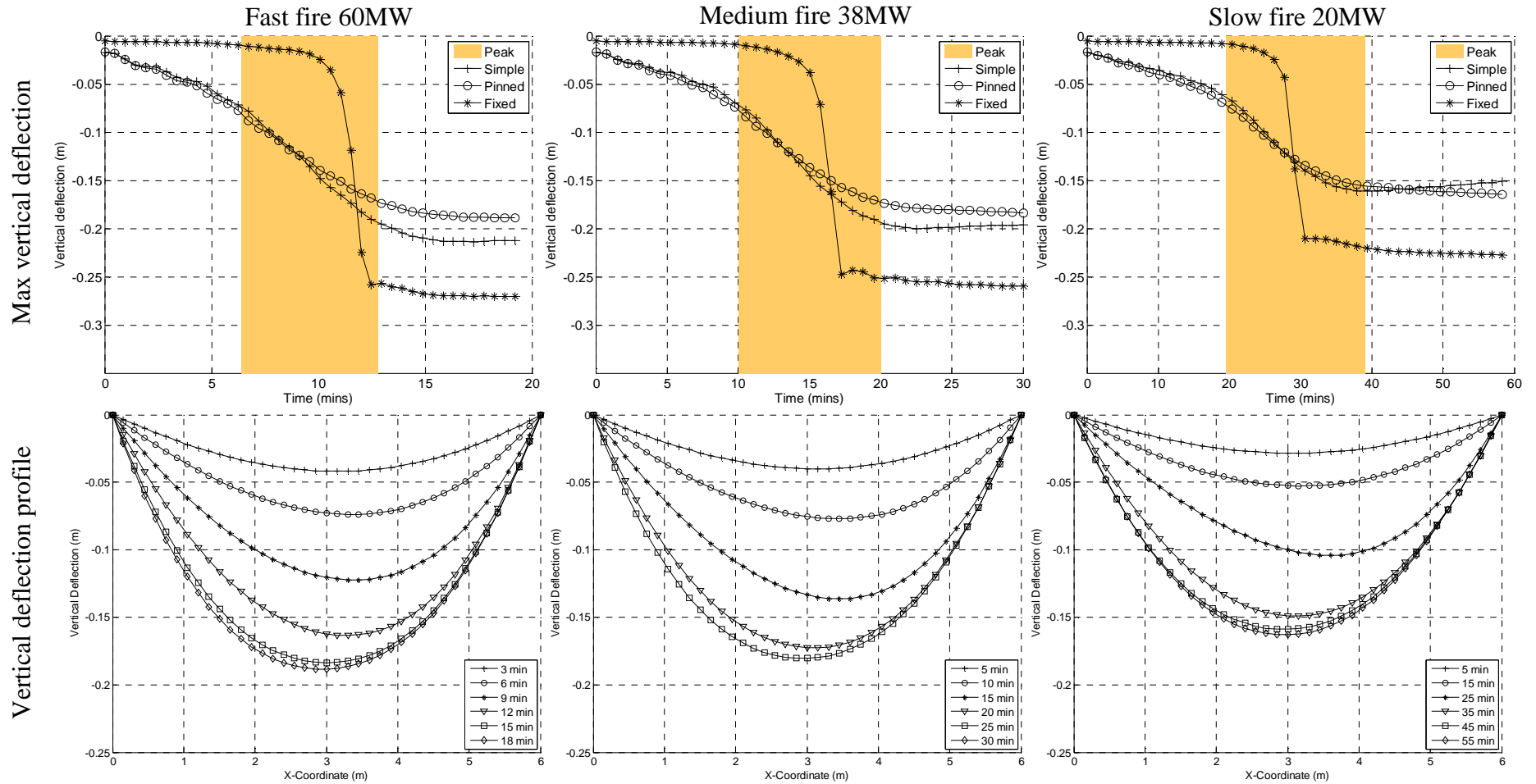


Figure 5-20 Effect of temporal and spatial variation of gas temperature upon the deformation behaviour of a slender two-way spanning reinforced concrete slab

Effect of spatial and temporal T_g variation upon the compressive ring

In section 5.2 it was shown that by locally increasing the thermal curvature the formation of the compressive ring is distorted. Figure 5-21 presents the minimum principle stress resultant for the fast, medium and slow fires at the end of exposure from which the shape of the compressive ring is discernible.

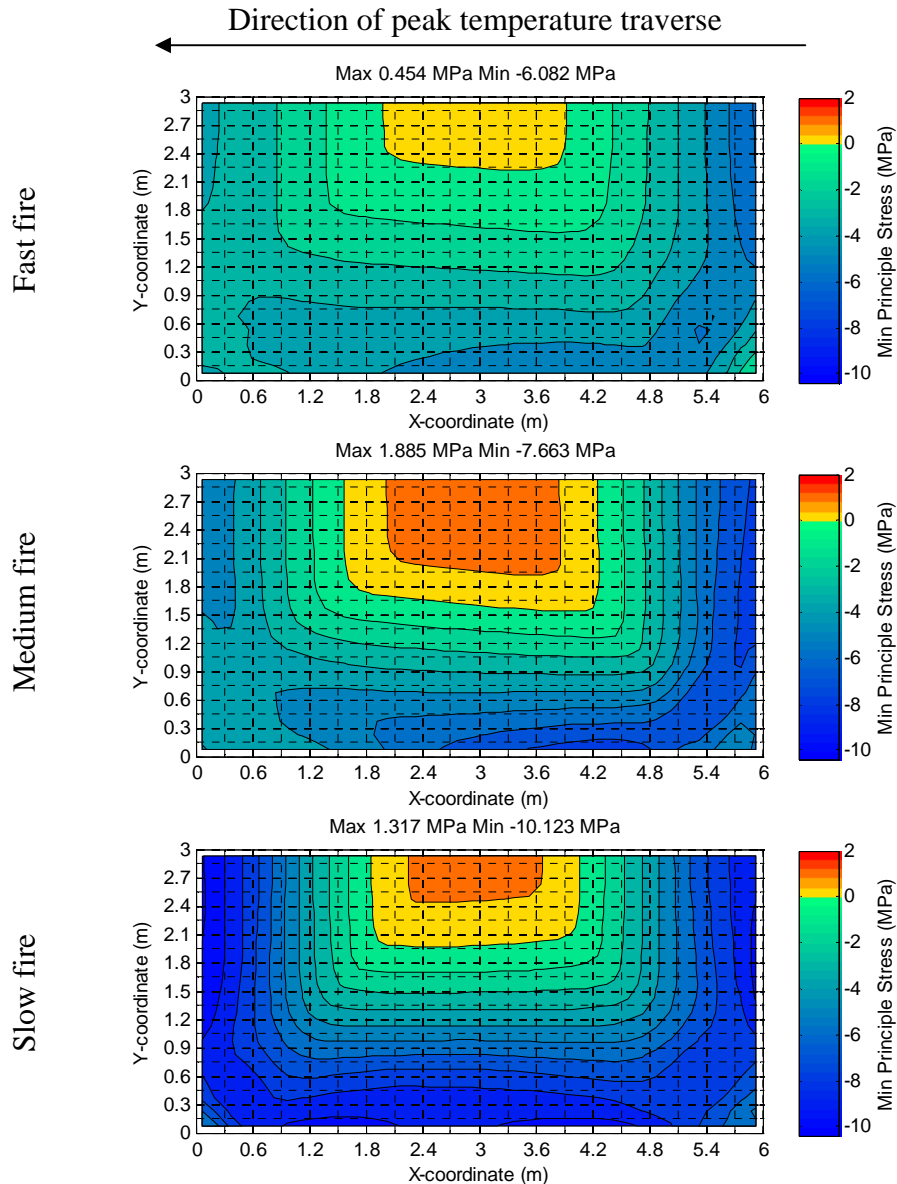


Figure 5-21 Effect of spatial and temporal variation of gas temperature upon the compressive ring: Minimum principle stress resultants under pinned boundary conditions

Under each exposure a small amount of distortion is visible at the end of exposure; this distortion is most clearly visible for the fastest burning fire. For the fast and

medium rate fires the stresses are concentrated in the right hand corner of the slab. In the slab subjected to the slow fire where distortion is less evident there is some stress concentration at the left hand corner of the slab.

A consequence of this distortion is unsymmetrical crushing behaviour as was seen in section 5.2. The influence of spatial and temporal variation upon the evolution of maximum crushing strains is presented in Figure 5-22. In this figure the maximum crushing strain for the left hand side ($x = 0-3\text{ m}$) and the right hand side ($x = 3-6\text{ m}$) of the slab are presented separately.

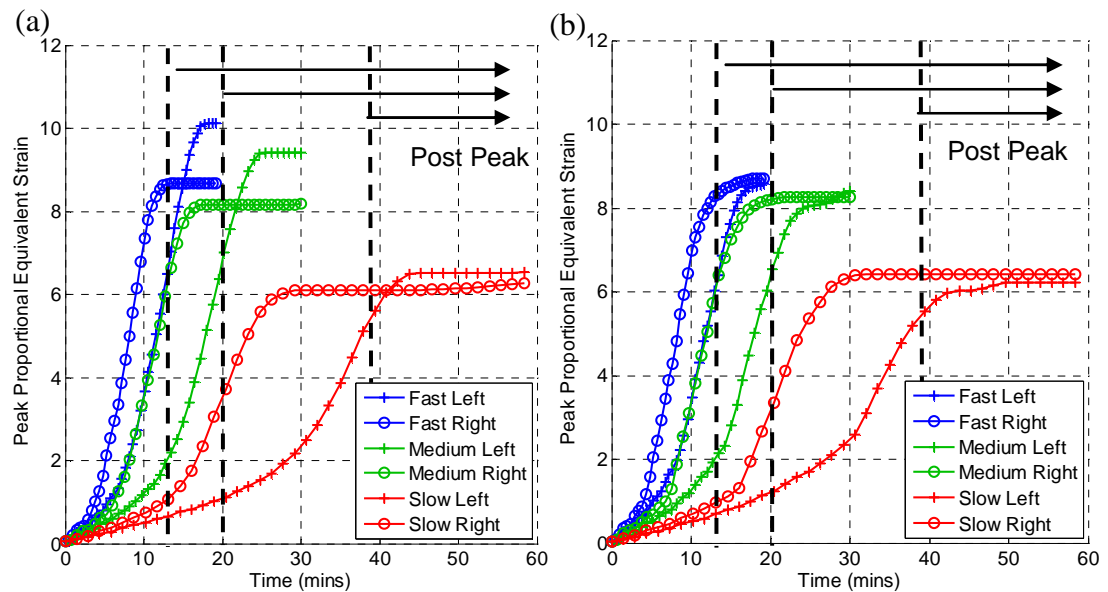


Figure 5-22 Corner crushing strains for different burning rates: Proportional plastic equivalent strains (a) Unrestrained slab (b) laterally restrained slab

By presenting the evolution of peak crushing strain for each side of the slab separately the unsymmetrical crushing behaviour is evident in all fires by the lag between the right hand side and left hand side values. As was seen in the deflection profiles (Figure 5-20) the peak curvature traverses right to left following the peak gas temperature during exposure. Thus the magnitude of crushing at the right hand side increases more rapidly initially and there is a lag in the development of the left hand side crushing strains.

Where the slab is unrestrained the crushing strains achieved at the left hand side exceed those of the right hand side which level off after the peak temperature has traversed to the left hand side. Figure 5-23 contrasts the final distribution of crushing

strains for the slab exposed to the medium fire under simply support and pinned boundary conditions.

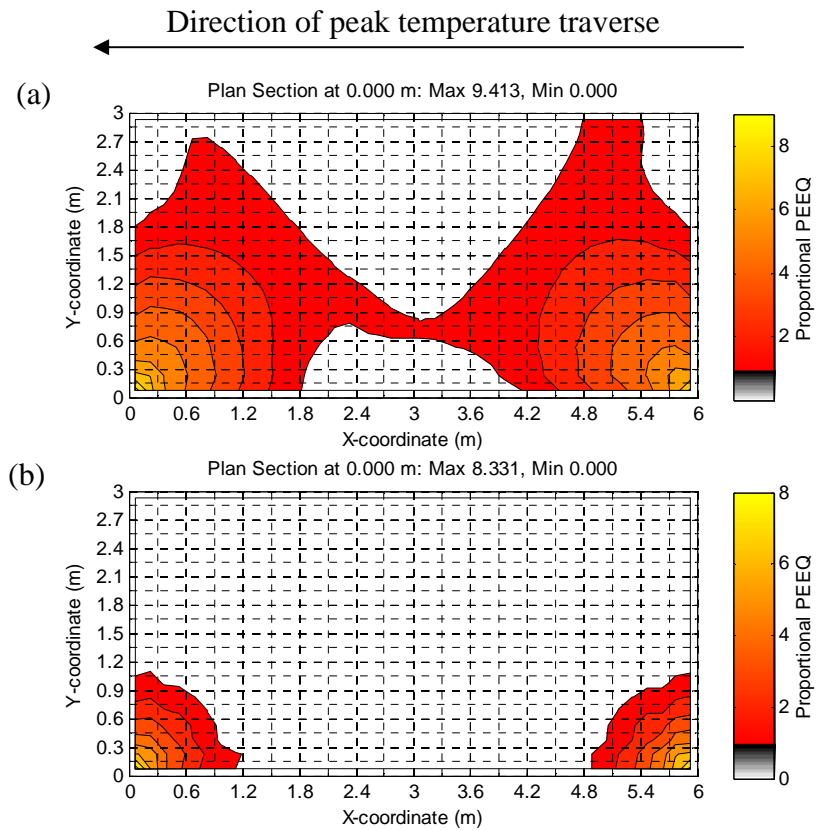


Figure 5-23 Effect spatial and temporal variation of gas temperature upon the distribution of concrete crushing strains: Plan contour of top surface proportional plastic equivalent compressive strains (a) simply supported slab (b) pinned slab

For each thermal exposure the effect of temporal variation is to produce an effectively symmetrical distribution of compressive crushing strains. The localised increase in compressive crushing under static gas temperature distributions is absent at the end of exposure due to the peak temperature traversing the entire length of the slab.

Effect of spatial and temporal T_g variation upon the reinforcement

In Figure 5-24 the evolution of the reinforcement mechanical strain distribution in the top and bottom reinforcement layers is presented in a series of plan contour plots. The initial effects of the spatial gas temperature variation are evident after 12 and 15 minutes where strains are concentrated at the right hand side of the slab. As seen in the deflection and crushing strain comparison (Figure 5-20 and Figure 5-23) at the

end of exposure the distribution of reinforcement strains is similar to that produced under uniform thermal exposure (Figure 5-7 (a & b)).

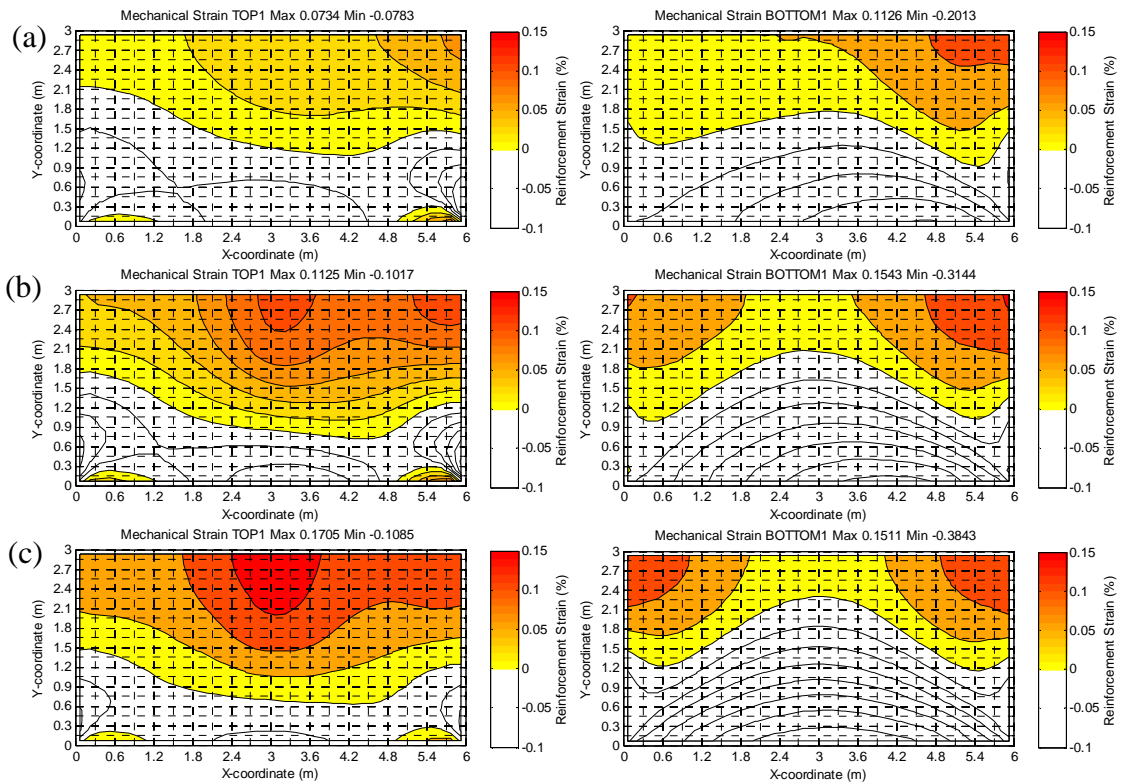


Figure 5-24 Evolution of reinforcement strain distribution under pinned boundary conditions and fast fire exposure (a) 12 min (b) 15 min (c) 19 min

Figure 5-25 contrasts the final distribution of reinforcement mechanical strains for each fire exposure. There is a noticeable difference in the fastest and slowest fires.

For the fast and medium fires the peak strain in the top mid-span reinforcement is much higher than the slow fire. This is potentially caused by two factors: The deflections of the slabs exposed to the fast and medium fire is much greater than the slow fire; and secondly the strength of the bottom reinforcement in the fast and medium fires is lower due to the higher temperature associated with these fires placing greater demands on the top reinforcement.

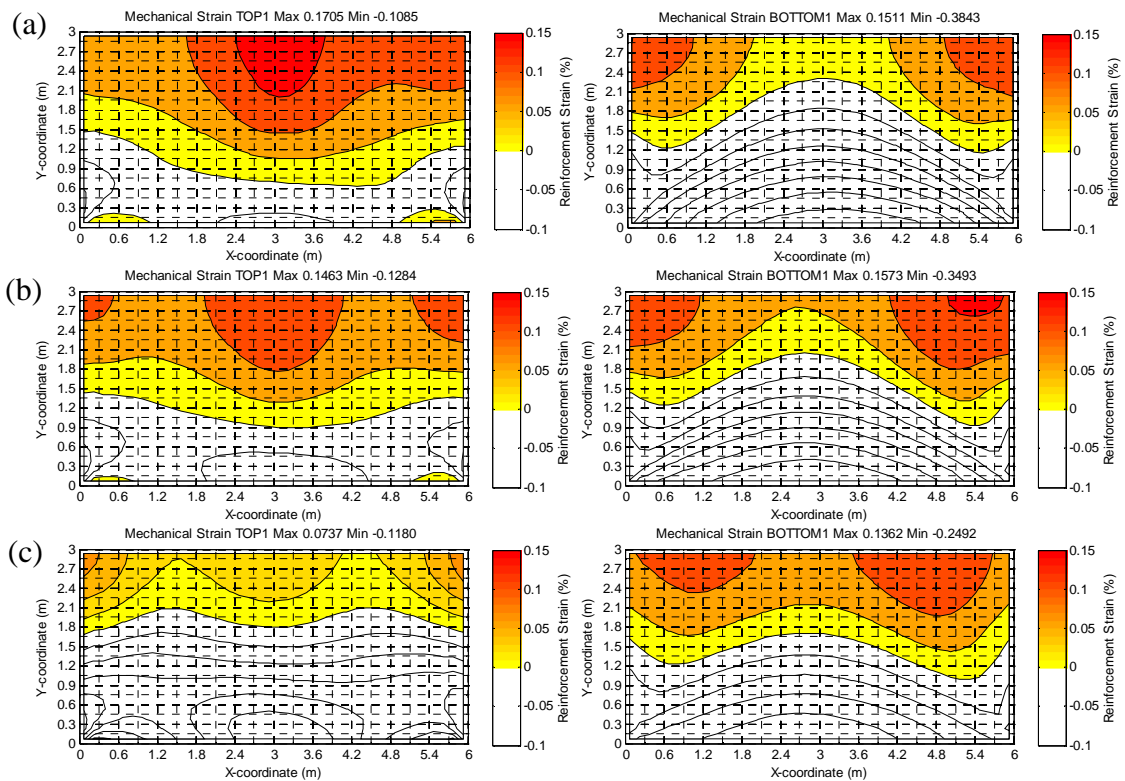


Figure 5-25 Effect of temporal changes in temperature spatial distribution for reinforcement behaviour: Pinned slab rebar mechanical strains (a) Fast fire 19 min (b) Medium fire 30 min and (c) Slow fire 58 min

The structural performance under each fire (fast, medium and slow) is however quite different. The fast fire produces the largest deflections and consequently the highest reinforcement strains and compressive crushing strains.

For each fire, however, the investigation has demonstrated that the localised increases in compressive crushing and reinforcement strain caused by spatial gas temperature variations are not evident under temporal variation.

5.3.2 Uniform and non-uniform thermal exposures

In this section the behaviour of the slab under spatial and temporal gas temperature variations is contrasted with behaviour caused by uniform temperature conditions. In the previous investigation it was shown that the temporal variation ‘evened’ out the localised effects of gas temperature spatial variation. By contrasting the structural performance under non-uniform and uniform thermal conditions the effectiveness of the uniform temperature assumptions can be judged.

Figure 5-26 (b) presents the temperature-time history of the uniform temperature assumptions for the fast, medium and slow fires. Two assumptions of uniformity are made: the maximum gas temperature and the average gas temperature. Figure 5-26 (a) shows schematically the maximum and average gas temperature for two time steps.

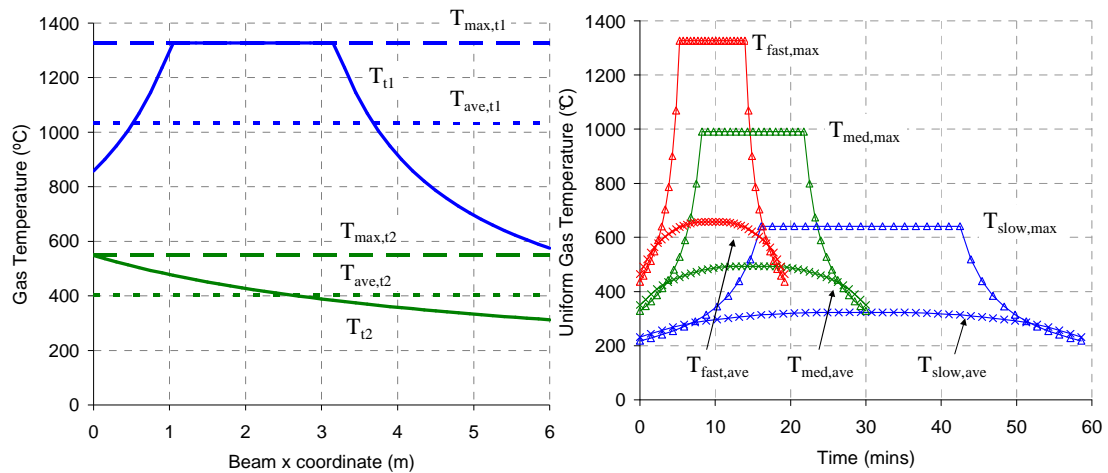


Figure 5-26 Maximum and average uniform temperature exposures for the fast, medium, and slow fires

Figure 5-27 contrasts the evolution of slab maximum vertical deflection under each non-uniform fire with the average and maximum uniform gas temperature exposure deflections. The deflections presented are for the pinned boundary condition only as the behaviour the same behaviour was exhibited under all conditions (simply supported, pinned and fixed).

For each fire the uniform maximum gas temperature assumption predicts a larger deflection than both the uniform average and non-uniform gas temperature definition. The deflection caused by the uniform average gas temperature assumption is initially greater than the non-uniform exposure deflection; however, the uniform average gas temperature assumption fails to capture the sharp increase in deflection caused by the peak temperature traversing the length of the slab span. Consequently the average assumption ultimately under predicts the maximum slab deflection.

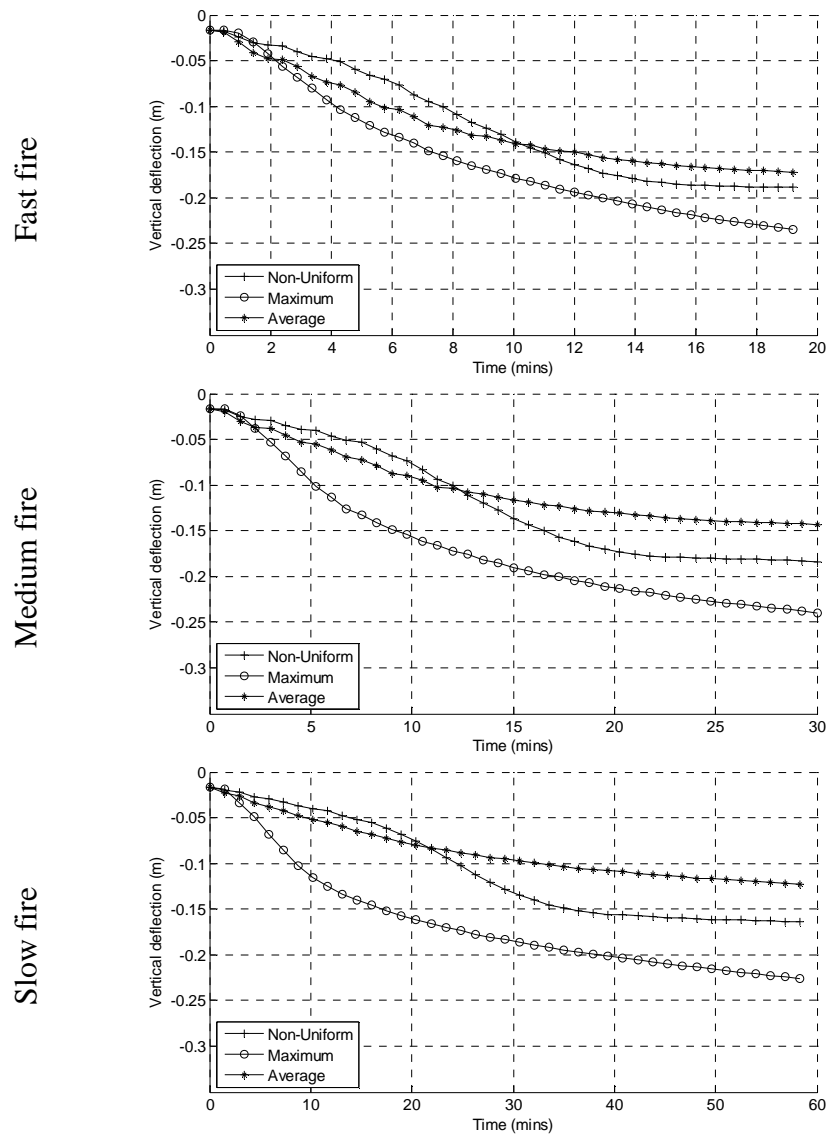


Figure 5-27 Evolution of maximum slab vertical deflection for non-uniform and uniform thermal exposure

There is a significant difference in the contrast of uniform and non-uniform thermal exposure final deflections for each fire. The uniform assumptions of temperature for the fast fire produced deflections closest to the non-uniform thermal exposure (Maximum T_g +24 % and average T_g -9%). The slow fire analysis produced the greatest difference in predicted deflections (Maximum T_g +38 % and average T_g -25%).

This is potentially due to the behaviour of the slow fire exposed slab being dominated by thermal expansion as opposed to the bowing dominated behaviour of the fast and medium fires. The peak temperature has a more substantial effect for

slow fire exposed slab deflections than the fast and medium fires; therefore the uniform maximum gas temperature assumption also produces substantially bigger deflections. Likewise the uniform average gas temperature assumption which fails to capture the deflection influence of the peak temperature predicts a much smaller deflection.

It was shown in section 5.3 that spatial and temporal variation of gas temperature ultimately produced a uniform like distribution of concrete compressive strains and reinforcement tensile strains, that is, symmetrical.

The contrast of reinforcement and compressive strains arising from uniform and non-uniform thermal exposure therefore reflects the contrast indicated by the deflections in Figure 5-27. As an example the evolution of maximum crushing strain and the maximum reinforcement strains at the slab mid span and slab edge are presented in Figure 5-28 and Figure 5-29 respectively for the pinned slab boundary condition.

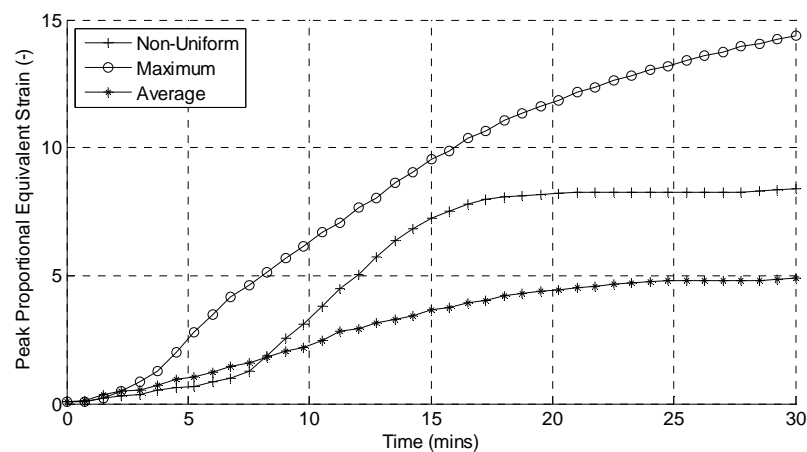


Figure 5-28 Evolution of maximum crushing strain in the pinned slab under uniform and non-uniform thermal exposure

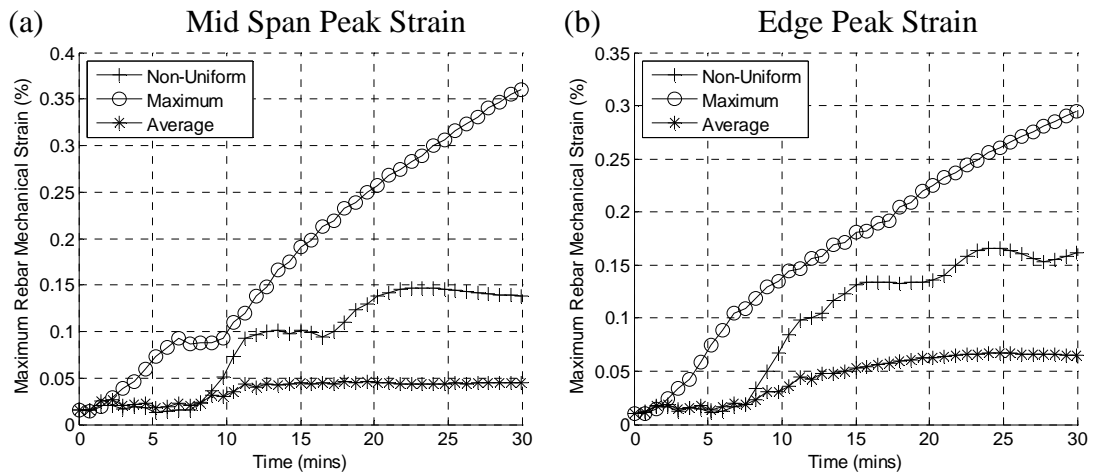


Figure 5-29 Evolution of maximum reinforcement strains under uniform and non-uniform thermal exposure at (a) slab mid-span ($x = 1.275 - 4.725$) and (b) edges ($x = 0 - 1.275, 4.725 - 6$)

5.3.3 Summary of spatial and temporal temperature variation effects

From this study we can conclude that the strain localisations that were caused by spatial variations in gas temperature are eventually evened out by simultaneous temporal variations.

The ability of uniform temperature assumptions to make adequate predictions of behaviour induced by these non-uniform thermal environments was therefore subsequently examined. Performance under non-uniform thermal exposure was contrasted with two assumptions of uniformity; uniform maximum gas temperature and uniform average gas temperature.

The most commonly used design fires the standard temperature time curve and the parametric temperature time curve from Eurocode 1 {, 2002 #30} both make uniform temperature assumptions. The standard-temperature time curve has no physical basis therefore it is not possible to establish what this temperature represents. The parametric temperature time curve, however, is based on the Swedish curves {Pettersson, 1976 #41} which derive compartment temperatures from 'energy balance'. The solution of the energy balance is simplified by using a single average compartment temperature. We can therefore consider the parametric temperature-time curve to represent an average temperature assumption.

Broadly for each fire the uniform maximum gas temperature assumption provides a conservative estimate of slab performance over predicting maximum deflections. The

uniform average temperature assumption unconservatively under predicts slab deflections by failing to capture the influence of the peak temperature for deflections. For each fire, fast, medium and slow the relative difference between uniform and non-uniform gas temperature predicted deflections differs. The uniform maximum gas temperature assumption produced the most conservative estimate of behaviour for the slow fire and the least conservative for the fast fire. The uniform average gas temperature assumption was the most unconservative for the slow fire and the least unconservative for the fast fire. This indicates that the ability of uniform temperature assumptions to characterise non-uniform thermal exposures for structural analysis is dependent upon the type of fire.

5.4 Conclusions

This chapter has focused on establishing implications of the deflection behaviour induced by spatial and temporal variations of gas temperature for the structural performance of a two-way spanning reinforced concrete slab.

The findings of this investigation challenge the singular focus of material strength in structural fire engineering design by demonstrating the influence of deformation behaviour for structural performance

Undoubtedly material strength is important for determining performance however it has also been shown that the tensile membrane action exhibited by slender slabs is sensitive to the deflection profile distortions caused by spatial variation of gas temperature. This variation resulted in localised increases in both the concrete and reinforcement strains used to indicate performance. The compressive membrane behaviour of stocky slabs however, was found to insensitive to spatial variation of gas temperature.

The sensitivity of slender and stocky slabs differs for two reasons:

- Slender slabs are dominated by thermal bowing and therefore are more susceptible to the deflection distortions caused by spatial variation of temperature. Stocky slabs which have lower thermal vertical deflections are substantially less susceptible to these distortions

- Slender slabs exhibit tensile membrane action at high temperatures; this mechanism has been shown to be influenced by distortions in the deflection profile. Stocky slabs exhibit compressive membrane behaviour which has been shown to be insensitive to the small distortions caused by spatial variation in stocky concrete sections.

Under temporal variation it was found that the localised peaks in reinforcement and concrete strains caused by static spatial distributions of temperature were not evident. These localisations were evident during exposure but ultimately the final distribution of strains was symmetric, akin to the distributions caused by uniform temperature exposure.

The performance of the slab was therefore contrast with the performance predicted under two uniform temperature assumptions, a uniform maximum gas temperature assumption and a uniform average gas temperature assumption. These uniform temperatures assumptions were found to provide unconservative (average) and conservative (maximum) predictions of behaviour. It was also found that the degree of conservativeness (or not) was dependent upon the type of fire (fast, medium or slow).

The results of this study indicate that uniform temperature assumptions can provide both conservative and unconservative predictions. The implications of spatial variation need to be considered very carefully for the design context.

Identifying the appropriate design fire is a function of the compartment fire dynamics and the structural behaviour. This investigation has demonstrated the differing vulnerabilities possible in structural behaviour (slender versus stocky behaviour). It is therefore necessary in identifying the worst case scenario to consider both fire and structural parameters to avoid overly conservative or conversely unconservative designs.

6 Consequences of Spalling

Spalling is a phenomenon of concrete behaviour at elevated temperatures involving the breaking off of layers or pieces of concrete from the exposed face at high and rapidly rising temperatures. The physical effect of spalling is to reduce the cross-sectional area and potentially expose reinforcement to high gas temperatures. It is therefore thought that spalling poses a potential threat to the stability of concrete structures in fire.

The severity of spalling for structural fire performance will depend upon the affected structural arrangement. A simply supported beam is reliant purely upon flexure for stability, for example. Exposure of the reinforcement to high gas temperatures causes a rapid decline in steel strength and consequently the flexural strength of the beam. Due to the absence of alternative load paths spalling accelerates failures of the beam at high temperatures.

However structural elements rarely act in isolation and this is particularly true in fire where the effect of thermal expansion can change both the restraint and loading conditions of a structure (Chapter 3). Restrained thermal expansion induces large in-plane compressive stresses which enhance the load bearing capacity. Consequently the reduction in flexural strength due to spalling is less critical for stability in these structures due to alternative support mechanisms such as arching action.

Such behaviour has been witnessed experimentally {Bailey, 2002 #4}. A full scale fire test of a concrete structure resulted in severe spalling of a flat slab exposing the majority of the sagging reinforcement but during and after the test no signs of collapse were evident. It is thought that large in plane compressive stresses resulting from restrained thermal expansion increased the severity of concrete spalling. However, these compressive stresses also have played an important role in maintaining the stability of the slab by enhancing the load-carrying capacity. This case demonstrates the complex interaction of behaviour which dictates the performance of concrete structures at high temperatures. This interaction is a delicate balance between detrimental and beneficial effects; to be able to design concrete

structures for fire confidently we must be able to quantify these effects, and to do this we must be able to:

- (1) fully understand the load carrying mechanisms of concrete in fire,
- (2) understand the mechanisms of spalling and quantify spalling severity; and
- (3) consider the interaction of concrete structural mechanisms with concrete spalling behaviour.

In this thesis we look specifically at points (1) and (3). Chapters 2-5 have looked in detail at the load carrying mechanisms of two-way spanning slabs and our ability to model this behaviour numerically. In this chapter we look at implementing the effect of spalling in a structural analysis to achieve point (3).

Point (2) is not addressed in this research. In sections 6.1 and 6.2 background information is presented to identify the motivation for decoupling spalling prediction from high temperature concrete structural analysis. Section 6.1 presents background information on the current understanding of spalling behaviour, the initiating mechanisms and current predictive capabilities. This section demonstrates the complexity of spalling and considerable challenges facing spalling prediction. Section 6.2 reviews the current guidelines for spalling behaviour in the design of concrete structures for fire and the applicability of those guidelines to modern concrete structures. This discussion demonstrates the need for calculation methods in the design of concrete structures against spalling.

Section 6.3 outlines a new design methodology intended to address point (3). The section explains how the methodology decouples spalling prediction from the structural analysis; the spalling severity then becomes an input for the structural analysis therefore some reference is made to spalling prediction techniques developed by others. In Section 6.4 and Section 6.5 two case studies are presented to demonstrate the implementation of the design methodology.

6.1 Spalling behaviour of concrete

A substantial body of research concerning the mechanisms of spalling of concrete at high temperatures exists. In this section the types of spalling, the governing mechanisms and predictive techniques are discussed. This discussion highlights the

complexity of spalling prediction and the feasibility of spalling predictive techniques in a design or structural analysis context.

6.1.1 Types and consequences of spalling

Spalling has been classified into 3 different types namely, explosive spalling, aggregate spalling and corner spalling {CIRIA, 1984 #222}:

Aggregate Spalling – This type of spalling occurs in the early stages of the fire and involves small pieces flying off from the surface. Damage to the concrete cross-section is cosmetic.

Explosive spalling – Typically occurs in the early stage of a fire and has been witnessed at temperatures as low as 200°C {Both, 1999 #25}. This type of spalling is violent and destructive, involving rapid expulsion of pieces of concrete from the exposed surface.

Corner Spalling – this type occurs in the later, and often, decay stages of the fire. It is characterised by large corner pieces falling off the concrete. Tensile cracks develop at the corners and edges where reinforcement is often located {Connolly, 1995 #29}.

Explosive spalling is generally considered to be the most detrimental to concrete structural behaviour by removing concrete cross section and reinforcement cover in the early stages of the fire when gas temperatures are high and rapidly rising. Aggregate spalling results in only superficial damage to the concrete structure. Although corner spalling occurs in the loss of large concrete pieces this concrete is already significantly weakened because this type of spalling occurs late on in the fire. In a real fire, temperatures are reducing at this stage unlike in the fire resistance test where the temperature rises indefinitely and corner spalling can result in failure of the member {Bailey, 2002 #4}.

The majority of research is therefore concerned with explosive spalling; in the following sections the mechanisms of explosive spalling and prediction techniques are described. All future references to spalling refer to explosive spalling.

6.1.2 Mechanisms of spalling

The precise conditions under which spalling occurs is still the source of much debate {Khoury, 2000 #81}. Broadly, the proposed mechanisms fall under three categories; pore pressure spalling, thermal stress spalling and combined pore pressure and thermal stress spalling. Each is described briefly here.

Pore pressure spalling

In general terms pore pressure spalling occurs when evaporation and migration of free water from the heated surface increases pore pressure locally at some distance from the heated surface. Continued heating and moisture migration will result in the pore pressure reaching the tensile strength of the concrete, resulting in an explosive local failure.

Thermal stress spalling

At sufficiently high heating rates ceramics have displayed explosive spalling due to excessive differential thermal expansion {Khoury, 2000 #81}. This demonstrates that factors other than pore pressure contribute to the occurrence of spalling. When concrete is heated steep thermal gradients develop. The differential rates of thermal expansion through the cross section result in compressive stresses at the exposed face where expansion is highest and tension in the cool interior where thermal expansion is lower (chapter 3). The thermal expansion differential is thought to give rise to thermal spalling.

Combination thermal stress and pore pressure spalling

There is growing consensus that spalling of concrete arises from a combination of the tensile stresses induced by differential thermal expansion and increased pore pressure {Phan, 1997 #85; Khoury, 2000 #14}. This theory is given credence by the lack of experimental evidence directly supporting either pore pressure spalling or thermal stress spalling as being individually capable of inducing spalling. The combined stresses from increased pore pressure and thermal stress are, however, thought to be sufficient. There is continued debate surrounding the interaction of these two mechanisms and how this interaction results in spalling. Recent numerical modelling has suggested that the influence of each mechanism may change depending on the

scenario {Zhang, 2009 #91}. Much of the difficulty in understanding this lies in the experimental challenge of concrete micro structure behaviour during high temperature experiments.

6.1.3 Influencing parameters

Several substantial reviews of the experimental and numerical research in this field have been undertaken {Khoury, 2000 #81; Khoury, 2000 #14} therefore this section briefly summarises the current consensus concerning the mechanisms which give rise to spalling and the influencing parameters.

A large number of factors have been found to contribute to the occurrence of spalling. Khoury {, 2000 #14} has grouped some of the most significant parameters under the following categories: material factors, environmental factors and geometric factors. These are presented in Table 6.1.

Table 6.1 Factors contributing to the spalling behaviour of concrete

Category	Contributing Factor
Material	Moisture Content Concrete Permeability Cracks Aggregate Type and Size Reinforcement
Environmental	Heating rate Heating profile Thermal Restraint
Geometric	Section shape Section size

Moisture Content

Moisture content is considered one of the main factors in the occurrence of spalling. Concrete with a moisture content above 2-3% by weight has a much higher propensity to spalling than that of drier concrete; however, a high moisture content is not a prerequisite for the occurrence of spalling {Khoury, 2000 #14}. Increased

moisture content will correspondingly result in an increase in pore pressure due to the greater volume of evaporable free water at the heated surface.

Permeability, water/cement ratio

High strength concretes are considered more prone to explosive spalling than normal strength concrete even though high strength concretes are also stronger in tension. This increased propensity to spalling is not due to their higher strength, but due to the means by which the concrete has been strengthened. A common method is the inclusion of densifying additives such as silica fume or a low water/cement ratio. A side effect of this is a reduction in material permeability and it is this low permeability which is thought to increase their risk of spalling by preventing the ready escape of water and increasing pore pressure build up {Hertz, 2003 #1}.

Aggregate type and size

Thermal incompatibility between the aggregate and the cement matrix can contribute to spalling behaviour, and some aggregates are more prone to spalling than others. Siliceous aggregates tend to perform poorly with some such as Thames gravel breaking down at temperatures as low as 350°C {Khoury, 2000 #14} and quartz aggregates experiencing alpha-beta conversion at 570°C {Bazant, 1996 #22}. Calcareous aggregates owe their better performance to a lower thermal expansion coefficient and so a greater thermal compatibility with the cement paste.

Heating rate and profile

The heating rate has been shown to be a significant factor in explosive spalling. The likelihood of spalling increases when heating rates are fast. The faster the rate of heating the steeper the thermal gradient in the concrete cross-section and the larger the differential rates of thermal expansion increasing thermal stress. An approximate minimum thermal gradient in the section is 5K/mm and at 7-8K/mm spalling is very likely {Fletcher, 2007 #3}.

Restraint and applied load

Restraint against thermal expansion of a heated structural element induces mechanical strains equal and opposite to the thermal expansion strains. The

development of these mechanical strains results in compressive stresses which increase the likelihood of spalling. Application of load can also increase compressive stresses, resulting in a greater possibility of spalling {Hertz, 2003 #1}.

Cross section geometry

Sharp changes in geometry such as corners have demonstrated a tendency for spalling, due to the higher thermal stresses and a higher rate of heat influx.

There is experimental evidence that thinner cross-sections spall more readily than thicker cross sections; it has been suggested that pore pressure magnitudes in thinner cross-sections could be higher {Khoury, 2000 #81}.

6.1.4 Predictive capabilities

Coupled hydro-thermal-mechanical models

To model the mechanisms of spalling accurately the heat transfer, mass transfer and mechanical stress analyses must be coupled in what is termed hydro-thermal-mechanical modelling. Advances were made with this approach in the 1990s with major contributions from Gawin et al. {, 2003 #94}, Khoury et al. {, 2002 #38} and Khoury {, 1995 #95}. This was largely driven by the European wide HITECO (HIGH TEMPERATURE CONCRETE) project. Further developments have been made by Tenchev and Purnell {, 2005 #6} and Davie et al. {, 2008 #119}.

These models are able to describe accurately the thermal, hydro and mechanical processes that occur in concrete at elevated temperatures; however, the predictive capabilities of such models has been limited by our inability to clearly identify the conditions under which spalling occurs. There is considerable experimental difficulty in measuring conditions within a specimen at high temperature which has made it difficult to establish the exact criteria for spalling and also to validate predictions made by these models. Therefore the models have not yet provided effective predictions of spalling {Davie, 2008 #119} suitable for a design scenario.

Coupled hydro-thermal models

To simplify the modelling process for the purpose of combination with a structural analysis some have developed coupled hydro-thermal models which ignore the

thermal stress contribution by performing the structural analysis separately {Dwaikat, 2009 #68}; this simplification has yet to be justified experimentally or theoretically.

6.1.5 Summary of spalling mechanisms and modelling

It is clear that numerical modelling has made significant advances in our understanding of the conditions in heated concrete specimens. Predictive techniques are limited by experimental validation and confirmation of the conditions which lead to spalling. Simplified prediction models are undermined by limited theoretical justification.

The mechanisms that govern spalling have been described here; the scale at which these occur is not compatible with a structural analysis. In addition the accuracy of current prediction techniques is not yet sufficient for design purposes. It is therefore concluded that current spalling predictive techniques are not suitable to be coupled with a structural analysis. This does not, however, negate the need for the ability to capture the detrimental effects of spalling in a structural analysis which is described in section 6.2.

6.2 Design of concrete structures for spalling

In this section the guidelines concerning the spalling behaviour of concrete under Eurocode 2 {, 2004 #27} are reviewed and the assumptions behind those guidelines are discussed in the context modern concrete structures.

6.2.1 European spalling guidance

In Eurocode 2 three design approaches are described for the design of concrete structures in fire; the tabulated data, simplified calculation methods and advanced calculation models. Only principles are provided for the advanced calculation models; however, more detailed guidance is provided for the tabulated data and simplified calculation method approach. The nature of these approaches and the spalling guidance provided are described in the following sections.

Tabulated data

The tabulated data consists of sets of minimum cross section dimensions and reinforcement cover levels to achieve a particular fire resistance rating for different structural elements (beams, walls, slabs etc). The origins of the tabulated data are empirical, primarily derived from standard fire resistance tests of isolated concrete structural elements conducted in the 1940s {Lennon, 2004 #225}.

When a design is compliant with the geometric requirements of the tabulated data no consideration of spalling is deemed necessary. As the origins of the tabulated data are empirical it is assumed that the detrimental effects of spalling are already implicitly accounted for by the experimental process.

However, an inherent limitation of empirical methods is that their applicability is determined by the conditions under which their data was obtained. Spalling behaviour is influenced by a large number of material, geometric and thermal parameters (for example, as discussed above, the aggregate type). There is a natural degree of variation in these parameters which should be covered by the range of tested specimens; however, these parameters have also changed over time.

Kelly and Purkiss {, 2008 #220} have investigated the validity of applying historical test data to modern concrete structures, particularly focusing on spalling behaviour. They found that typical concrete porosity and permeability has decreased since the tests in the 1940s as a by product of increasing early day concrete strengths. Permeability is a significant contributing factor to the spalling behaviour of concrete; therefore the ability of an empirical approach which uses historical data to adequately address the issue of spalling is questionable.

It should also be noted that material changes in concrete are not the only difference between the test data and modern concrete structures. The tabulated data are largely based on unrestrained concrete specimens subject to a single heating condition, the standard temperature time curve. Restraint of thermal expansion and the heating rate have strong influences upon the development of the thermal stress, indeed Ali et al. {, 2004 #5} have shown the likelihood and severity of spalling are affected by both of these parameters.

Simplified calculation method

When using a calculation method to estimate fire resistance, either the simplified methods of Eurocode 2 Annex B {, 2004 #27} or advanced calculation models, spalling risk is determined only by the concrete moisture content by weight. According to the UK Eurocode 2 Annex {, 2004 #221} the critical moisture content of concrete by weight is 3%. The moisture content may be assumed to be below this if the member is designed for an X0 or XC1 exposure class; these exposure classes represent internal exposure. Where the designer feels the moisture content may be above 3% it is recommended to check for the effect of spalling by assuming loss of cover to one reinforcing bar or bundle of bars. Thus this assumes only localised spalling. This check may also be avoided if where the number of reinforcement bars is large as it is thought that an acceptable redistribution of stress is possible without loss of stability. This may be assumed for the following situations:

- solid slabs with evenly distributed rebar; and
- beams with a width of greater than 400mm and more than 8 reinforcement bars in the tensile area.

For high spalling risk scenarios the use of spalling mitigation measures such as polypropylene fibres are advocated. Polypropylene fibres melt at 160°C; it is thought that this process reduces spalling by providing channels to relieve the build up of pore pressures {Khoury, 2000 #81}.

Although moisture content is a significant contributing parameter in the spalling behaviour of concrete it is not solely responsible. The use of a singular parameter to determine spalling risk ignores the effect and interactions of other contributing parameters; neglect of these has not been justified {Kelly, 2008 #220}. The use of moisture content alone also focuses on pore pressure spalling as being predominantly responsible for spalling. Recent numerical research {Zhang, 2009 #91} has indicated that the relative importance of thermal stress and pore pressure could be scenario specific.

6.2.2 Summary of spalling design guidance

Spalling is only considered in a small number of cases under European concrete fire design guidance. Some of the underlying assumptions are difficult to justify, such as the use of historical data to ensure fire resistance; some have not been justified, such as the use of a singular parameter for the determination of spalling risk. Modern concrete structures are typically lighter than traditional concrete construction thus making them more vulnerable to the effects of spalling and fire.

Spalling risk assessment methods need to be improved and it needs to be recognised that this is a two-stage process:

- the likelihood of spalling occurring; and
- the consequences for the structure should spalling occur.

6.3 Spalling design framework

A new design framework has been developed here which aims to directly address the design of concrete structures for the effects of fire and concrete spalling.

This framework improves on previous approaches by decoupling the spalling prediction from the structural analysis. The spalling design framework developed here focuses on the implementation of the spalling effect in a structural analysis. This provides the opportunity to pursue design solutions which minimise the consequences of spalling for structural performance. In addition to current spalling mitigation measures this will increase the available options for designing concrete structures for the effects of spalling.

The spalling design framework is appropriate for use in performance based design. Performance based design is used when it can add value to a design; this is typically achieved with new and innovative designs which fall outside the boundaries of prescriptive guidance. As discussed in section 6.2 the current European guidance provides limited information for determining spalling risk; this impedes the use of calculation techniques necessary for ensuring concrete structural fire resistance under performance based design approaches.

A key feature of this framework is to separate the tasks of determining *spalling risk* and investigating the *consequences of spalling* for structural performance. The advantage of determining spalling risk and structural response separately is greater freedom and flexibility to choose the most appropriate spalling tool or structural analysis for the given situation. Additionally within a design there is likely to be a substantial amount of variation in parameters contributing to spalling behaviour. Combined with the variation in structural form this produces a potentially large number of analyses to be conducted; by separating the task of spalling risk and structural analysis this may be reduced.

6.3.1 Spalling design framework overview

The proposed spalling design framework is summarised in the flow chart in Figure 6-1.

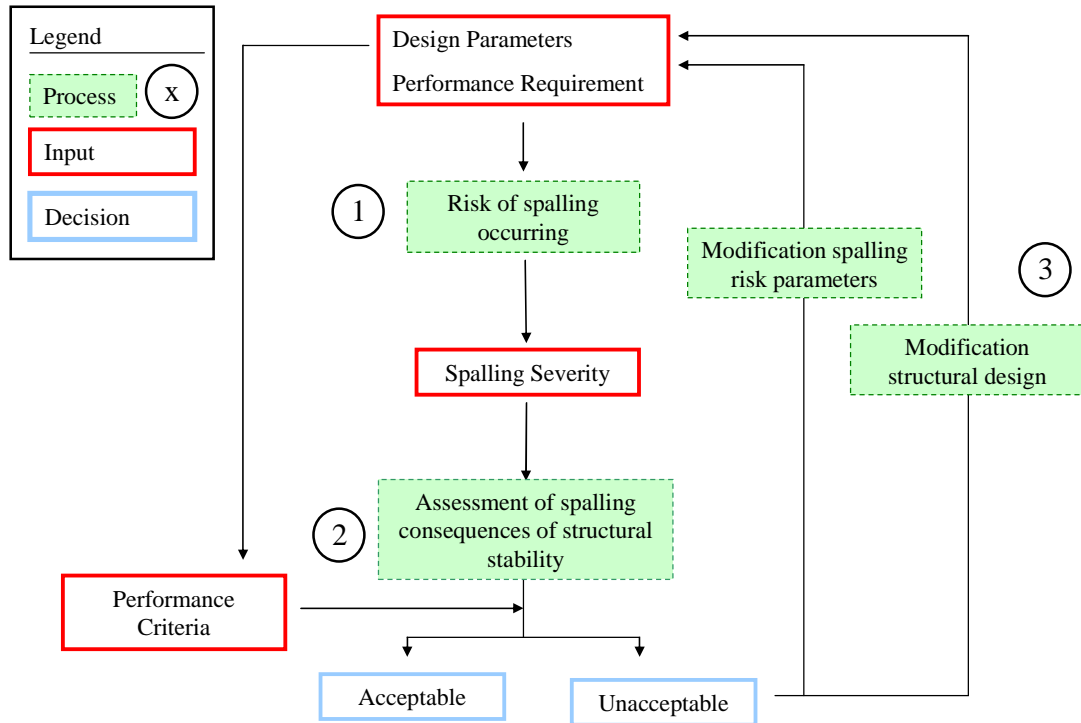


Figure 6-1 Flow chart of proposed design procedure for the consideration of spalling effects for concrete structural performance in fire

The procedure consists of two separate sequential analyses. The first analysis considers the likelihood of spalling; the second calculates the spalling affected structural performance and assesses the consequences for structural fire performance.

The first stage of the analysis examines the likelihood of spalling. Spalling prediction may be undertaken using a variety of methods: empirically observed spalling rates, numerical spalling models or risk-based assessments. These methods are discussed more fully in section 6.3.2. The inputs to the design procedure are the spalling risk factors, that is, the thermal, material and geometric factors summarised in section 6.1.3. The thermal conditions are defined by the appropriate design fire, the material factors are determined by the concrete mix design and the geometric factors are determined by the structural design and structural conditions, that is, restraint and applied load. Whichever method is used, the output is a quantification of spalling

severity which is input to the structural analysis. This quantification is expressed as an area of cross-section lost.

The consequences of spalling upon the structural performance are assessed in the second analysis. The spalling affected structural fire performance is first calculated and then the consequences of spalling for structural fire performance are judged on the basis of the design performance criteria. The type of structural analysis used is dictated by the performance requirement. Simple analyses might omit thermal expansion (for example) but are typically conservative; more detailed calculation techniques such as frame and finite element analysis are more accurate but require more assumptions to be made. Inputs will therefore depend upon the type of analysis adopted but will include the spalling severity established in the first analysis.

To determine the consequences of spalling the predicted structural performance is compared with the performance requirements to determine acceptability. Where the interpreted performance meets the fire resistance requirements the design is acceptable and the process comes to an end; where it is unacceptable the process must be repeated following modification of the design. The performance may be improved by either:

- reducing spalling risk factors;
- spalling mitigation measures; or
- improving structural stability in the event of spalling.

Reducing the spalling severity entails changing spalling risk factors such as high levels of restraint against thermal expansion or concrete mix design. Measures to mitigate spalling include application of protective insulation layers such as plasterboard and the use of polypropylene fibres in the concrete mix. These approaches constitute the current treatment of spalling in design. The spalling design framework offers a third alternative. Where the severity of spalling is not excessively onerous it may be possible to design out the effects of spalling. This will require identifying the consequences of spalling for structural support mechanisms, and therefore an understanding of concrete structural support mechanisms.

6.3.2 Spalling prediction

Spalling predictions can be made using empirical data or numerical model predictions. The spalling prediction methodologies presented in this section is the work of others. They are presented to demonstrate how they can fit in with the spalling design framework developed by the author in section 6.3.1.

Empirical data derived from material and structural tests has allowed us to develop an understanding of the conditions likely to cause spalling. However, by its very nature it is limited to the test conditions under which it was derived, limiting its applicability.

Numerical models vary in their sophistication, the most complex models are able to accurately model the physical processes responsible but have been limited by poor definition of the critical conditions for spalling and a lack of experimental validation. Simplified models naturally suffer from the same limitations. The gap has yet to be closed between empirical data and modelling capability.

While both numerical and empirical based predictions individually have limitations, the combination of knowledge amassed from both these methods provides a wealth of understanding concerning the conditions likely to lead to spalling and the potential severity of spalling.

These approaches can be combined by using a risk-based methodology to make spalling predictions. Risk based approaches are already in wide spread use with the fire safety community. Risk is calculated as a function of the frequency of occurrence, the probability of occurrence and the consequence of occurrence. Each of these depend upon a large number of contributing factors, thus prediction of spalling for a full design can be a laborious task. A risk-based approach is substantially faster than detailed modelling making it attractive in a design context; it allows detailed analysis to focus upon high risk elements of a structure. The framework of many risk-based approaches allows for classification of risk to be continually updated as research in the field advances.

Two risk-based methods that have been developed to determine the risk of spalling are Lennon et al. {, 2007 #223} and Lamont et al. {, 2007 #219}.

Lennon risk based approach

Lennon et al. {, 2007 #223} developed a risk based approach for demonstration purposes in the design guide, *Concrete structures in fire*. Risk is calculated according to the equation:

$$\text{Risk} = \text{frequency} \times \text{probability} \times \text{consequences} \quad \text{Equation 6-1}$$

Frequency refers to the number of fires that are likely to occur in a building, which is a function of building size and usage. Probability refers to the likelihood of spalling occurring; this is determined by the interaction of the contributing factors (such as moisture content, aggregate type, thermal exposure) which were summarised in section 6.1.3. Consequences in this context must be considered the consequences of structural failure occurring due to spalling for the fire safety strategy, rather than the consequences of spalling specifically for structural performance. Therefore consequence is a function of the application of the structural element for example location and role in the structural arrangement. When considering the consequences of structural failure due to spalling for life safety or property protection Lennon et al. assume the consequences to be proportional to the height of the building.

To demonstrate how the method can be used Lennon created a hazard scoring system for the likelihood of spalling; an extract is included in Table 6.2. Each factor is attributed a weighted score 1, 3 or 5 depending on their effect upon spalling likelihood. A score of 1 indicates a small effect, 5 a large effect.

Table 6.2 Example of hazard based scoring system for spalling of concrete structures {Lennon, 2007 #223}

Condition	Factor	Suggested Hazard Score		
		Low	Med	High
Thermal Exposure	Normal (Standard Fire curve)	1		
	Severe (Hydrocarbon curve)		3	
	Extreme (Modified Hydrocarbon curve, RWS)			5
	1 sided exposure	1		
	> 1 side exposed		3	

Spalling risk categories are attributed to bands of total hazard score; Lennon et al.'s categorisation is included here in Table 6.3

Table 6.3 Hazard categorisation for spalling of concrete structures {Lennon, 2007 #223}

Hazard Category	Risk of Spalling	Overall hazard score	Key factors
Low	Very low	<10	Normal strength, lightweight concrete, standard fire exposure, mc <3%, I side exposure, unloaded
	Low	11-15	Normal strength, normal weight concrete, calcareous aggregate, standard fire exposure, internal environment, restrained, unloaded
Medium	Medium	16-20	Normal strength, normal weight concrete, siliceous aggregate, hydrocarbon fire exposure, internal environment, restrained, loaded
High	High	21-25	High strength (Class 2 of EN 1992-1-2) Hydrocarbon fire, siliceous aggregate
	Very high	>25	High strength concrete (Class 3 of EN 1992-1-2), tunnel fire exposure, high moisture content, siliceous aggregate

Once the spalling hazard has been identified Lennon uses a matrix in Table 6.4 and the categories in Table 6.5 to judge the overall risk category in terms of the spalling hazard and spalling failure consequences (the failure of an element due to spalling) and suggests possible actions.

Table 6.4 Risk Assessment – possible template for risk profiling {Lennon, 2007 #223}

Hazard Category	Consequence class – function of building height (m)				
	1 (0-5m)	2 (5-18m)	3 (18-30m)	4 (30-60m)	5 (>60m)
Low					
Med					
High					

Table 6.5 Possible risk categories {Lennon, 2007 #223}

Colour Code	Risk Category	Action Required
	Acceptable risk	No action required
	Tolerable	Consider the use of passive fire protection
	Unacceptable risk	Measures to reduce or mitigate consequences of spalling essential

This method demonstrates how spalling *likelihood* can be quantified. The focus for risk profiling is, however, upon spalling mitigation which is only one potential solution to minimising the threat of spalling behaviour. The consequence of structural failure is considered in relation to life safety by linking the risk to building height.

Lamont risk based approach

Lamont et al. {, 2007 #219} adopts a similar methodology to Lennon {, 2007 #223} to determine spalling hazard. Factors affecting spalling likelihood are designated a weighted score of 1, 3 and 5 to represent low, medium and high hazard. Table 6.6 allows the total risk score (column 3) to be translated into different spalling risk categories. Five risk categories are defined with a severity of spalling associated with each category. These spalling severities correlate with experimental evidence.

Table 6.6 Spalling hazard classification and spalling severities {Lamont, 2007 #219}

Category	Risk of spalling	Total Risk	Key factors	Spalling Level
A	Very Low	≤11	Ordinary Strength, normal weight, unloaded, unrestrained, standard fire exposure, reinforced, moisture < 3%, one side exposure	Zero or minimal
B	Low	12-20	Ordinary Strength, normal weight, unloaded, restrained, standard fire exposure Significant no. of key variables likely to promote spalling	Up to the level of the reinforcement
C	Med	21-28	Ordinary Strength, normal weight, unloaded, restrained, standard hydrocarbon fire exposure Small no. of key variables likely to promote spalling	3 mm/min
D	High	29-37	Ordinary Strength, normal weight, unloaded, restrained, standard hydrocarbon fire exposure Significant no. of key variables likely to promote spalling	7 mm/min
E	Very high	>37	High strength (design strength > 55 MPa), standard hydrocarbon fire exposure	Un-quantifiable

Lamont et al.'s method fails to consider the consequences of spalling-induced structural failure in the hazard scoring. The consequences of failure are, however, an important contribution to the total risk. Relying purely on spalling hazard to determine risk neglects scenarios where the consequences of structural failure are sufficiently severe to warrant consideration of lower risk events (such as in nuclear applications).

This approach has the advantage of attributing physical spalling rates to different risk categories. These spalling rates may be used as a direct input into the structural analysis in section 6.3.3. The spalling severities are currently based on experimental evidence and are tied to the standard temperature time curve, the methodology is open however to modification as numerical and experimental research advances.

Summary

Risk based approaches provide a more robust design solution for spalling prediction than current numerical solutions are capable of providing. The framework of a risk based approach is open to development as numerical and experimental research advances.

The risk based approaches reviewed here represent the first attempts to quantify spalling risk. Naturally, there is room for improvement. Immediate improvements include:

- Inclusion of consequences of structural failure for fire safety strategy in hazard scoring; and
- more experimental evidence of spalling severities

6.3.3 Structural Analysis

The structural analysis stage of the design framework assesses the structural performance should spalling occur. The inputs to the structural analysis are: material properties, structural arrangement, design fire, spalling severity and the performance requirements.

The type of structural analysis depends upon the design requirements and can vary from simple estimates of flexural strength to more detailed frame and finite element analyses. In both cases the heat transfer and structural analysis is typically performed separately but the analysis must correctly model the thermal distribution due to the loss of concrete section when spalling occurs.

The predicted structural performance (e.g. time to collapse) must then be compared with the performance requirements. The degree of fire resistance required is normally specified in terms of the stability, insulation and integrity performance of the structure (the three essential fire resistance criteria). For load bearing structures, we are primarily concerned with stability, but insulation and integrity can also become the limiting performance requirements.

In section 6.4 and section 6.5 two case-studies are used to demonstrate the implementation of this new design framework for (i) a simple calculation technique and (ii) a finite element analysis.

6.4 Case Study 1: Continuous two span RC beam

This case study demonstrates the implementation of the spalling design framework for the simple structural analysis of a concrete structural element in fire. The structure analysed is a two span continuous reinforced concrete beam which is 600 mm deep, 300 mm wide and has 6 m spans. The ambient concrete strength f_{cu} is 30 MPa. Figure 6-2 shows the reinforcement quantities and curtailment. The ambient reinforcement yield strength is $f_y = 500$ MPa and the cover level to top and bottom reinforcement is 35 mm. Temperature dependent material properties for both the concrete and reinforcing steel are taken from Eurocode 2.

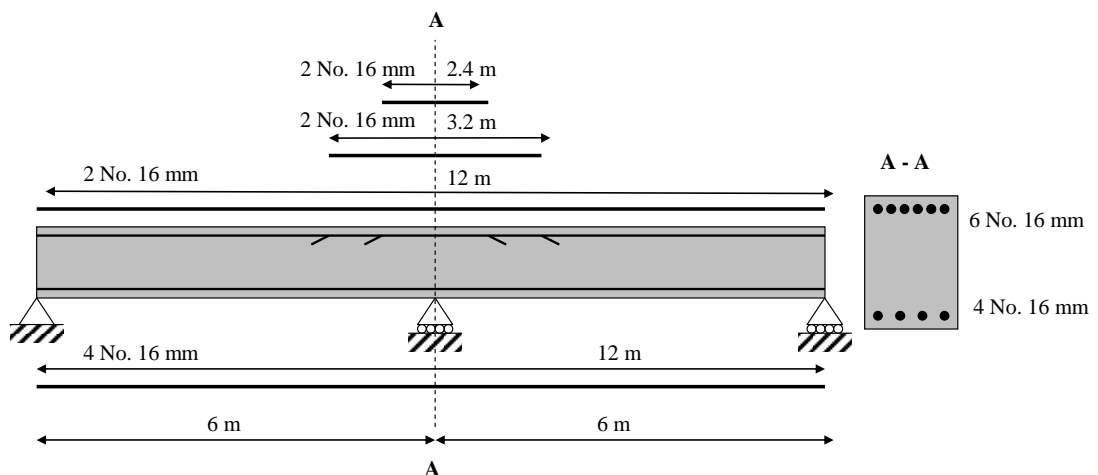


Figure 6-2 Two span continuous beam reinforcement distribution

The beam load ratio is 0.5. Load ratio compares the applied bending moment in fire conditions (M^*_{fire}) to the beam ambient ultimate moment capacity (R_{cold}):

$$r_{load} = M^*_{fire} / M_{cold} \quad \text{Equation 6-2}$$

6.4.1 Step 1: Spalling assessment

The spalling assessment by Lamont et al. {, 2007 #219} is used here to define the spalling severity (Table 6.6). The structure investigated is an ordinary strength,

unrestrained beam exposed to the standard fire curve. It is assumed that a significant number of key material variables likely to promote spalling are present, for example high moisture content. The spalling hazard category is therefore B for which the spalling severity is the loss of reinforcement cover.

If the category had been C or D, the most severe categories the loss of cover to the reinforcement and the reinforcement (spalling progresses beyond the reinforcement level) would occur in 12 min and 5 min respectively. The consequence of these spalling classifications for flexural structural elements is so severe as to make it impossible to design out the effects of spalling, and so measures need to be taken to minimise spalling risk or spalling mitigation measures should be adopted.

6.4.2 Step 2: Structural performance

The spalling affected thermal response of the beam is calculated using the finite element method. The structural response is subsequently calculated using plastic hand calculation analysis and moment redistribution (as commonly used for ambient design). The standard temperature time curve is used to define the thermal exposure. The failure mechanism is considered to be the formation of two plastic hinges within a single span and the duration of exposure to the standard fire required to cause this is the failure time.

The moment capacity of the beam cross-section during heating is calculated using the 500°C isotherm method from Appendix B1 of Eurocode 2 {, 2002 #30}. This method assumes that concrete heated above 500°C has zero strength and below 500°C the strength is unaffected by temperature. The 500°C isotherm method is the simplest calculation technique available for the design of concrete structures for fire. The thermal and mechanical analyses are performed separately. The mechanical analysis is performed in two-steps:

- Sectional analysis to calculate spalling affected moment capacity
- Structural analysis to calculate implications for the continuous beam

Thermal analysis

The thermal analysis is performed for a 2D cross section of the beam using commercial finite element software ABAQUS [1, 2008 #120]. During the heat transfer analysis finite elements are removed to the reinforcement cover depth. Spalling is assumed to occur instantly and at a prescribed rate of 3mm/min to compare the effect for temperature evolution of both the reinforcement and the concrete cross section. Each time a layer of concrete elements is removed from the analysis the thermal boundary conditions are reapplied. Figure 6-3 presents a contour plot of cross section temperatures during the heat transfer. Elements coloured white represent spalled material and have been removed from the analysis.

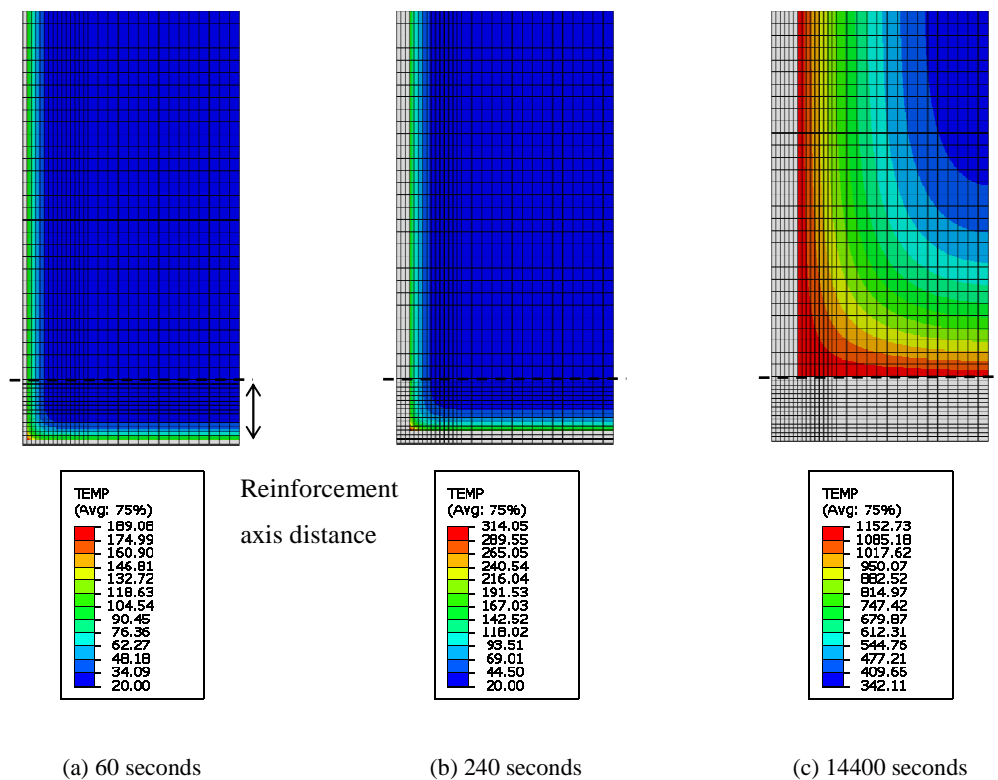


Figure 6-3 Beam cross section temperature profiles ($^{\circ}\text{C}$)

The thermal response of the cross section is summarised in terms of the temperature of the bottom reinforcement steel and the effective cross-sectional area in Figure 6-4. The effective cross sectional area is the cross-sectional area of concrete below 500°C . Three cases are compared in Figure 6-4: no spalling, category B spalling instant removal and category B spalling progressive. Figure 6-4 (a) compares the

evolution of bottom reinforcement temperature and Figure 6-4 (b) the reduction in effective cross-sectional area.

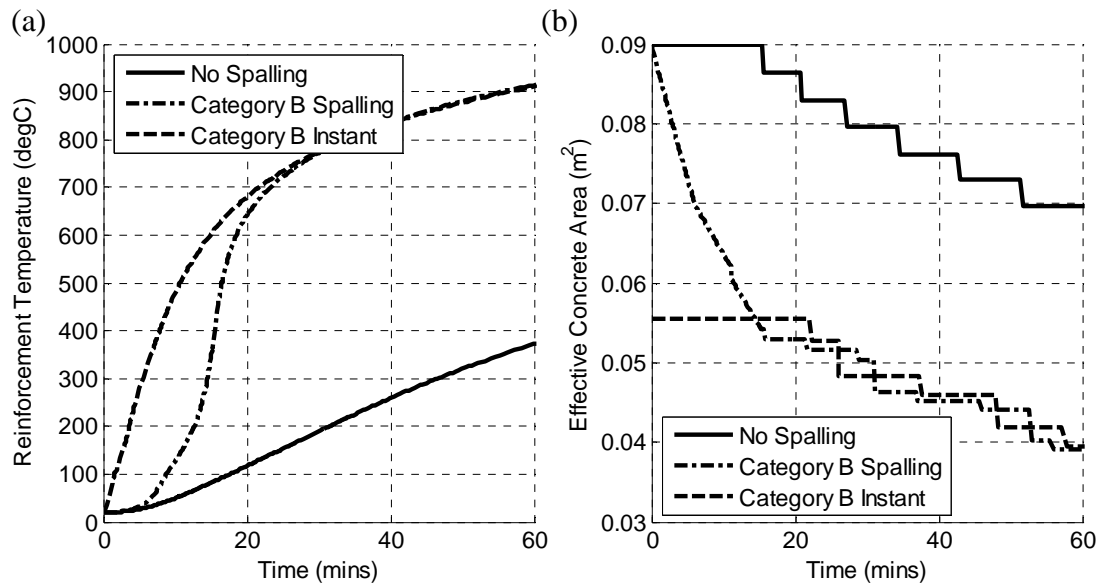


Figure 6-4. Effect of spalling characterisation for (a) Bottom reinforcement temperature and (b) effective cross section area upon exposure to the standard temperature time curve

Spalling increases the rate of temperature rise of the reinforcement and increases the reduction in effective cross-sectional area. Removing all of the spalled material prior to the start of the analysis as opposed to gradually during the analysis results in a faster initial rise in reinforcement temperature; after 20 minutes of exposure when all the spalled material has been removed the spalling affected reinforcement temperatures are almost the same. Similarly instant removal of the spalled material results in initially a much higher reduction in effective cross-sectional area. However, once all of the spalled material has been removed the effective cross sectional areas are equal; it is therefore possible when spalling of the reinforcement cover is considered to simplify the analysis by assuming the loss of concrete cover prior to the start of the analysis.

Section capacity

The effect of temperature for the beam moment capacity is calculated using the 500°C isotherm method from Appendix B1 Eurocode2 {, 2002 #30}. Figure 6-5 presents the reduction in normalised sagging and hogging moment capacities for the case of no spalling, Figure 6-5 (a), and category B spalling, Figure 6-5 (b).

It is apparent from both figures that the mid span sagging moment capacity is most adversely affected by fire exposure and spalling due to the proximity of the sagging reinforcement to the exposed beam surface. The rapid decline of moment capacity will lead to yielding of the reinforcement at mid span.

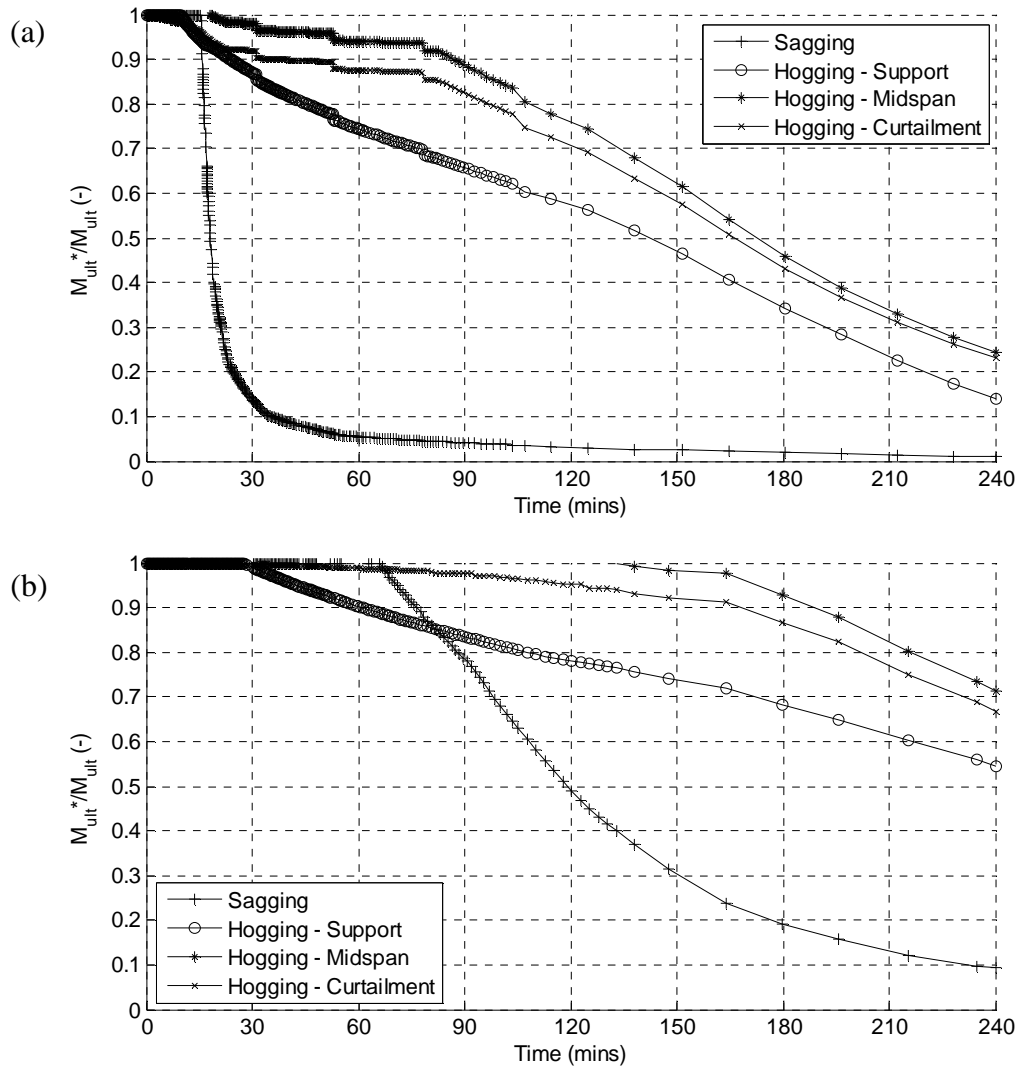


Figure 6-5 Cross section sagging and hogging moment capacity for (a) No spalling and (b) Category B spalling under standard fire exposure

Structural analysis

The structural response of the beam is calculated using plastic analysis and moment redistribution. Thermal expansion effects are not considered in this calculation. Figure 6-6 demonstrates the moment redistribution that occurs during heating of the beam. The ambient temperature bending moment diagram and moment capacity

envelope are presented in Figure 6-6 (a). In Figure 6-6 (b) the rapid decline in mid span sagging moment has led to the development of a plastic hinge. As the sagging moment capacity continues to decrease so too does the mid span moment, redistributing moment towards the central support. This is evident in Figure 6-6 (c) where a third plastic hinge forms at the central support due to a reduction in hogging moment capacity and redistributed mid span moment which will result in failure of the slab.

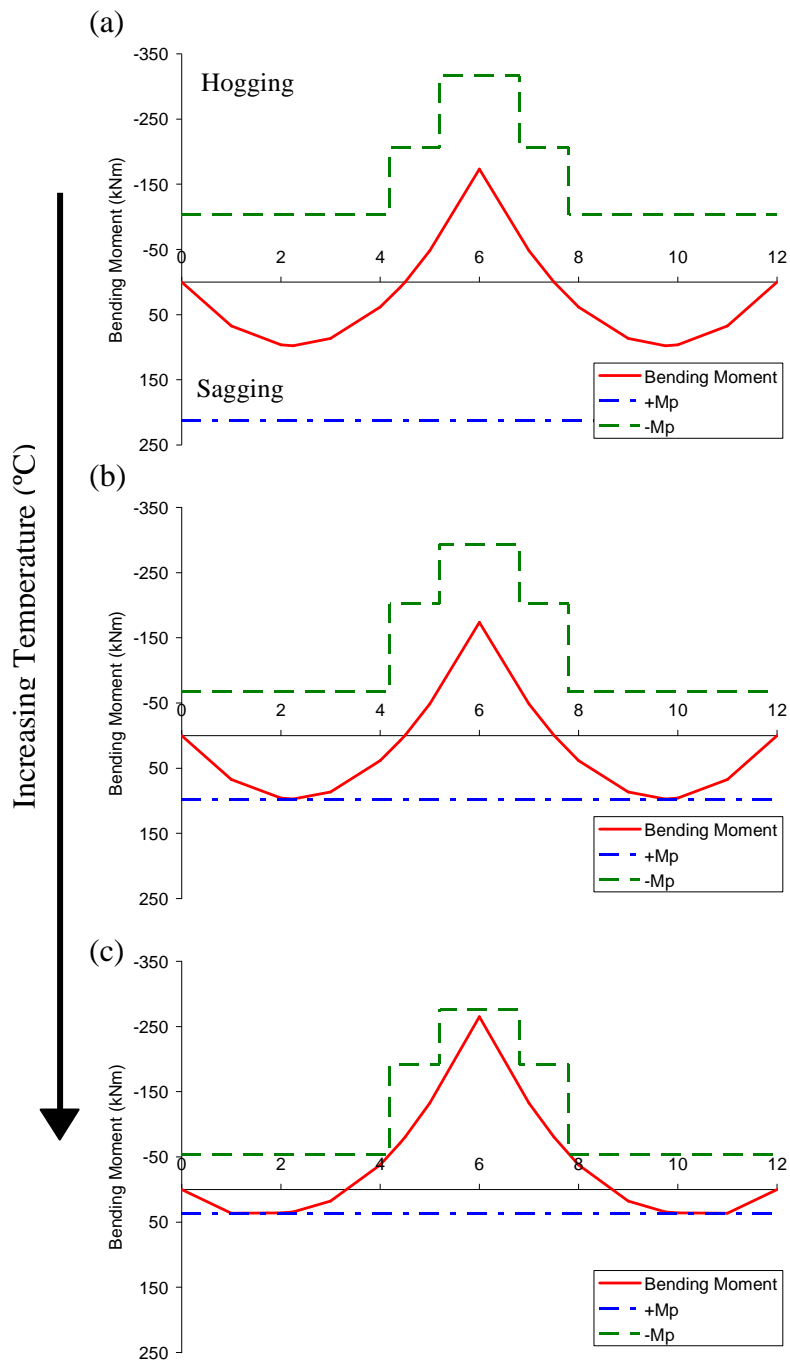


Figure 6-6 Moment Redistribution in a two span continuous beam exposed to a fire (a) Ambient conditions (b) plastic hinge development at beam mid spans (c) plastic hinge develops at support – failure mechanism

The duration of exposure to the standard temperature time curve that causes this failure is used to determine the fire resistance period. Table 6.7 summarises the duration of exposure which causes the first and second plastic hinge to form which correspond to the failure times of a simply supported beam and a continuous beam respectively.

Table 6.7 Fire resistance periods of continuous two span beam under spalling categories A-D

Spalling Designation	First Yield (min)	Second Yield (min)	Fire Resistance (min)
No Spalling	125	180	180
Category B Spalling	19	30	30

Spalling significantly reduces the fire performance of the beam by causing a rapid decline in the sagging flexural capacity. The first yield of the beam is due to the reducing sagging capacity. In Table 6.7 we can see that spalling reduces the first yield time from 125 minutes to just 19 minutes. The second yield occurs at the continuous support due to moment redistribution. In Table 6.7 it can be seen that continuity improves the performance time of the non-spalling and spalling cases to 180 minutes and 30 minutes respectively. For the spalling case the improvement is less significant than for the non-spalling case. It is clear that the sagging moment capacity is critical to the performance of the beam.

A structural element may be attributed a fire resistance rating of 30, 60, 90, 120, 180 or 240 minutes, which ever is less than the predicted failure time; the fire resistance times of the continuous beam based on the calculations in this section are included in Table 6.7.

Consideration of the spalling effect has shown the performance of the two way spanning beam to be inadequate. The designer now has two options, (1) to reduce the spalling risk or (2) having identified the consequences of spalling for the structure they can design out the effect of spalling. This process is demonstrated in the following section

6.4.3 Step 3: Spalling re-design

The analysis of the structure demonstrated that the rapid deterioration in mid span sagging capacity was critical for the behaviour of the beam. If the designer is able to attenuate that decline, the fire resistance period of the beam can be improved.

The reduction in cross section sagging capacity is chiefly due to the rise in temperature of the steel reinforcement. To improve performance it is therefore

necessary to limit this temperature rise. This could be achieved by redistributing the bottom steel layer into two layers (Figure 6-7). With this arrangement of reinforcement only the lowest layer of reinforcement is exposed and 50% of the reinforcement is insulated. Figure 6-7 presents the new reinforcement detailing.

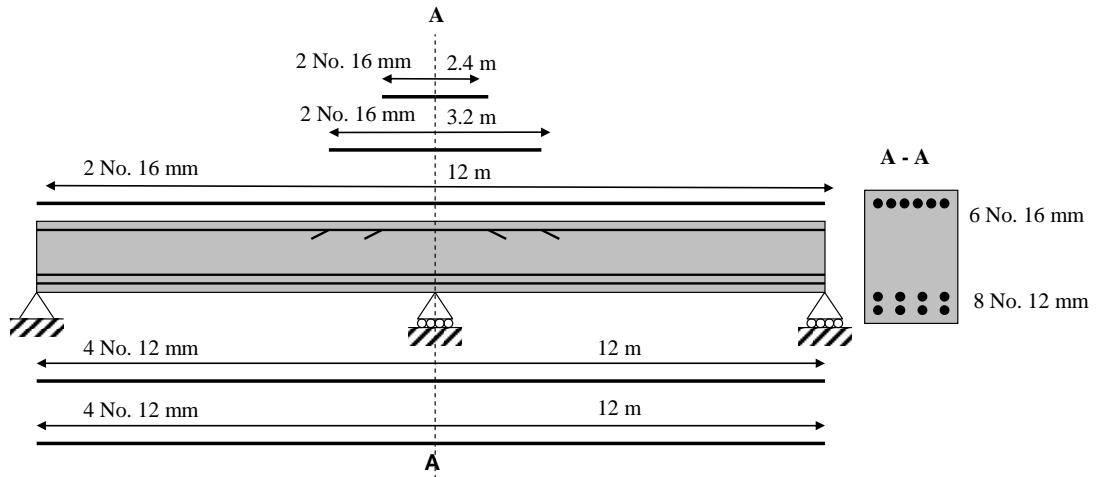


Figure 6-7 Reinforcement redistribution to improve spalling performance of a two span continuous reinforced concrete beam

Figure 6-8 compares the reduction in capacity when a double layer of reinforcing steel is used in the bottom layer for the case of spalling and no spalling.

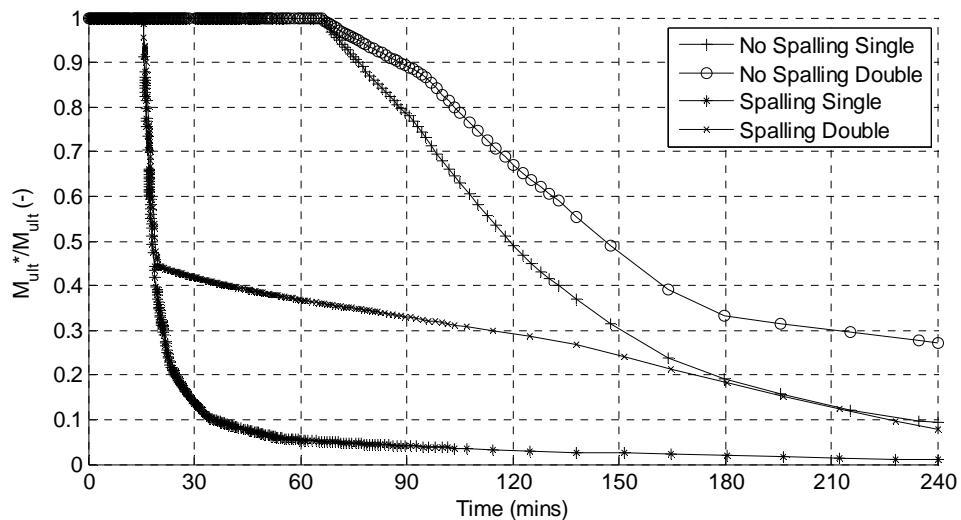


Figure 6-8 Effect of redistribution of sagging reinforcement for the sagging moment capacity without spalling (Cat A) and with spalling (Cat B)

The decrease in sagging capacity is attenuated by partially maintaining insulation to the bottom reinforcement. The moment redistribution has been calculated to

determine the failure time under exposure to the standard temperature time curve, this is summarised in Table 6.8.

Table 6.8 Effect of sagging reinforcement distribution upon fire resistance periods in the event of spalling (Cat B) and without spalling

Spalling	1 st Yield	2 nd Yield	Fire Resistance
No Spalling	180	216	180
Category B Spalling	20	107	60

The fire resistance rating for category B spalling is significantly improved achieving the predefined performance criterion of 60 minutes fire resistance. This demonstrates that by understanding the consequences of spalling for structural behaviour it is possible to design out the effects of spalling.

6.5 Case Study 2: Two-way spanning slender slab

In this case-study the spalling affected performance of a two-way spanning reinforced concrete slab is analysed. The reinforced concrete slab spans 6m x 6m and 100mm deep as shown in Figure 6-9. This model is similar to that used in the chapters 4 and 5. In this model only tensile reinforcement is provided (12 mm diameter mesh with 200mm spacings). The reinforcement axis distance (from the slab soffit to the reinforcement mesh mid depth) is 30 mm. The applied load is 5 kN/m².

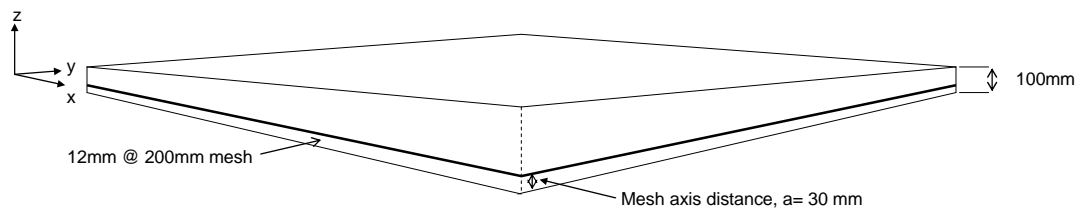


Figure 6-9 Reinforced concrete slab geometry

The ambient concrete strength f_{cu} is 30 MPa. The ambient reinforcement yield strength is $f_y = 500$ MPa and the reinforcement cover is 35 mm. Temperature

dependent material properties for both the concrete and reinforcing steel are taken from Eurocode 2. The fire is defined by the standard temperature time curve.

As discussed in chapter 4 two-way spanning slabs experience tensile membrane action in fire. This mechanism is heavily dependent upon the reinforcement to support the concrete slab by catenary action so any increase in reinforcement temperature due to spalling could have important consequences for the slabs performance. In this investigation the effect of spalling upon a slab experiencing tensile membrane action is investigated.

6.5.1 Step 1: Spalling assessment

As in the previous section Lamont et al.'s {, 2007 #219} spalling assessment is used here to define the spalling severity (Table 6.6). The inputs are the same as case study 1 therefore the spalling hazard category is B for this case study also; only the reinforcement cover is removed.

6.5.2 Step 2: Structural performance

The performance of the slab is analysed using the finite element method using the slab shell model employed in chapters 4 and 5. The analysis is a sequential heat transfer–stress analysis, with spalling implemented using the method described in the following sections.

Unlike the previous example of a continuous beam, the failure point or limiting performance of the slab is not readily apparent for the two-way spanning slab. Careful and considered interpretation of the finite element result is required.

The typical failure mechanism for a slender two way spanning slab which develops tensile membrane action is rupture of the mid span reinforcement but it is not possible to model this localised behaviour with the shell model used due to smearing of both the concrete tensile behaviour and the reinforcement (chapter 5). The design of composite steel-concrete structures for tensile membrane action instead uses a deflection limit {Bailey, 2001 #65}; this is currently considered conservative but is limited by experimental validation.

Thermal analysis

The thermal analysis is conducted using the finite element software ABAQUS {, 2008 #120}. In section 6.4.2 it was demonstrated that immediate removal of the spalled material has a conservative effect for the thermal response of the structure. This simplification is adopted here and the thermal distribution for the spalling affected depth of slab established.

Stress analysis

The stress analysis employs the shell model used in chapters 4 and 5 to analyse the behaviour of the slab. Alternative solutions include the use of solid elements where elements maybe physically removed from the analysis. Solid elements are computationally more expensive than shell elements. Specialist finite element codes such as Vulcan {Huang, 2007 #224} have also begun to include techniques in their code to mimic the effect of spalling.

The analysis contains two steps: (i) the load is applied first under ambient temperature and then (ii) the slab is heated. The spalled material must therefore be removed between the load step and the heating step. It is not possible to change the shell thickness during an analysis. The spalling effect is therefore approximated by using a composite shell cross section where different material properties can be assigned through the shell depth. Figure 6-10 presents a schematic of the slab cross-section and the composite shell section used to characterise it.

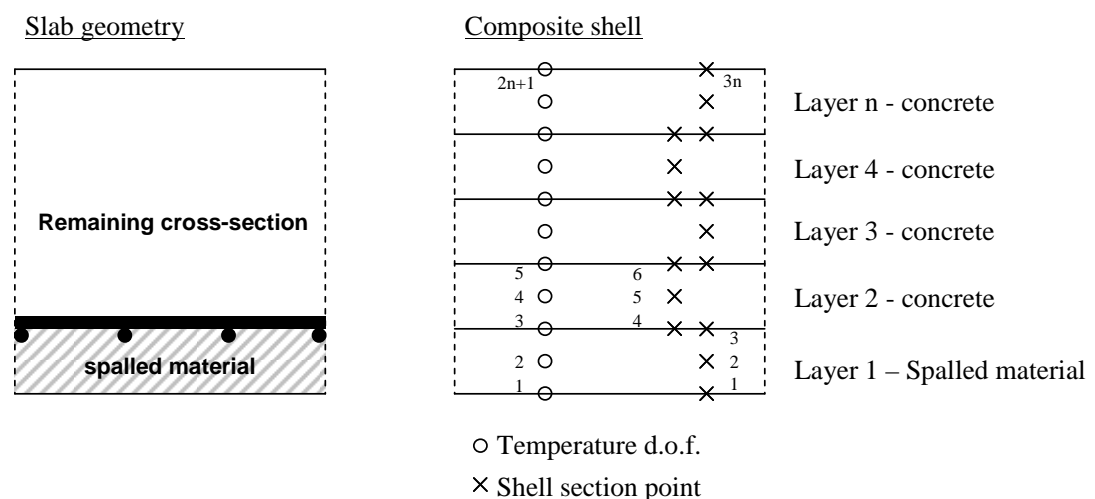


Figure 6-10 Composite shell section for approximation of spalling affected slab cross-section

Layer 1 represents the spalled material; this layer is not physically removed from the model but is assigned modified material properties, such that it has full strength at ambient temperature and no strength at elevated temperatures. The material properties assigned to the spalling layer are presented in Figure 6-11. The 20°C line represents Eurocode 2 ambient temperature concrete material properties. The 50°C has minimal strength.

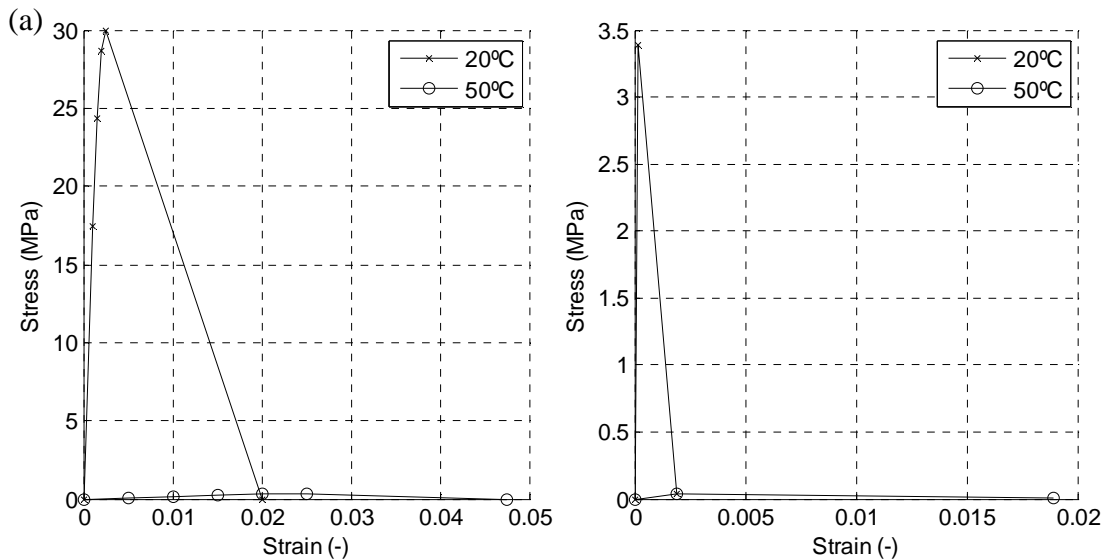


Figure 6-11 Spalled material properties under (a) compression (b) tension. Above 50 °C material properties assumed unchanging showing how material properties are modified to effectively remove the concrete

Figure 6-12 demonstrates the variation of the (a) temperature (b) thermal strain and (c) material strength through the shell thickness during the analysis. This demonstrates that the spalling layer makes no contribution to structural strength, nor does it affect differential thermal expansion, through the use of material properties.

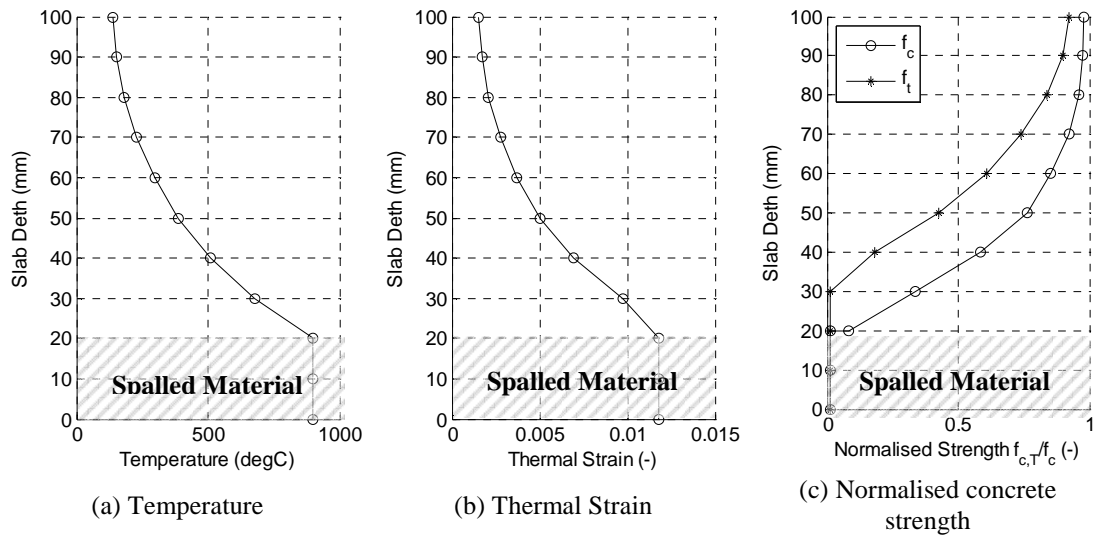


Figure 6-12 (a) Temperature (b) thermal strain and (c) normalised concrete strength profile after sixty minutes exposure for spalling affected slab

Slab analysis

Thermal response

Figure 6-13 presents the thermal profile after a sixty minute exposure to the standard fire and the evolution of reinforcement temperature for the spalling and non spalling case.

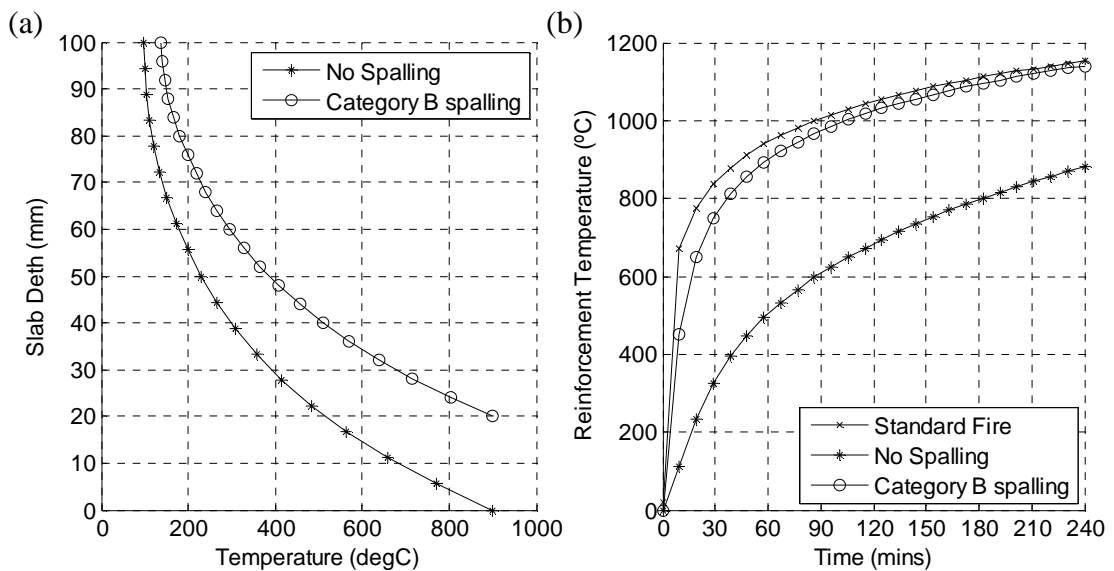


Figure 6-13 (a) Thermal profile after sixty minute standard fire exposure (b) Evolution of reinforcement temperature during exposure to the standard fire.

Material response

Figure 6-14 (a) and (b) present the decrease in reinforcement strength and the drop in average concrete compressive strength for the cross section. Spalling reduces the concrete effective area in Figure 6-14 by not only removing concrete cross section but also by increasing the average temperature rise of the cross section. Exposure of the reinforcement causes a rapid decline in reinforcement strength. After about 30 minutes the steel strength is less than 20% of the ambient temperature strength, while for the no spalling case the strength remains unaffected. The reinforcement strength is critical for tensile membrane action, where the reinforcement supports the central portion of the slab in catenary.

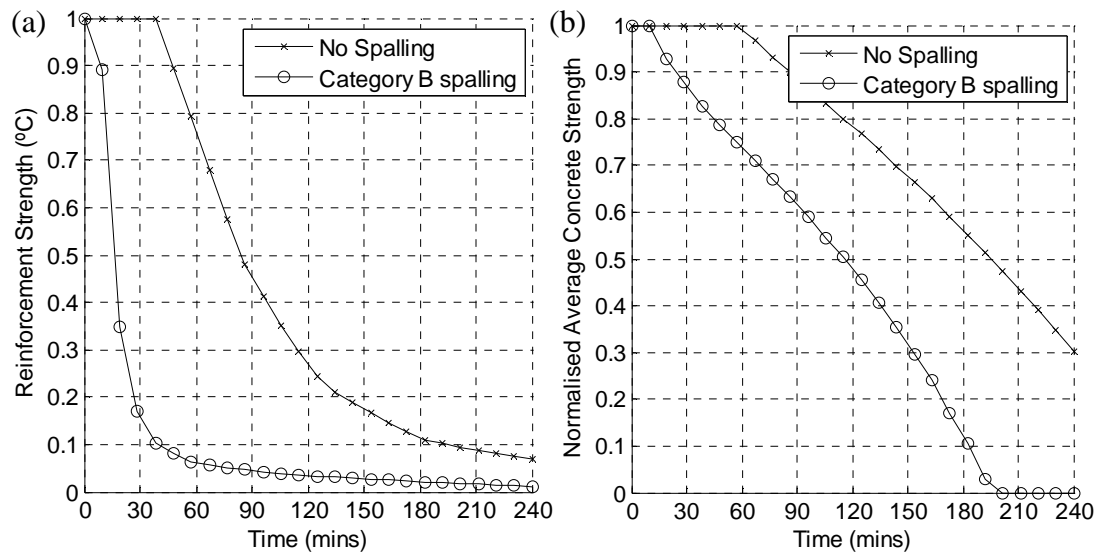


Figure 6-14 (a) Reinforcement strength (b) average concrete compressive strength through shell cross-section

Structural response

Figure 6-15 presents the deformation history of the slab for the case of spalling and non-spalling. Spalling results in an immediate increase in slab central deflection; after approximately 90 minutes of exposure the analysis predicts runaway deflections. The increased rate of deflection and runaway deflection associated with the spalling case is due to the decrease in reinforcement strength. Larger deflections increase the strength enhancement from tensile membrane action therefore the

deflections increase more rapidly to compensate for the loss of reinforcement strength.

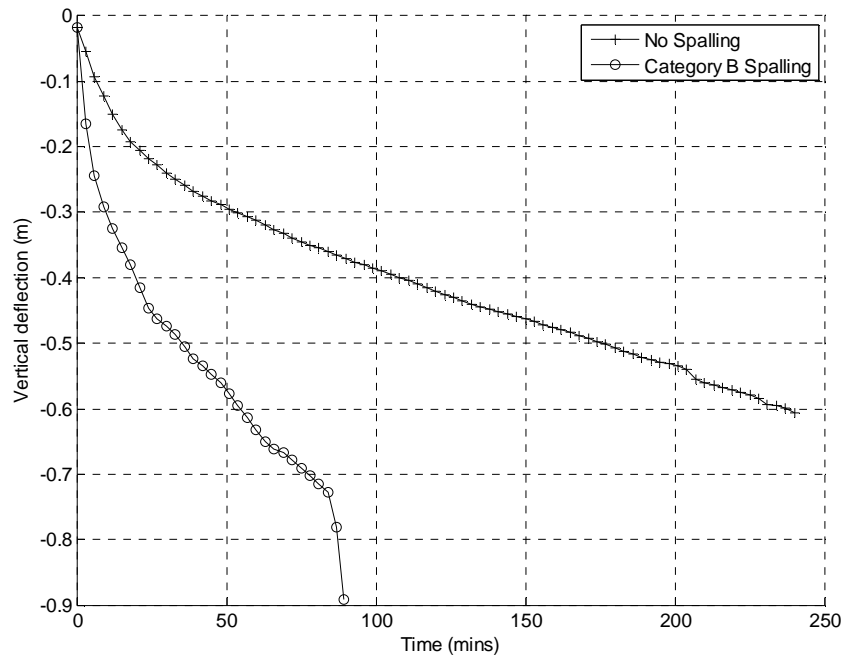


Figure 6-15 Central slab deflection of a laterally restrained two way spanning slender concrete slab for the case of spalling and no spalling

These rapidly increasing deflections are important for the reinforcement behaviour which is critical for the catenary action which is supporting the central portion of the slab. The peak reinforcement strains are contrasted at the slab edge and the slab mid-span in Figure 6-16. After less than 30 minutes spalling affected reinforcement strain deviate from the no spalling case, increasing significantly in line with the slab deflections. In the steel constitutive curve used in this analysis total strength loss occurs at 15% mechanical strain. It is at approximately this percentage strain that deflections runaway.

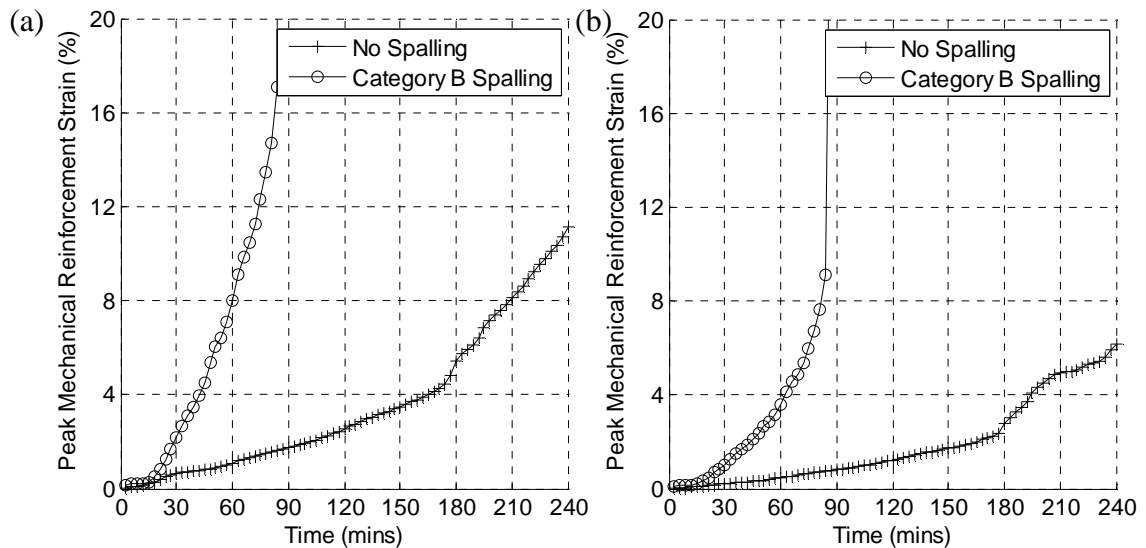


Figure 6-16 Peak reinforcement strain (a) Slab edge (0-1.2 m) (b) slab mid-span (1.2 – 3m)

From these results it is evident that the rapid decline in reinforcement strength is critical for the performance of the slab. The increased deflections required to mobilise tensile membrane action induce large strains at both the slab edge and the slab mid span. These spalling model strains are in excess of 15% after 90 minutes which is defined as the rupture strain in the analysis; these strains are not achieved in the no spalling model after 240 minutes of exposure. This explains the runaway deflections as the slab fails to maintain stability. In section 6.5.3 alternative designs are investigated to try to design out this spalling effect.

6.5.3 Step 3: Spalling re-design

As the reinforcement strength is critical to the performance of the slab under tensile membrane behaviour, to reduce the detrimental effect of spalling for the slab it will be necessary to reduce the loss of reinforcement strength. Two solutions are considered:

- (1) Redistribution of the sagging steel layer into two layers.
- (2) No curtailment of the hogging reinforcement.

Figure 6-17 presents the reinforcement layouts for the original design and the alternative design options.

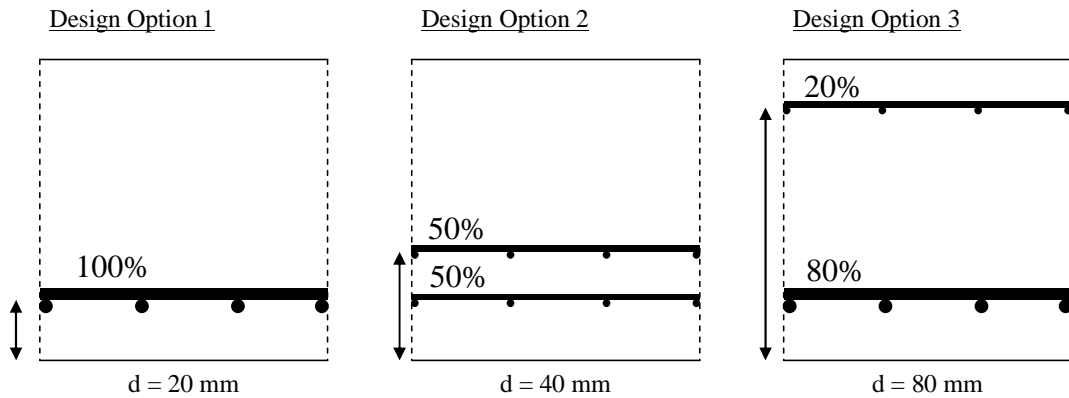


Figure 6-17 Design option 1 and alternative design options 2 & 3 slab cross section showing the exposure cover (d) for each reinforcement layer

The spalling designation remains the same, that is, spalling removes only the reinforcement cover. Therefore in the alternative design solutions insulation is maintained for a portion of the reinforcement.

Thermal response

Figure 6-19 compares the evolution of reinforcement temperature for the depths of cover present in design options, 1, 2 & 3 for the case of spalling and no spalling.

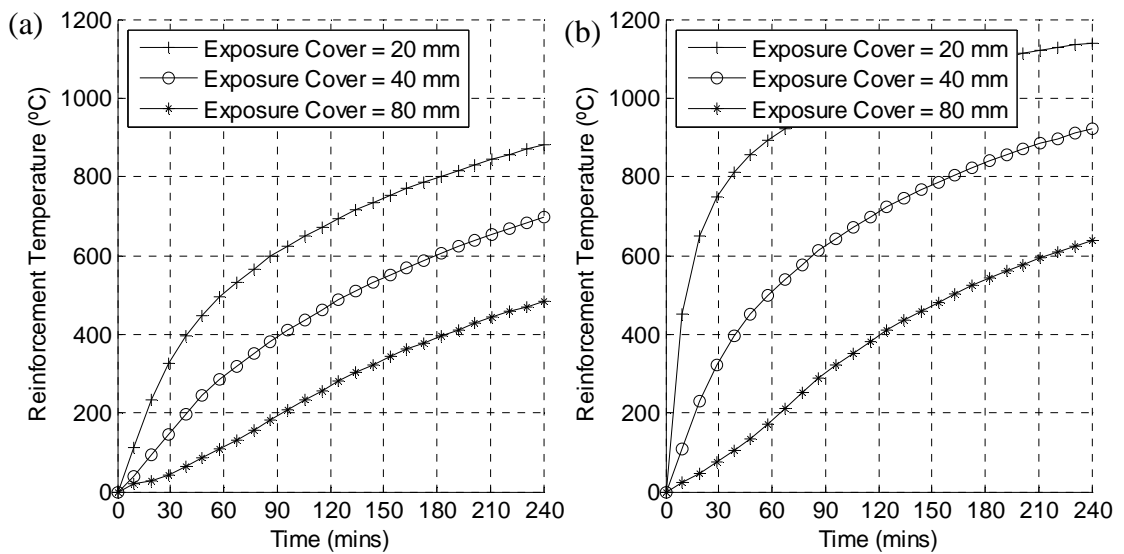


Figure 6-18 (a) No spalling and (b) Spalling affected temperature evolution for each reinforcement layer

Material response

To compare the relative reduction in reinforcement strength for each design option the equivalent reinforcement area is presented in Figure 6-19 for no spalling and spalling. The equivalent reinforcement area is the area of reinforcement modified by the high temperature reduction in steel strength. It is calculated as per the following equation:

$$A_{s,eq} = A_s * \left(\frac{f_{y,T}}{f_y} \right) \quad \text{Equation 6-3}$$

In Figure 6-19 the normalised areas represent both the top and bottom reinforcement.

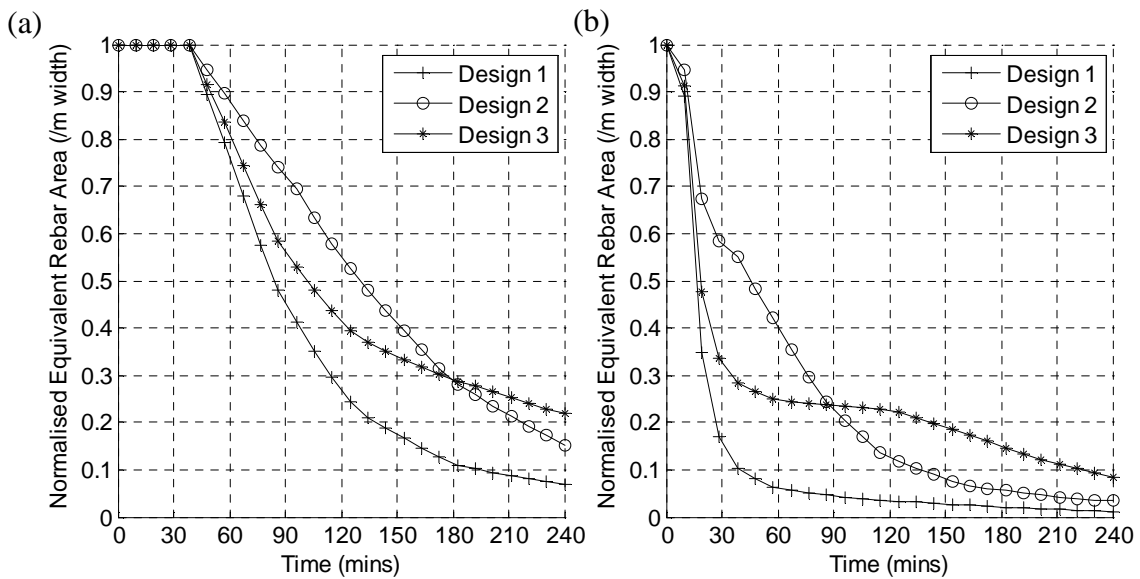


Figure 6-19 (a) no spalling (b) spalling affected normalised equivalent reinforcement area.

By maintaining cover to a portion of the steel reinforcement the alternative design options 2 and 3 retain a greater proportion of their steel strength under increasing exposure to high temperatures. The proportional decrease in reinforcement strength is lowest initially in design option two as a greater percentage of the slab reinforcement maintains cover. For a longer duration of exposure the reduction in reinforcement strength for design option 3 is lowest due to the large amount of cover to the top reinforcement. The performance of each design solution is investigated using reinforcement mechanical strain and concrete compressive proportional equivalent plastic strain as performance indicators.

Slab Performance

In Figure 6-20 the slab central deflections are presented for the spalling and no spalling case. For the case of no spalling the influence of the reinforcement distribution is small initially. Under the effects of spalling, there is a significant difference in the deflection response of the slab. The analysis was run for a 4 hour exposure; the runaway failure exhibited by the first design is delayed in design option 2 and never seen in design option 3. For up to three hours the second design where the sagging reinforcement is redistributed into two layers exhibits the lowest deflections due to the lowest reduction in overall reinforcement strength.

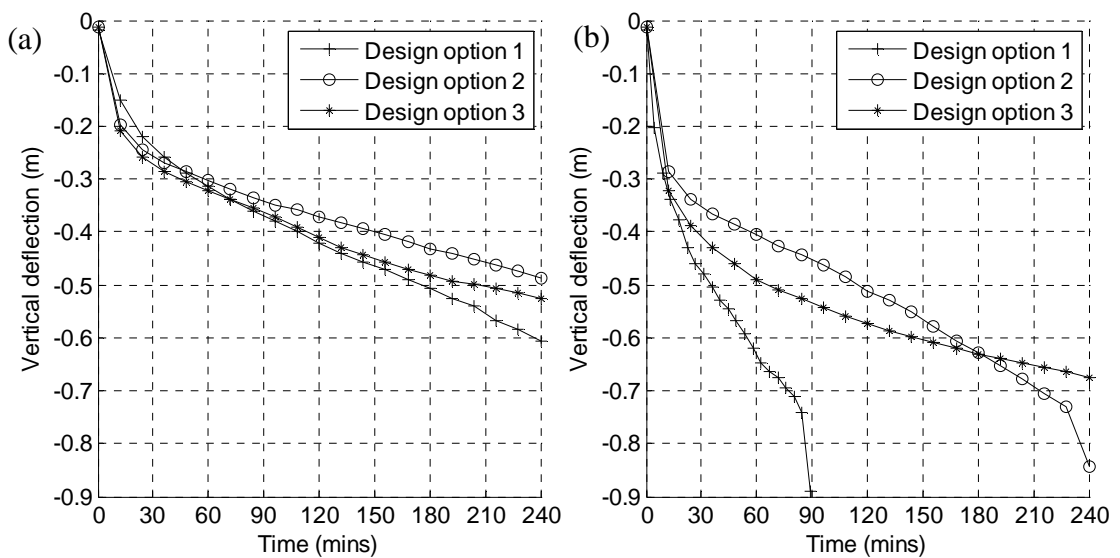


Figure 6-20 Slab central deflection (a) No spalling (b) Spalling

The reinforcement mechanical strains are used to contrast the performance of the two alternative design options. In Figure 6-21 the reinforcement performance is compared for the case of spalling and no spalling.

For the case of no spalling, reinforcement strains are substantially lower due to the higher reinforcement strength and lower deflections. For the duration of exposure the reinforcement strains are below the 15% rupture strain. The reinforcement strains in design option 3 are significantly higher than options 1 and 2. The additional reinforcement in this design is much cooler than the reinforcement present in options 1 and 2 therefore the strain relieving effects of thermal expansion are less.

For the case of spalling, the magnitude of reinforcement strains is considerably higher than the no spalling case. As seen in the previous analysis rapid loss of reinforcement strength induces large deflection strain rates. For design options 1 and 2 runaway failure is exhibited when peak reinforcement strains reach 15%. For design option 3 peak reinforcement strains reach up to 40%, well in excess of the rupture strain. Stability is maintained by the other layers of reinforcement.

Improving slab performance by informed redistribution of the reinforcement is a balance between ensuring sufficient cover is retained to minimise strength loss and limiting that cover to prevent large mechanical strains developing in the reinforcement. Both alternate design options improve the slab performance in the event of spalling. The appropriate design solution will also depend on other factors such as build ability and cost.

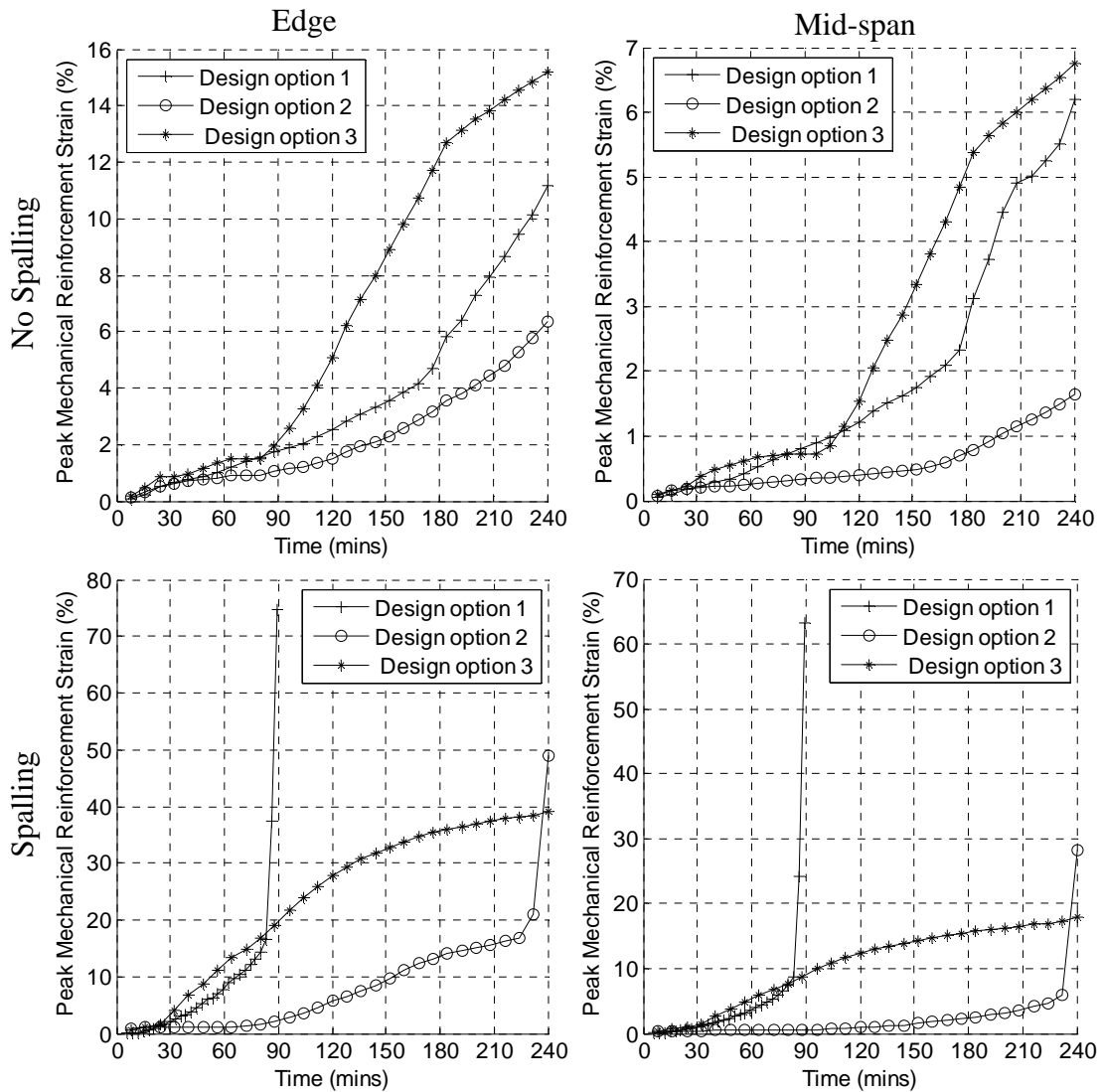


Figure 6-21 Peak reinforcement strains for design options 1, 2 and 3 at the slab edge and mid-span

6.6 Conclusions

The current method of designing concrete structures for the effects of spalling is predominantly based on empirical data. This approach was sufficient at the time of its development, however, the applicability of this data to modern concrete mix design and modern concrete construction is questionable. Neither is this approach applicable to performance based design.

In this chapter a spalling design framework has been developed which directly addresses the effects of spalling upon structural performance. In this framework the spalling prediction and structural analysis are decoupled. The analyses are performed sequentially; the spalling prediction output of spalling severity is used as an input to the structural analysis. Advantages of the framework include:

- Spalling prediction and structural analysis are decoupled. Comprehensive review of the mechanisms of spalling and spalling prediction techniques found that they are not compatible with structural analyses
- Structural analysis can be used in conjunction with any spalling prediction technique provided the output quantifies spalling severity as an area of concrete lost
- risk based approaches to spalling prediction provide the most robust solution for design purposes as the accuracy of numerical models is not yet sufficient for design purposes.

The spalling design framework was applied in two case studies: an analytical calculation of a two span continuous beam and a finite element analysis of a two-way spanning slab.

These case studies demonstrated how the critical effects of spalling for structural stability can be identified and subsequently designed out. It was found in both cases that spalling poses a serious threat to structural stability; it was also demonstrated that informed re-design of the structure can improve structural performance and is a viable design solution for addressing the issue of spalling risk.

7 Conclusions and further work

7.1 Introduction

Detailed research of high temperature concrete structural behaviour is necessary to help facilitate the advancement of performance based design in this area. The research conducted in this thesis makes an important contribution to furthering our understanding of the mechanisms of concrete structural performance in fire.

The relationship between fire compartment gas phase temperature variation and reinforced concrete slab structural performance was specifically examined. This relationship was investigated numerically and a detailed review of the necessary background knowledge undertaken. These areas included:

- material modelling of reinforced concrete,
- finite element modelling of reinforced concrete structures; and
- compartment fire thermal variation.

Preliminary studies identified the relationship between gas phase temperature variation and concrete's thermal expansion behaviour which is fundamental to understanding structural behaviour at high temperatures. These preliminary studies provided the necessary fundamental behaviour to understand the implications of gas phase temperature variation for reinforced concrete structural performance.

The behaviour of a two-way spanning reinforced concrete slab under a range of non-uniform thermal definitions was investigated. These analyses were contrasted with behaviour exhibited under uniform thermal exposure to judge the ability of uniform temperature assumptions to predict behaviour.

These investigations of behaviour did not consider the influence of concrete spalling. The incorporation of spalling into structural analysis is not straightforward. The influence of spalling upon behaviour was therefore dealt with separately. The current approaches and capabilities of spalling prediction techniques were reviewed and a methodology to include the effects of spalling in structural analysis developed. The consequences of spalling for two case-studies were investigated to identify the critical effects upon performance.

In this chapter the key conclusions from this research are identified in section 7.2 and the need for further research which has been identified by this work is presented in section 7.3.

7.2 Summary and conclusions

The research conducted is briefly summarised and the key conclusions from this research presented in bullet points.

7.2.1 Finite element & material modelling of RC two way spanning slabs

Under increasing thermal deformation two-way spanning slabs exhibit compressive membrane action at low deflections and tensile membrane action at large deflections. Under tensile membrane action the central portion of the slab is supported by the reinforcement in catenary action, this in turn is supported by lateral restraint and/or a self supporting ring of concrete compression at the slab periphery.

A finite element model was developed to analyse the high temperature behaviour of a two-way spanning reinforced concrete slab. During this development the assumptions of reinforced concrete material modelling and structural assumptions of finite element modelling were reviewed in detail.

- This review found finite element modelling able to provide reasonable predictions of high temperature tensile membrane behaviour in concrete slabs using simplifying assumptions. Finite element modelling of the tensile membrane mechanism has been validated against full-scale experimental studies by others.

The investigation of finite element model sensitivity to material definitions included: tension stiffening, load induced thermal strain and reinforcement rupture strain.

- The model was found to be quite sensitive to the concrete tensile definition. Load induced thermal strains were also found to affect behaviour. The sensitivity of the finite element model to the tension definition is particularly important
- Varying the amount of tension stiffening found that large tension stiffening definitions smothered the cracking behaviour of concrete producing an overly

stiff deflection response and underestimating reinforcement strains. This sensitivity is important for design where it is difficult to accurately know material properties. Too little tension stiffening was found to create numerical instabilities for the analysis

- Inclusion of the LITS component in the analysis of the two way spanning slab was found to reduce deflections and reinforcement strains during tensile membrane action. Detailed examination of the slab behaviour indicated this was due to the non-recoverable transient strain component of LITS which develops when the slab is initially loaded by in plane compression from thermal restraint. In this context inclusion of the LITS has been shown to make a more conservative prediction of behaviour. The LITS term has not been widely adopted in structural engineering. The findings of this study further our understanding of the manifestation of LITS in high temperature structural behaviour.

Ultimate stability failure of two-way spanning slabs under tensile membrane action has been shown experimentally by others to be by either mid-span reinforcement rupture or where the reinforcement ratio and/or ductility are high compressive crushing at the slab corners.

- Comparison of the mechanism of failure with the simplifying assumptions of the finite element model has demonstrated the inability of the model to analyse behaviour under failure conditions.
- The simplifying assumptions to most profoundly limit the ability of the model to analyse behaviour at failure is the smeared reinforcement and smeared concrete tensile cracking assumptions. These assumptions are not able to capture the large discrete cracks and subsequent reinforcement rupture at slab failure.

Where it is not possible to model the final failure mode of the slab it is possible to contrast performance using the indicators developed in this thesis. The performance of the tensile membrane mechanism is dependant upon the reinforcement for the mid-span catenary action and the ring of concrete compression for lateral support. (This investigation assumes continuity of vertical support).

In this research it has been shown that slab performance can be indicated by the performance of the compressive ring and the tensile net.

The performance of the compressive ring is measured by the development of post peak compressive strains. Equivalent plastic compressive strains are expressed as a proportion of the strain at peak stress. This ratio is used to indicate extent of crushing; a value greater than unity indicates the onset of concrete crushing.

The performance of the reinforcement is measured by the magnitude of tensile mechanical strains. Smearing of concrete tensile cracking and concrete-steel bond properties will lead to possible under prediction of the reinforcement mechanical strains. However, the accuracy of these predictions is adequate for relative measures of behaviour.

- The thermal and mechanical behaviour of reinforced concrete is complex and provides serious numerical challenges. Simplifying assumptions can provide reasonable estimates of behaviour however the limitations of those assumptions must be understood when using numerical modelling of reinforced concrete as a structural fire engineering research or design tool.

Investigation of geometric parameters for slab performance found slenderness ratio to have a significant effect upon the behaviour exhibited by the slab.

- The high temperature behaviour of slabs with reduced slenderness was found to be dominated by compressive membrane action. This markedly different behaviour is important for identifying the critical weakness in fire of different types of structures. For example the implications of non-uniform thermal environments for slender and stocky slabs will differ due to the different mechanisms of stability exhibited at high temperature by both.

7.2.2 Structural implications of spatial & temporal variations in T_g

Compartment fire thermal variation

The variation of gas temperature within a fire compartment is both spatial and temporal. This considerably increases the complexity of the relationship between structural behaviour and gas temperature variation. The timescales associated with changes in gas phase spatial distributions and concrete heating are considerably

different. Therefore to establish the implications of thermal variation for structural behaviour the response of the concrete was investigated in stages;

- the RC response to a static spatial distribution of gas temperature was first established; and
- then the sensitivity of the RC response to different temporal variations (fast, medium and slow) of spatial gas temperature distribution was investigated.

Concrete thermal expansion behaviour

The behaviour of structures at elevated temperatures is also complex being influenced by thermal expansion, temperature dependant material properties and structural restraint. The influence of gas temperature variation upon structural behaviour was investigated by first establishing the relationship between gas temperature variation and concrete thermal expansion behaviour.

- Thus it has been demonstrated that complex structural behaviour can be explained by understanding the role of underlying fundamental behaviour such as thermal expansion

The thermal expansion behaviour of concrete was found to be sensitive to spatial variations in gas temperature. The sensitivity of shallow and deep concrete elements was significantly different however.

- Shallow concrete elements are susceptible to thermal bowing due to the steep vertical thermal gradients which develop in concrete cross-sections upon heating. Exposure to spatial distributions of gas temperature produced distorted vertical deflection profiles due to variation in thermal curvature laterally. The peak deflection shifts towards the location of the peak gas temperature
- In deep concrete elements the influence of the high surface temperatures diminishes thus expansion behaviour dominates over thermal bowing behaviour. The vertical deflection profile is therefore significantly less affected by spatial distributions of temperature.
- For both the shallow and deep concrete elements the gas temperature variation does not substantially influence lateral displacements.

The thermal expansion behaviour of shallow concrete elements was also found to be sensitive to the effects of spatial variation in gas temperature at a range of temporal variations. The vertical deflection profile of a deep beam is however, significantly less affected by the temporal variations in gas temperature.

- The sensitivity of shallow concrete elements sensitivity to changing distributions of gas temperature is due to concrete's insulating nature and the susceptibility of shallow elements to thermal bowing. The insulating properties of concrete mean that the near surface temperatures respond quickly to changes in the thermal environment. In shallow concrete elements the near surface temperatures dominate the thermal gradient and influence the thermal bowing behaviour. This explains the reduced sensitivity of deeper concrete cross-sections where the influence of the near surface temperatures for the thermal expansion behaviour is reduced.

Two-way spanning slab behaviour

The implications of the thermal expansion distortions caused by spatial and temporal variation of gas temperature for the structural performance of a two-way spanning reinforced concrete slab were investigated under static gas temperature distributions and temporally varying distributions separately

The effect of spatial variation was investigated for a slender and a stocky slab the high temperature behaviour of which are dominated by tensile membrane action and compressive membrane action respectively.

- The tensile membrane mechanism exhibited by the slender RC slab was found to be sensitive to the distortions caused by spatial variation. The distorted vertical profile produced localised peaks in both the reinforcement mechanical strains used and concrete crushing strains used to indicate performance.
- The compressive membrane action exhibited by the stocky RC slab was found to be not significantly affected by the vertical distortions caused by spatial variation of gas temperature. These distortions were significantly less than in the slender slab. The compressive membrane performance of the slab was not further investigated under temporal conditions.

The effect of temporal variation was investigated for the slender slab exhibiting tensile membrane action. The behaviour exhibited under temporal and spatially varying temperatures was then contrasted with behaviour caused by uniform temperature exposures. These investigations provided the following specific findings:

- Under temporal variation the localised peaks in reinforcement strain and crushing strain seen in the slender slab behaviour is not evident. This is due to the complete traverse of the peak temperature across the slab span. The distribution of reinforcement strains and concrete crushing strains used to measure behaviour are symmetric for all temporal variations. The traverse of the localised peak temperature does cause an increased rate of peak deflection.
- Contrasting performance with different uniform temperature assumptions it was found that a uniform maximum gas temperature assumption provided a conservative estimate of behaviour. A uniform average gas temperature assumption provided an unconservative estimate of performance. The average assumption could not capture the increased rate of deflection caused by the traverse of the peak temperature across the slab span.
- The relative accuracy of the uniform temperature assumptions varied for each fire considered also. The uniform maximum temperature assumption was the least conservative for the fast fire and the most conservative for the slow fire. Similarly the uniform average gas temperature assumption as the least unconservative for the fast fire and the most unconservative for the slow fire.

From the findings of the investigations of spatial and temporal variation of gas temperature effects upon reinforced concrete structural performance we can make the following conclusions:

- The findings of this investigation challenge the purely strength based approach commonly adopted for the design of concrete structures at high temperatures. Slab deformations have been shown to be capable of influencing performance in structures where stability is heavily dependent on deformation dependent mechanisms like tensile membrane action.

- Structural fire engineering commonly makes uniform temperature assumptions. The results of this study indicate that uniform temperature assumptions can provide both conservative and unconservative predictions. The implications of spatial variation need to be considered very carefully for the design context.
- Previous research has shown the thermal variation within a compartment to be statistically significant; this research has demonstrated that non-uniform thermal distributions do have implications for the behaviour of structures susceptible to thermal bowing and changes in near surface temperatures.
- Identifying the appropriate design fire is a function of the compartment fire dynamics and the structural behaviour. This investigation has demonstrated the differing vulnerabilities possible in structural behaviour (slender versus stocky behaviour). It is therefore necessary in identifying the worst case scenario to consider both fire and structural parameters to avoid overly conservative or conversely unconservative designs.

7.2.3 Consequences of spalling for concrete structural behaviour

Explosive spalling poses a serious threat to reinforced concrete structural stability by reducing the concrete cross-sectional area and potentially exposing the reinforcement to high gas temperatures. To properly quantify the consequences of spalling for structural performance it is necessary to implement the effects of spalling in a structural analysis.

A review of the current understanding of the mechanisms responsible for spalling and current predictive capabilities came to the following conclusion:

- The mechanisms responsible for the occurrence of spalling occur at the micro-scale which is not captured in a typical high temperature concrete structural analysis. They are also complex requiring coupling of the thermal, hydro and mechanical processes occurring as concrete is heated. This is beyond the scope of a structural analysis particularly in a design context.

This research has therefore developed a spalling design framework for the consideration of spalling in a structural analysis without explicitly modelling the mechanisms of spalling. This has been achieved by decoupling the spalling

prediction and the structural analysis. The prediction of spalling severity (by others) becomes an input to the structural analysis. The spalling design framework that has been developed here is concerned with the structural analysis and establishing and the consequences of spalling for structural performance rather than spalling prediction.

The spalling design framework has been demonstrated using two case studies employing two different structural analyses; a simply supported continuous two span beam and a two-way spanning slab. The case studies have demonstrated the implementation of the methodology and how it can be used to identify the critical effects of spalling and design the structure accordingly.

- The spalling affected analytical analysis of the continuous two-span simply supported beam demonstrated that the sharp decrease in flexural strength due to the exposure of the reinforcement was critical for performance. Moment redistribution from continuity was not sufficient to improve performance to an acceptable level. It then demonstrated through the same analysis procedure that performance could be improved by attenuating the decrease in reinforcement strength by redistribution of the reinforcement steel.
- The performance of the restrained two-way spanning slab was analysed using the finite element method. This analysis demonstrated that the loss of reinforcement strength was critical not only for the flexural strength but for the tensile membrane mechanism. By maintaining reinforcement cover by either redistribution of the sagging reinforcement or continuation of the hogging reinforcement tensile membrane action could be mobilised and the effect of spalling for performance minimised.
- It has been shown in this investigation that the consequences of spalling are critical for the structural fire performance of the structures analysed. It has also been shown that by understanding the critical effect spalling has upon a structure those effects can potentially be mitigated by designing out the detrimental effects of spalling upon structural performance.
- Spalling is not currently explicitly considered in concrete structural fire design. The effects of spalling are assumed to be implicitly accounted for in the

empirical data which underpins most of concrete structural fire engineering. This research offers a methodology for the structural fire design of modern structures that fall out with the applicability of that empirical data.

7.3 Further work

The investigations conducted in this thesis have highlighted the need for further research.

This thesis has focused on establishing the fundamental behaviour of singular structural elements. To do this the structural boundary conditions needed to be simplified and behaviour was investigated under an envelope of idealised boundary conditions. The restraint conditions imposed in a real building are much more complex. The next logical step is to therefore investigate whole building response to non-uniform thermal environments. This is particularly important for non-uniform thermal exposures where the location of the peak temperature changes with time causing the boundary conditions for each structural element to change also.

This thesis has also focused on the implications of non-uniform thermal variation for slender structural elements where deformations strongly influence behaviour. Investigations of slenderness effects showed the behaviour of stockier concrete elements to be quite different and less susceptible to the effects of distorted deformations arising from thermal variation. These types of structures should be further investigated by undertaking a more detailed examination of the effect of non-uniform thermal exposures upon structural capacity and the implications of that for performance.

This research into the relationship between compartment fire thermal environments and structural behaviour would benefit from additional full scale fire testing in large compartments typical of open plan offices found today. Detailed instrumentation of the fire tests would provide valuable additional data on the thermal variation present in compartment fires.

The investigation of our current predictive capabilities of concrete spalling has demonstrated that their accuracy is not currently sufficient for use in a design context. Nevertheless there is a need for providing spalling estimates for the design

of structures which fall outside the limits of applicability of the tabulated data. Given the current limitations of numerical predictions risk based methodologies provide the most robust solution for design. Some initial efforts have been made to develop a risk based approach; these methodologies would benefit from further numerical and experimental research characterising spalling rates under different conditions.

References
